

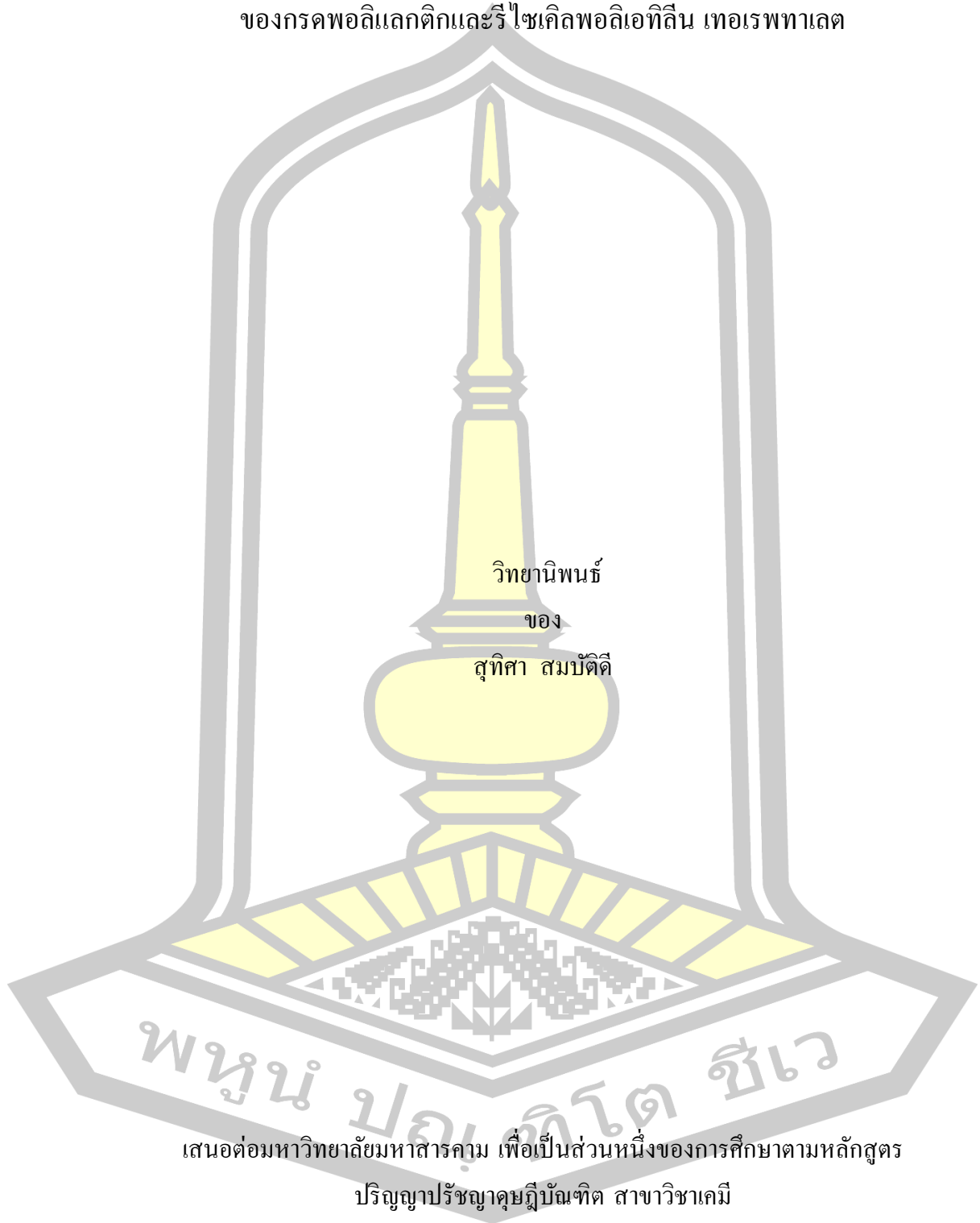
Polyethylene-Based Composite Fibers *In Situ* Reinforced with Poly(lactic acid) and Recycled Poly(ethylene terephthalate) Microfibrils

Suthisa Sombatdee

A Thesis Submitted in Partial Fulfillment of Requirements for
degree of Doctor of Philosophy in Chemistry
Academic Year 2017

Copyright of Maharakham University

เส้นใยเชิงประกอบของพอลิเอทิลีนที่มีการเสริมแรงแบบอิน-ซิทู ด้วยเส้นใยขนาดเล็ก
ของกรดพอลิแลคติกและรีไซเคิลพอลิเอทิลีน เทอเรพทาเลต



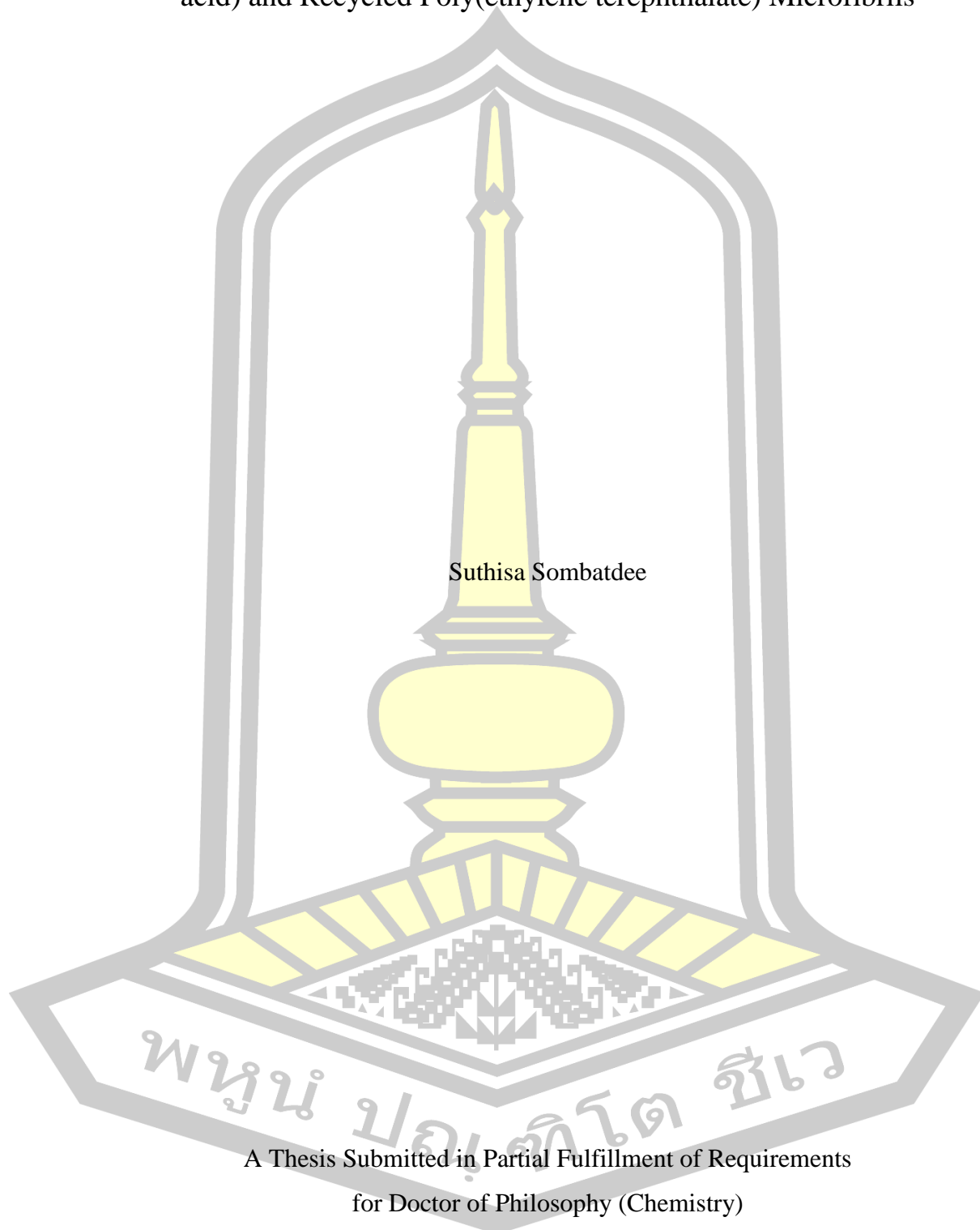
เสนอต่อมหาวิทยาลัยมหาสารคาม เพื่อเป็นส่วนหนึ่งของการศึกษาตามหลักสูตร

ปริญญาปรัชญาดุษฎีบัณฑิต สาขาวิชาเคมี

ปีการศึกษา 2560

สงวนลิขสิทธิ์เป็นของมหาวิทยาลัยมหาสารคาม

Polyethylene-Based Composite Fibers *In Situ* Reinforced with Poly(lactic acid) and Recycled Poly(ethylene terephthalate) Microfibrils



Suthisa Sombatdee

A Thesis Submitted in Partial Fulfillment of Requirements
for Doctor of Philosophy (Chemistry)

Academic Year 2017

Copyright of Mahasarakham University



The examining committee has unanimously approved this Thesis, submitted by Miss Suthisa Sombatdee , as a partial fulfillment of the requirements for the Doctor of Philosophy Chemistry at Mahasarakham University

Examining Committee

Chairman

(Assoc. Prof. Sayant Saengsuwan
Ph.D.)

Advisor

(Assoc. Prof. Sunan Saikrasun ,
Ph.D.)

Co-advisor

(Assoc.Prof. Taweechai
Amornsakchai , Ph.D.)

Committee

(Asst. Prof. Banchob Wannoo ,
Ph.D.)

Committee

(Asst. Prof.
Widchaya Radchatawedchakoon ,
Ph.D.)

Mahasarakham University has granted approval to accept this Thesis as a partial fulfillment of the requirements for the Doctor of Philosophy Chemistry

(Prof. Pairoit Pramual , Ph.D.)

Dean of the Faculty of The Faculty of
Science

(Asst. Prof. Krit Chaimoon , Ph.D.)

Dean of Graduate School

Day..... Month..... Year.....

TITLE Polyethylene-Based Composite Fibers *In Situ* Reinforced with Poly(lactic acid) and Recycled Poly(ethylene terephthalate) Microfibrils

AUTHOR Suthisa Sombatdee

ADVISORS Associate Professor Sunan Saikrasun , Ph.D.
Associate Professor Taweechai Amornsakchai , Ph.D.

DEGREE Doctor of Philosophy **MAJOR** Chemistry

UNIVERSITY Mahasarakham **YEAR** 2017
University

ABSTRACT

In this work, polyethylene (PE)-based composite fibers reinforced by polylactic acid (PLA), recycled polyethylene terephthalate (rPET) and liquid crystalline polymer (LCP) compatibilized with polyethylene-grafted-maleic anhydride (PE-g-MA) were prepared using extrusion and hot drawing process. The rheology, morphology, thermal stability and tensile properties of the composites were investigated. All polymers exhibited non-Newtonian behavior except PLA and rPET. The results of viscosity ratios of PE/PLA and PE/rPET systems suggested the fibrillation ability of PLA and rPET. The larger droplet size of PLA domains was observed in as-extruded strands. The fibrillation of PLA was observed in the as-spun sample whereas rPET appeared as droplets. However, fibrillation of PLA and rPET domains was obviously observed for the composite fibers. The droplet size of PLA and rPET were smaller than those of LCP in as-extruded strands. Thermal stability of the composites seemed to progressively decrease with PLA loading both in nitrogen and in air atmospheres. The addition of rPET or LCP into PE/PLA clearly improved the thermal stability of the composite. The reinforcing performance of the composite fibers was remarkably improved with PLA loading and further improvement in reinforcing performance was observed with addition of PLA and rPET. The tensile strength of PE-10PLA or PE-10PLA-10rPET composite fiber was ~ 600 times higher than that of its corresponding as-spun sample. Moreover, the tensile properties of the fiber were also depended on draw ratios and contents of dispersed phases. It was found that PE-10PLA-10rPET or PE-10PLA-10LCP fibers showed better improved reinforcing performance compared with PE-10PLA. For the present work, the addition of PE-g-MA compatibilizer has a little effect on the tensile properties of the composites. All obtained results suggested the high potential of rPET minor blend component as a good reinforcing for PE/PLA composite fibers, in replacing the more expensive LCP. The high performance composite fibers prepared in the present work has a high potential for load bearing application.

Keyword : composite fiber, polyethylene, poly(lactic acid), recycled PET

ACKNOWLEDGEMENTS

I would like to thank Nakhon Ratchasima Rajabhat University and the Center of Excellence for Innovation in Chemistry (PERCH-CIC) for financial support. I also thank the Department of Chemistry, Faculty of Science, Mahasarakham University for partially supports of chemicals, instruments and facilities, and the Graduate School, Mahasarakham University for the guidance in preparing the thesis.

The dissertation would not have been accomplished if without the help from several people. First of all, I would like to thank my advisor, Assoc.Prof.Dr. Sunan Saikrasun, for his kind supervision, valuable guidance, teaching encouragement, advice, taking care and helpful discussion throughout this research. Sincere gratefulness is also extended to my co-advisor, Assoc.Prof.Dr. Taweechai Amornsakchai for helpful suggestions and comments for completion of this thesis.

I am grateful to thank Assoc.Prof.Dr. Sayant Saengsuwan, Department of Chemistry, Faculty of Science, Ubon Ratchathani University, Asst.Prof.Dr. Banchob Wannoo and Asst.Prof.Dr. Widchaya Radchatawedchakoon, Department of Chemistry, Faculty of Science, Mahasarakham University for they kind comments and supports as members of my examining committee.

I was very fortunate to have many friends both within and outside the Faculty of Science during my doctoral life. I thank them all for their being very supportive my mind.

Most of all, I wish to express my heartfelt gratitude here to my family for their tender loves, definitely care encouragement and constant support throughout my study. The usefulness of this dissertation, I dedicate to my parents and all the teachers who have taught me since my childhood.

Suthisa Sombatdee

TABLE OF CONTENTS

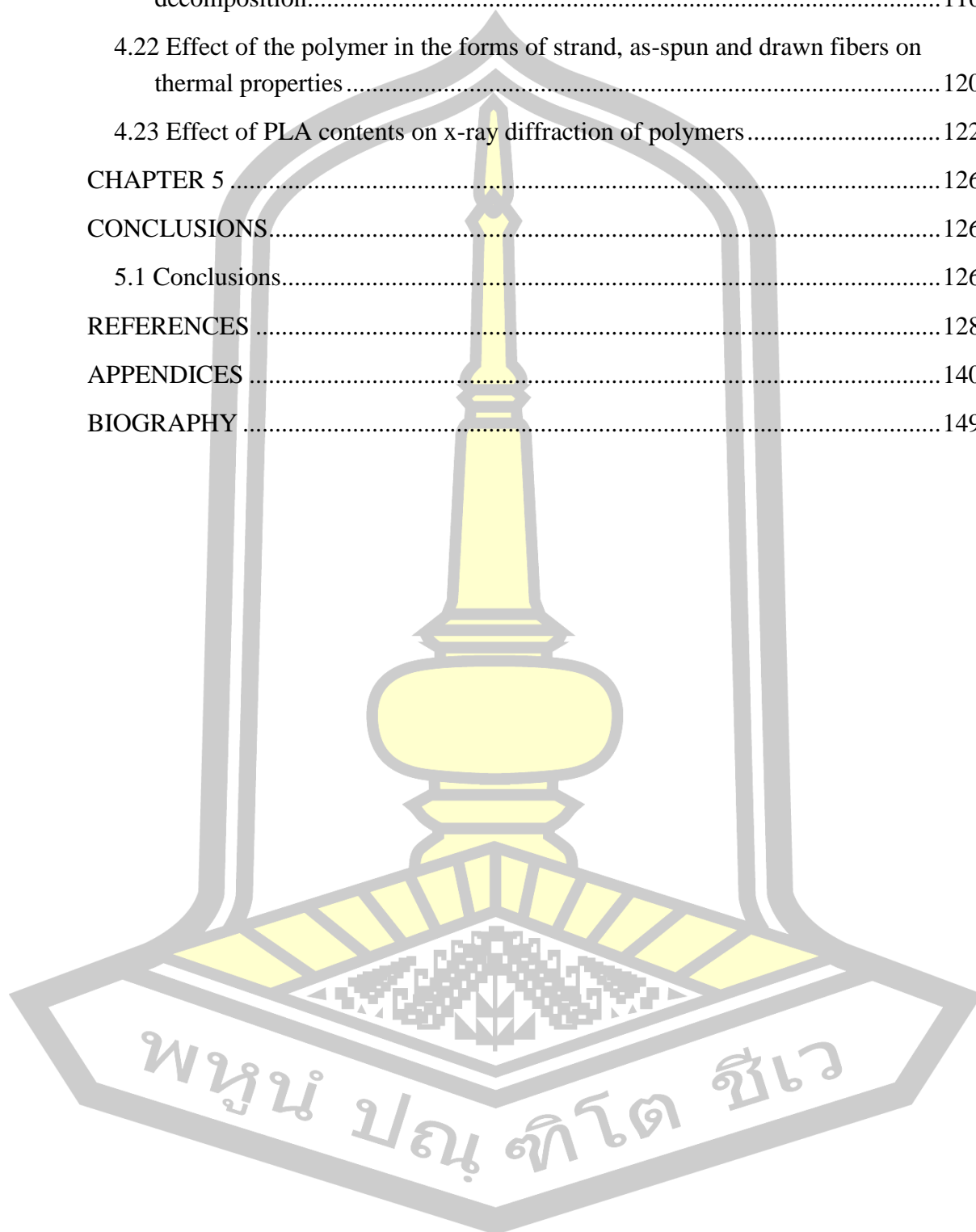
	Page
ABSTRACT.....	D
ACKNOWLEDGEMENTS.....	E
TABLE OF CONTENTS.....	F
LIST OF TABLES.....	K
LIST OF FIGURES.....	L
LIST OF ABBREVIATIONS.....	P
CHAPTER 1.....	1
INTRODUCTION.....	1
1.1 Background.....	1
1.2 Purposes of the Research.....	3
1.3 Scope of the Research.....	3
1.4 Definition of terms.....	4
CHAPTER 2.....	5
LITERATURE REVIEW.....	5
2.1 Composites.....	5
2.2 Fiber-reinforced composites.....	6
2.2.1 Fibers.....	7
2.2.2 Matrix.....	7
2.2.3 Incorporation of fibers into thermoplastic resins.....	8
2.3 Poly(ethylene terephthalate) (PET).....	8
2.3.1 Virgin PET.....	8
2.3.2 Recycled PET (rPET).....	8
2.4 rPET reinforced polymer composites.....	9
2.5 Biocomposites and bio-based composites.....	12
2.5.1 Fiber source.....	13

2.5.2 Matrices for biocomposites	13
2.5.2.1 Petrochemical based matrices.....	13
2.5.2.2 Bio-based matrices	15
2.6 Poly(lactic acid)	16
2.7 PLA composites.....	18
2.8 Potential applications of PLA composites	20
2.9 Compatibilization	22
2.9.1 Compatibilized PLA-containing blends	23
2.10 Composite structure	24
2.11 Rheology.....	26
2.11.1 The important of rheological properties	28
2.11.2 Types of fluids.....	28
2.11.3 Measurements of viscosity	32
2.11.4 Rheometers	33
2.11.4.1 Plate-and-plate rheometer.....	34
2.11.5 Effect of some parameters on rheological behavior.....	36
2.11.5.1 Effect of temperature on viscosity.....	36
2.11.5.2 Effect of pressure on viscosity	36
2.11.5.3 Effect of time, stress, shear rate and molecular weigh.....	37
2.12 Scanning Electron Microscope (SEM)	37
2.13 Thermal Analysis.....	39
2.13.1 Definition.....	39
2.13.2 Characteristics of thermal analysis.....	39
2.13.3 Conformation of thermal analysis instruments	40
2.13.4 Thermal analysis techniques	41
2.13.4.1 Differential scanning calorimetry (DSC)	41
2.13.4.2 Differential thermal analysis (DTA)	41
2.13.4.3 Thermomechanical analysis (TMA).....	41
2.13.4.4 Thermogravimetry (TG).....	42

2.14 Mechanical properties.....	55
2.14.1 Stress-strain behavior	55
2.15 Dynamic Mechanical Analysis (DMA).....	58
2.16 X-Ray Diffraction analysis (XRD).....	60
CHAPTER 3	61
METHODOLOGY	61
3.1 Materials	61
3.1.1 Dispersed phases	61
3.1.1.1 Liquid crystalline polymer (LCP)	61
3.1.1.2 Recycled poly(ethylene terephthalate) (rPET).....	61
3.1.1.3 Poly(lactic acid) (PLA).....	61
3.1.2 Matrix phase	61
3.1.3 Compatibilizer	62
3.2 Composite preparation.....	63
3.2.1 Mixing process	63
3.2.1 Hot drawing process.....	63
3.3 Characterizations	64
3.3.1 Measurements of rheological behavior in the molten state.....	64
3.3.2 Morphological characterization.....	65
3.3.3 Measurements of thermal decomposition behavior.....	65
3.3.3.1 Non-isothermal heating	65
3.3.4 Fourier transform IR (FTIR) analysis.....	65
3.3.5 Measurements of tensile properties.....	65
3.3.6 Differential scanning calorimetric (DSC) analysis	66
3.3.7 X-Ray Diffraction analysis (XRD).....	66
CHAPTER 4	69
RESULTS AND DISCUSSION	69
4.1 Effect of LCP and rPET contents on melt rheological properties of PLA-based composites	69

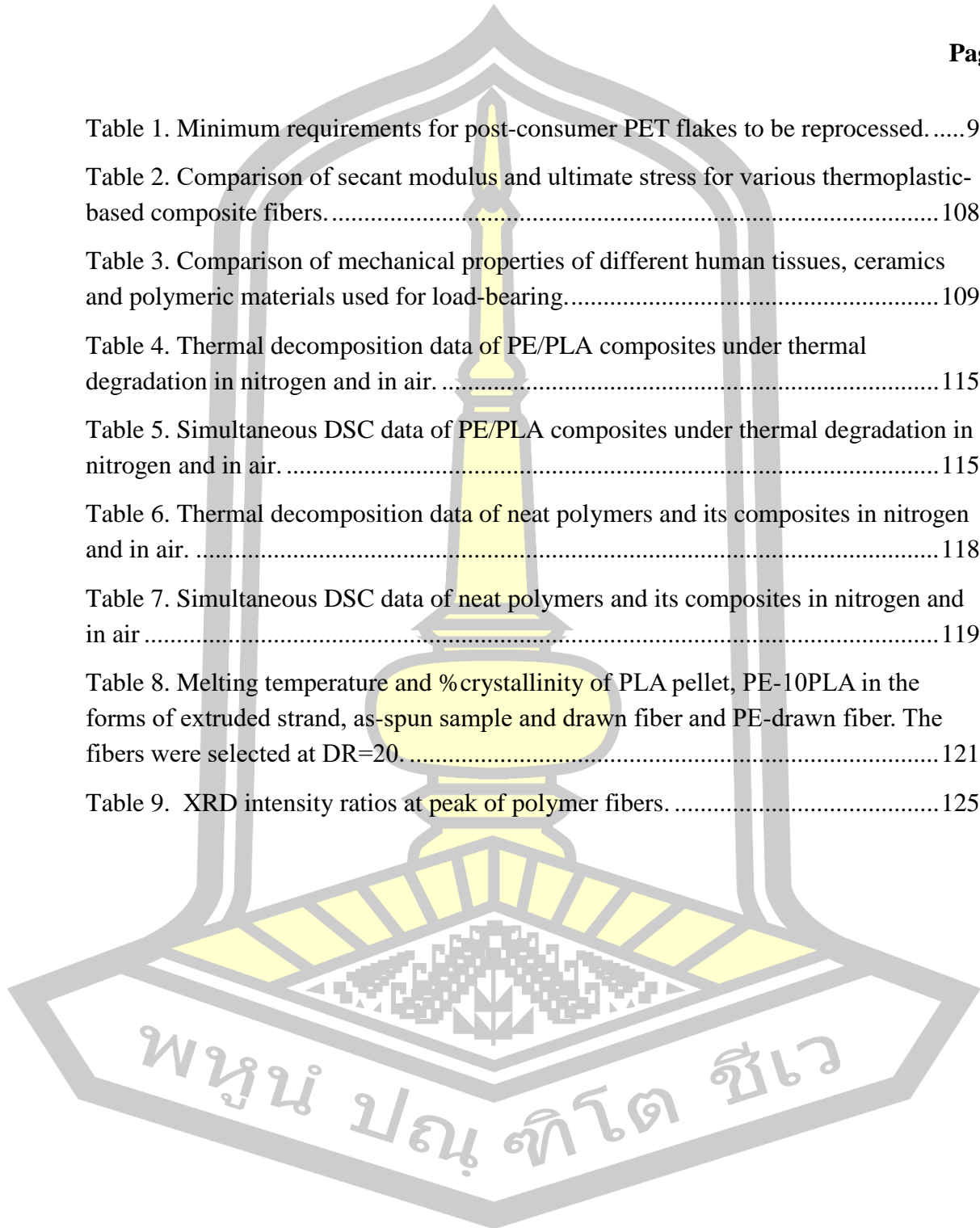
4.2 Effect of PLA contents on melt rheological properties of PE/PLA blends	73
4.3 Effect of rPET and compatibilizer on melt rheological properties of PE/PLA blends.....	75
4.4 Viscosity ratios of LCP/PLA and rPET/PLA blends.....	78
4.5 Viscosity ratios of rPET/PE and PLA/PE blends	80
4.6 Effect of LCP and rPET minor contents on morphology of the PLA-based composite strands	81
4.7 Effect of PLA contents on morphology of the PE based-composite	83
4.8 Effect of rPET contents on morphology of the PE/PLA/rPET extruded strands	85
4.9 Effect of PE-g-MA compatibilizer on morphology of the PE/PLA and PE/PLA/rPET extruded strands	87
4.10 Effect of PLA contents on morphology of the PE/PLA as-spun and drawn fibers	88
4.11 Effect of PE-g-MA compatibilizer on morphology of the PE/PLA and PE/PLA/rPET as-spun and drawn fibers	90
4.12 Effect of draw ratios on morphology of PE/PLA/rPET composite fibers	93
4.13 Tensile properties of polymers	94
4.13.1 Effect of PLA contents on tensile properties of the as-spun composites	94
4.13.2 Effect of PE-g-MA compatibilizer on tensile properties of PE-10PLA and PE-10rPET as-spun composites.....	94
4.13.3 Effect of rPET and PE-g-MA compatibilizer on tensile properties of the as-spun composites	97
4.14 Effect of draw ratios on stress-strain behavior of the polymer fibers.....	99
4.15 Effect of PLA contents on tensile properties of polymer fibers	101
4.16 Effect of rPET and PE-g-MA compatibilizer on tensile properties of polymer fibers	103
4.17 Effect of rPET and LCP on tensile properties of polymer fibers.....	106
4.18 Discussion on reinforcing performance	107
4.19 Composition of thermal stability of extruded strands, as-spun and drawn fibers	110
4.20 Effect of PLA contents on nonisothermal decomposition behavior	112

4.21 Effect of rPET, LCP and PE-g-MA compatibilizer on nonisothermal decomposition.....	116
4.22 Effect of the polymer in the forms of strand, as-spun and drawn fibers on thermal properties	120
4.23 Effect of PLA contents on x-ray diffraction of polymers	122
CHAPTER 5	126
CONCLUSIONS.....	126
5.1 Conclusions.....	126
REFERENCES	128
APPENDICES	140
BIOGRAPHY	149



LIST OF TABLES

	Page
Table 1. Minimum requirements for post-consumer PET flakes to be reprocessed.....	9
Table 2. Comparison of secant modulus and ultimate stress for various thermoplastic-based composite fibers.....	108
Table 3. Comparison of mechanical properties of different human tissues, ceramics and polymeric materials used for load-bearing.....	109
Table 4. Thermal decomposition data of PE/PLA composites under thermal degradation in nitrogen and in air.....	115
Table 5. Simultaneous DSC data of PE/PLA composites under thermal degradation in nitrogen and in air.....	115
Table 6. Thermal decomposition data of neat polymers and its composites in nitrogen and in air.....	118
Table 7. Simultaneous DSC data of neat polymers and its composites in nitrogen and in air.....	119
Table 8. Melting temperature and % crystallinity of PLA pellet, PE-10PLA in the forms of extruded strand, as-spun sample and drawn fiber and PE-drawn fiber. The fibers were selected at DR=20.....	121
Table 9. XRD intensity ratios at peak of polymer fibers.....	125



LIST OF FIGURES

	Page
Figure 1. Classification of composite material.	6
Figure 2. Optical isomers of lactic acid.	16
Figure 3. Synthesis of poly(lactic acid).	17
Figure 4. Basic building blocks in fiber-reinforced composites.	26
Figure 5. Shear stress-shear rate relationships for Bingham bodies, dilatant fluids and pseudoplastic fluids and a Newtonian material. τ_y is the yield point.	29
Figure 6. Apparent viscosity-shear rate curves for a dilatant fluid, a Newtonian fluid and a pseudoplastic fluid which have the same apparent viscosity at zero shear rate.	31
Figure 7. Logarithmic plots between stress and shear rate for (a) a dilatant material obeying the power law, (b) a Newtonian material, (c) a pseudoplastic material obeying the power law and (d) a conventional polymer melt which is pseudoplastic but does not obey the power law.	31
Figure 8. Schematic diagrams for the measurements of (a) shear viscosity and (b) elongation or tensile viscosity.	32
Figure 9. Idealized illustration for (a) plate-and-plate, and (b) capillary rheometers.	34
Figure 10. Electron signals from samples in different.	38
Figure 11. Block diagram of TA instrument.	40
Figure 12. Three modes of thermogravimetry: (a) Isothermal thermogravimetry, (b)	43
Figure 13. Comparison (a) integral TG and (b) derivative TG (DTG) mass-loss curves.	45
Figure 14. Typical stress-strain curves for plastic.	56
Figure 15. Schematic of stress-strain testing.	58
Figure 16. Chemical structures of (a) Rodrun LC3000 (LCP), (b) poly(ethylene terephthalate) (PET), (c) poly(lactic acid) (PLA), (d) polyethylene (PE) and (e) polyethylene-graft-maleic anhydride (PE-g-MA).	62
Figure 17. Schematic diagram of a single-screw extruder and pelletizer.	64
Figure 18. The schematic diagram of the mini-extruder.	64

Figure 19. Flow charts of the whole experiments of preparation and characterization of preparation and characterization of extruded strands.....	67
Figure 20. Flow charts of the whole experiments of preparation and characterization of Preparation and characterization of composite fibers.....	68
Figure 21. η^* vs. ω for (A) PLA/LCP and (B) PLA/rPET blends containing various dispersed phase contents measured at 225 and 260 °C, respectively.....	70
Figure 22. G' (column I) and G'' (column II) versus ω for (A) PLA-LCP and (B) PLA-rPET blends containing various contents of dispersed phase. The measurements of G' and G'' for PLA/LCP and PLA/rPET blends are carried out at 225 and 260°C, respectively.....	72
Figure 23. η^* (A), G' (B) and G'' (C) for PE, PE-10PLA, PE-20PLA, and PE-30PLA and viscosity ratio (D) for PE/PLA blend system at 260°C.....	74
Figure 24. η^* (A), G' (B) and G'' (C) for PE-10PLA, PE-10PLA-10rPET and PE-10PLA-10rPET-5MA, and viscosity ratio (D) for PE/PLA blend system at 260°C. ..	76
Figure 25. η^* (A), G' (B) and G'' (C) versus ω for PE-10PLA, PE-10PLA-5MA, PE-10rPET-5MA, PLA and rPET at 260°C.	77
Figure 26. Viscosity ratio versus ω for (A) PLA-LCP and (B) PLA-rPET blending systems, measured at 225 and 260°C, respectively.....	79
Figure 27. Viscosity ratio versus ω for (A) PE-PLA and (B) PE-rPET blending systems, measured at 225 and 260°C, respectively.....	80
Figure 28. SEM micrographs of the fracture surface for PLA/LCP (column I) and PLA/rPET (column II) blends containing (A) 10, (B) 20, and (C) 30 wt% dispersed phase.	82
Figure 29. SEM micrographs of the fracture surface for PE/PLA blends containing (A) 10, (B) 20, and (C) 30 wt% dispersed phase.	84
Figure 30. Fracture surfaces of the extruded strands for PE-10PLA-10rPET (A), PE-10PLA-20rPET (B) and PE-20PLA-10rPET (C).	86
Figure 31. The fracture surface of uncompatibilized (column I) and compatibilized .	87
Figure 32. Fracture surface of the as-spun samples (column I) and its composite fibers (column II) of PE-10PLA (A), PE-20PLA (B) and PE-30PLA (C), drawn at DR = 20.	89
Figure 33. Fracture surfaces of the as-spun (column I), and DR20-fiber (column II) samples for PE-10PLA (row A) and PE-10PLA-5MA (row B).	90

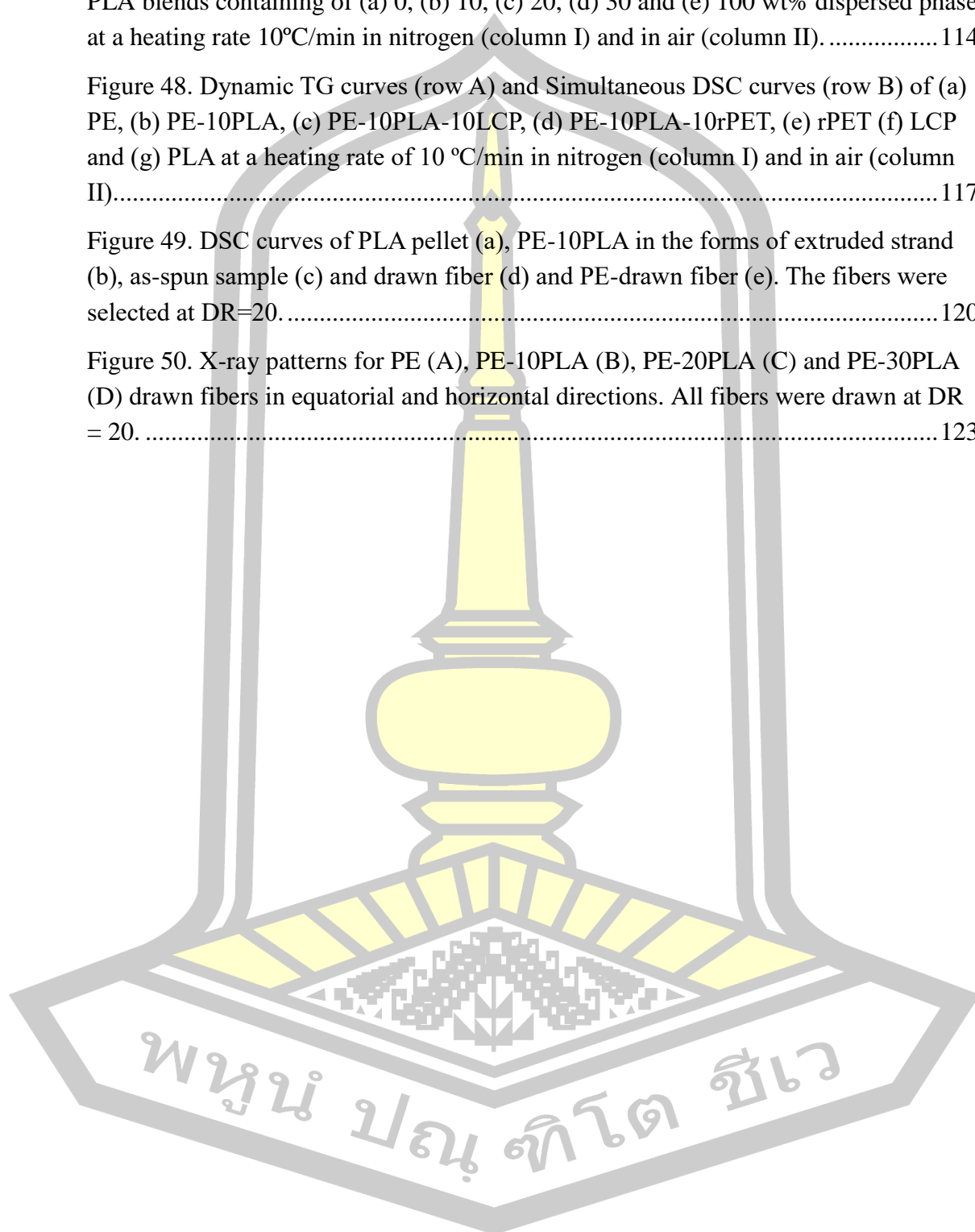
Figure 34. Fracture surfaces of the as-spun (column I), and DR20-fiber (column II) samples for PE-10PLA-10rPET (row A), PE-10PLA-10rPET-5MA (row B).	91
Figure 35. SEM images of fiber surfaces for PE-10PLA (A), PE-20PLA (B), PE-30PLA (C), PE-10PLA-10rPET (D) and PE-10PLA-10rPET-5MA (E).....	92
Figure 36. Fracture surface of PE-10PLA-10rPET composite fibers drawn at DR = 12 (A), 14 (B), and 20 (C).....	93
Figure 37. Stress-strain curves (A), stress-strain curves with expanded strain region from 0 to 20% (B), secant modulus (C), and ultimate strength (D) for the as-spun samples of PE (a), PE-10PLA (b), PE-20PLA (c), and PE-30PLA (d).	95
Figure 38. Stress-strain curves (A), stress-strain curves with expanded strain region from 0% to 20% (B), secant modulus (C), and ultimate strength (D) for the as-spun samples of PE (a), PE-10PLA (b), PE-10PLA-5MA(c), and PE-10rPET-5MA (d)....	96
Figure 39. Stress-strain curves (A), stress-strain curves with expanded strain region from 0% to 20% (B), secant modulus (C), and ultimate strength (D) for the as-spun samples of PE (a), PE-10PLA (b), PE-10PLA-5MA(c), and PE-10rPET-5MA (d)....	98
Figure 40. Effect of draw ratios on stress-strain behavior for PE-10PLA (A) and PE-10PLA-10rPET (B) composite fibers.	100
Figure 41. Stress-strain curves (A), secant modulus (B), ultimate strength (C), and elongation at break (D) for PE, PE-10PLA, PE-20PLA, and PE-30PLA composite fibers at DR = 20.....	102
Figure 42. Stress-strain curves (A), secant modulus (B), tensile strength (C) and elongation at break (D) for PE, PE-10PLA, PE-10PLA-10rPET and PE 10PLA-10rPET-5MA composite fibers drawn at DR = 20.	104
Figure 43. Stress-strain curves (A), secant modulus (B), tensile strength (C) and elongation at break (D) for PE, PE-10PLA, PE-10PLA-5MA and PE-10rPET-5MA composite fibers drawn at DR = 20.	105
Figure 44. Stress-strain curves (A), secant modulus (B), ultimate strength (C), and elongation at break (D) for PE, PE-10PLA, PE-10PLA-10LCP, and PE-10PLA-10rPET composite fibers at DR = 20.....	106
Figure 45. Dynamic TG curves of PE-10PLA-10rPET composite systems in the forms of extruded strand (a), as-spun (b) and drawn fiber (c) at a heating rate 10°C/min in nitrogen and air.	110
Figure 46. Dynamic TG curves of PE-10PLA (a) and PE-10PLA-10rPET (b) composite fiber at a heating rate 10°C/min in nitrogen and air.	111

Figure 47. Dynamic TG curves (row I) and Simultaneous DSC curves (row B) for PE-PLA blends containing of (a) 0, (b) 10, (c) 20, (d) 30 and (e) 100 wt% dispersed phase at a heating rate 10°C/min in nitrogen (column I) and in air (column II). 114

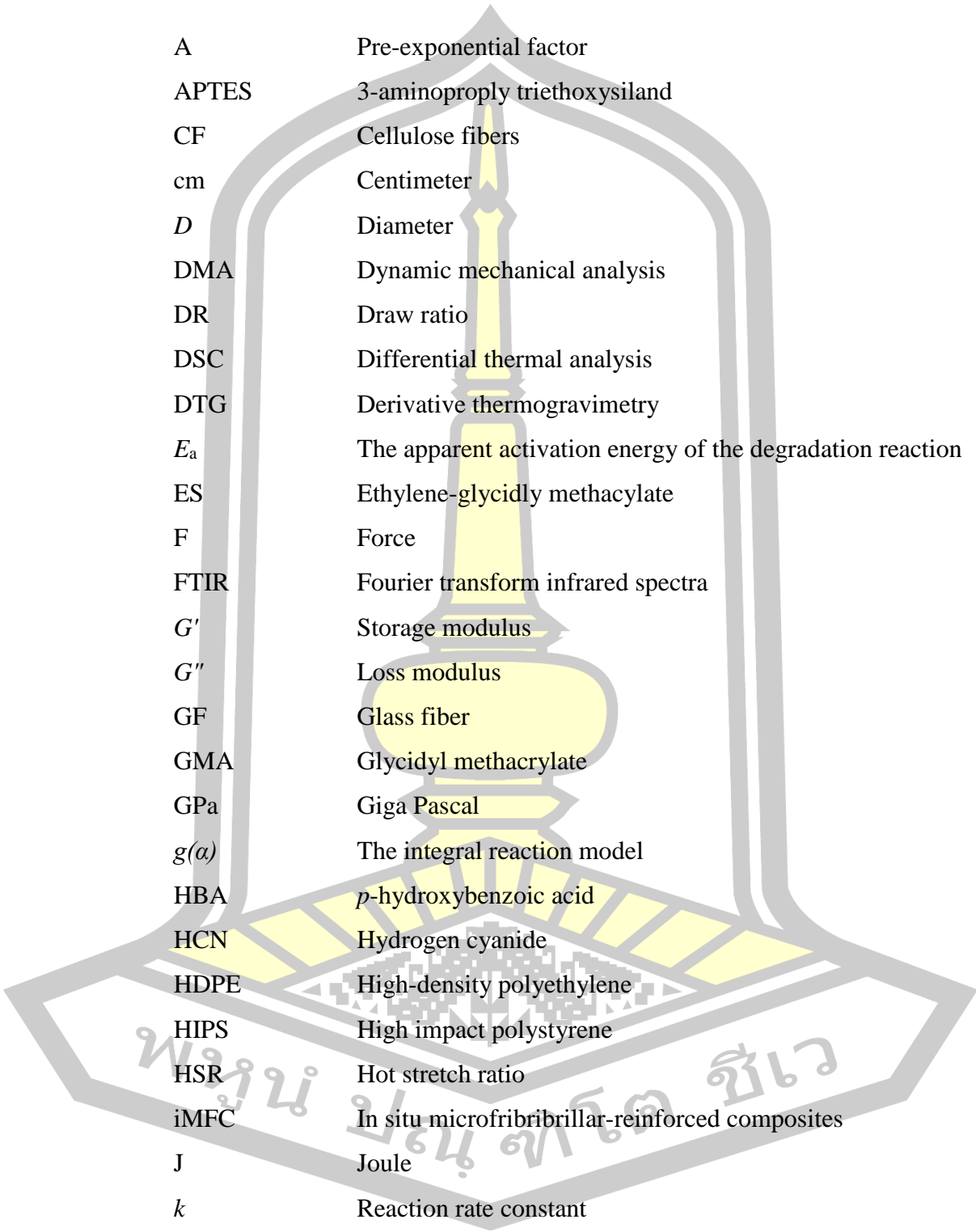
Figure 48. Dynamic TG curves (row A) and Simultaneous DSC curves (row B) of (a) PE, (b) PE-10PLA, (c) PE-10PLA-10LCP, (d) PE-10PLA-10rPET, (e) rPET (f) LCP and (g) PLA at a heating rate of 10 °C/min in nitrogen (column I) and in air (column II). 117

Figure 49. DSC curves of PLA pellet (a), PE-10PLA in the forms of extruded strand (b), as-spun sample (c) and drawn fiber (d) and PE-drawn fiber (e). The fibers were selected at DR=20. 120

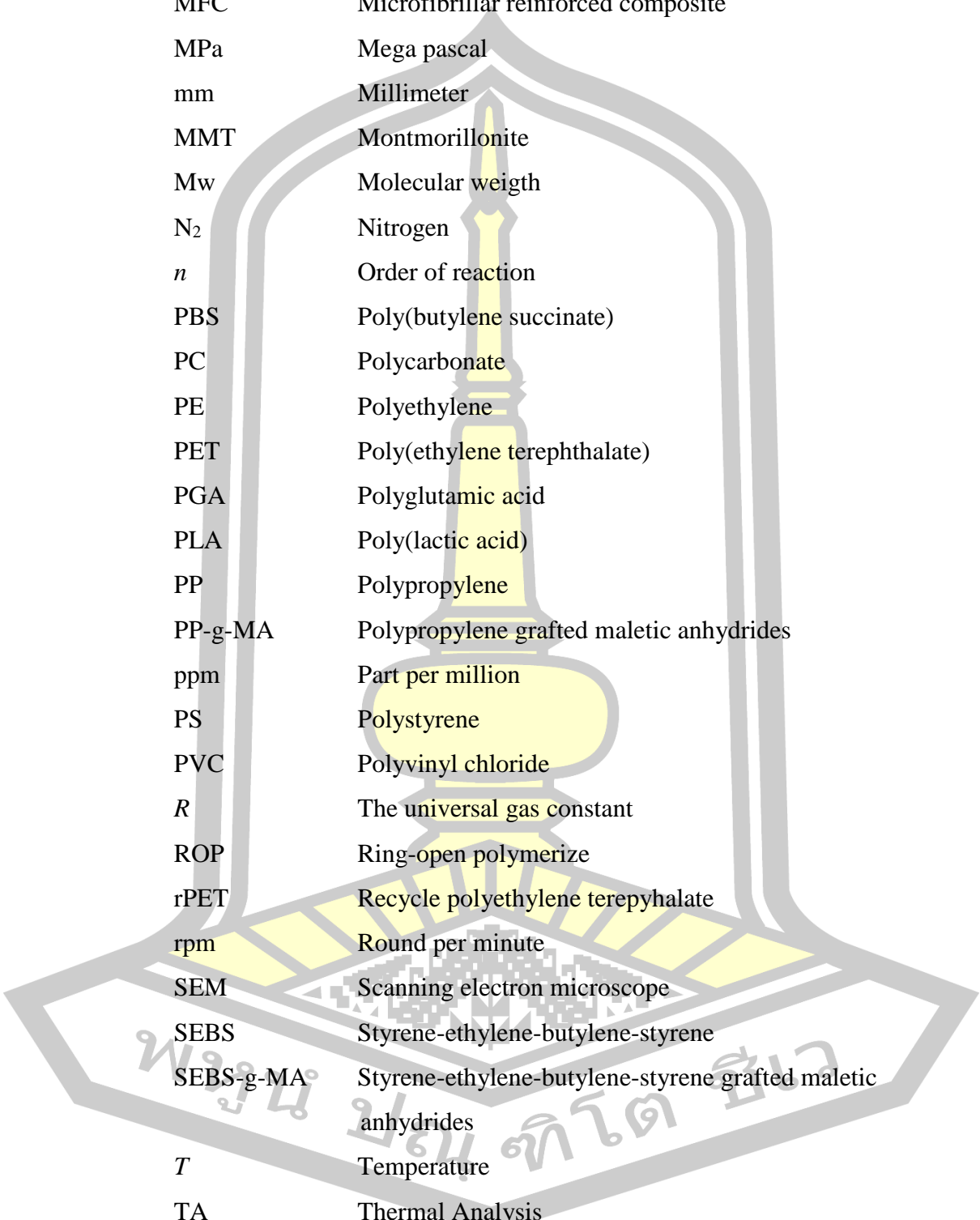
Figure 50. X-ray patterns for PE (A), PE-10PLA (B), PE-20PLA (C) and PE-30PLA (D) drawn fibers in equatorial and horizontal directions. All fibers were drawn at DR = 20. 123



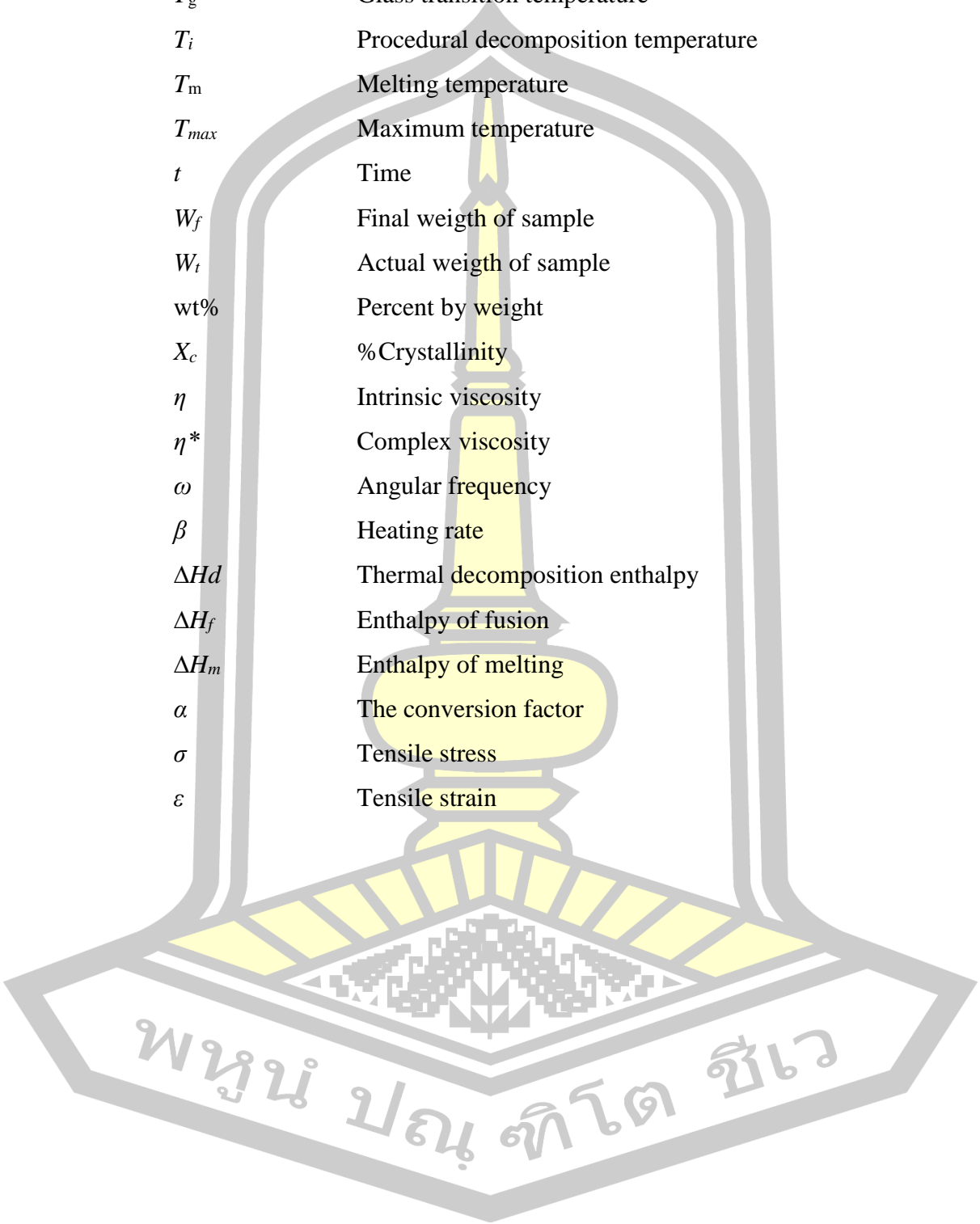
LIST OF ABBREVIATIONS



A	Pre-exponential factor
APTES	3-aminopropyl triethoxysilane
CF	Cellulose fibers
cm	Centimeter
<i>D</i>	Diameter
DMA	Dynamic mechanical analysis
DR	Draw ratio
DSC	Differential thermal analysis
DTG	Derivative thermogravimetry
E_a	The apparent activation energy of the degradation reaction
ES	Ethylene-glycidyl methacrylate
F	Force
FTIR	Fourier transform infrared spectra
G'	Storage modulus
G''	Loss modulus
GF	Glass fiber
GMA	Glycidyl methacrylate
GPa	Giga Pascal
$g(\alpha)$	The integral reaction model
HBA	<i>p</i> -hydroxybenzoic acid
HCN	Hydrogen cyanide
HDPE	High-density polyethylene
HIPS	High impact polystyrene
HSR	Hot stretch ratio
iMFC	In situ microfibrillar-reinforced composites
J	Joule
<i>k</i>	Reaction rate constant
<i>kJ</i>	Kilojoules
LCP	Liquid crystalline polymer
LDPE	Low density polyethylene



LLDPE	Linear low density polyethylene
MFC	Microfibrillar reinforced composite
MPa	Mega pascal
mm	Millimeter
MMT	Montmorillonite
Mw	Molecular weight
N ₂	Nitrogen
<i>n</i>	Order of reaction
PBS	Poly(butylene succinate)
PC	Polycarbonate
PE	Polyethylene
PET	Poly(ethylene terephthalate)
PGA	Polyglutamic acid
PLA	Poly(lactic acid)
PP	Polypropylene
PP-g-MA	Polypropylene grafted maleic anhydrides
ppm	Part per million
PS	Polystyrene
PVC	Polyvinyl chloride
<i>R</i>	The universal gas constant
ROP	Ring-open polymerize
rPET	Recycle polyethylene terephthalate
rpm	Round per minute
SEM	Scanning electron microscope
SEBS	Styrene-ethylene-butylene-styrene
SEBS-g-MA	Styrene-ethylene-butylene-styrene grafted maleic anhydrides
<i>T</i>	Temperature
TA	Thermal Analysis
TG	Thermogravimetry
TGA	Thermogravimetric analysis
TPU	Thermoplastic polyurethane



T_f	Final tempertaure
T_g	Glass transition temperature
T_i	Procedural decomposition temperature
T_m	Melting temperature
T_{max}	Maximum temperature
t	Time
W_f	Final weigth of sample
W_t	Actual weigth of sample
wt%	Percent by weight
X_c	%Crystallinity
η	Intrinsic viscosity
η^*	Complex viscosity
ω	Angular frequency
β	Heating rate
ΔHd	Thermal decomposition enthalpy
ΔH_f	Enthalpy of fusion
ΔH_m	Enthalpy of melting
α	The conversion factor
σ	Tensile stress
ε	Tensile strain

CHAPTER 1

INTRODUCTION

1.1 Background

Poly(ethylene terephthalate) (PET) is one of the most important engineering polymers widely used for many applications. This results from its attractive properties such as excellent tensile and impact strength, chemical resistance, clarity, process ability, color ability and reasonable thermal stability [1]. However, extensive utilization of PET results in waste management difficulties. Landfill of PET is undesirable because of space limitations and ground pollution. Incineration is also not the preferred option, because of the inevitable emission of toxic gases that are generated from the decomposition of PET molecular chains and residual additives, although incineration produces energy [2, 3]. The conversion of the recycled PET (rPET) into fibers and reinforcement in structural concrete was one of possible ways in order to reduce the waste problems [4, 5]. Moreover, the blending of rPET with different polyolefins, with the objective of saving time, needing relatively less investment for machinery, and obtaining a composite material with an increased value with respect to the starting polymers is a possible upgrading and recycling approach. Recently, the use of rPET as a reinforcing filler for polyethylene-based composite fiber remarkable is found to improve not only the modulus but also the thermal resistance of the materials [6]. Moreover, cross-ply laminate prepared from the rPET-containing composite exhibited much better impact resistance compared with PE laminate. This is due to the flexibility and elasticity of rPET microfibrills [7].

Poly(lactic acid) (PLA) is linear aliphatic polyester derived from renewable sources such as corn and potato, sugar from beets and sugar cane, and so on [8, 9, 10, 11]. It is one of the most promising biodegradable polymer due to its high strength, high stiffness, and resistance to fats and oil [12]. Despite of many advantages gained from PLA composite, PLA are low viscosity, low thermal stability and high moisture sensitivity [13, 14]. Moreover, PLA is a brittle behavior with low deformation, poor

crystallization, and low gas barrier properties, representing one of its main limitations for the sustainable development of PLA [15, 16]. Therefore, toughening and reinforcing improvements of PLA are important to extend its applications. Blends of PLA with more flexible polymers such as natural rubber [15] and common thermoplastics such as linear low density polyethylene (LLDPE) [13, 17], polypropylene [18, 19] is one of the way to toughen PLA. Most of the modifications have been found to improve the brittleness and crystallization ability of PLA-based composites. However, the addition of plasticizers sometimes sacrifices the stiffness of the materials. Therefore, the new toughener such as linear low density polyethylene [17, 20, 21, 22] has been used to overcome the brittleness, nevertheless significantly reducing the stiffness of the material.

PLA has been investigated for tissue engineering applications, such as bone scaffolds, because of the good biocompatibility of this polymer, but it had poor mechanical properties for applications to tissue engineering. The mechanical properties of PLA were improved using a range of methods, such as blending and composites forming. PLA have been blended with polypropylene (PP) [23], polystyrene (PS) [24, 25], and polyethylene (PE) [26, 27] obtain materials with improved properties. Although the tensile strength and young's modulus (good stiffness) of PLA could be improved by adding the polymer blending, the poor impact strength limited its use in applications requiring load bearing in bone.

As known that rPET microfibrils show good flexibility, elasticity and high reinforcing performance, the use of rPET as the reinforcement for PLA-based composites are one primarily motivation. Moreover, the blending of rPET with PLA have been prepared in an effort to enhance the properties of PLA and also to obtain novel composite materials with good stiffness and high impact resistance. The bio-compatible material with high strength and high impact resistance is possibly applicable to the structural parts for load bearing in bone applications [28]. However, to provide the effective reinforcing, the rPET phase should be elongated as the microfibrils within the PLA matrix. Therefore, the fabrication of the composite in the form of composite fiber is required. The fabrication in the form of fiber is one of the processing methods that molecular orientation of polymer is better improved than those in the form of a sheet and those formed by injection molding [29]. Due to the

low melt viscosity of PLA, it is difficult to draw as the fiber with high draw ratio. To improve drawability, high density PE was used to assist the drawing process. To the best of the author's knowledge, investigation on polymer reinforced composite using PLA as a minor reinforcing phase has rarely been reported. In this study, polyethylene (PE)-based composite fibers reinforced by PLA and high impact resistant rPET fibrils were prepared using extrusion and hot drawing process. The high performance composite fibers prepared in the present work could have a high potential for load bearing application.

In this work, PE melt blended with PLA and rPET was prepared using extrusion process. All extruded polymers were further fabricated as fiber using hot drawing process. The rheology, morphology, thermal stability and mechanical properties were investigated and compared.

1.2 Purposes of the Research

1. To investigate the effects of PLA and rPET minor components on melt rheology, morphology, thermal stability and mechanical properties of PE-based composites.
2. To fabricate the PE-based composites containing hybrid fillers in the fiber form using melt extrusion and hot drawing process.
3. To investigate the effects of PE-g-MA compatibilizer on properties of the PE-based composites.

1.3 Scope of the Research

In this work, Polyethylene (PE)-based composite fibers reinforced by PLA and high impact resistant rPET fibrils were prepared using extrusion process in the first step and further fabricated as the fiber using hot drawing process at different draw ratio. The effects of PLA, rPET, and compatibilizer on rheological properties, morphology, thermal stability and mechanical properties were investigated and compared.

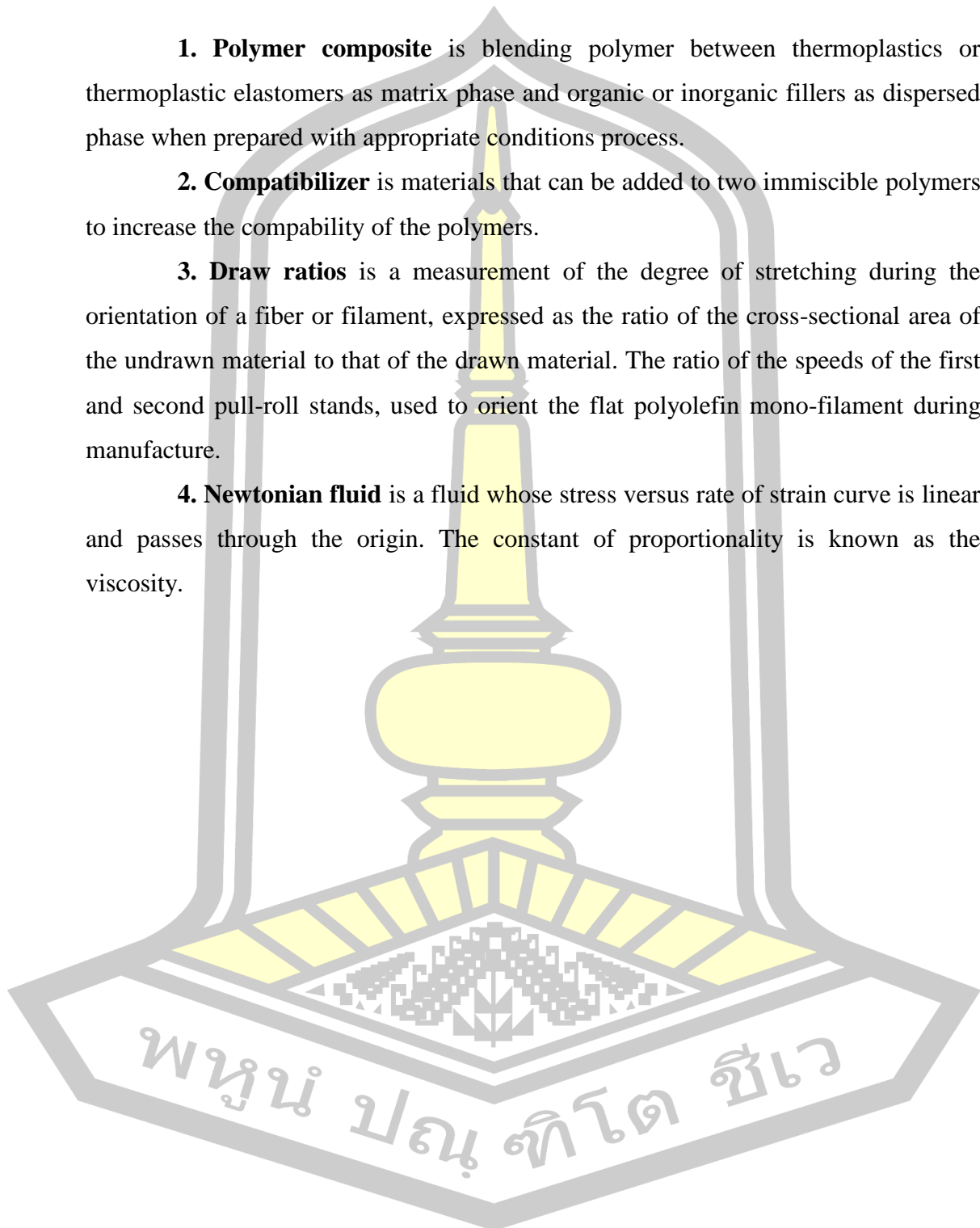
1.4 Definition of terms

1. **Polymer composite** is blending polymer between thermoplastics or thermoplastic elastomers as matrix phase and organic or inorganic fillers as dispersed phase when prepared with appropriate conditions process.

2. **Compatibilizer** is materials that can be added to two immiscible polymers to increase the compability of the polymers.

3. **Draw ratios** is a measurement of the degree of stretching during the orientation of a fiber or filament, expressed as the ratio of the cross-sectional area of the undrawn material to that of the drawn material. The ratio of the speeds of the first and second pull-roll stands, used to orient the flat polyolefin mono-filament during manufacture.

4. **Newtonian fluid** is a fluid whose stress versus rate of strain curve is linear and passes through the origin. The constant of proportionality is known as the viscosity.



CHAPTER 2

LITERATURE REVIEW

2.1 Composites

Composites are materials that contain strong fibers embedded in a continuous phase. The fibers are called “reinforcement” fibers and the continuous phase is called the matrix [30]. While the continuous phase can be a metallic alloy or inorganic material, the continuous phase is typically an organic polymer that is termed a “resin”. Because of the use of new fibers and technology, most of the composites discussed in this section are referred to as “space-age” and “advanced materials” composites. Composites can be fabricated into almost any shape, and after hardening they can be machined, painted, ect., as desired.

Composites have high tensile strengths (on the order of thousands of MPa), Young’s modulus (on the order of hundreds of GPa), and good resistance to weathering exceeding the bulk properties of most metals. The resinous matrix, by itself, is typically not particularly strong relative to the composite. Further, the overall strength of a single fiber is low. In combination, the matrix-fiber composite becomes strong. The resin acts as a transfer agent, transferring and distributing applied stresses to the fibers. Generally, the fibers should have aspect ratios (ratio of length to diameter) exceeding 100, often much larger. Most fibers are thin (less than 20 μm thick, about a tenth the thickness of a human hair). Fibers should have a high tensile strength and most have a high stiffness, i.e., low strain for high stress or little elongation as high forces are applied.

One simple scheme for the classification of composite materials is shown in Figure 1, which consists of three main divisions: particle-reinforced, fiber-reinforced, and structural composites; also, two subdivisions exist for each.

The dispersed phase for particle-reinforced composites is equiaxed (i.e., particle dimensions are approximately the same in all the directions); for fiber-reinforced composites, the dispersed phase has the geometry of a fiber (i.e., a large

length-to-diameter ratio). Structural composites are combinations of composites and homogenous materials.

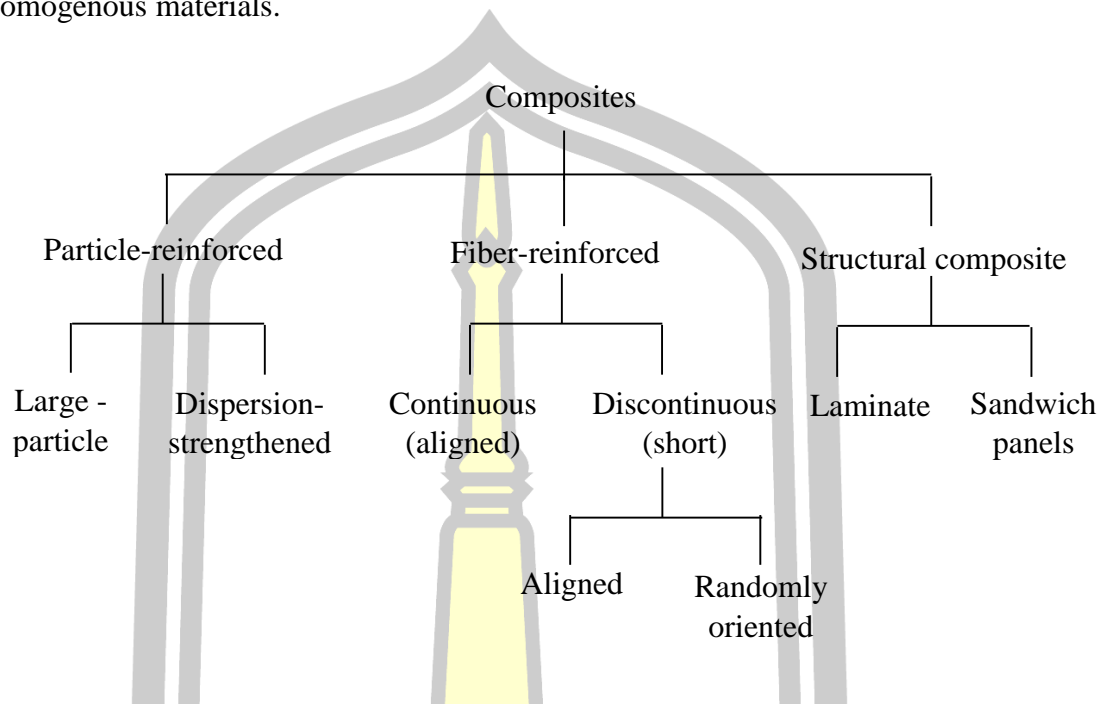


Figure 1. Classification of composite material.

2.2 Fiber-reinforced composites

Fiber-reinforced composite [31] materials consist of fibers of high strength and modulus embedded in or bonded to a matrix with distinct interfaces (boundaries) between them. In this form, both fibers and matrix retain their physical and chemical identities, yet they produce a combination of properties that cannot be achieved with either of the constituents acting alone. In general, fibers are the principal load-carrying members, while the surrounding matrix keeps them in the desired location and orientation, acts as a load transfer medium between them, and protects them from environmental damages due to elevated temperatures and humidity, for example. Thus, even though the fibers provide reinforcement for the matrix, the latter also serves a number of useful functions in a fiber reinforced composite material. The most common form in which fiber-reinforced composites are used in structural applications is called a laminate, which is made by stacking a number of thin layers of fibers and matrix and consolidating them into the desired thickness. Fiber orientation in each layer as well as the stacking sequence of various layers in a composite laminate can

be controlled to generate a wide range of physical and mechanical properties for the composite laminate.

2.2.1 Fibers

Fibers are the principal constituents in a fiber-reinforced composite material. They occupy the largest volume fraction in a composite laminate and share the major portion of the load acting on a composite structure. Proper selection of the fiber type, fiber volume fraction, fiber length, and fiber orientation is very important, since it influences the following characteristics of a composite laminate:

1. Density
2. Tensile strength and modulus
3. Compressive strength and modulus
4. Fatigue strength as well as fatigue failure mechanisms
5. Electrical and thermal conductivities
6. Cost

2.2.2 Matrix

The roles of the matrix in a fiber-reinforced composite are: (1) to keep the fibers in place, (2) to transfer stresses between the fibers, (3) to provide a barrier against an adverse environment, such as chemicals and moisture, and (4) to protect the surface of the fibers from mechanical degradation (e.g., by abrasion). The matrix plays a minor role in the tensile load-carrying capacity of a composite structure. However, selection of a matrix has a major influence on the compressive, interlaminar shear as well as inplane shear properties of the composite material. The matrix provides lateral support against the possibility of fiber buckling under compressive loading, thus influencing to a large extent, the compressive strength of the composite material. The interlaminar shear strength is an important design consideration for structures under bending loads, whereas the in-plane shear strength is important under torsional loads. The interaction between fibers and matrix is also important in designing damage-tolerant structures. Finally, the processing and defects in a composite material depend strongly on the processing characteristics of the matrix. For example, epoxy polymers used as matrix in many aerospace composites, the processing characteristics include the liquid viscosity, the curing temperature, and the curing time.

2.2.3 Incorporation of fibers into thermoplastic resins

Incorporating fibers into high-viscosity thermoplastic resins and achieving a good fiber wet-out are much harder than those in low-viscosity thermoset resins. Nevertheless, several fiber incorporation techniques in thermoplastic resins have been developed, and many of them are now commercially used to produce thermoplastic prepregs. These prepregs can be stored for unlimited time without any special storage facilities and, whenever required, stacked and consolidated into laminates by the applications of heat and pressure.

2.3 Poly(ethylene terephthalate) (PET)

2.3.1 Virgin PET

Poly(ethylene terephthalate) (PET) is the most commonly used thermoplastic polyester. It is often called just polyester, which often causes confusion, because polyester resin are thermosetting materials. It has excellent tensile and impact strength, chemical resistance, clarity, processability, color ability and reasonable thermal stability [1, 2]. Commercial PET has a melting temperature (T_m) of between 255 and 265°C and the glass transition temperature (T_g) of virgin PET varies between 67°C and 140°C. The rate of crystallisation of virgin PET depends on temperature and reaches its maximum at the temperature of 150-180 °C. PET is used broadly in products such as: bottle, food packaging, textile fibers, electrical and electronic instruments (e.g. X-rays sheets, recording tapes and insulator), sporting goods and blood vessel tissue engineering.

2.3.2 Recycled PET (rPET)

PET is a non-degradable polymer in the natural environment, leading to environmental pollution when it is discarded after use [2]. Moreover, the extensive use of PET products leads to waste management difficulties. In view of the increasing environmental awareness in the society, recycling processes are the best way to economically reduce PET waste. There are many studies describing methods for successful PET recycling, and the minimum requirements that recycled PET flakes should meet are reported in Table 1 [1]. Recycled PET should fulfill the following quality objectives for suitability in high-value applications. The quality objectives are

color separation, minimum contamination, intrinsic viscosity close to the original values, and consistent batch-to-batch quality.

Table 1. Minimum requirements for post-consumer PET flakes to be reprocessed.

Property	Value
$[\eta]$	> 0.7 dl/g
T_m	$> 240^\circ\text{C}$
Water content	$< 0.02\text{wt}\%$
Flake size	$0.4 \text{ mm} < D < 8 \text{ mm}$
Dye content	< 10 ppm
Yellowing index	< 20
Metal content	< 3 ppm
PVC content	< 50 ppm
Polyolefin content	< 10 ppm

2.4 rPET reinforced polymer composites

rPET can be recycled in many way including chemical and mechanical methods. The conversion of the rPET into reinforcement in thermoplastics was one of possible ways in order to reduce the waste problems. There are a number of previous studied on the PET/thermoplastic blends. The following are a number of research works concerning thermoplastics reinforced with rPET.

The low density polyethylene (LDPE) and recycled poly(ethylene terephthalate) (PET) from bottles were melt blended and extruded, followed by continuous drawing, palletizing and injection molding of dogbone samples were investigated by Evstatiev et al. [32]. They found that the MFC dogbone samples showed impressive mechanical properties the elastic modulus is about 10 times higher than that of LDPE and about three times higher than reinforced LDPE with glass spheres, approaching the modulus of LDPE reinforced with 30 wt% short-glass fibers (GF). The tensile strength is at least two times higher than that of LDPE or of reinforced LDPE with glass spheres, approaching that of reinforced LDPE with 30

wt% GF. The impact strength of LDPE increases by 50% after reinforcement with PET.

Mbarek et al. [33] studied the thermal and mechanical properties of PET/PC blends prepared in a twin-extruder by melt blending in the absence and presence of stannous octoate as a transesterification catalyst. Blending of PET with PC improve the tensile properties in comparison to neat components for compositions of PET higher than 50 % and these properties are improved by the addition of a transesterification catalyst. The melting temperature of PET was decreased with increasing PC content. Also, the temperatures of the cold crystallization of PET were higher than those of similar blends without catalyst.

Mantia et al. [34] studied the influence of small amounts of PLA on the recycling properties of post-consumer PET from bottles, and determined their rheological, mechanical, morphological and thermogravimetric. They found that the amount of PLA used was up to 5% by weight. Shear viscosity measurements showed that the blends have lower viscosities than PET. Rheological tests in non-isothermal elongational flow showed that the main rheological properties of PET significantly decreased in the presence of even small amounts of PLA. Mechanical tests results showed that the main tensile properties are not much affected by the presence of small amounts of PLA. DSC analysis revealed changes in the crystallinity of the blends which were in agreement with the trends of the tensile properties. SEM analysis clearly showed a biphasic morphology in all of the blends. Thermogravimetric analysis showed that the thermal stability was not significantly affected by the presence of PLA, except in the temperature range around 400°C, in any case with only small variations.

Saikrasun et al. [35] studied the rheological behavior, morphology, and thermal stability of LCP/PS and rPET/PS blends. They found that all blends and LCP exhibited shear thinning behavior, whereas Newtonian fluid behavior was observed for rPET. The incorporation of both LCP and rPET into PS significantly improved the processability. An addition of LCP and rPET into PS matrix improved the thermal resistance in air significantly. The obtained results suggested the high potential of rPET as a processing aid and thermally stable reinforcing-material similar to LCP. At

the same composition, the LCP-containing blends showed better tensile properties when compared with the corresponding rPET-containing blends.

The styrene-(ethylene butylene)-styrene (SEBS) triblock copolymer was melt blended with LCP and rPET using extrusion process were investigated by Saikrasun et al. [36]. It was found that the incorporation of small amount of LCP and rPET (10 wt %) into SEBS significantly reduces the melt viscosity of the blend system. SEBS/LCP displays fibrillar morphology at 20 and 30 wt% LCP whereas SEBS/rPET does not. The results obtained from thermogravimetric analysis suggested that an addition of LCP and rPET into the SEBS matrix improved the thermal resistance significantly in air but not in nitrogen.

Sombatdee et al. [37] prepared and studied properties of LCP/PP and rPET/PP blends containing various dispersed phase contents; the blends were prepared separately using a single screw extruder. The obtained results effectively demonstrate the high potential of using rPET in replacing the more expensive LCP as processing aids by bringing down the melt viscosity of the blend system and also to improve the thermal resistance of PP polymer matrix in air atmosphere. However, the morphology of LCP and rPET domains in the composite strand mostly appear as droplets which is found to have poor reinforcing performance. Therefore, PP/LCP and PP/rPET composites were prepared as fiber using hot drawing process [24]. It was found that the better dispersion with smaller droplets of LCP and rPET domains are observed in the as-spun samples with addition of compatibilizer. Tensile strength and extensibility of both composites system were significantly improved with compatibilizer loading. The tensile strength of compatibilized rPET-composite fibers was higher than that of the compatibilized LCP system [38].

Kayaisang et al. [39] studied the effects of the LCP and rPET reinforcing materials on rheology, morphology, and thermal decomposition behavior of the LCP/PE and rPET/PE blends. They found that the addition of rPET and LCP into PE matrix significantly improved processability. The results obtained from TGA suggested that the addition of LCP or rPET into the PE matrix improved the thermal resistance, especially in air atmosphere. However, the morphology of LCP and rPET domains in the composite strand mostly appear as droplets which is expected to have little effect on reinforcing performance. Therefore, PE/LCP and PE/rPET composites

were prepared as fiber using hot drawing process [6]. After drawing, good fibrillation of LCP and rPET domains is remarkably observed especially in the composite fibers with compatibilizer loading. The mechanical properties of the composite fibers were strongly depended on the fibrillation of the dispersed phases which directly related the levels of draw ratio and compatibilizer loading. The obtained results suggested the high potential of rPET as a processing aid and good thermally resistant material similar to LCP. Moreover, the rPET-containing composite fiber was further used for cross-ply laminate preparation. The results showed that the rPET-composite laminate have a high impact-resistance than PE laminate [7].

2.5 Biocomposites and bio-based composites

Biocomposites are composite materials comprising one or more phase(s) derived from a biological origin. In terms of the reinforcement, this could include plant fibres such as cotton, flax, hemp and the like, or fibres from recycled wood or waste paper, or even by-products from food crops. Regenerated cellulose fibres (viscose/rayon) are also included in this definition, since ultimately they too come from a renewable resource, as are natural ‘nano fibrils’ of cellulose and chitin [40].

Bio-based composites are materials produced from renewable agricultural and forestry feedstock. A sustainable bio-based product should have both recycling capability and biodegradability. Bio-based composites typically consist of a combination of biofiber and bioplastic. For bioplastic derived from renewable resources, thermoplastics play a more important role than thermosets due to their recyclability [41].

Natural biobased polymers are another class of biobased polymers which are formed naturally, such as nucleic acids, proteins, and polysaccharides (collagen, chitosan, etc.). These biobased polymers have shown tremendous growth in the recent years in terms of technological developments and their commercial applications. There are three principal ways to produce biobased polymers using renewable resources [42]:

1. Employing natural biobased polymers with partial alteration to meet the requirements (e.g., starch, protein).

2. Making biobased monomers by fermentation/traditional chemistry followed by polymerization (e.g., poly(lactic acid) (PLA)).

3. Synthesizing biobased polymers directly by microbial fermentation (e.g., polyhydroxyalkanoates (PHA)).

2.5.1 Fiber source

The plants, which produce natural fibers, are classified as primary and secondary depending on their utilization. Primary plants are those grown for their fiber content while secondary plants are plants in which the fibers are produced as a by-product. Jute, hemp, kenaf, and sisal are examples of primary plants. Pineapple, oil palm and coir are examples of secondary plants.

2.5.2 Matrices for biocomposites

Matrices may be polymers, ideally derived from renewable resources such as vegetable oils or starches. Alternatively, and more commonly at the present time, synthetic, fossil-derived polymers preponderate and may be either 'virgin' or recycled thermoplastics such as polyethylene, polypropylene, polystyrene and polyvinyl chloride, or virgin thermosets such as unsaturated polyesters, phenol formaldehyde, isocyanates and epoxies [43].

2.5.2.1 Petrochemical based matrices

The effects of the incorporation of natural fibers in petrochemical based thermoplastics and thermoset matrixes were extensively studied. Polypropylene (PP), polyethylene (PE), polystyrene (PS), and polyvinyl chloride (PVC) were used for the thermoplastic matrixes. Polyester, epoxy resin, phenol formaldehyde, and vinyl esters were used for the thermoset matrices and are reportedly the most widely used matrices for natural fiber reinforced polymer composites.

Development of a simple manufacturing technique for sisal fibre-reinforced polypropylene composites, that minimises fibre degradation and can be used in developing countries were investigated by Jayaraman [44]. The best possible mechanical properties for the sisal fiber/PP composites were achieved when the fiber length was greater than 10 mm and the fiber mass fraction was in the range of 15-35%. The aged sisal fiber showed lower tenacity, breaking strength and elongation with in comparison to fresh sisal fibers.

Li et al. [45] studied the interfacial properties of sisal fiber reinforced high density polyethylene (HDPE) composites. Fiber surface treatment methods are quite useful for the improvement of the interfacial properties between sisal fibers and the HDPE resin. Permanganate (KMnO_4) and dicumyl peroxide (DCP) roughen the fiber surface and introduced mechanical interlocking with the HDPE. Sisal fiber reinforced HDPE shows a stable de-bonding process with KMnO_4 and DCP treatment. Silane treated sisal fiber reinforced HDPE exhibits an unstable debonding process.

Flax fiber-reinforced HDPE biocomposites with various fiber fractions were prepared and their thermal properties were studied by Li et al. [46]. They found that the thermal conductivity, thermal diffusivity, and specific heat of the flax/HDPE composites decreased with increasing fiber content, but the thermal conductivity and thermal diffusivity did not change significantly at temperatures in the range (170-200 °C) studied. The specific heat of the biocomposites increased gradually with temperature.

Wang et al. [47] investigated the impact of the properties of bamboo including moisture content, granule size of bamboo and the ratio of bamboo and PVC on the dimensional stability and mechanical properties. They found that enhancement of the content of PVC will improve the mechanical properties of bamboo-PVC composites. Also a higher content of PVC will improve the dimensional stability of bamboo-PVC composites. An optimum granule size of bamboo is 40 mesh, in which bamboo and PVC can get a fixed composition. When bamboo moisture content was less than 8%, there was no direct relationship between moisture content of bamboo and modulus of elastic of bamboo-PVC composites. Dimensional stability and strength properties of the composites can be improved by increasing the polymer content.

The PS composites reinforced with agave fiber were also studied regarding their fiber surface modification were studied by Singha and Rana [48]. They found that 20% fiber content gives optimum mechanical properties. The particle reinforcement gives better mechanical properties than short and long fiber reinforcement. The surface modified fiber reinforced composites have been found to be thermally more stable than that of raw fiber reinforced composites.

2.5.2.2 Bio-based matrices

Public concern about the environment, climate change and limited fossil fuel resources are important driving forces, which motivate researchers to find alternatives to crude oil. Bio-based plastics may offer important contributions by reducing the dependence on fossil fuels and, in turn the related environmental impacts. Biopolymers have experienced a renaissance in the recent years. Many new polymers were developed from renewable resources, such as starch, which is a naturally occurring polymer that was re-discovered as a plastic material. Others are poly(lactic acid) (PLA) that can be produced via lactic acid from fermentable sugar and polyhydroxyalkanoate (PHAs), which can be produced from vegetable oils next to their bio-based feed stocks.

Alvarez et al. [49] studied the effect shear rate, temperature, fiber content and treatment of starch matrixes with sisal fibers. They found that shear rate was the most influential processing condition, while, from the point of view of the material structure, the intercalation effectiveness of the matrix in the fibers is directly linked to the rheological behavior. In fact, processing techniques with high stresses and more efficient mechanical mixing promote the opening of fiber bundles, increasing the aspect ratio of the fibers and the average viscosity of the molten composite. A similar effect on the increase of the aspect ratio and composite viscosity is observed when treated fibers are used.

The interfacial improvement of PHB/flax composites were investigated by Wong et al. [50]. The addition of 4,4-thiodiphenol (TDP) at various concentrations (up to 10% v/v) brought advantageous changes in the dynamic flexural properties and thermal stability (favorable shift of degradation temperatures to higher values). With increases of the TDP content, improvements were observed in the fiber-matrix bonding and a change in the matrix from brittle to ductile.

Arbelaiz et al. [51] studied the mechanical properties of flax fibre bundles/PCL composites with different amounts of synthesized PCL-g-MA coupling agent and fibre content. The results obtained by TG showed that fibre addition and matrix modification slightly reduce the thermal stability of PCL. SEM confirmed adhesion improvement between flax fibre bundles and PCL-g-MA matrix. Both mechanical properties and crystallinity of composites increased with increasing the

PCL-g-MA coupling agent. The improvements obtained for tensile and flexural strength are 54 and 44%, respectively. For flax/PCL composites, above 0.2 fibre volume fraction experimental values are lower than predicted value ones as a consequence of lack of adhesion between flax fibre and PCL matrix.

Liu et al. [52] studied the mechanical properties of poly(butylene succinate) (PBS) biocomposites reinforced with surface modified jute. They found that the mechanical strength or modulus are all gradually increased with the increasing fibre content from 0 to 20 wt%, and with 30 wt% fibre content they are decreased or nearly remain constant, however the breaking elongation are evidently decreased than pure PBS film. The mechanical strength or modulus of biocomposites exits an optimum value at certain fibre content, which is 20 wt% in this study. Surface modification by alkali or coupling agent both can improve the mechanical properties of biocomposites. And the stronger fibre-matrix interface can lead to lowering of the critical fibre length for effective stress transfer.

2.6 Poly(lactic acid)

Poly(lactic acid) or polylactide (PLA) is a kind of polyester that has become a major topic of industry literature and even mainstream media, making it the key, representative biopolymer of current interest. PLA is a thermoplastic, high-strength, high-modulus, biodegradable and bio-based aliphatic polyester derived from renewable resources [8, 9, 10, 11]. The chemistry of PLA involves the processing and polymerization of lactic acid monomer. Lactic acid is a simple chiral molecule which exists as two enantiomers, L- and D-lactic acid as shown in Figure 2, the differing in their effect on polarized light. The L isomer rotates the plane of polarized light clockwise, the D isomer rotates it counterclockwise [53].

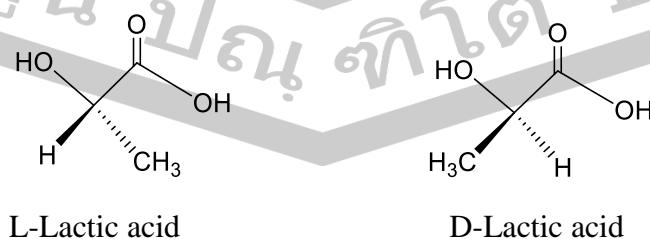


Figure 2. Optical isomers of lactic acid.

Lactic acid is the starting material for the PLA production process. The synthesis of lactic acid into high molecular weight PLA can follow two different routes of polymerization, as shown in Figure 3 [8]. Lactic acid is condensation polymerized to yield a low-molecular-weight, brittle, glassy polymer, which, for the most part, is unusable for esterification of any applications unless external coupling agents are used to increase the molecular weight of the polymer. The molecular weight of this condensation polymer is low due to the viscous polymer melt, the presence of water, impurities, the statistical absence (low concentration) of reactive end-groups, and the “back-biting” equilibrium reaction that forms the six-member lactide ring. The second route of producing PLA is to collect, purify, and ring-open polymerize (ROP) lactide to yield high-weight average molecular weight (MW>100,000) PLA. The lactide method was the only method of producing pure, high molecular weight PLA until Mitsui Toatsu Chemicals recently commercialized a process wherein lactic acid and catalyst are azeotropically dehydrated in a refluxing, high-boiling, aprotic solvent under reduced pressures to obtain PLA with weight average molecular weights greater than 300,000 [8].

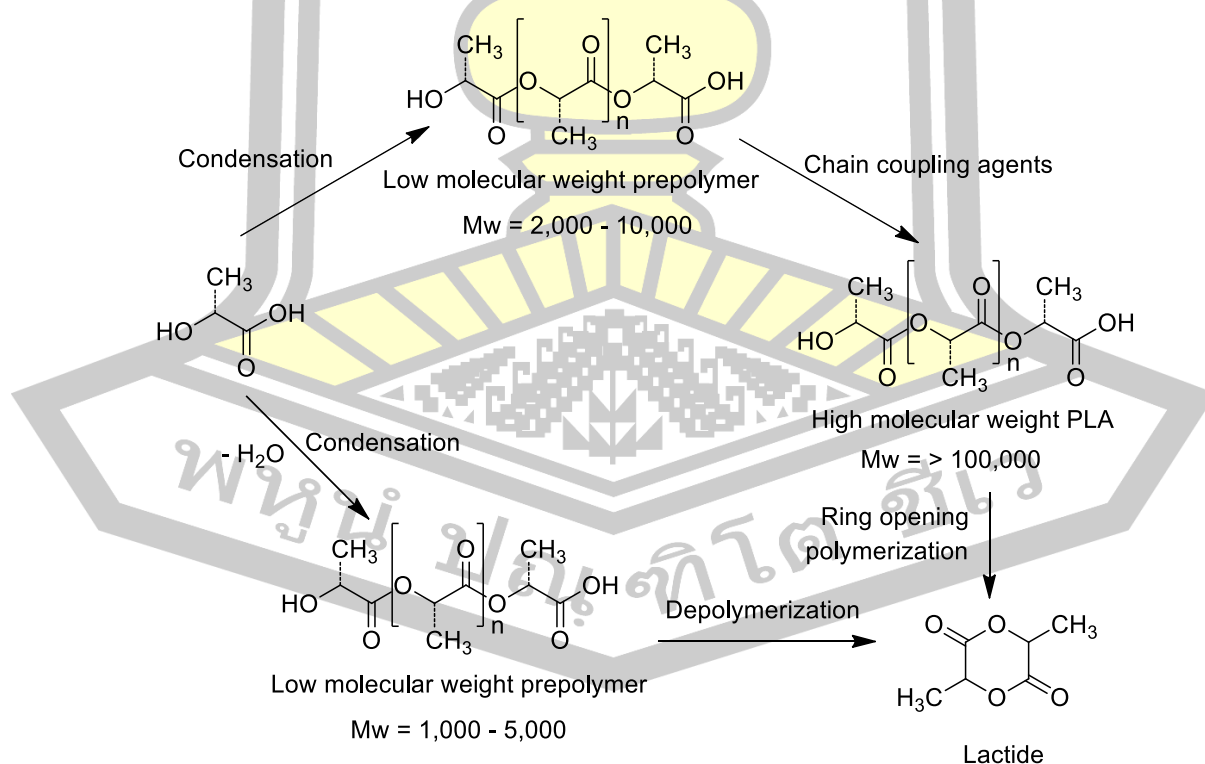


Figure 3. Synthesis of poly(lactic acid).

PLA was selected for its high biocompatibility and biodegradability. It has become an alternative to traditional commodity plastics for everyday applications as an environmental friendly polymer due to its some unique properties such as high tensile strength and Young's modulus, good flexural strength [13, 54], which are even higher than those of PS, PP, PE, or other polymers [11]. However, brittleness and other properties such as low viscosity, low thermal stability, high moisture sensitivity, medium gas barrier properties, high cost and low solvents resistance (e.g., against water) of the pure polymer are often insufficient for a lot of applications.

PLA has potential for use in a wide range of applications; medical and pharmaceutical applications to environmentally benign film and fibres for packaging, houseware and clothing. PLA is also used in composite materials. Primary applications are in fibres, fibrefill (pillows, comforters, mattresses, duvets), apparel (sport, active, underwear and fashion wear), and nonwoven applications (agricultural and geo textiles, hygiene products, wipes) [11, 15, 55].

2.7 PLA composites

PLA has been limited from wide spread use because of its brittle polymer, low toughness, low heat stability, and low moisture stability. The improvement of the properties of PLA is added of fillers or reinforcement material and polymer blending is an effective way to develop new materials with superior properties.

Jiang et al. [56] studied the failure behavior and toughening mechanisms of PLA/MMT and PLA/NPCC nanocomposites. The both nanocomposites were prepared by melt compounding using a twin-screw extruder and injection molded into test specimens. The morphology showed good dispersions of both nanoparticles were achieved when the filler concentration was 5 wt%. The strain-at-break of PLA increased with NPCC concentration ranging from 0 to 7.5 wt%, whereas it only increased with MMT concentration up to 2.5 wt% and decreased at higher concentrations. The tensile strength of PLA nanocomposites decreased with NPCC, whereas it increased with MMT up to 5 wt%.

The effects of two different types of nanosized fillers (silica and montmorillonite) at three different weight fractions as well their mixtures on the

thermomechanical properties of polylactide (PLA) were investigated by Kontou et al [57]. The results suggest that silica and montmorillonite have different reinforcing and toughening effects on PLA, while the combination of the two different nanofillers has a detrimental effect on the tensile properties of the material. Both nanofiller types acted as nucleating agents, leading to an increment of crystallinity content. On the other hand, the combination of the two nanofillers reduced the crystallinity of the material. Furthermore, the T_g of all PLA/nanocomposites is lower than the T_g of neat PLA. The concurrent addition of two nanofillers caused the yield stress to decrease and the Young's modulus to increase compared with neat PLA.

Piekarska et al. [58] studied the effect of cellulose fibers (CF) and different nanofillers (montmorillonite, MMT and calcium carbonate nanoparticles, NCC) on the properties of PLA nanocomposites. From this research they can conclude that, the fillers practically did not affect the glass transition temperature of PLA but intensified its cold crystallization, due to nucleating effect, which was reflected in decreased cold-crystallization and enlarged cold-crystallization enthalpies. The exfoliation of MMT in PLA/MMT did not affect significantly the stability of PLA during heating in N_2 but enhanced it during heating in air. All the fillers improved storage modulus and tensile properties of the materials.

Bledzki et al. [59] have reported the results of mechanical properties of composites based on PLA, reinforced with 30% man-made cellulose and abaca fibres. By adding of man-made cellulose the Charpy impact strength at ambient temperature increased by factor 3.60, compared to unreinforced PLA. Tensile strength rose by factor 1.45 and stiffness by approx. 1.75. Reinforcing with abaca fibres enhanced both E-Modulus and tensile strength by factor 2.40 and 1.20, respectively. The Charpy A-notch impact resistance of PLA/abaca could be improved by factor 2.4.

Xia et al. [60] investigated PLA/Flax composites were fabricated by extrusion and injection molding processes. They found that the impact strength and elongation at break of PLA/Flax composites were remarkably higher than PLA. The thermal behavior of composites was analyzed by DSC Differential, it was found that incorporation of fiber improved the crystallinity of PLA. The toughening mechanism of PLA/Flax composites was discussed according to the results.

The rheological and mechanical properties of PLA/PS blends were studied by Hamad et al. [25]. The blends were prepared using a single screw extruder. They found that PLA/PS blend exhibited a typical shear-thinning behavior over the range of the studied shear rates, and the viscosity of the blend decreased with increasing PLA content. Also it was found that no equal-viscosity temperature exists between PLA and PS. The mechanical results showed immiscibility between PLA and PS in the blend.

Li et al. [61] studied the fibrous blends of PET and PLA prepared by electrospinning (ES) from a common solvent. Morphology of as-spun amorphous fibers showed that addition of PLA into the ES solution prevents occurrence of beads. The degree of crystallinity of each blend component is reduced by the presence of the other blend component, and the overall crystallinity of the blend fibers is less than that of the homopolymer fibers. Also, it was found that oriented crystals were formed in the blended electrospun fibers collected on a rotating collector.

2.8 Potential applications of PLA composites

PLA is a biodegradable, biocompatible, non-toxic and eco-friendly polymer. PLA and its composites are currently used in in biomedical and pharmaceutical applications, e.g. drug delivery systems, sutures, implants for bone fixation, etc. They are widely used in orthopedic medicine, soft tissue repair, synthetic grafts, etc [28, 62, 63].

Sankaran et al. [64] prepared using the poly(L-lactic acid) (PLA) and poly(ϵ -caprolactone) (PCL) physical blends in the ratios of 75:25 and 25:75 by electrospinning using dynamic collector (1500 RPM). They found that the PLA-PCL blend ratio of 25:75 exhibit better thromboresistivity, faster adhesion, and proliferation of HUVEC and promoted better cell extension along the direction of alignment. Human umbilical vascular endothelial cells (HUVEC) adhesion on the scaffolds was observed within 24 h. Cell viability and proliferation were rationally influenced by the aligned nanofibers. Gene expression reveals the grafts thromboresistivity, elasticity, and aided neovascularization. Thus, these scaffolds could be an ideal candidate for small diameter blood vessel engineering.

The polylactic acid (PLA) and thermoplastic polyurethane (TPU) were melt blended with a twin-screw extruder and microcellular injection molded to mass produce tissue engineering scaffolds with different ratios and resulting mechanical properties and phase morphologies were studied by Mi et al. [65]. They found that the PLA was dispersed as spheres or islands inside the TPU matrix and that this phase morphology further influenced the scaffold's microstructure and surface roughness. The blends exhibited a large range of mechanical properties that covered several human tissue requirements. The elongation-at-break improved dramatically as the TPU content increased in the blends.

Hamad et al. [13] studied the rheological properties of PLA/LDPE blends. The experiments were carried on a capillary rheometer. The results showed that the PLA/LDPE polymer blends are pseudo plastic in nature, where their viscosity decreases with increasing shear stress. Also it was found the melt viscosity of the blends decreases with increasing PLA content in the blend.

Balakrishnan et al [26] investigate the properties of PLA/LLDPE blends at various LLDPE loadings. They found that the impact strength of PLA improved by 53% with addition of 10 wt% LLDPE. However, the tensile modulus and strength, and elongation at break of PLA/LLDPE blends decreased with increasing weight ratio of LLDPE. Similarly, flexural modulus and strength also dropped with addition of LLDPE. DSC results showed that glass transition temperature (T_g) and crystallinity (X_c) of PLA increased with blending of LLDPE. The LLDPE particles size was seen to increase with increasing loadings of LLDPE which explains the unexpected decrease of impact strength after 10 wt%.

The LLDPE/PLLA polymer blends with and without compatibilizer with grafted low-density polyethylene MA were prepared and investigated by Singh et al. [27]. They found that the polymer blend LLDPE 80 [80 wt % LLDPE and 20 wt % poly(L-lactic acid) (PLLA)] and MA-g-lowdensity polyethylene 80/4 (80 wt % LLDPE, 20 wt % PLLA, and 4 phr compatibilizer) had the optimum tensile strengths and elongations at break. The FTIR analysis indicated the specific interaction in the blend with compatibilizer. Those specific interactions morphological studies indicated that the compatibilizer influenced the morphology of the LLDPE/PLLA blends. This blend may be used for packaging applications.

Lisa et al. [66] investigated electrospun blends of PLA and PGA via scanning electron microscopy, tensile testing, differential scanning calorimetry, and phase contrast microscopy to gain a better understanding of these blended structures for potential use in biomedical applications. They report the morphology and mechanical properties of electrospun blends of PLA and PGA indicate that these materials are promising and may be utilized in soft tissue engineering.

2.9 Compatibilization

Compatibilization is important that most commercial polymer blends are immiscible systems [67]. The phase separated typically exhibited by immiscible system usually lead to poor blends properties. The challenge here is to modify immiscible blend by induction, typically referred to as blend compatibilization, is mostly based on interfacial modification. Compatibilization aims at modifying the interfacial properties, which is highly critical for the performance of immiscible polymer blend. An efficient compatibilization assists in the development of the required morphology during the compounding stage and help to preserve this optimized phase structure during the subsequent forming steps. This process is thus a prerequisite for manufacturing polymer blends with stable and reproducible properties. The design of a good compatibilization strategy is the key factor required for achieving high quality polymer blends. It is usually recognized that an efficient compatibilization method must complete is three tasks.

1. A reduction of interfacial tension between the blend's components to permit the production of a finer dispersion during the compounding step.
2. A decrease in coalescence rate to stabilize the morphology during compounding and prevent phase coarsening during the subsequent forming processes.
3. An efficient stress transfer between the solid components to provide mechanical strength and integrity to parts manufactured from the polymer blend.

The most common compatibilizing technique relies on the of selected copolymer that is added to the blends. The chemical structure of the copolymer is chosen in such a way that their different segments are selectively miscible with each of

the blends components. The simplest approach is to use a copolymer A-B for compatibilizing a blend of polymer A and B.

2.9.1 Compatibilized PLA-containing blends

The polymer blends quite often have poor mechanical properties because of high interfacial tension, which promotes segregation and poor adhesion between the components. Therefore, many polymer pairs have been compatibilized by the addition of a third component, such as block or graft copolymer, which possess segment capable of interaction with each blend component. Such copolymers behave as macromolecular emulsifiers, providing polar bonds that strengthen and stabilize the blend interface.

Anderson and Hillmyer [68] studied the mechanical properties of PLA/PE blends compatibilized by polylactide–polyethylene block copolymers (PLA-*co*-PE). Blending of PLA with PE improves the impact strength of the material comparing to pure PLA and it was more pronounced, when compatibilizers were used, whereas the tensile properties including the tensile strength, elongation, and Young's modulus in both compatibilized and non-compatibilized materials were less than those of pure PLA.

Yoo et al. [69] studied the effect of SEBS-*g*-MA and PP-*g*-MA as compatibilizers for PLA/PP (80/20 wt%) blend prepared using a twin screw extruder. The results showed that PP-*g*-MA is more effective for improving tensile strength of the blend, whereas the impact strength of the blend was significantly enhanced by addition of SEBS-*g*-MA. The tensile and impact strengths of the PP/PLA (80/20) blends, it is suggested that the PP-*g*-MAH acts as an effective compatibilizer to increase the tensile strength of the blends, while the SEBS-*g*-MAH is an effective impact modifier to increase the impact strength of the PP/PLA blends.

The effects of MAH-*g*-PP and GMA as compatibilizing agents for PLA/PP blends were investigated by Choudhary et al. [70]. Mechanical test results indicated an increase in the tensile modulus, tensile strength, flexural strength, and impact properties of PLA with the incorporation of PP. Further addition of MAH-*g*-PP increased tensile modulus, tensile strength, flexural strength, and impact strength. Thermal studies employing TGA revealed an increased thermal stability in the blend matrix. Storage modulus (E') of PLA was found to increase in the blend matrix

compatibilized with MAH-g-PP in comparison with that of the virgin PLA. SEM of impact-fractured samples showed that the soft PP phase was dispersed within the PLA matrix, and a decrease in the domain size of the dispersed phase was observed with the incorporation of MAH-g-PP, which acted as a compatibilizer to improve the compatibility between PLA and PP.

Lai et al. [71] studied the physical and thermal properties of the PLA/TPU blends prepared through a melt-blending process were investigated with 3-aminopropyl triethoxysilane (APTES) as a compatibilizer to enhance their interfacial interaction. They found that the addition of the compatibilizer showed improved compatibility between TPU and PLA. The addition of a high dosage of APTES into the PLA/TPU blends depressed the crystallization temperature. A low dosage of APTES (1 phr) also increased the viscosity because of the improved interaction between TPU and PLA at all of the investigated shear rate regions, but a higher dosage of compatibilizer induced another plasticizing effect to reduce the viscosity.

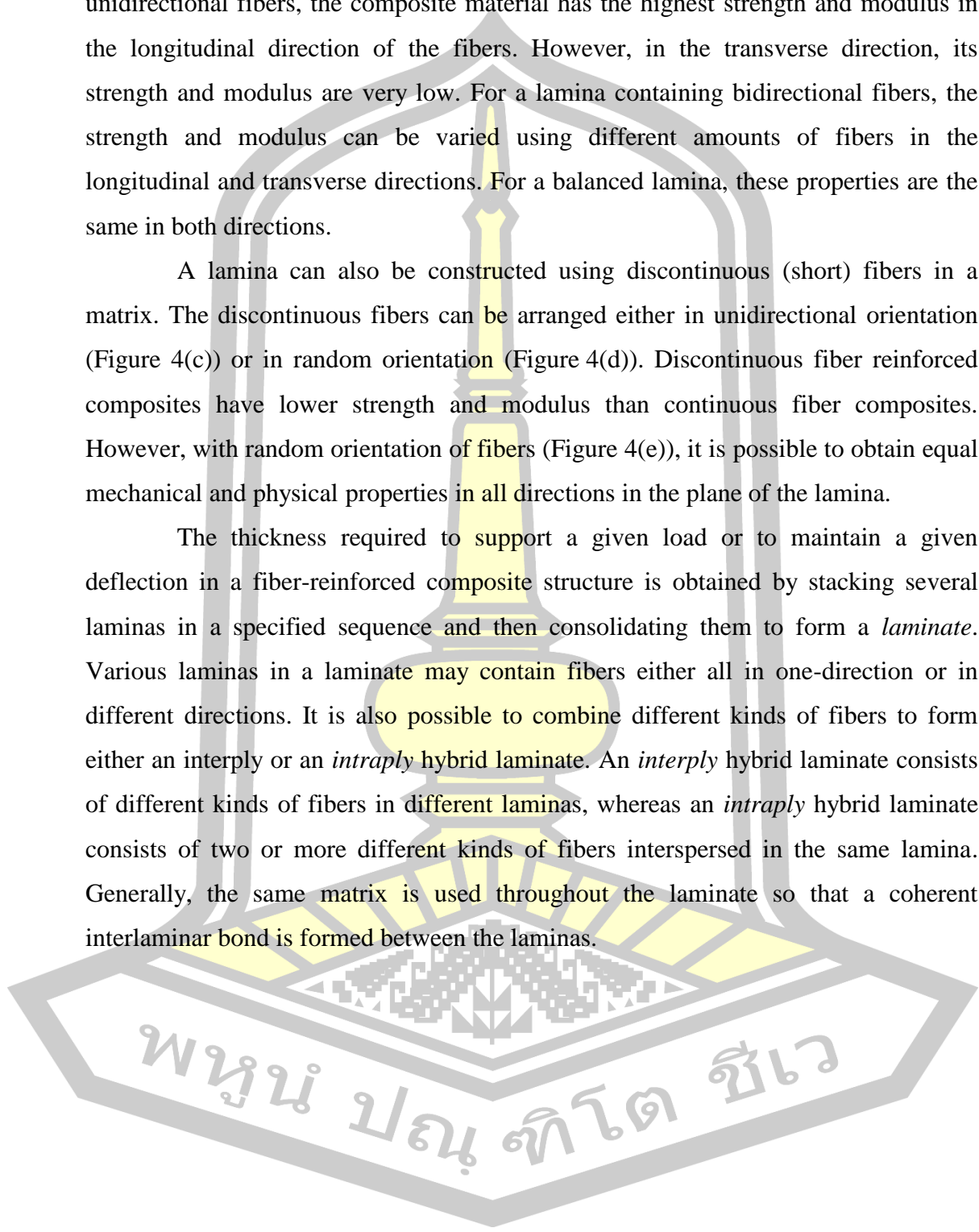
2.10 Composite structure

Major constituents in a fiber-reinforced composite material are the reinforcing fibers and a matrix, which acts as a binder for the fibers. Other constituents that may also be found are coupling agents, coatings, and fillers. Coupling agents and coatings are applied on the fibers to improve their wetting with the matrix as well as to promote bonding across the fiber–matrix interface. Both in turn promote a better load transfer between the fibers and the matrix. Fillers are used with some polymeric matrices primarily to reduce cost and improve their dimensional stability. Manufacturing of a composite structure starts with the incorporation of a large number of fibers into a thin layer of matrix to form a *lamina* (ply). The thickness of a lamina is usually in the range of 0.1-1 mm (0.004-0.04 in.) [72]. If continuous (long) fibers are used in making the lamina, they may be arranged either in a unidirectional orientation (i.e., all fibers in one direction, Figure 4(a)), in a bidirectional orientation (i.e., fibers in two directions, usually normal to each other, Figure 4(b)), or in a multidirectional orientation (i.e., fibers in more than two directions, Figure 4(c)). The bi- or multidirectional orientation of fibers is obtained by

weaving or other processes used in the textile industry. For a lamina containing unidirectional fibers, the composite material has the highest strength and modulus in the longitudinal direction of the fibers. However, in the transverse direction, its strength and modulus are very low. For a lamina containing bidirectional fibers, the strength and modulus can be varied using different amounts of fibers in the longitudinal and transverse directions. For a balanced lamina, these properties are the same in both directions.

A lamina can also be constructed using discontinuous (short) fibers in a matrix. The discontinuous fibers can be arranged either in unidirectional orientation (Figure 4(c)) or in random orientation (Figure 4(d)). Discontinuous fiber reinforced composites have lower strength and modulus than continuous fiber composites. However, with random orientation of fibers (Figure 4(e)), it is possible to obtain equal mechanical and physical properties in all directions in the plane of the lamina.

The thickness required to support a given load or to maintain a given deflection in a fiber-reinforced composite structure is obtained by stacking several laminas in a specified sequence and then consolidating them to form a *laminate*. Various laminas in a laminate may contain fibers either all in one-direction or in different directions. It is also possible to combine different kinds of fibers to form either an interply or an *intraply* hybrid laminate. An *interply* hybrid laminate consists of different kinds of fibers in different laminas, whereas an *intraply* hybrid laminate consists of two or more different kinds of fibers interspersed in the same lamina. Generally, the same matrix is used throughout the laminate so that a coherent interlaminar bond is formed between the laminas.



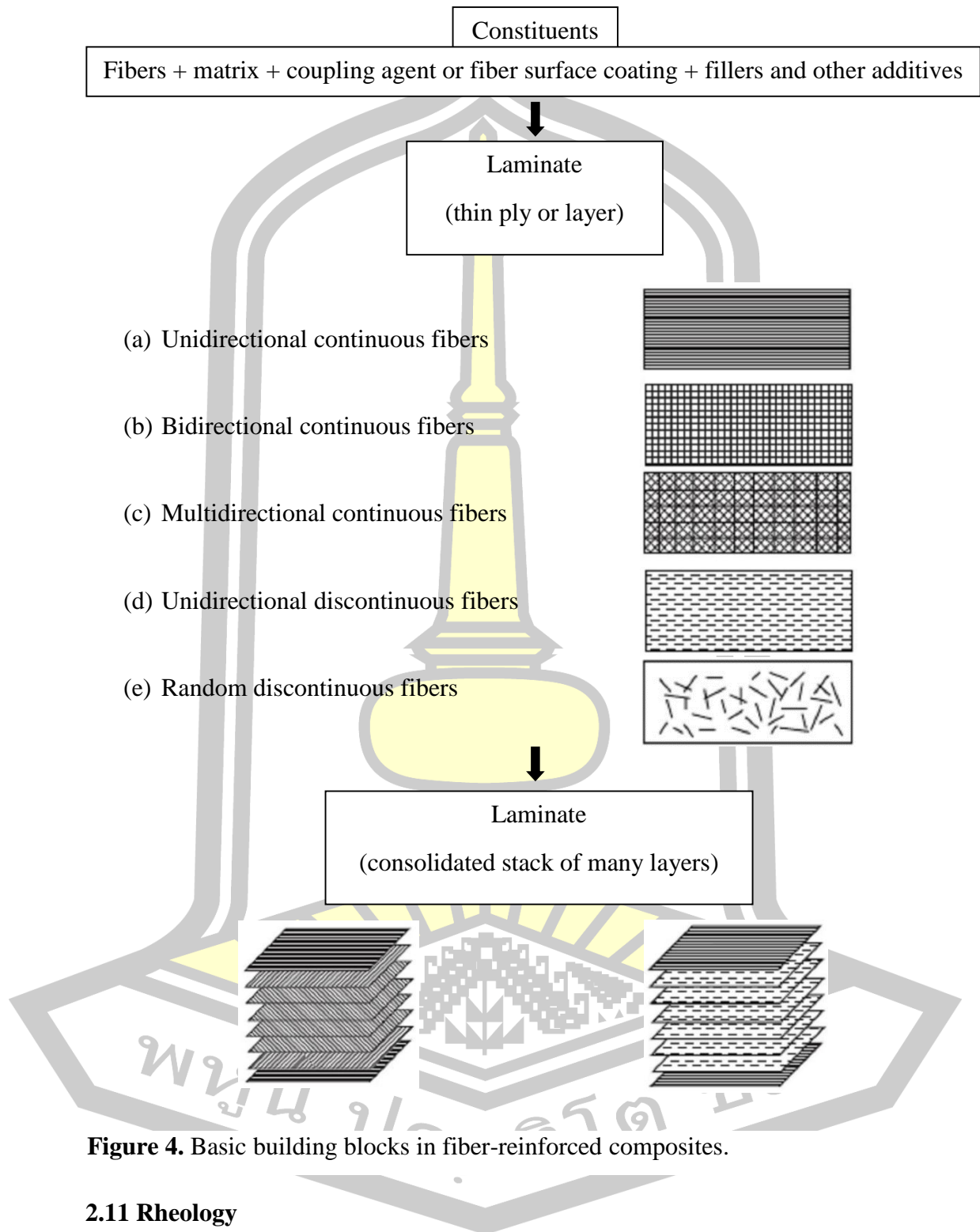


Figure 4. Basic building blocks in fiber-reinforced composites.

2.11 Rheology

It is anticipated that many readers will have little previous knowledge about rheology but will wish to find out how it can be useful to them in solving practical

problems involving the flow of molten polymers [73]. For this reason, it is our intention to supply sufficient basic information about rheology to enable the reader to understand and make use of the methods described. With this in mind, the term of “rheology” is defined at the beginning “rheology” is the science that deals with the deformation of materials when forces are applied to them. The term is most commonly applied to the study of liquids and liquid-like material such as paint, catsup, blood, polymer in solutions or in molten state. Moreover, this includes the study of the deformation of solids such as the metal forming and the stretching of rubber. There are two principal aspects of rheology. One involves the development of quantitative relationships between deformation and force for a material of interest. The information for the development of such a relationship is obtained from experiment measurements. For example, for the foam pillow, it might be observed that the force required to compress it a certain distance is proportional to the distance. In the case of the lubrication oil, it might be found that the speed with which it flows through a small hole in the bottom of a can is proportional to the height of the oil remaining in the can.

For a linear elastic material or a Newtonian fluid, such simple observations are sufficient to establish a general equation describing how such a material will respond to any type of deformation. Such an equation of state is called a “constitutive equation” or a rheological equation of state. However, for more complex material such as molten plastics, the development of a constitutive equation is a much more difficult task, which may require the result of many type of experiment.

The second aspect of rheology is the development of relationships that show how rheological behavior is influenced by the structure and composition of the material and the temperature and pressure. Ideally, one would like to know how these parameters affect the constitutive equation, but this has not been accomplished at the present time, except for very simple materials such as Newtonian fluids. In the case of more complex material, one can at least develop relationships showing how specific rheological properties such as the viscosity and the relaxation modulus are influenced by molecular structure, composition, temperature and pressure.

Molten plastics are rheologically complex materials that can exhibit both viscous flow and elastic recoil. An exactly general constitutive equation has not been

developed for these materials. This complicates the description and measurement of their rheological properties but makes polymer rheology an interesting and challenging field of study.

2.11.1 The important of rheological properties

The forces that develop when a lubricant is subjected to a high-speed shearing deformation are obviously of central importance to mechanical engineers. The rheological property of interest in this application is the viscosity. The stiffness of a steel beam used to construct a building is of great importance to civil engineers, and the relevant property here is the modulus of elasticity [74].

The viscoelastic properties of molten polymers are of importance to plastics engineers, because these properties directly affect the flow behavior whenever plastic are processed in the molten state. For example, in order to optimize the design of an extruder, the viscosity must be known as a function of temperature and shear rate. In injection molding, the same information is necessary in order to design the mold in such a way that the melt will completely fill it in every shot. In blow molding, the processes of parison sag and swell are governed entirely by the rheological properties of the melt.

2.11.2 Types of fluids

The viscosity of the Newtonian fluid is independent of shear rate, thus if we draw the relationships between shear stress-shear rate for an ideal fluid, the slope is equal to the viscosity of the fluid. However, real materials, particularly polymer melts, solutions and suspension of particles in liquid do not exhibit the characteristics of a Newtonian fluid. Thus, it is called non-Newtonian behavior. The flow behavior of material can be classified into three classes [74].

- i) Time-independent fluids: fluids in which the rate of shear at a given point is some functions of the shear stress at the point and nothing else.
- ii) Time-dependent fluids: more complex systems in which the shear stress-shear rate relationships depend on how the fluid has been sheared and on its previous history.

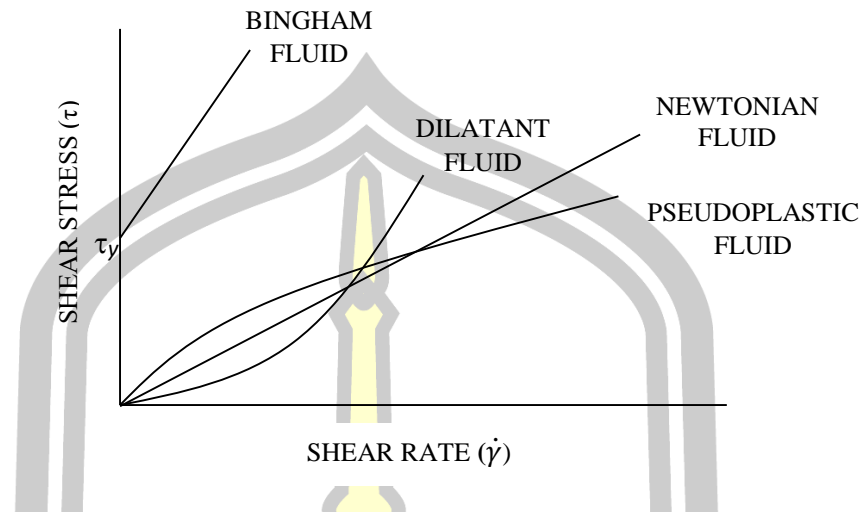


Figure 5. Shear stress-shear rate relationships for Bingham bodies, dilatant fluids and pseudoplastic fluids and a Newtonian material. τ_y is the yield point.

iii) Viscoelastic fluids: systems which are predominantly viscous but which exhibit partial elastic recovery after deformation. The four basic types are indicated in Figure 5; Newtonian fluid, pseudoplastic fluid, dilatant fluid and Bingham fluid. The Bingham body is an idealized material which it is considered to have an internal structure which collapses above a yield stress τ_y , above which the rate increases linearly with shear stress;

$$\dot{\gamma} = \frac{\tau - \tau_y}{\eta} \quad \text{when } \tau \geq \tau_y \quad (2.1)$$

Bingham bodies, even for shear stress-shear rate above τ_y may be non-linear. Examples are suspensions, slurries and pulps.

Pseudoplastic flow is when the shear rate increases at a more than linear rate with increasing in shear stress. In other words, there is no constant of proportionality between shear stress and shear rate. Therefore, instead of talking about the viscosity, used in Newtonian liquids, it is more common to refer to the “*apparent viscosity*” defined as *shear stress/shear rate*. Such an apparent viscosity decreases with rate of shear for pseudoplastics and increases with shear rate for dilatant fluids while it is independent of shear rate for Newtonian fluids as shown in Figure 6 These behaviors are all found in common polymer melts.

Pseudoplastic behavior can arise in several ways but two explanations are commonly offered:

i) There are extensive entanglements and/or random orientation at rest. The number of entanglements reduces and the orientation of molecules increases under high shear rate. At very high shear rate, the orientation may be complete in which a near Newtonian behavior may be observed.

ii) There may be present highly solvated molecules or particle. With increasing shear rate, solvated layers may be sheared away resulting in a less interaction of the particles (due to their smaller effective size) leading to a reduction in viscosity. These processes must occur at a finite rate. Apparently, the time-independent properties are due to the differences in the time-scale of the experiment compared with the time required for the removal of the solvated layers.

There have been a numerous equations used to describe the behavior of pseudoplastic fluids. Equations of state are often dispensed within rheological calculations. Instead, conservation from shear rate to shear stress (or vice versa) is achieved by reading directly from a flow curve, i.e. a plot of shear stress against the shear rate.

However, the only equation used for any real case is the power law equation (also know as the Ostwald-de Waele equation), which it is expressed as:

$$\tau = K \left(\dot{\gamma} \right)^n \quad (2.2)$$

Or in logarithmic form, this equation may be written as:

$$\log \tau = \log K + n \log \dot{\gamma} \quad (2.3)$$

where K and n is the power law constant and power index, respectively. This indicates that log-log plot of τ versus $\dot{\gamma}$ will give a straight line (see Figure 7)

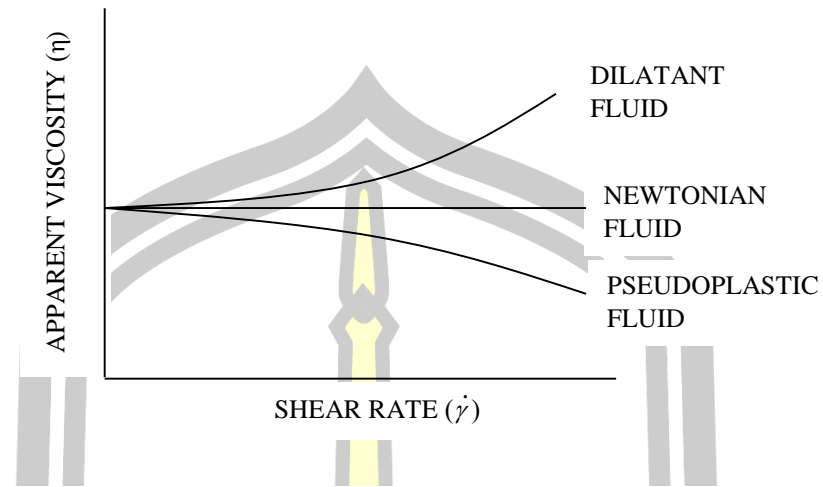


Figure 6. Apparent viscosity-shear rate curves for a dilatant fluid, a Newtonian fluid and a pseudoplastic fluid which have the same apparent viscosity at zero shear rate.

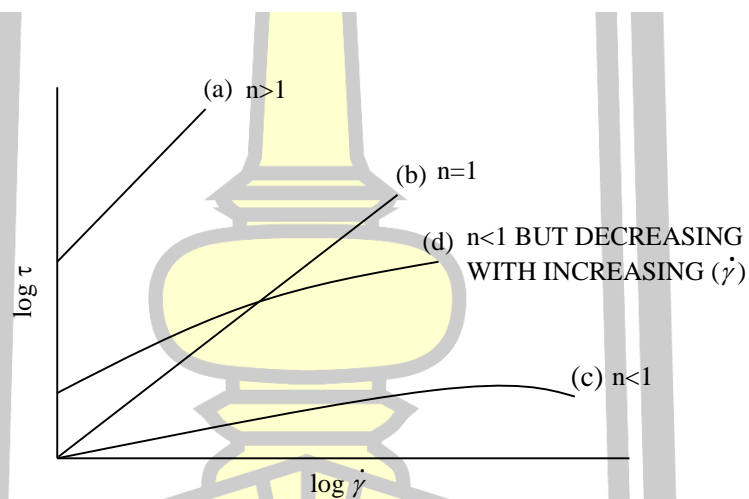


Figure 7. Logarithmic plots between stress and shear rate for (a) a dilatant material obeying the power law, (b) a Newtonian material, (c) a pseudoplastic material obeying the power law and (d) a conventional polymer melt which is pseudoplastic but does not obey the power law.

and if $n = 1$, it is the Newtonian fluid. By combining Eq.2.8 and Eq.2.2 together, it obtains:

$$\eta = K \left(\dot{\gamma} \right)^{n-1} \quad (2.4)$$

Thus, it is possible to relate the viscosity to shear rate and n in terms which do not involve K . From Eq. 2.4, the viscosity (η) at other shear rates ($\dot{\gamma}$) can also be estimated if the viscosity (η_r) at some arbitrary shear rate ($\dot{\gamma}_r$) is known by using the following equation:

$$\frac{\eta}{\eta_r} = \left| \frac{\dot{\gamma}}{\dot{\gamma}_r} \right|^{n-1} \quad (2.5)$$

The dilatancy has the opposite behavior to pseudoplasticity. Dilatant materials present an increase in the apparent viscosity with increasing shear rate, which is often exhibited by highly concentrated suspensions.

2.11.3 Measurements of viscosity

Ideal fluids are called Newtonian. Their viscosities are independent of the rate of shear. The measurement of Newtonian shear viscosity is schematically shown in Figure 2.8 from 8(a), a liquid is confined between two parallel plates of area, A , separated by a distance, D . A force, F , is required to move the top plate at a constant velocity relative to the lower plate. The force is directly proportional to the viscosity of the liquid. The important quantities involved in measuring shear viscosity may be defined as follows with the help of Figure 8(a).

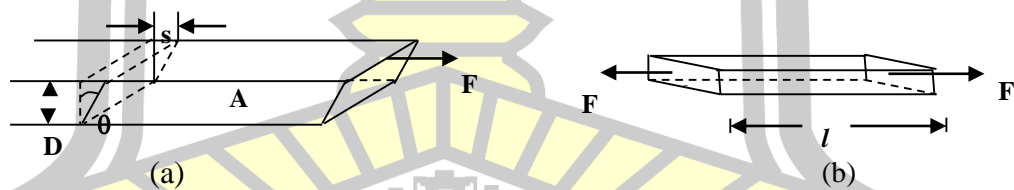


Figure 8. Schematic diagrams for the measurements of (a) shear viscosity and (b) elongation or tensile viscosity.

$$\text{Shear } (\tau) \text{ stress} = \frac{\text{Shear force}}{\text{Area of shear force}} = \frac{F}{A} \quad (2.6)$$

$$\text{Shear strain } (\dot{\gamma}) = \frac{\text{Amount of shear displacement}}{\text{Distance between shearing}} = \frac{S}{D} = \tan \theta \quad (2.7)$$

$$\text{Viscosity } (\eta) = \frac{\text{Shear stress}}{\text{Rate of shear strain}} (\eta) = \frac{\tau}{\frac{d\dot{\gamma}}{dt}} = \frac{\tau}{\dot{\gamma}} \quad (2.8)$$

Another type of viscosity can be measured in tension mode instead of in shearing test. The measurement of tensile or extensional viscosity is illustrated in the Figure 2.8(b) in which a strip or thread of material is stretched. The tensile stress, σ , is expressed as

$$\sigma = \frac{F}{A} \quad (2.9)$$

While the tensile strain or elongation, ε , is

$$\varepsilon = \int_0^l \ln \frac{dl}{l} = \frac{l-l_0}{l} \quad (2.10)$$

where l_0 is the initial length while l is the length at some later time. The tensile viscosity, η_t is:

$$\eta_t = \frac{\sigma}{\frac{d\varepsilon}{dt}} \quad (2.11)$$

For a Newtonian liquid, the tensile viscosity is three times the shear viscosity, but in polymeric liquids, the tensile viscosity may be many times the shear viscosity. For polymers, the tensile viscosity is comparable in importance to the shear viscosity. Tensile viscosity is of great practical importance when polymer flows through channels or tubes in which the cross section area is progressively decreased. Examples include the spinning of fibers and the filling of moulds in injection moulding [75].

The conservative unit of viscosity is the poise (with dimensions of dyne second per cm^2 or gram cm/s). The SI units for viscosity are $\text{Pa}\cdot\text{s}$. To convert the poise to Pascal seconds, multiply the number of poises by 0.001.

2.11.4 Rheometers

A great variety of instruments have been used to measure the viscosity and other rheological properties of liquid and molten polymers. Most of these instruments are capable of measuring the rheological properties as a function of temperature and shear rate. The relationship between shear stress and shear rate, and therefore the dependence of viscosity upon shear rate, can be determined over a wide temperature range. The common methods include capillary, cone-and-plate, plate-

and-plate and parallel-plate rheometer, which can also give information concerning normal stresses through measurements by force transducers mounted in the direction normal to the plane of shear.

2.11.4.1 Plate-and-plate rheometer

For plate-and-plate rheometer (Figure 9(a)) a circular disk of viscous sample is held between two parallel plates. The applied force is normal to the plates. The advantages of this method are the variable gap, simpler sample preparation and loading. It is the best choice for oscillation tests. The main disadvantage of this geometry is that the shear rate a function of the radius and therefore not constant throughout the sample. The shear stress, τ , is proportional to the torque, M , and to the stress factor, A , as follows:

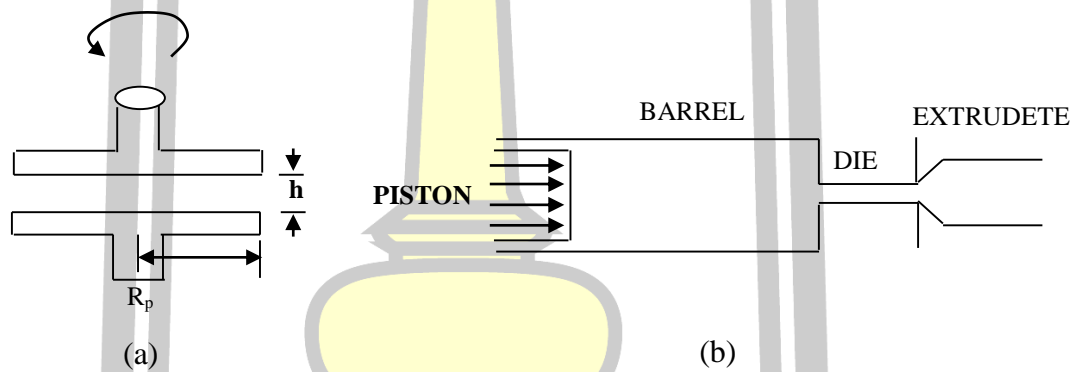


Figure 9. Idealized illustration for (a) plate-and-plate, and (b) capillary rheometers.

$$\tau = A \cdot M \quad (2.12)$$

The A factor is calculated as following:

$$A = \frac{2}{\pi \cdot R_p^3} \quad (2.13)$$

where R_p is the plate radius. Thus it has the unit of an inverse volume.

While the shear rate, $\dot{\gamma}$, is proportionally linked to the angular velocity or speed and the shear factor, N , expressed as:

$$\dot{\gamma} = N \cdot \omega \quad (2.14)$$

where ω is the angular viscosity (rad/s) calculated according to $(2\pi n/60)$ from the speed n . The N factor is calculated from:

$$N = \frac{R_p}{h} \quad (2.15)$$

where h is the gap distance. This is the viscosity in the case of parallel-plate rheometers can be obtained as:

$$\eta = \frac{\tau}{\dot{\gamma}} = \frac{A \cdot M}{N \cdot \omega} = \frac{2}{\pi \cdot R_p^3} = \frac{M \cdot h}{R_p \cdot \omega} = \frac{2 \cdot M \cdot A}{\pi \cdot R_p^4 \cdot \omega} \quad (2.16)$$

Complex viscosity is determined from the amplitudes of the stress and strain and the phase angle between them (δ). In oscillatory measurements, the melt is subjected to a sinusoidal varying shear strain (γ) and shear stress (σ) as follows:

$$\dot{\gamma} = \dot{\gamma}_0 \cos \omega t \quad (2.17)$$

$$\sigma = \sigma_0 \sin(\omega t + \delta) \quad (2.18)$$

The maximum values of the sinusoidal shear strain and shear stress are γ_0 and σ_0 , respectively. The shear stress and shear strain are commonly dealt with by using complex notation:

$$\dot{\gamma}^* = \dot{\gamma}_0 (\cos \omega t + i \sin \omega t + \delta) = \dot{\gamma}_0 \exp i(\omega t) = \dot{\gamma}' + i \dot{\gamma}'' \quad (2.19)$$

$$\sigma^* = \sigma_0 (\cos(\omega t + \delta) + i \sin(\omega t + \delta)) = \sigma_0 \exp(i(\omega t + \delta)) \quad (2.20)$$

The complex shear modulus is defined as:

$$G^* = \frac{\sigma^*}{\dot{\gamma}^*} = \frac{\sigma_0}{\dot{\gamma}_0} \cdot \cos \delta + i \frac{\sigma_0}{\dot{\gamma}_0} \cdot \sin \delta = G' + iG'' \quad (2.21)$$

where $G'(\omega)$ is the storage modulus associating with the stored energy and $G''(\omega)$ is the loss modulus associating with the dissipation of energy as heat, while $I = (-1)^{1/2}$. The complex viscosity (η^*) is the defined as:

$$\eta^* = \frac{\sigma^*}{\dot{\gamma}^*} = \frac{\sigma^*}{i\omega\dot{\gamma}^*} = \frac{\sigma_0}{\dot{\gamma}_0} \cdot \sin \delta \cdot \frac{1}{\omega} - i \frac{\sigma_0}{\dot{\gamma}_0} \cdot \cos \delta \cdot \frac{1}{\omega} \quad (2.22)$$

where η^* is the dynamic viscosity or the real part of the viscosity associating with the dissipation of energy, and η'' is the imaginary part or the associating with the energy storage.

2.11.5 Effect of some parameters on rheological behavior

2.11.5.1 Effect of temperature on viscosity

The viscosity of most polymers changes greatly with temperature. For a Newtonian liquid and for polymer fluid at temperatures far above the glass transition temperature (T_g) or the melting point, the viscosity follows the Arrhenius equation to a good approximation [75].

$$\eta = Ae^{\frac{E_a}{RT}} \quad (2.23)$$

where A is a constant characteristic of the polymer at a given shear stress and its molecular weight, E_a is the activation energy for the flow process, R is the universal gas constant and T is the absolute temperature. The low value of E_a is a result of the great flexibility of the polymer chain. The energy of activation for flow increases as the polymer chain becomes more rigid [76].

2.11.5.2 Effect of pressure on viscosity

The greater the free volume the easier it is for flow to take place. The free volume increases with temperature (due to thermal expansion) and is much influenced by the pressure. An increase in the hydrostatic pressure decreases free volume and increases the viscosity of liquid. One approach is the modified *Andrade* equation:

$$\eta = K \exp \left[\frac{E_a}{RT} + \frac{CV_0}{V_f} \right] \quad (2.24)$$

where V_0 is the close packed volume, V_f is the free volume defined as $V - V_0$ where V is the observed volume and C is the constant generally being 5-1.0.

2.11.5.3 Effect of time, stress, shear rate and molecular weight

An increase in time and shear rate will cause a decrease in melt viscosity of the polymer while an increase in stress and molecular weight will result in an increase in melt viscosity of polymer, Moreover, it is found that the polymers having the greater molecular weight distribution exhibit the higher melt viscosity than the one having the narrower molecular weight distribution.

2.12 Scanning Electron Microscope (SEM)

Another instrument employed for studies of fracture surface is the scanning electron microscope (Figure 10). This instrument makes use of a beam scattering mode of operation. A fine electron beam scans the surface of the specimen previously coated with a conducting layer in a two-dimensional raster. The back scattered or the secondary electron are analyzed with a scintillation counter, and the signal from the counter is fed into a cathode-ray tube which is set to scan synchronously with the electron beam. As a result, a point-by-point image of the specimen is displayed on the cathode-ray tube. This instrument has an extremely large depth of focus and is therefore applicable to fracture studies. The resolution of this instrument depends on several factors but resolution of ~ 5 nm has been achieved. The most important factors limiting the resolution, in addition to instrumental parameters, are the specimens and their preparation.

To avoid damage to the fibrillous structure and the creation of artifacts during scanning electron imaging, a special protective coating composed of rigid and well-conducting amorphous layers must be applied by low energetic sputtering. From the preparation of sample, a penning-sputtering device with neutralization electrodes has proven to be very effective, producing a layer of tantalum of ca 5-nm thickness. In order to increase the electric conductivity of the tantalum layer, a subsequent carbon layer has to be deposited by flash evaporation of carbon yarn.

Examining fatigue-fracture surfaces by detailed fractography, size and appearance of the broken-craze fibrils, and other surface structures can be determined, whereas micromechanical data such as craze length can only be estimated. On the other hand, direct SEM observation of the crack-tip area, including the craze, facilitates measurement of the crack opening as well as craze thickness and length. Increasing magnification also allow comparison of fibril thickness with fibril diameters as measured by such indirect methods as the deflection technique. In addition, fibril strain can be estimated by comparing the thickness of craze fibril in both the loaded and broken state.

The SEM method can also be used during crack propagation. For example very slow crack propagation has been measured in PS with rubber content of different toughening. Brittle in low rubber-phase, high impact PS (HIPS) is observed, whereas high rubber-phase systems exhibit a ductile tearing mode of fracture. With increasing rubber-phase volume, craze density increase, which leads to a reduction in width of material between the crazes; subsequent failure leaves bridging ligaments. Under increasing load, these fail in a manner dependent on their thickness with a brittle ductile transition at a ligament thickness ca 3 μm .

The application of SEM to micromechanical investigation at the crack-tip process zone has overcome many limitation of other method. Its high magnification and resolution and its high depth of field offer advantages over light microscopy (qv). Although SEM is limited by the low speed of the scanning process and by charging effects during the examination, as well as by poor contrast in the case of small differences in the sample profile [77].

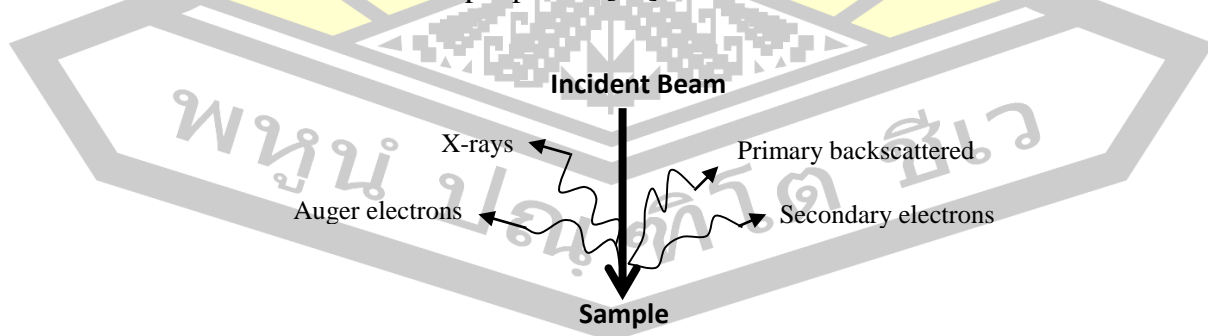


Figure 10. Electron signals from samples in different.

2.13 Thermal Analysis

2.13.1 Definition

Thermal analysis (TA) [78] is frequently used to describe analytical experimental techniques which investigate the behavior of a sample as a function of temperature. In this report, TA refers to conventional TA techniques such as differential scanning calorimetry (DSC), differential thermal analysis (DTA), thermogravimetry (TG), thermomechanical analysis (TMA) and dynamic mechanical analysis (DMA) and so on. TA, in its various guises, is widely employed in both scientific and industrial domains.

The ability of these techniques to characterize, quantitatively and qualitatively, a huge variety of materials over a considerable temperature range has been pivotal in their acceptance as analytical techniques. Under normal conditions only limited training of personnel is required to operate a TA instrument. This coupled with the fact that results can be obtained relatively quickly, means that TA is employed in an ever increasing range of applications. However, the operational simplicity of TA instruments belies the subtlety of techniques which, if improperly practiced, can give rise to misleading or erroneous results. The abundance of results of dubious integrity in both the academic literature and industrial performance reports underlines the extent and seriousness of this problem.

2.13.2 Characteristics of thermal analysis

The advantages of TA over other analytical methods can be summarized as follows:

- (a) The sample can be studied over a wide temperature range using various temperature programmers.
- (b) Almost any physical form of sample (solid, liquid or gel) can be accommodated using a variety of sample vessels or attachments.
- (c) A small amount of sample (0.1 μg - 10 mg) is required.
- (d) The atmosphere in the vicinity of the sample can be standardized.
- (e) The time required to complete an experiment range from several minutes to several hours.

(f) TA instruments are reasonably priced.

In polymer science, preliminary investigation of the sample transition temperature and decomposition characteristics is routinely performed using TA before spectroscopic analysis is begun.

2.13.3 Conformation of thermal analysis instruments

The general conformation of TA apparatus, consisting of a physical property sensor, a controlled - atmosphere furnace, a temperature programmer and a recording device, is illustrated in Figure 11. Modern TA apparatus is generally interfaced to a computer (work station) which oversees operation of the instrument controlling the temperature range, heating and cooling rate, flow of purge gas and data accumulation and storage. Various types of data analysis can be performed by the computer [78].

For TA apparatus without computers is also used where the analogue output signal is plotted using a chart recorder. Data are accumulated on chart paper and calculations performed manually. The quality of the data obtained is not diminished in any way. The accuracy of the results is the same provided that the apparatus is used properly and the data are analyzed correctly.

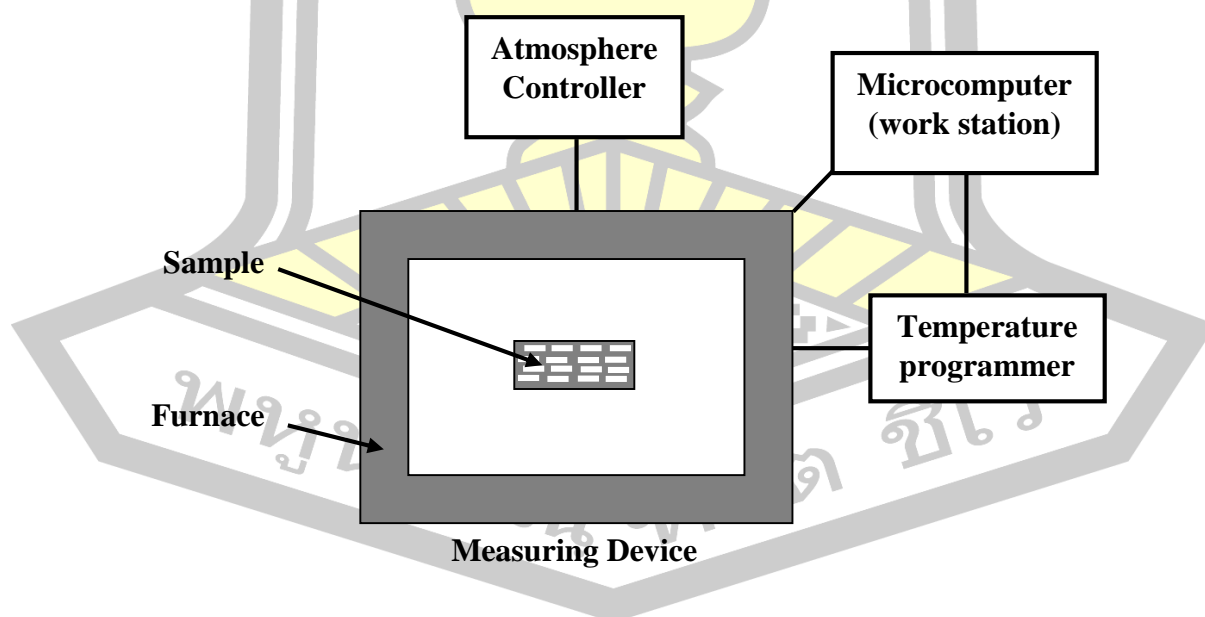


Figure 11. Block diagram of TA instrument.

2.13.4 Thermal analysis techniques

2.13.4.1 Differential scanning calorimetry (DSC)

DSC is of more recent vintage, and has become the method of choice for quantitative studies of thermal transitions in polymer. A polymer sample and inert reference are heated, usually in a nitrogen atmosphere, and thermal transition in the sample are detected and measured. The sample holder most commonly used is a very small aluminum cup (gold or graphite is used or analyses above 800°C), and the reference is either an empty cup or a cup containing an inert material in the temperature range of interest. For the sample and reference are provided with individual heaters, and energy is supplied to keep the sample and reference temperatures constant.

2.13.4.2 Differential thermal analysis (DTA)

DTA is a thermal technique in which the temperature of a sample, a polymer sample and inert reference are heated, usually in a nitrogen atmosphere, and thermal transition in the sample are detected and measured. The sample holder most commonly used is a very small aluminum cup and the reference is either an empty cup or a cup containing an inert material in the temperature range of interest. Both sample and reference are heated by the same heat source, and the difference in temperature (ΔT) between the two is recorded. When a transition occurs in the sample for example, the glass transition or a crossing reaction the temperature of the sample will lag behind that of the reference if the transition is endothermic, and will surge ahead if the transition is exothermic.

2.13.4.3 Thermomechanical analysis (TMA)

TMA can be used to measure the deformation characteristics of solid polymers, film, fibers, thin film, coatings, viscous fluids and gels. Selection of the most appropriate load and deformation mode is important.

TMA curves are plotted with deformation on the vertical axis against temperature or time on the horizontal axis. TMA is used to determine the linear thermal expansion coefficient (α) of polymers, defined as

$$\alpha = \frac{dL}{dt} \cdot \frac{1}{L_0} \quad (2.25)$$

where L_0 is the original length of the sample and dL/dT is the slope of the TMA curve. TMA is generally more sensitive than DSC or DTA for detecting thermal transitions.

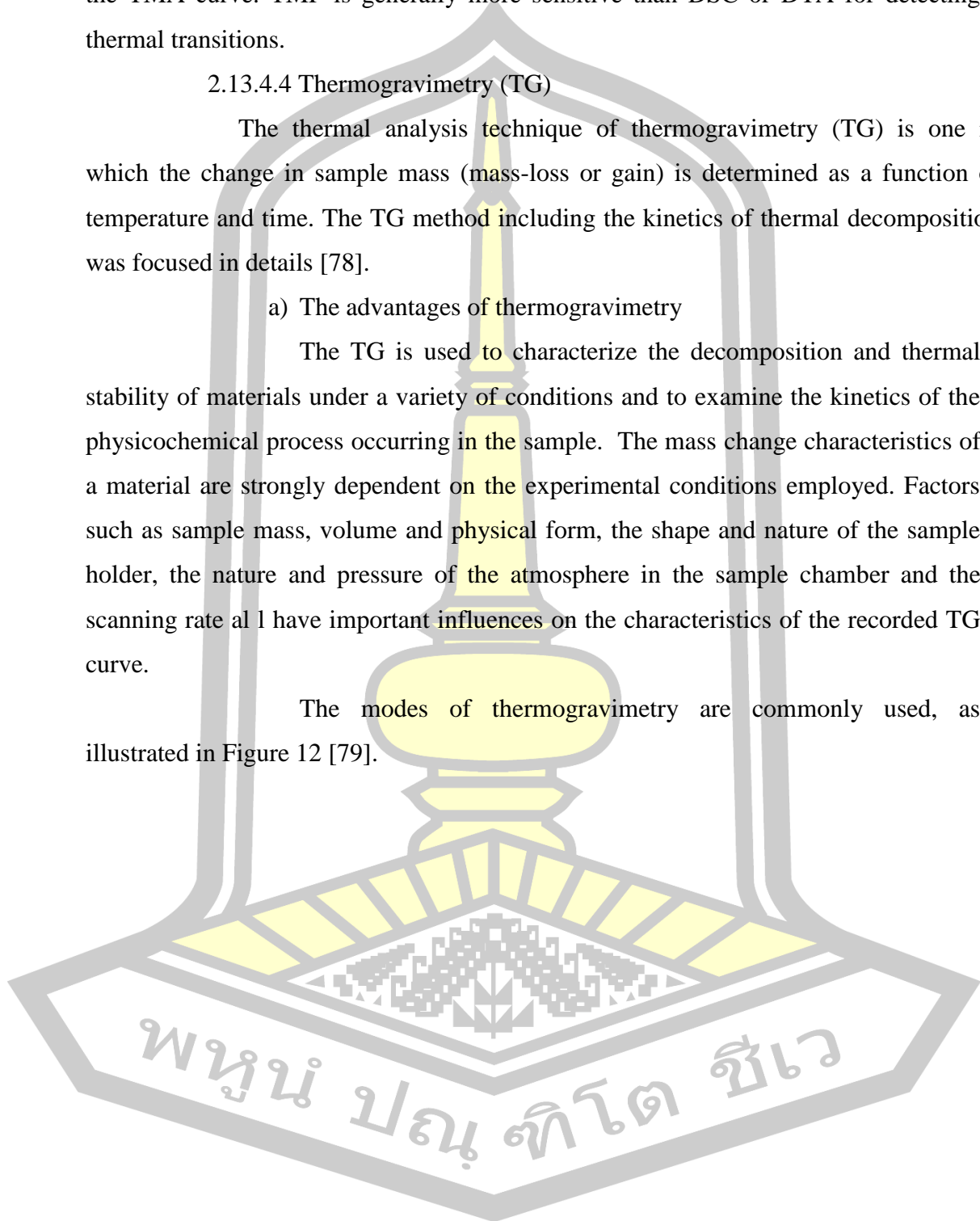
2.13.4.4 Thermogravimetry (TG)

The thermal analysis technique of thermogravimetry (TG) is one in which the change in sample mass (mass-loss or gain) is determined as a function of temperature and time. The TG method including the kinetics of thermal decomposition was focused in details [78].

a) The advantages of thermogravimetry

The TG is used to characterize the decomposition and thermal stability of materials under a variety of conditions and to examine the kinetics of the physicochemical process occurring in the sample. The mass change characteristics of a material are strongly dependent on the experimental conditions employed. Factors such as sample mass, volume and physical form, the shape and nature of the sample holder, the nature and pressure of the atmosphere in the sample chamber and the scanning rate all have important influences on the characteristics of the recorded TG curve.

The modes of thermogravimetry are commonly used, as illustrated in Figure 12 [79].



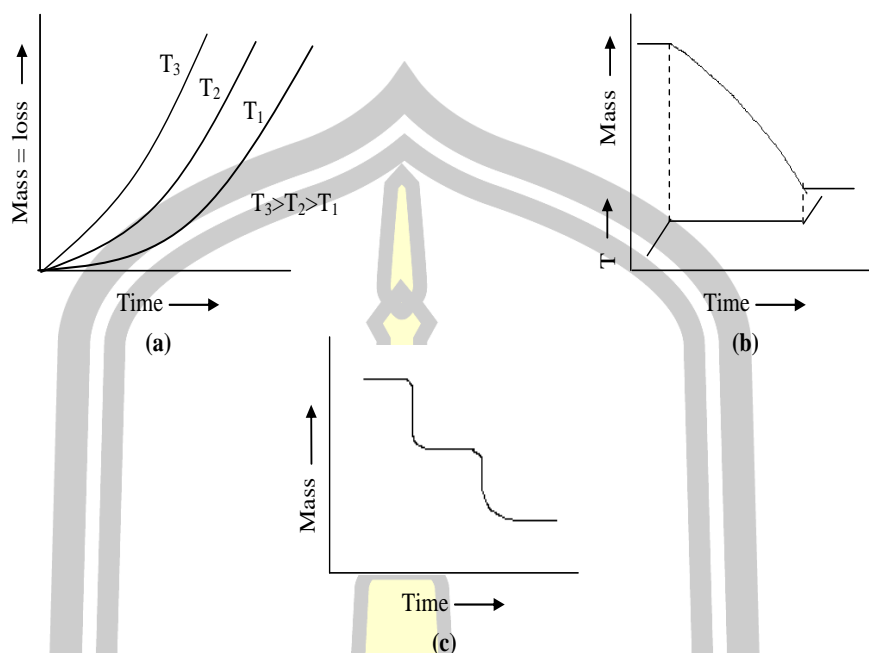


Figure 12. Three modes of thermogravimetry: (a) Isothermal thermogravimetry, (b) quasi-isothermal thermogravimetry, (c) dynamic thermogravimetry.

(I) Isothermal thermogravimetry in which the sample mass is recorded as a function of time at constant temperature.

(II) Quasi-isothermal thermogravimetry, in which the sample is heated to constant mass at each of a series of increasing temperatures.

(III) Dynamic thermogravimetry in which the sample is heated in an environment whose temperature is changing in a predetermined manner, preferably at a linear rate.

TG curves are normally plotted with the mass change (Δm) expressed as a percentage on the vertical axis and temperature (T) or time (t) on the horizontal axis. The reaction is characterized by two temperatures, T_i and T_f , which are called the procedural decomposition temperature and the final temperature, respectively. T_i merely represents the lowest temperature at which the onset of a mass change can be detected for a given set of experimental conditions. Similarly, T_f represents the lowest temperature by which the process responsible for the mass change has been completed. The values of T_i and T_f have no absolute significance as

both the reaction temperature true and the reaction interval ($T_i - T_f$) has no definition value but depend on the experimental condition.

Interpretation of TG data is often facilitated by comparison with data from other experimental techniques. Many TA instrument manufactures offer simultaneous TG-DTA apparatus. The advantage of simultaneous apparatus is that the sample and experimental conditions are identical, and therefore directly comparative data can be quickly obtained.

b) Derivative thermogravimetry (DTG)

In conventional thermogravimetry the mass of a sample, m , is continuously recorded as a function of temperature, T , or time, t ,

$$m = f(T \text{ or } t) \quad (2.26)$$

Quantitative measurements of the mass-changes are possible by determination of the distance, on the curve mass axis, between the two points of interest or between the two horizontal mass levels. In derivative thermogravimetry, the derivative of the mass-change with respect to time, dm/dt , is recorded as a function of time (t) or temperature (T).

$$\frac{dm}{dt} = f(T \text{ or } t) \quad (2.27)$$

A series of peaks are obtained, instead of the step wise curve, in which the areas under the peak are proportional to the total mass-change of the sample. A horizontal plateau in the TG curve gives a corresponding horizontal plateau in the DTG curve because $dm/dt = 0$. A maximum in the DTG curve is obtained when the TG curve has an inflection point where mass is being lost the most rapidly.

A comparison between a conventional (a) and a derivative (b) mass-loss curves is given in Figure 13. The derivative curve may be obtained either from the TG curve by manual differentiation methods or by electronic differentiation of the TG signal.

Accessory equipment is available for most thermobalances so that the DTG curve can be easily recorded along with the TG curve. The DTG curve,

whether derived mathematically or recorded directly. Contains no more information than does an integral TG curve obtained under the same experiment conditions; it simply displays the data differently.

I. Information obtainable from the DTG curve has been summarized by Dunn [68]:

- The DTG curve presents this information in a form that is more visually accessible, whereas the DTG curve contains no more information than does the TG curve.

- The DTG curve allows the ready determination of the temperature at which the rate of mass-change is maximum, T_{max} , and this provides additional information to the extrapolated onset temperature, however, respond to changes in experimental conditions, and T_{max} values are no more characteristic of a material than is T_i or T_f .

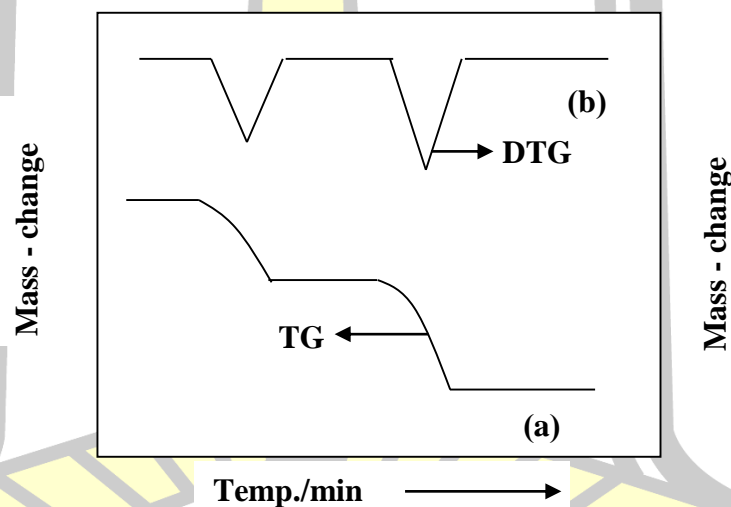


Figure 13. Comparison between (a) integral TG and (b) derivative TG (DTG) mass-loss curves.

- The area under the DTG curve is directly proportional to the mass change.

- The height of the DTG peak at any temperature gives the rate of mass-change at that temperature. These values can be use to obtain kinetic information since equations can be written of the form [80, 81]:

$$\frac{-dm}{dt} = Ae^{\left(\frac{-E}{RT}\right)} f(m) \quad (2.28)$$

II. The advantages of DTG have been summarized

1. The curves may be obtained in conjunction with TG and DTG measurements.

2. The curves for DTA and DTG are comparable, but the results of the former method indicates even those changes of state that are not accompanied by loss in mass. The curves by the latter method are more reproducible.

3. Although the curves for DTA extend over a wider temperature interval, due to subsequent warming of the material after reaction, the DTG measurements indicate exactly the temperature of the beginning, the maximum rate, and the end of the change.

4. On the TG curves, changes following each other very closely cannot be distinguished, as the corresponding stages coincide. The DTG curves of the same change indicate by sharp maxima that the thermogravimetric stages can be divided in to two parts.

5. The DTG curves are exactly proportional to the derivatives of the TG curves; therefore, the area under the curves gives the change in mass precisely. Accordingly, DTG can give exact quantitative analysis.

6. The DTG method can be used for the investigation of materials which for some reason or another cannot be analyzed by DTA. For example, some Organic compounds melt during heating, but even so the DTG method yields fairly good results.

c) Some factors affecting thermogravimetric curves

I. Instrumental (Thermobalance) factors

i) Heating rate

The effect of heating rate change on the procedural decomposition temperature of a sample has been widely studied perhaps the only other parameter that has been studied more is that of the effect of atmosphere on the TG curve. For a single-stage endothermic reaction Simons and Newkirk [82] have

pointed out the following changes for T_i and T_f , as a function of fast (F) and slow (S) heating rates. For the initial procedural decomposition temperature, T_i .

$$(T_i)_F > (T_i)_S$$

For the final procedural temperature, T_f

$$(T_f)_F > (T_f)_S$$

while the reaction interval, $T_f - T_i$, varies according to $(T_f - T_i)_F > (T_f - T_i)_S$

For any given temperature interval, the extent of decomposition is greater at a low rate of heating than for a similar sample heated at a faster rate. If the reaction involved is exothermic, the sample temperature will rise above that of the furnace, and it has been shown that the difference between the furnace temperature and the sample temperature is greatest for the faster rate of heating when a reaction is occurring. When successive reactions are involved, the rate of heating may well determine whether or not this reaction will be separated. The appearance of a point of inflection in the TG curve at a faster heating rate.

ii) Recording or chart speed

The recording of the mass-loss curves for either rapid or slow reaction can have a pronounced effect on the shape of the curves. The lower-chart speed curves shows less separation of the decomposition steps than the higher-chart speed curve.

iii) Effect of furnace atmosphere

The effect of the atmosphere on the mass-change curve depends upon (1) the type of reaction, (2) the nature of the decomposition products, and (3) the type of atmosphere employed. For the atmosphere TG analysis can be performed under a variety of atmosphere conditions, which include high pressure (up to 300 MPa), vacuum (down to 10^{-3} Pa) and atmosphere pressure in the presence of inert, corrosive, oxidizing or reducing gases. High-pressure work requires a metal casing and high-pressure sealing around the sample housing, Gases employed in TG

analysis include air, Ar, Cl₂, CO₂, H₂, HCN, H₂O, He, N₂, O₂ and SO₂. Before attempting to use Cl₂, HCN, or SO₂ it is strongly recommended to consult with a safety officer to ensure the safe use and proper disposal of these harmful gases.

iv) Sample holder

Sample holders range from flat plates to deep crucibles of various capacities. Materials used in their construction may vary from glass, alumina, and ceramic compositions to various metals and metallic alloys. The melting point of the crucible should be at least 100 K greater than the temperature range of the experiment and there must be no chemical reaction between the crucible and the sample. The crucible should transfer heat as uniformly and as efficiently as possible to the sample. The shape, thermal conductivity and thermal mass of the crucible are therefore important. Flat crucibles with a small lip are recommended for powdered samples, but if swelling or spattering is likely then a walled crucible is better. Liquid samples also require a walled crucible. The form of the crucible will to a large extent determine the temperature gradient in the sample.

v) Condition for optimum sensitivity

Greater sensitivity of the thermobalance permits the use of smaller samples with improved determination of mass plateaus of intermediate compounds and the use of faster heating rates. However, thermobalances with sensitivities greater than 1 µg can be attained only under conditions where sample hangs down tubes of 9 mm inside diameter or less if used at atmospheric pressure. Larger-diameter tubes if used at reduced pressure. Unfortunately, the use of the 9 mm tubes limits the sample size to 8-10 mg.

II. Sample Characteristics

i) Sample Mass

The sample mass can affect the TG curve in three ways:

- The extent to which endothermic or exothermic reactions of the sample will cause sample temperature to deviate from a linear temperature change (the larger the sample mass is, the greater the deviation is).
- The degree of diffusion of the product gas through the void space around the solid particles (under static conditions, the atmosphere immediately

surrounding the reacting particles will be somewhat governed by the bulk of the sample).

- The existence of large thermal gradients throughout the sample, particularly if it has a low thermal conductivity. Concerning the effect of sample mass on T_i and T_f values, Richer and Vallet [82] found that T_i was virtually constant for calcium carbonate in the mass range 0.25-1.0 g, both in nitrogen and carbon dioxide. On the other hand, once the decomposition reaction has begun, it generally does not occur uniformly in every particle throughout the entire mass of the sample. Under such non homogeneous condition, it would be expected that time required for complete decomposition of a powdered solid would increase with increase sample mass. Because the furnace heating rate is linear, there would be a resultant increase in the observed value of T_f .

ii) Sample particle size

The effect of sample particle size on the TG curve has been comparatively little studied. Various particle sizes will cause a change in the diffusion of product gases, which will alter the reaction rate and hence the curve shape. Most of studies in this area that have been reported have been concerned with the effect of particle size on the kinetics parameter. Large crystals of the sample may decrepitate, causing sudden the greater will be the extent to which equilibrium is reached, and at any given temperature, the greater the extent of decomposition will be.

Likewise, for a chrysotile sample, Martinez found that the decomposition temperature decreased with a decrease in sample particle size. For the ground material there was a continuous loss in mass from about 50-850 °C, with the most rapid decomposition between 600 and 700°C. For the massive material, there was little mass-loss until a temperature of about 600°C was attained. Similar results were obtained for serpentine and a brucine-carbonate mixture. In general, a decrease in particle size of the sample lowers the temperature at which thermal decomposition begins, as well as the temperature at which the decomposition reactions are completed.

iii) Miscellaneous sample effect

The effect of the heat of reaction of the sample on the mass-loss curve has been studied by Newkrirk [82]. The heat of reaction will affect the

difference between the sample temperature and the furnace temperature causing the sample temperature to lead or lag behind the furnace temperature, depending on whether the heat effect is exothermic or endothermic. Since this temperature change may be 10°C or more, depending on the heating rate employed, the calculation of kinetic constant from mass-loss curves may be unavoidably and significantly in error.

d) Theory of thermal decomposition

One of the most important applications of TGA is the determination of kinetic parameters of the degradation process, such as rate constants, apparent activation energies, reaction orders and pre-exponential factors. The values of the computed parameters will depend not only on the experimental conditions of tests, such as atmosphere, gate rate, sample weight and heating rate, but also on the particular choice of the kinetic model and on the mathematical treatment of data. Many kinetic models were in fact proposed in order to simplify the general kinetic equation and determine the parameters of the degradation process. In the present work the following symbols are used: Apparent activation energy, E_a (kJ/mol); pre-exponential factor, A (min^{-1}); reaction orders, n and m ; gas constant, R (8.3136 J/mol K); absolute, T (K); time, t (min); degree of conversion, α , and heating rate, β (K/min).

The reaction rate in TGA studies can be defined as the variation of degree of conversion with time or temperature where the conversion is calculated in terms of mass loss accordingly Eq.(2.29)

$$\alpha = \left(\frac{W_0 - W_t}{W_0 - W_f} \right) \quad (2.29)$$

where, W_0 , W_t and W_f are respectively, weight at the beginning of the degradation step, actual weight at each point of curve and the final weight measured after the specific degradation process considered. The conversion rate for a kinetic process can be typically indicated as the product of two contributions; one of them is the temperature, which affects the kinetic constant and the other is the concentration of reactive species. Therefore, the most general kinetic model for the degradation process is shown in Eq. (2.30)

$$\frac{d\alpha}{dt} = k(T) \cdot f(\alpha) \quad (2.30)$$

where k is the reaction rate constant, $f(\alpha)$ the reaction model and α the conversion fraction. Integrating the above equation gives the integral rate law

$$g(\alpha) = kt \quad (2.31)$$

where $g(\alpha)$ is the integral reaction model. The temperature dependence of the rate constant is usually described by the Arrhenius-type equation, such as Eq. (2.32).

$$k(T) = A \exp\left(\frac{-E_a}{RT}\right) \quad (2.32)$$

On the other hand, following the complexity of the multiple degradation reaction, the function $f(\alpha)$ is generally very complex and it is not possible to solve the differential equation (Eq. 2.37) leading to the necessity to introduce some simplifications for the determination of the kinetic parameters. The simplest expression proposed for $f(\alpha)$ is the use of the n^{th} -order model represented in Eq. (2.33).

$$f(\alpha) = (1-\alpha)^n \quad (2.33)$$

while a slightly higher complexity is introduced by the use of the autocatalytic model represented in Eq. (2.34)

$$f(\alpha) = (1-\alpha)^n \alpha^m \quad (2.34)$$

A lot of effects are been dedicated to the computation of the apparent activation energy of the thermal degradation of polymers, and some reported approaches have become a classic in the scientific literature.

So the combination of Eq. (2.30), (2.31) gives the following equation:

$$\frac{d\alpha}{dt} = A \exp\left(\frac{-E_a}{RT}\right) (1-\alpha)^n \quad (2.35)$$

$$g(\alpha) = A \exp\left(\frac{-E_a}{RT}\right) \quad (2.36)$$

about the heating, $\beta = (dT/dt)$ Eq. (2.35) modifies to

$$\frac{d\alpha}{(1-\alpha)^n} = \frac{A}{B} \exp\left(\frac{-E_a}{RT}\right) dT \quad (2.37)$$

$$g(\alpha) = \int_0^\alpha \frac{d\alpha}{f(\alpha)} = \frac{A}{B} \int_0^T \exp\left(\frac{-E_a}{RT}\right) dT = \frac{AE_a}{\beta R} p(x) \quad (2.38)$$

where $x = \frac{E_a}{RT}$ and $p(x) = -\int_\infty^x \frac{\exp(-x)}{x^2} dx$

Based on the degree of conversion measurement, α , and on the heating rate, β there are several methods available for the calculations of the apparent activation energy. Hence, the determinations of the kinetic parameters for the degradation from the TGA data are strongly depend on the method of calculation. The number of methods to determine the apparent activation energy based on one or multiple heating rates of the TGA curve namely, Flynn-Wall-Ozawa [80, 81, 82]

Ozawa's method is based on Doyle's approximation

$$\log p(x) \approx -2.315 - 0.457x$$

or

$$\log p(x) \approx -5.330 - 1.052x$$

For $20 < x < 60$, Eq. (2.38) can be written as

$$\ln g(\alpha) = \ln \frac{AE_a}{\beta R} - 5.330 - 1.052 \frac{E_a}{RT} \quad (2.39)$$

Here, A and R is constants and for a particular α or weight loss percentage, $g(\alpha)$ is a constant. Then Eq. (2.39) becomes

$$\ln \beta = C - 1.052 \cdot \left(\frac{E_a}{R} \right) \cdot \Delta \left(\frac{1}{T} \right) \quad (2.40)$$

Where C is a constant and is given by

$$C = \ln \frac{AE_a}{g(\alpha)R} - 5.330$$

Hence, the value of E_a can be computed by Ozawa's method for any particular weight loss, being determined from the linear dependence of $\ln \beta$ vs $1/T$ plot at different heating rates.

Another isoconversional procedure, introduced by Friedman technique based on single-rate method, has been widely used. This method utilizes the following natural logarithmic differential equation:

$$\ln \left(\frac{d\alpha}{dt} \right) = \ln \left(\beta \frac{d\alpha}{dt} \right) = \ln A + n \ln(1-\alpha) - \frac{E_a}{RT} \quad (2.41)$$

By plotting $\ln d\alpha/dt$ or $\ln(1-\alpha)$ against $1/T$ for a constant heating rate, a straight line could be obtained with a slope of $-E/R$. Additionally, the E/nR value could be slope of the linear plot of $\ln(1-\alpha)$ versus $1/T$.

The standard isoconversional method is based on taking the natural logarithm of Eq. (2.36) giving,

$$\ln(t) = \ln \left(\frac{g(\alpha)}{A} \right) + \frac{E}{RT} \quad (2.42)$$

Equation (2.42) has been used as the kinetic method to study the isothermal TG of degradation. The natural logarithm of the time taken to reach a fixed weight loss is linearly depending on the reciprocal of the temperature, provided that the order of the decomposition reaction n remains constant within the temperature and weight-loss interval under consideration, the E and $\ln A$ can be, respectively,

calculated by the value of slope and intercept of the linear relationship of $\ln(t)$ versus $1/T$ for the whole range of α values.

e) Prediction of lifetime estimates (t_f)

The lifetime, if, of polymer failure at a constant temperature can be predicted by using the following equation:

$$t_f = \left(1 - (1 - \alpha)^{1-n}\right) \frac{e^{\frac{E}{RT}}}{(A(1-n))} \quad (n \neq 1) \quad (2.43)$$

f) Applications of TG

The method of thermogravimetry is basically quantitative in nature in that the mass change can be accurately determined. However, the temperature ranges in which the mass- changes occur are qualitative in that they depend on the instrumental and sample characteristic [71]. With the wide use of commercial thermobalances. TG data of a sample can be correlated from laboratory to laboratory if similar conditions of pyrolysis are employed. The application of thermogravimetry to a particular problem if a mass – change is observed on the application of heat.

Some of the many applications of thermogravimetry are listed as follows:

1. Thermal decomposition of inorganic, organic, and polymeric substances.
2. Corrosion of metals in various atmospheres at elevated temperatures.
3. Solid-state reactions.
4. Roasting and calcimine of minerals.
5. Distillation and evaporation of liquids.
6. Pyrolysis of coal, petroleum, and wood.
7. Determination of moisture, volatiles, and ash contents.
8. Rates of evaporation and sublimation.

The applications to polymer materials include comparisons of the relative thermal stability, the effect of additives on the thermal stability, moisture and

additive contents, studies of degradation kinetic, direct quantitative analysis of various copolymer systems, oxidation stability and many others.

2.14 Mechanical properties

Discussion of the mechanical properties of solid polymers often contains two interrelated objectives. The first of these is to obtain adequate macroscopic description of the particular facet of polymer behavior under consideration. The second objective is to seek an explanation of this behavior in molecular term, which may include details of chemical and physical structures [79].

The results obtained from mechanical tests are very considerable, due to many factors, such as the difference in shape or size of the test piece or perhaps its preparation. The storage of material, test method or conditions can all make substantial differences to the test results. Polymer behavior is particularly sensitive to the preconditioning of the test piece and the actual test conditions. Comparable test results can never be obtained unless care is taken to ensure uniform temperature, humidity levels and testing rates. To ensure reproducible results, standardized equipment design and test procedures must be used. Standard also help in indicating suitable test conditions and techniques as well as revealing possible sources of test error.

In this section, some basic methods used for testing the mechanical properties of the polymer materials will be described.

2.14.1 Stress-strain behavior

In stress-strain tests the buildup of force (or stress) is measured as the specimen is being deformed at constant rate. Occasionally, stress-strain tests are modified to measure the deformation of a specimen as the force is applied at a constant rate, and such tests are becoming ordinary with the advent of commercially available load controlled test machines. Stress-strain tests have traditionally been the most popular and universally used of all mechanical tests and are described by ASTM standard tests, such as D638, D883 and D412. Since the properties of polymer are time dependent, the shape of the observed curve will depend on the strain rate and temperature. The great variation in stress-strain behavior of polymer as measured at a

constant rate of strain can be classified into five main types as shown in Figure 14. The soft and weak class (a) of polymer, including polyisobutylene, is characterized by a low modulus of elasticity, low yield (stress) point, and moderate time dependent elongation. The Poisson ratio, i.e., the ratio of contraction to elongation, for class (a) polymer is 0.5, which is similar to that of liquids.

In contrast, the Poisson ratio of hard and brittle class (b) polymers such as polystyrene, approaches 0.3. Class (b) polymers are characterized by a high modulus of elasticity, a poorly defined yield point, and little elongation before failure. However, class (c) polymers stretch after the yield point, the area under the entire curve, which represents toughness, is greater than that in class (b).

Rigid PVC is representative of hard and strong class (d) polymers. These polymers have a high modulus of elasticity and high yield strength. The curve for hard and tough class (e) polymers, such as ABS copolymers, shown moderate elongation prior to the yield point followed by nonrecoverable elongation. In general, the behavior of all classes is Hookean prior to the yield point. The reversible recoverable elongation prior to the yield point, called the elastic range, is primarily the result of bending and stretching covalent bonds in the polymer backbone. This useful portion of the stress-strain curve may also include some recoverable uncoiling of polymer chain. Irreversible slippage of polymer chain is the predominant mechanism after the yield point. Since these properties are time dependent, class (a) polymers may resemble class (d) polymers if the stress is applied rapidly, and vice versa. These properties are also temperature dependent. Hence, the properties of class (c) polymers may resemble class (b) polymers when the temperature is decreased.

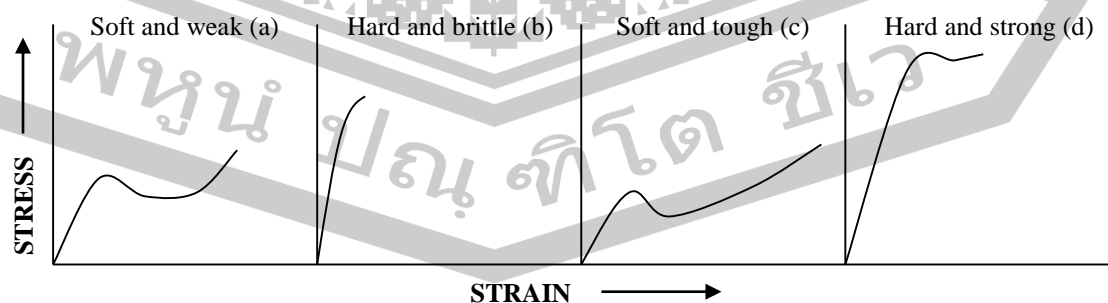


Figure 14. Typical stress-strain curves for plastic.

Figure 15 [71] Illustrates the terminology used for stress-strain testing. The slope of the initial straight-line portion of the curve is the elastic modulus of the material. In tensile test, this modulus is Young's modulus (E) [80].

$$E = \frac{d\sigma}{d\varepsilon} \quad (2.44)$$

The maximum in the curve denotes the stress at yield, σ_y , and the elongation at yield, ε_y . The end of the curve denotes the failure of the material, which is characterized by the tensile strength, σ_B , and the ultimate strain or elongation to break ε_B . The slope of the stress-strain curve evaluating at the origin is termed the elastic modulus, E , and is taken to be a measure of the stiffness of the materials. Finally, the area under the stress-strain curve is called the toughness and has units of energy per volume. These values are determined from a stress-strain curve while the actual experimental values are generally reported from a stress-strain curves. Thus, the experimental curves require a transformation of scales to obtain the desired stress-strain curves. This is accomplished by the following definitions for tensile test, the stress (σ) is expressed by:

$$\sigma = \frac{F}{A} \quad (2.45)$$

where, F is the force and A is the cross-section area. If the cross-section is that of undeformed specimen, this is called the *engineering stress*. If the area is continuously monitored or known during test, this is the *true stress*. The strain (ε) can be defined as:

$$\varepsilon = \frac{L - L_0}{L_0} \quad (2.46)$$

where L_0 is the initial sample length and its stretched length is L . This definition, ε is known as the engineering strain.

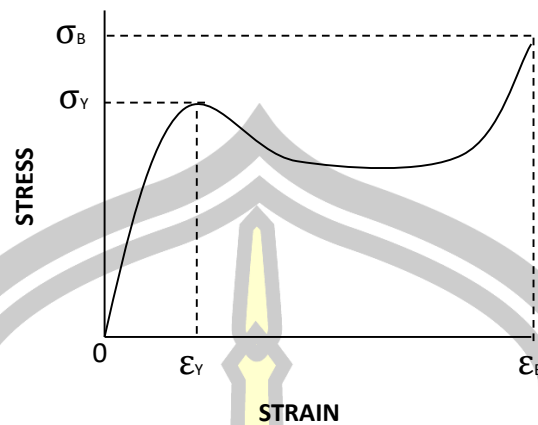


Figure 15. Schematic of stress-strain testing.

2.15 Dynamic Mechanical Analysis (DMA)

Dynamic mechanical properties [83] refer to the response of a material as it is subjected to a periodic force. These properties may be expressed in terms of a dynamic modulus, a dynamic loss modulus, and a mechanical damping term. Typical values of dynamic moduli for polymers range from 10^6 - 10^{12} dyne/cm² depending upon the type of polymer, temperature, and frequency.

For an applied stress varying sinusoidally with time, a viscoelastic material will also respond with a sinusoidal strain for low amplitudes of stress. The sinusoidal variation in time is usually described as a rate specified by the frequency ($f = \text{Hz}$; $\omega = \text{rad/sec}$). The strain of a viscoelastic body is out of phase with the stress applied, by the phase angle, δ . This phase lag is due to the excess time necessary for molecular motions and relaxations to occur. Dynamic stress, σ , and strain, ε , given as:

$$\sigma = \sigma_o \sin(\omega t + \delta) \quad (2.47)$$

$$\varepsilon = \varepsilon_o \sin(\omega t) \quad (2.48)$$

where ω is the angular frequency. Using this notation, stress can be divided into an “inphase” component ($\sigma_o \cos\delta$) and an “out-of-phase” component ($\sigma_o \sin\delta$) and rewritten as,

$$\sigma = \sigma_o \sin(\omega t) \cos \delta + \sigma_o \cos(\omega t) \sin \delta \quad (2.49)$$

Dividing stress by strain to yield a modulus and using the symbols E' and E'' for the inphase (real) and out-of-phase (imaginary) moduli yields:

$$\sigma = \varepsilon_o E' \sin(\omega t) + \varepsilon_o E'' \cos(\omega t) \quad (2.50)$$

$$E' = \frac{\sigma_o}{\varepsilon_o} \cos \delta \quad E'' = \frac{\sigma_o}{\varepsilon_o} \sin \delta \quad (2.51)$$

$$\varepsilon = \varepsilon_o \exp(i\omega t) \quad \sigma = \sigma_o \exp(\omega t + \delta)i \quad (2.52)$$

$$E^* = \frac{\sigma}{\varepsilon} = \frac{\sigma_o}{\varepsilon_o} e^{i\delta} = \frac{\sigma_o}{\varepsilon_o} (\cos \delta + i \sin \delta) = E' + iE'' \quad (2.53)$$

Equation (2.53) shows that the complex modulus obtained from a dynamic mechanical test consists of “real” and “imaginary” parts. The real (storage) part describes the ability of the material to store potential energy and release it upon deformation. The imaginary (loss) portion is associated with energy dissipation in the form of heat upon deformation. The above equation is rewritten for shear modulus as,

$$G^* = G' + iG'' \quad (2.54)$$

where G' is the storage modulus and G'' is the loss modulus. The phase angle δ is given by

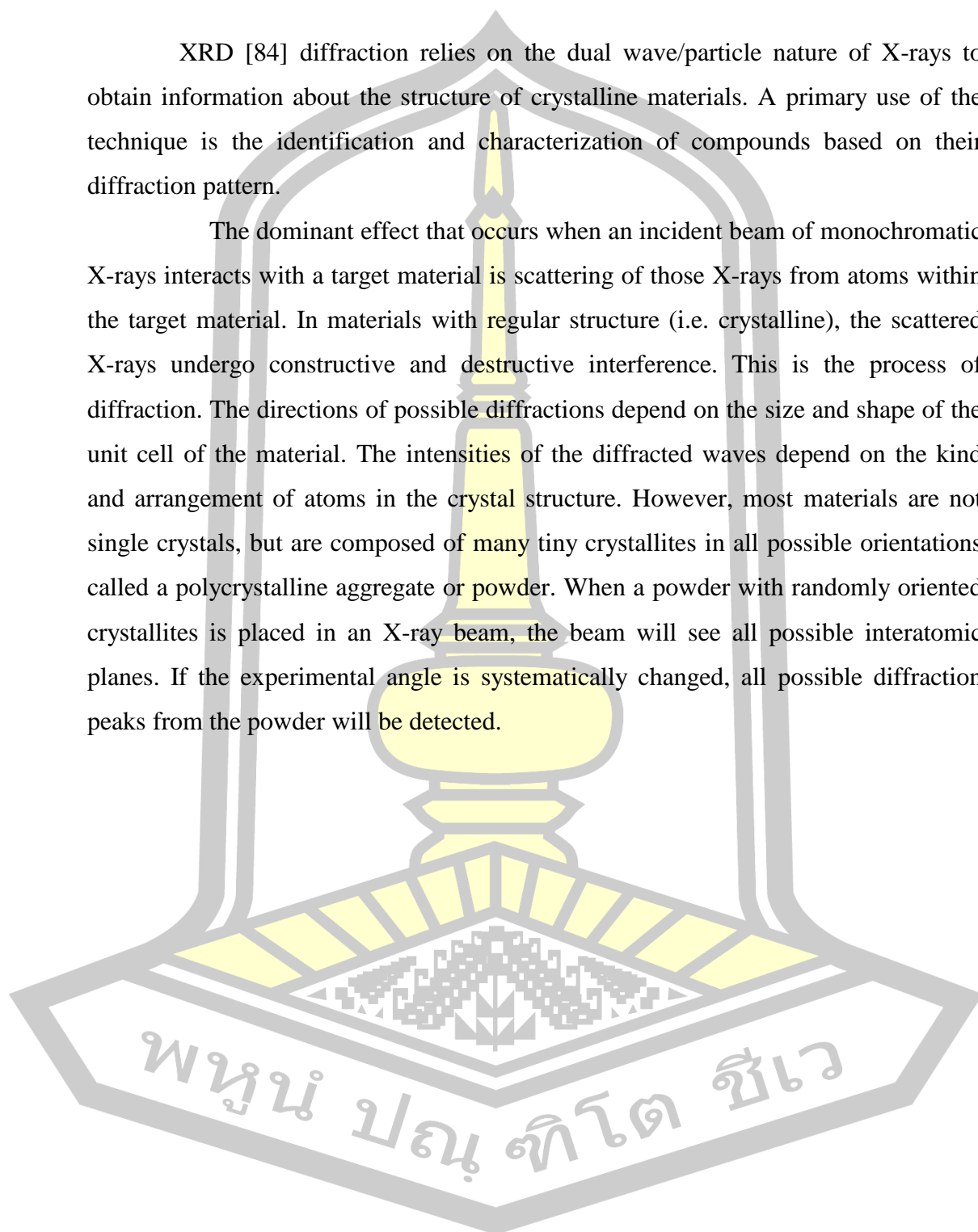
$$\tan \delta = \frac{G''}{G'} \quad (2.55)$$

The storage modulus is often times associated with “stiffness” of a material and is related to the Young’s modulus, E . The dynamic loss modulus is often associated with “internal friction” and is sensitive to different kinds of molecular motions, relaxation processes, transitions, morphology and other structural heterogeneities. Thus, the dynamic properties provide information at the molecular level to understanding the polymer mechanical behavior.

2.16 X-Ray Diffraction analysis (XRD)

XRD [84] diffraction relies on the dual wave/particle nature of X-rays to obtain information about the structure of crystalline materials. A primary use of the technique is the identification and characterization of compounds based on their diffraction pattern.

The dominant effect that occurs when an incident beam of monochromatic X-rays interacts with a target material is scattering of those X-rays from atoms within the target material. In materials with regular structure (i.e. crystalline), the scattered X-rays undergo constructive and destructive interference. This is the process of diffraction. The directions of possible diffractions depend on the size and shape of the unit cell of the material. The intensities of the diffracted waves depend on the kind and arrangement of atoms in the crystal structure. However, most materials are not single crystals, but are composed of many tiny crystallites in all possible orientations called a polycrystalline aggregate or powder. When a powder with randomly oriented crystallites is placed in an X-ray beam, the beam will see all possible interatomic planes. If the experimental angle is systematically changed, all possible diffraction peaks from the powder will be detected.



CHAPTER 3

METHODOLOGY

3.1 Materials

3.1.1 Dispersed phases

3.1.1.1 Liquid crystalline polymer (LCP)

The polymer dispersed phases used in this study was Rodrun LC3000, supplied by Unikita Co., Ltd. (Tokyo, Japan). Rodrun LC3000 was a copolyester of 60 mol% *p*-hydroxy benzoic acid (HBA) and 40 mol% poly(ethylene terephthalate) (PET) with a melting point at 220°C and a density of 1.41 g/cm³. The chemical structure of this polymer is shown in Figure 16(a). In this report, Rodrun LC3000 was denoted as LCP.

3.1.1.2 Recycled poly(ethylene terephthalate) (rPET)

rPET dispersed phase used in this work was obtain from various brands of drinking water providing in the area of Mahasarakham Province. The rPET collected from post-consumer soft drink bottles were cleaned and cut into small pieces with dimension of about 3 x 3 mm². The chemical structure of PET is shown in Figure 16(b).

3.1.1.3 Poly(lactic acid) (PLA)

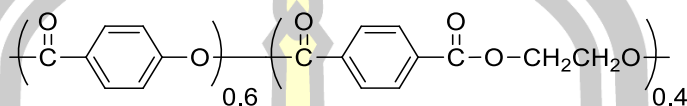
Poly(lactic acid) (PLA) (NatureWorks LLC, Ingeo™ Grade 3251D, MFI = 6 g/10 min, average Mw ~ 110,100 g/mol, $T_g = 57.1$ °C, $T_m = 149$ °C, density = 1.24 g/cm³) was purchased from BC Polymers Marketing Co. Ltd. (Thailand. The chemical structure of PLA is shown in Figure 16(c).

3.1.2 Matrix phase

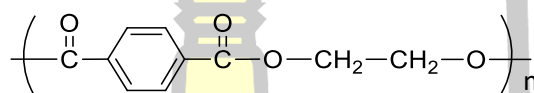
High density polyethylene (PE) trade name 5000s with an MFI of 0.80 g/10 min was also used as the matrix phase. The material has number average molecular weight of 59×10^3 g/mol and weight average molecular weight of 294.0×10^3 g/mol. This polymer was purchased from Bangkok Polyethylene, Thailand. The chemical structure of PE is shown in Figure 16(d).

3.1.3 Compatibilizer

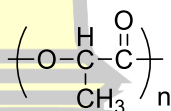
The compatibilizers used in this work was polyethylene-graft-maleic anhydride (PE-g-MA), supplied by S.M. Chemical Supplies Co.,Ltd., Thailand. From the Singma-Aldrich product literature, the compatibilizer contains MA about 3 wt%. The chemical structures of PE-g-MA is shown in Figure 16(e).



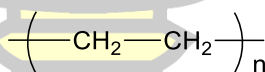
(a) Rodrun LC3000 (LCP)



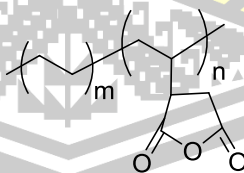
(b) poly(ethylene terephthalate) (PET)



(c) poly(lactic acid) (PLA)



(d) polyethylene (PE)



(f) polyethylene-graft-maleic anhydride (PE-g-MA)

Figure 16. Chemical structures of (a) Rodrun LC3000 (LCP), (b) poly(ethylene terephthalate) (PET), (c) poly(lactic acid) (PLA), (d) polyethylene (PE) and (e) polyethylene-graft-maleic anhydride (PE-g-MA).

3.2 Composite preparation

3.2.1 Mixing process

Before mixing with extrusion process, all materials were dried in vacuum oven at 70°C for at least 12 h. The PLA blends containing various contents of LCP and rPET and PE blends at various compositions were extruded using a single-screw extruder (Haake Rheomex, Thermo Electron (Karlsruhe) GmbH, Karlsruhe, Germany), with a screw diameter of 16 mm, length-to-diameter (L/D) ratio of 25, a die diameter of 2 mm and a screw speed of 100 rpm. The schematic diagram of the extruder is shown in Figure. 17. The temperature profiles used was 190-220-220-225°C for LCP and 190-225-250-255°C rPET containing composites. The temperature profiles shown here represent the temperatures at the hopper zone, two barrel zones and heating zone in the die head, respectively. The extruded strands were immediately quenched in a water bath and cut into pellets using pelletizing machine. The sample codes of the extruded strand blends are designated as PLA-*a*LCP (or rPET) and PE-*b*PLA-*c*rPET (orLCP)-*d*MA where *a*, *b*, *c* and *d* depicts the concentration of dispersed phase in wt%. For the compatibilized system, the content of PE-*g*-MA was fixed 5 wt% (*d* = 5).

3.2.1 Hot drawing process

To improve the fibrillation of dispersed phases, the pellets of polymer matrix and its composites were further fabricated as a composite fiber form using mini-single screw extruder (Randcastle, RCP-0625, Cedar Grove, USA, screw diameter = 16 mm, length-to-diameter ratio = 24, diameter of capillary die = 1.15 mm) conducted with a hot drawing machine. The spinning temperature was set at 180/190/230/255. The temperature profiles represent the temperatures at zone 1, zone 2, zone 3 and die, respectively. The as-spun fibers were drawn to different draw ratio in hot glycerol bath at 110°C. The schematic diagram of the mini-extruder is shown in Figure 18.

To improve drawability, the addition of various content of PE into the composites was carried out. Moreover, PE-*g*-MA is also used for enhancing of the compatibility of the composite systems. The mixing condition was the same as that of LCP-or rPET containing composites. The sample were designed as PE-*b*PLA-*c*rPET

(or LCP)-*d*MA, where *b*, *c* and *d* depicts the content of rPET or LCP, PLA, PE and PE-g-MA in wt%, respectively.

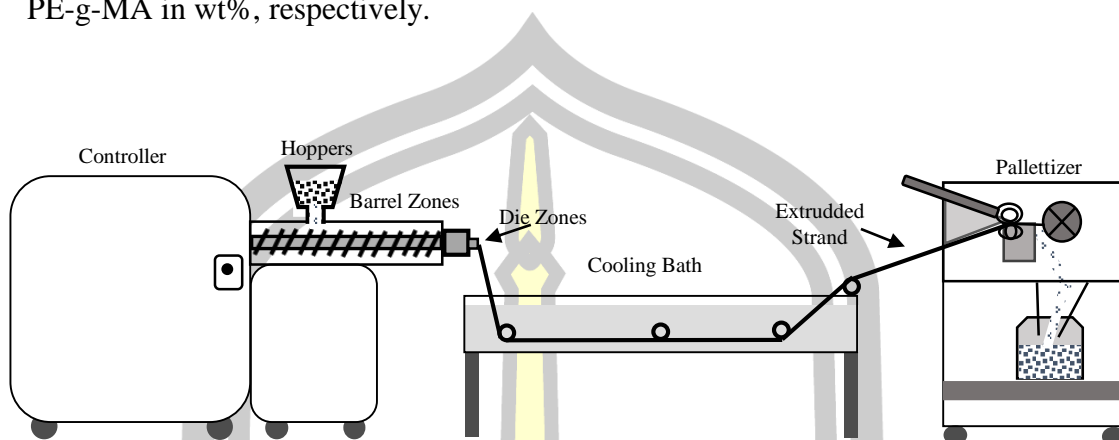


Figure 17. Schematic diagram of a single-screw extruder and pelletizer.

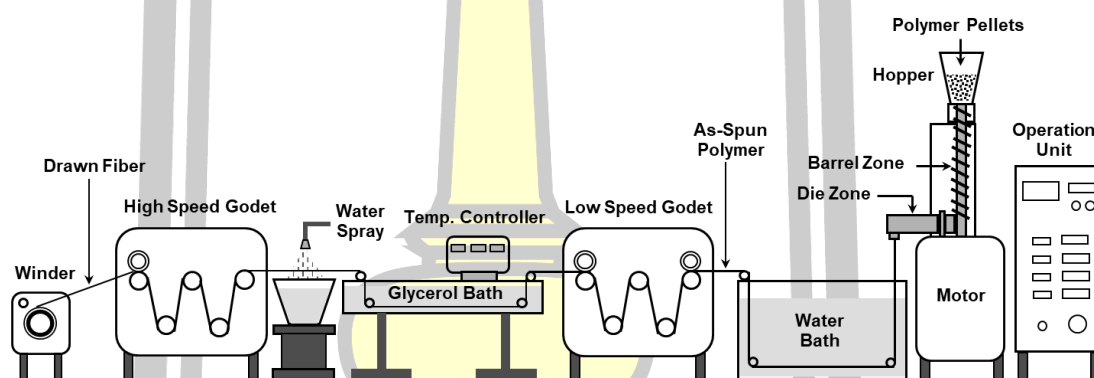


Figure 18. The schematic diagram of the mini-extruder. [85]

3.3 Characterizations

3.3.1 Measurements of rheological behavior in the molten state

The rheological behavior in the molten state for all neat polymers and its blends was characterized with a plate-and-plate rheometer (Physica Anton Paar, MCR5000, Physica Messtechnik GmbH, Stuttgart, Germany). The extruded strands were cut into pellets and compression-molded at 200°C (for 5 min) into a sheet about 1.5 mm thick. The sample sheet was punched into disk 25 mm in diameter. The complex viscosity (η^*), storage modulus (G') and loss modulus (G'') of all specimens were measured in an oscillatory shear mode with the strain amplitude of 5% within

the angular frequency (ω) range of 0.5-500 rad/s. The measuring temperatures for LCP and rPET systems are 225 and 260°C, respectively. The gap between the two plates is set at 0.9 mm.

3.3.2 Morphological characterization

The surfaces morphology of extruded strand, as-spun and drawn fibers was observed under the scanning electron microscope (SEM) (LEO-01455VP and LEO-1450, Cambridge JEOL, England) operated with an accelerating voltage of 20 kV. Prior to examination, the samples were immersed in liquid nitrogen for 30 min and then fractured. The specimens were sputter-coated with gold for enhanced surface conductivity.

3.3.3 Measurements of thermal decomposition behavior

3.3.3.1 Non-isothermal heating

The thermogravimetric analysis (TGA) were carried out using TA instruments, SDT Q600 (Luken's drive, New Castle, DE). The pellet cut from the extruded strand and the neat and composite fibers of 8-10 mg were loaded in alumina crucible and then nonisothermally heated from ambient temperature to 700°C at heating rates of 10°C/min. The measurement was performed in nitrogen and in air with the flow rate of 100 mL/min. The TG and DSC data were simultaneously recorded online in TA instrument's Q series Explorer software. The analyses of the TG data are done using TA Instrument's Universal Analysis 2000 software (version 3.3B).

3.3.4 Fourier transform IR (FTIR) analysis

For characterization of compatibilizing effect, the extruded strands were cut into pellets and compressed as thin film by compression molding using a two-piece stainless steel mold at 200°C. The functional groups of the compatibilized blends were characterized by using Fourier transform IR (FTIR) (Perkin Elmer, Spectrum GX FTIR system, United Kingdom). A resolution of 4 cm⁻¹ and a minimum of 32 scans was carried out.

3.3.5 Measurements of tensile properties

Tensile properties of the as-spun and drawn fibers were measured at room temperature with an Instron mechanical tester (Model 5566, Instron, Canton, MA, grip length = 25 mm, crosshead speed = 50 mm/min, full scale load = 1 kN). Stress-strain curves, Secant modulus, tensile strength, and elongation at break of the

polymers were recorded. The secant modulus used in this manuscript is defined as the slope of the line connecting the origin and a given point (1% strain) on the stress-strain curve, or the ratio of nominal stress to corresponding strain at any specified point (1% strain) on the stress-strain curve. The average value of five measurements for each sample was determined.

3.3.6 Differential scanning calorimetric (DSC) analysis

The melting temperature (T_m) and crystallization temperature (T_c) of the extruded strand, as-spun, neat polymers, and drawn fibers measured using a differential scanning calorimeter (DSC) (Perkin-Elmer, Pyris Diamond). Samples of about 3-5 mg were placed in aluminum pan and heated from 20 °C to 200 °C at a heating rate of 10°C/min under nitrogen atmosphere. The percentage crystallinity (X_c) of samples were calculated according to the following equation:

$$X_c = \frac{\Delta H_f}{\Delta H_f^0} \times 100$$

where X_c = % crystallinity

ΔH_f = the enthalpy of fusion (J/g)

H_f^0 = Heat of fusion of perfectly crystalline PLA and PE i.e., 93 J/g [86, 87] and 293 J/g [88], respectively.

3.3.7 X-Ray Diffraction analysis (XRD)

The structure of the drawn fibers will be measured using XRD (D8 advance, Bruker, Germany), in a reflection mode, using a computer controlled wide angle goniometer coupled to a sealed-tube source of $Cu K\alpha$ radiation, operating at 30 kV and 50 mA. The slit system used for collecting the 2θ scans allowed for the collection of the diffracted beam with a divergence angle of less than 0.05.

The summarized flow chart of the whole experimental are illustrated in Figure 19 and Figure 20.

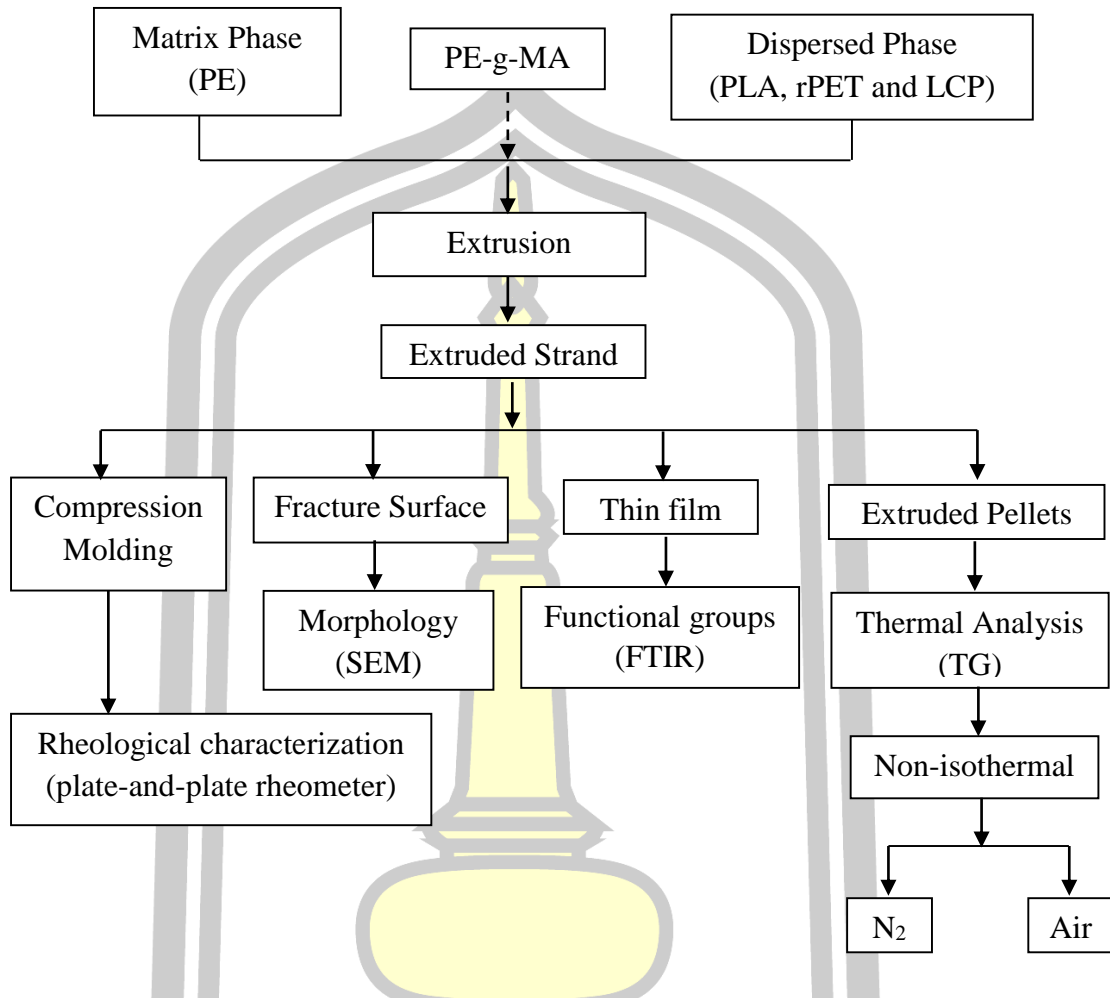


Figure 19. Flow charts of the whole experiments of preparation and characterization of preparation and characterization of extruded strands.



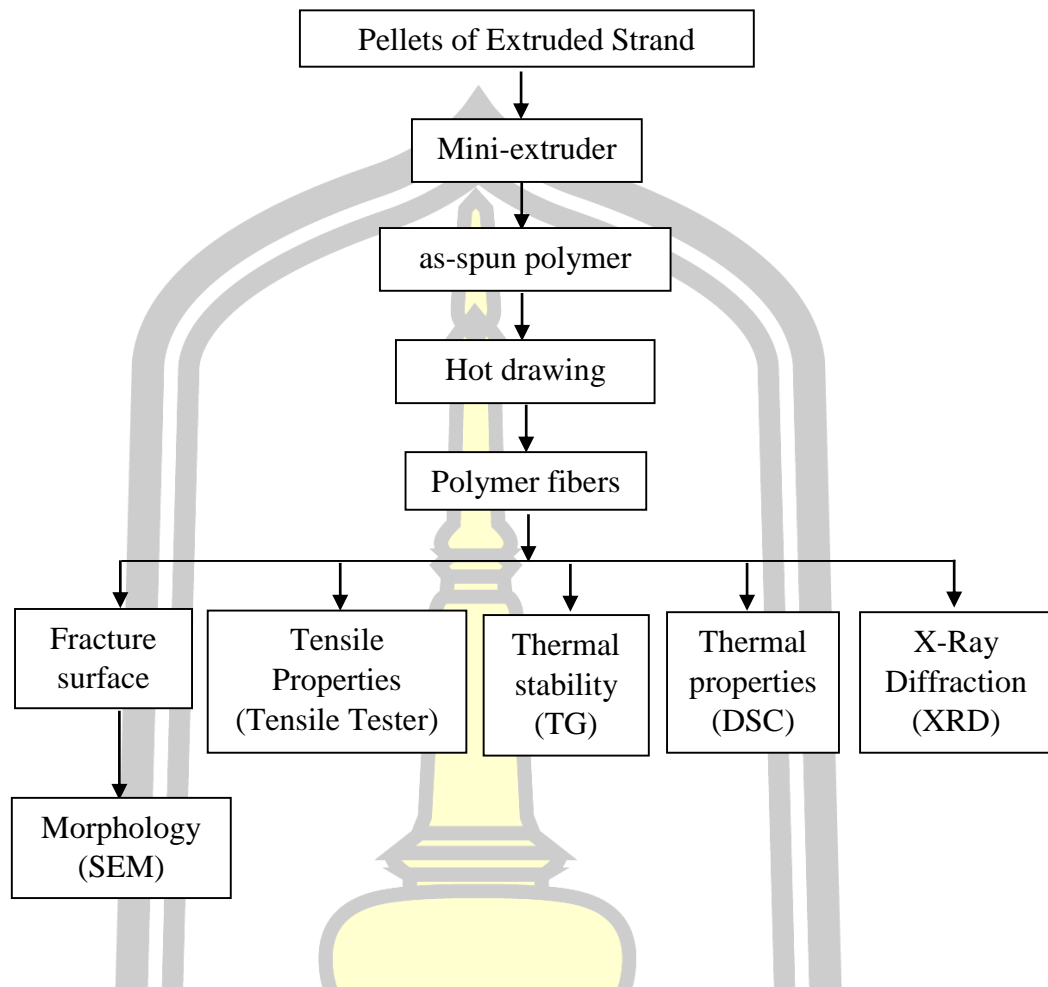


Figure 20. Flow charts of the whole experiments of preparation and characterization of Preparation and characterization of composite fibers.



CHAPTER 4

RESULTS AND DISCUSSION

4.1 Effect of LCP and rPET contents on melt rheological properties of PLA-based composites

To predict the fibrillation ability of rPET compared with LCP dispersed phase in PLA matrix, rheological measurement is a convenient method for investigation of morphological evolution.

In this study, different temperature profiles are used for the preparation PLA/LCP and PLA/rPET blends due to different melting temperatures of the dispersed phases. Rheological measurements in the molten state of PLA/LCP and PLA/rPET blends are carried out at 225 and 260°C, respectively. Figure 21 shows the frequency (ω) dependence of complex viscosity (η^*) for all analyzed samples. For PLA/LCP blends (Figure 21A), it is seen that LCP exhibits non-Newtonian behavior; the viscosity decreases with increasing shear rate (or shear frequency) due to the shear induced chain orientation, leading to a reduction in the chain entanglement density. PLA and its blends with 10-20 wt% LCP are seen to exhibit Newtonian behavior compared with LCP. However, non-Newtonian behavior is still observed for the blend containing 30 wt% LCP. From the rheological results, it can be summarized that the addition of 10 and 20 wt% LCP into PLA does not affect the intrinsic Newtonian behavior of PLA. In the case of the PLA/rPET system (Figure 21B), at low shear frequency ($\omega < 10^2$ rad/s), flow curves of PLA and rPET exhibit Newtonian behavior, whereas shear thinning behavior (η^* values of the blends decreased with increasing frequency) is observed for all composites. At high shear frequency ($\omega > 10^2$ rad/s), η^* values of all sample increase and converge to nearly the same value with increasing ω (an unknown error occurred). It is interesting to note that, at frequency range 10^1 - 10^2 rad/s, η^* of the blends are nearly the same and lower than those of PLA and rPET.

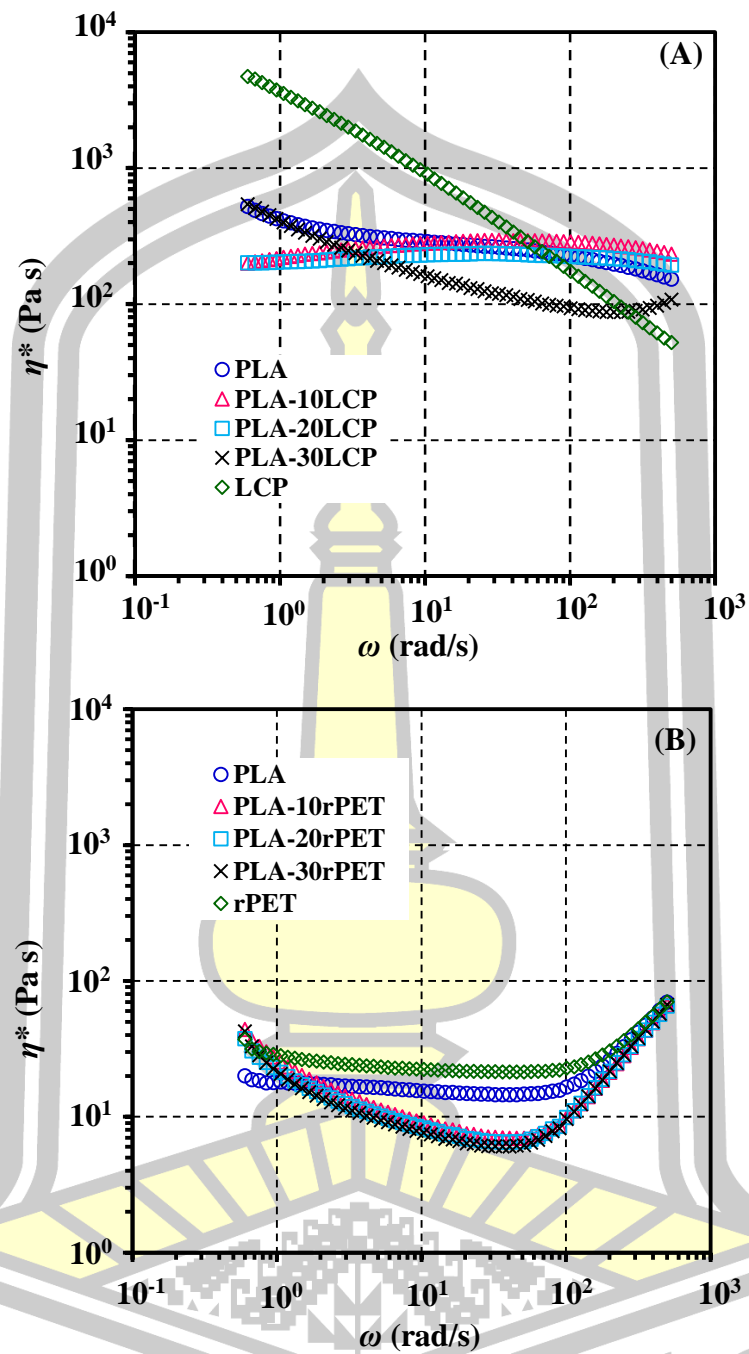


Figure 21. η^* vs. ω for (A) PLA/LCP and (B) PLA/rPET blends containing various dispersed phase contents measured at 225 and 260 °C, respectively.

Study on viscoelastic properties using melt rheological data is one of the simple techniques widely used for characterization of interaction in the polymer composites or blends. Figure 22 shows the elastic and viscous characteristics of the blend system which can be considered from the plots of the storage modulus (G') and loss modulus (G''), respectively, as a function of ω . The viscoelastic data at low frequency generally provide information about long-range (beyond entanglement distance) relaxation, while the values at high frequency provide information about short range (motion with entanglement) relaxation [89]. As seen from Figures 4.2, G' and G'' of all polymers increases with increasing frequency, indicating a viscoelastic properties dependence of the timescale of molecular motion. As seen Figure 4.2 IA, the LCP loading clearly affect G' at low ω region ($\omega < 10$ rad/s). At high frequency, the G' values are nearly the same. The results indicate that the LCP loadings, especially at high contents remarkably level up the elastic properties of the composites due to the rigid-chain structure of LCP. It is interesting to note that viscous properties of the neat polymer and its blends are not significantly different over the whole range of ω examined (Figure 22IIA). In the case of PLA/rPET blends (Figure 22IB), G' of the blends are nearly the same and lower than that of neat matrix, indicating a viscoelastic properties dependence of the timescale of molecular motion. The G'' of the blends are lower than those of PLA and rPET especially at higher angular frequency (Figure 22IIB). At the same composition for both types of the blends, G'' values of the neat polymers and all blends are mostly higher than the corresponding G' values in the whole frequency range. This indicates that the viscous characteristics for these samples are dominant factor.

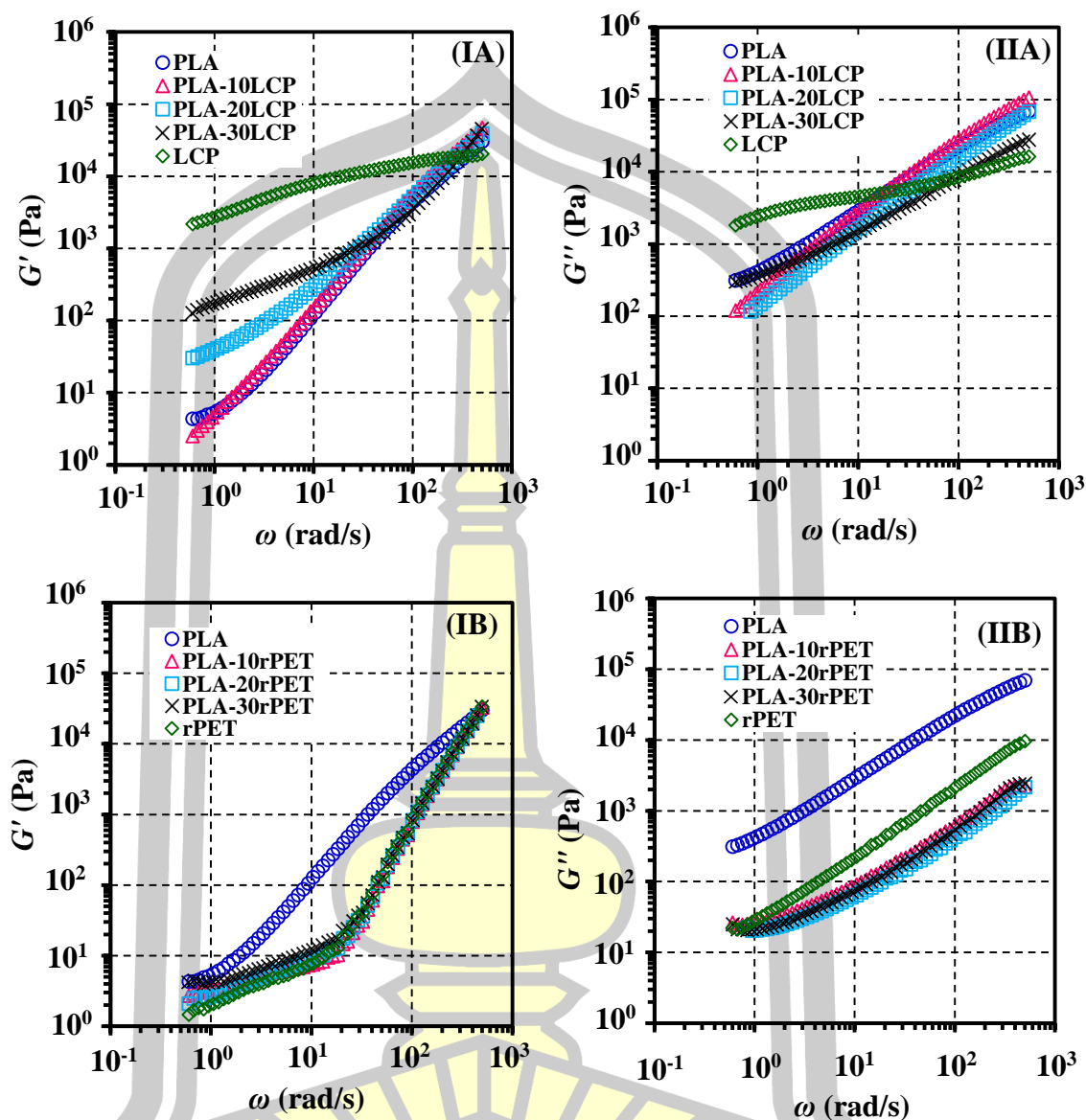


Figure 22. G' (column I) and G'' (column II) versus ω for (A) PLA-LCP and (B) PLA-rPET blends containing various contents of dispersed phase. The measurements of G' and G'' for PLA/LCP and PLA/rPET blends are carried out at 225 and 260°C, respectively.

4.2 Effect of PLA contents on melt rheological properties of PE/PLA blends

This research not only interested about the fibrillation of rPET and LCP dispersed phase in PLA matrix, but also studied fibrillation of PLA dispersed phase in PE matrix. The study on rheological properties using rheological measurement is one of the simple techniques used to predict fibrillation of dispersed phase in matrix phase.

The complex viscosity (η^*), storage modulus (G') and loss modulus (G'') as a function of angular frequency (ω) for the PE/PLA blends system are presented in Figure 23. As seen from Figure 4.3A, all polymers, except PLA, exhibit shear thinning behavior. The complex viscosity clearly decrease with 20-30 wt% PLA loading. At frequency range lower than 10^2 rad/s, PLA exhibits Newtonian fluid behavior due to the loss of entanglement density of the polymer chains. Moreover, at high shear frequency ($\omega > 10^2$ rad/s) PLA exhibits the shear hardening effect. As seen from Figure 23B, G' of all polymer samples increase with increase in ω indicating a dependence of G' on the time scale of molecular motion. The G' of the blends containing 20-30 wt% PLA are lower than that of the neat matrix, arising from the contribution of the dispersed PLA phases. This indicates that PLA containing blends with high enough content play an important role in promoting the chain mobility, leading to a decrease in chain rigidity. Figure 23C, it is seen that G'' values are slightly decrease with increase in dispersed phase contents. Note that, G'' values of the same sample are mostly higher than the corresponding G' values in the whole frequency range, indicating that the viscous characteristics for all polymers are dominant factor.

พหุ ประถมศึกษา

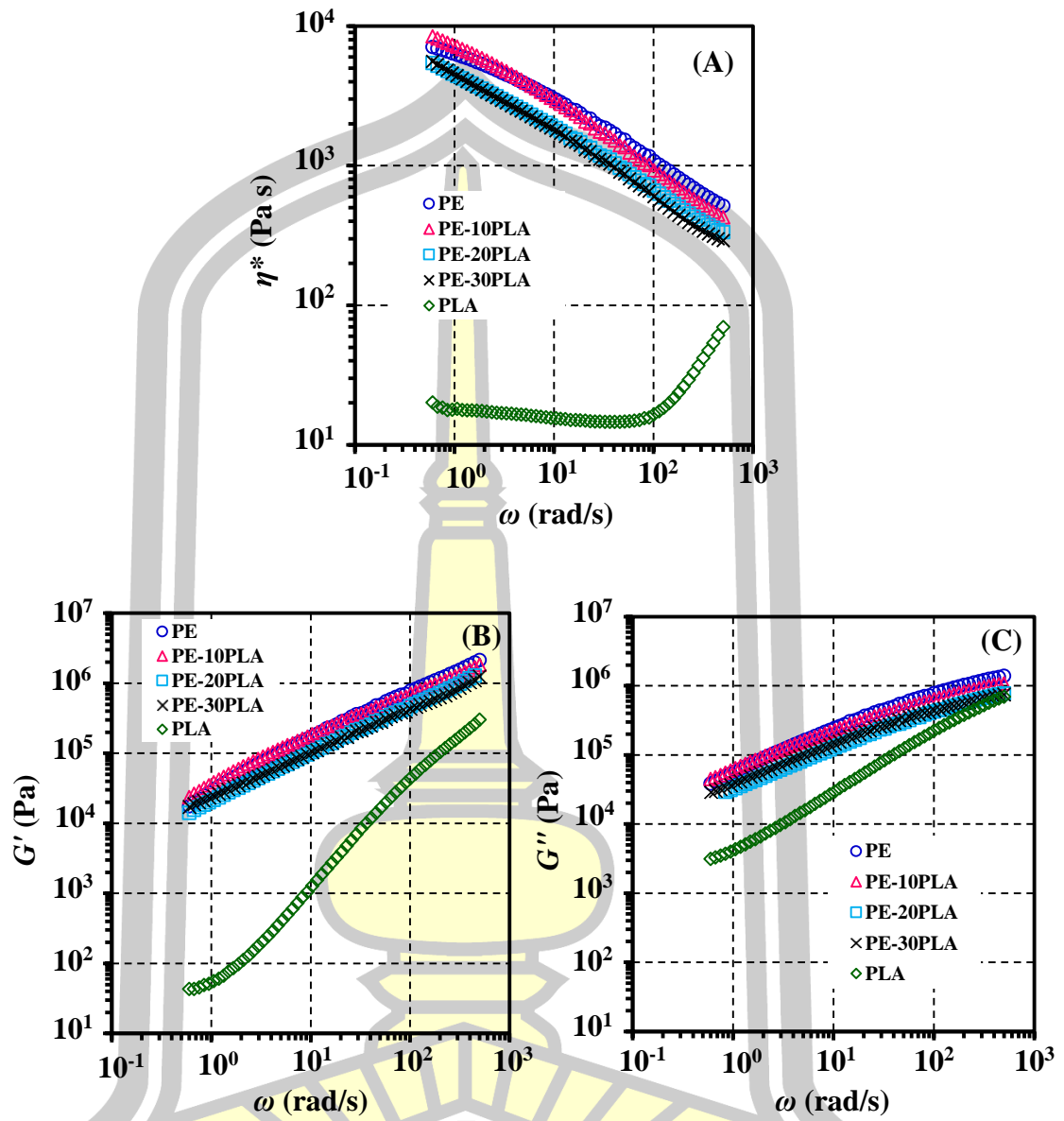


Figure 23. η^* (A), G' (B) and G'' (C) for PE, PE-10PLA, PE-20PLA, and PE-30PLA and viscosity ratio (D) for PE/PLA blend system at 260°C.

4.3 Effect of rPET and compatibilizer on melt rheological properties of PE/PLA blends

Figure 4.4 shows the complex viscosity (η^*), storage modulus (G') and loss modulus (G'') as a function of angular frequency (ω) of the PE-10PLA-10rPET and PE-10PLA-10rPET-5MA in comparison with those of PE, PLA and PE-10PLA. As seen from Figure 24A, the η^* of rPET exhibits Newtonian behavior at low shear frequency ($\omega < 10^2$ rad/s) and shows the shear hardening at high frequencies. The complex viscosity of the rPET-containing blends decrease when compared with PE-10PLA. This indicates that the addition of rPET into PE-10PLA improves melt processability. Figure 24B and C show the respective G' (elastic behavior) and G'' (viscous behavior) of polymers as a function of ω . As seen from Figure 24B, a dependence of G' on the time scale of molecular motion is appeared as a result from the increase in G' with ω for all samples. However, the viscoelastic characteristics (G' and G'') for all blends are nearly the same and much higher than those of rPET. At the same composition for neat and all blends G'' values are mostly higher than the corresponding G' values in the whole frequency range. This indicates that the viscous characteristics for these sample are dominant factor. In the case of compatibilized blend systems, the η^* of PE-10PLA-5MA and PE-10rPET-5MA (Figure 25A) show similar trend as that of PE-10PLA-10rPET-5MA (Figure 24A) indicating that blend systems exhibit shear thinning behavior. It is seen that the η^* of PE-10PLA-5MA is lower than those of PE-10rPET and PE-10rPET-5MA. It is found that G' and G'' of compatibilized blends are nearly the same. However, the presence of PE-g-MA compatibilizer slightly affects the melt rheological properties of the of the blend systems.

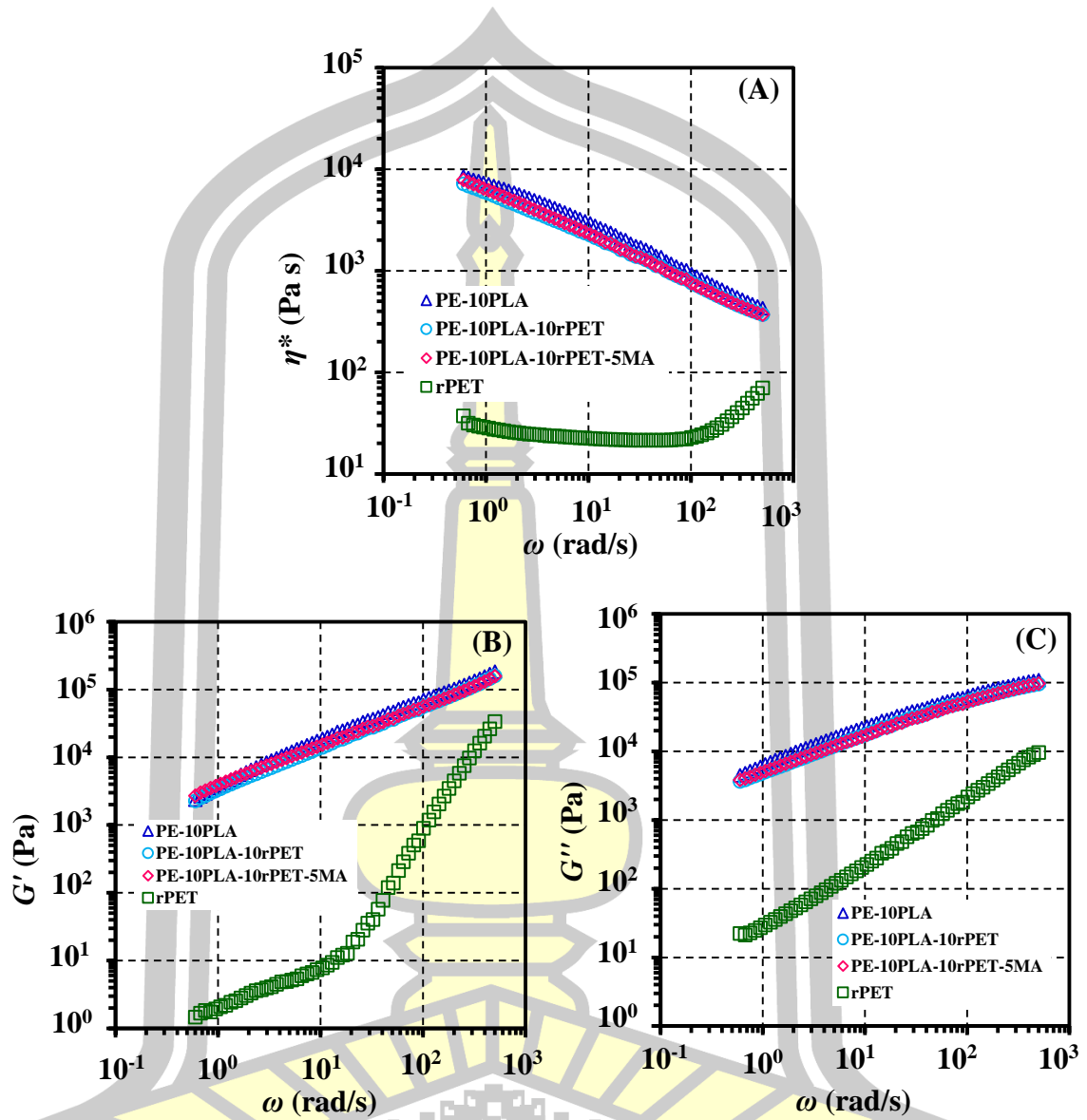


Figure 24. η^* (A), G' (B) and G'' (C) for PE-10PLA, PE-10PLA-10rPET and PE-10PLA-10rPET-5MA, and viscosity ratio (D) for PE/PLA blend system at 260°C.

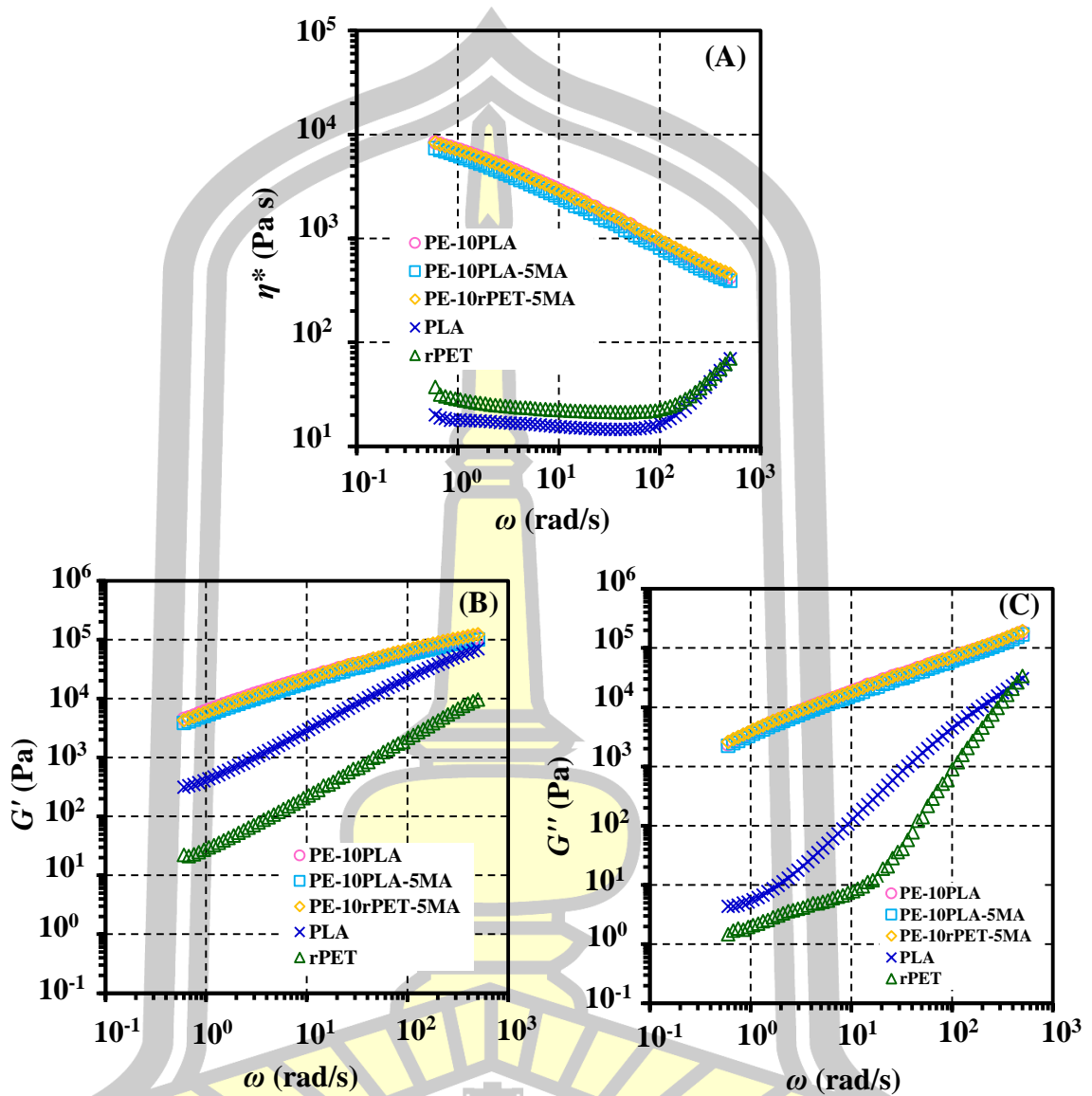
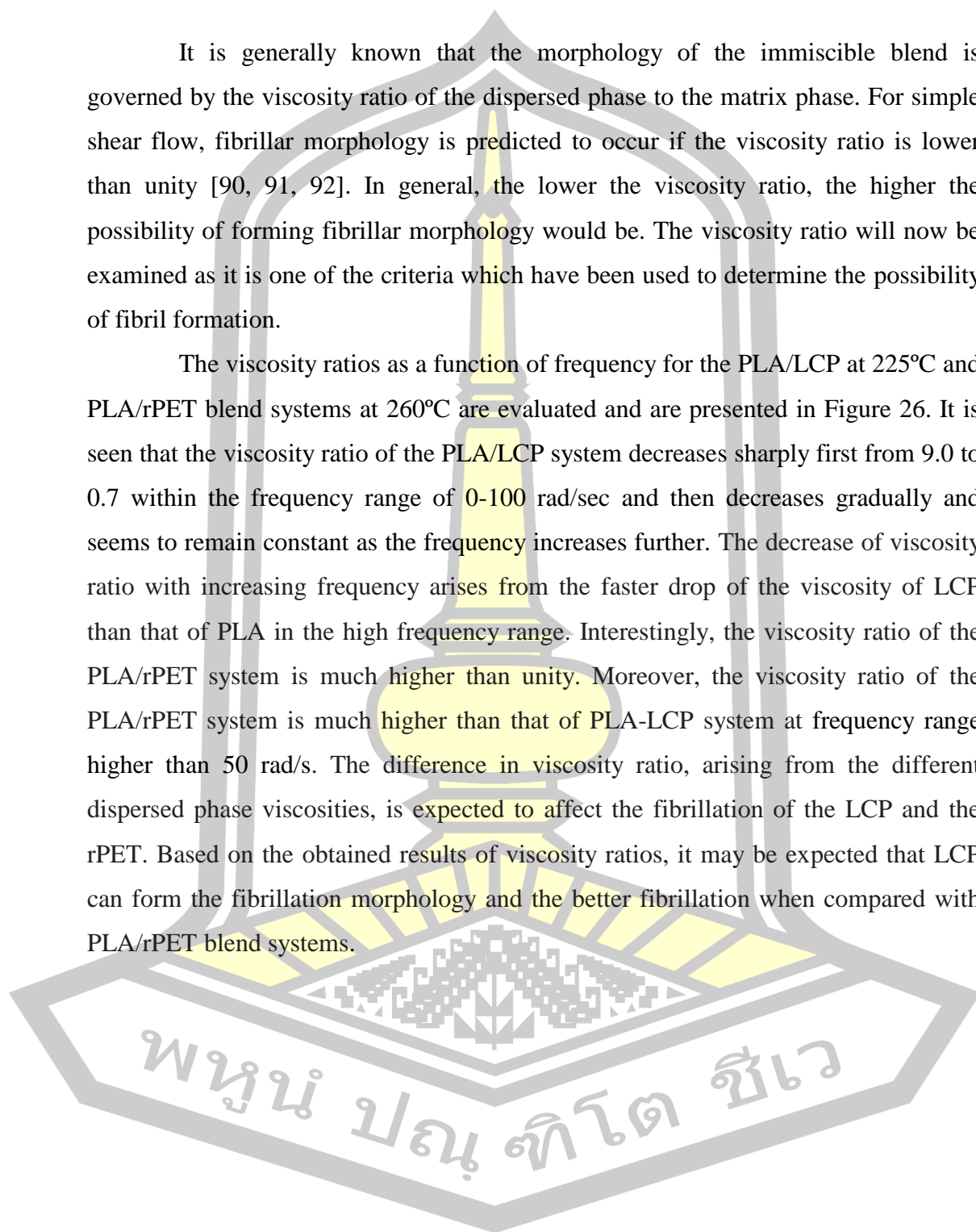


Figure 25. η^* (A), G' (B) and G'' (C) versus ω for PE-10PLA, PE-10PLA-5MA, PE-10rPET-5MA, PLA and rPET at 260°C.

4.4 Viscosity ratios of LCP/PLA and rPET/PLA blends

It is generally known that the morphology of the immiscible blend is governed by the viscosity ratio of the dispersed phase to the matrix phase. For simple shear flow, fibrillar morphology is predicted to occur if the viscosity ratio is lower than unity [90, 91, 92]. In general, the lower the viscosity ratio, the higher the possibility of forming fibrillar morphology would be. The viscosity ratio will now be examined as it is one of the criteria which have been used to determine the possibility of fibril formation.

The viscosity ratios as a function of frequency for the PLA/LCP at 225°C and PLA/rPET blend systems at 260°C are evaluated and are presented in Figure 26. It is seen that the viscosity ratio of the PLA/LCP system decreases sharply first from 9.0 to 0.7 within the frequency range of 0-100 rad/sec and then decreases gradually and seems to remain constant as the frequency increases further. The decrease of viscosity ratio with increasing frequency arises from the faster drop of the viscosity of LCP than that of PLA in the high frequency range. Interestingly, the viscosity ratio of the PLA/rPET system is much higher than unity. Moreover, the viscosity ratio of the PLA/rPET system is much higher than that of PLA-LCP system at frequency range higher than 50 rad/s. The difference in viscosity ratio, arising from the different dispersed phase viscosities, is expected to affect the fibrillation of the LCP and the rPET. Based on the obtained results of viscosity ratios, it may be expected that LCP can form the fibrillation morphology and the better fibrillation when compared with PLA/rPET blend systems.



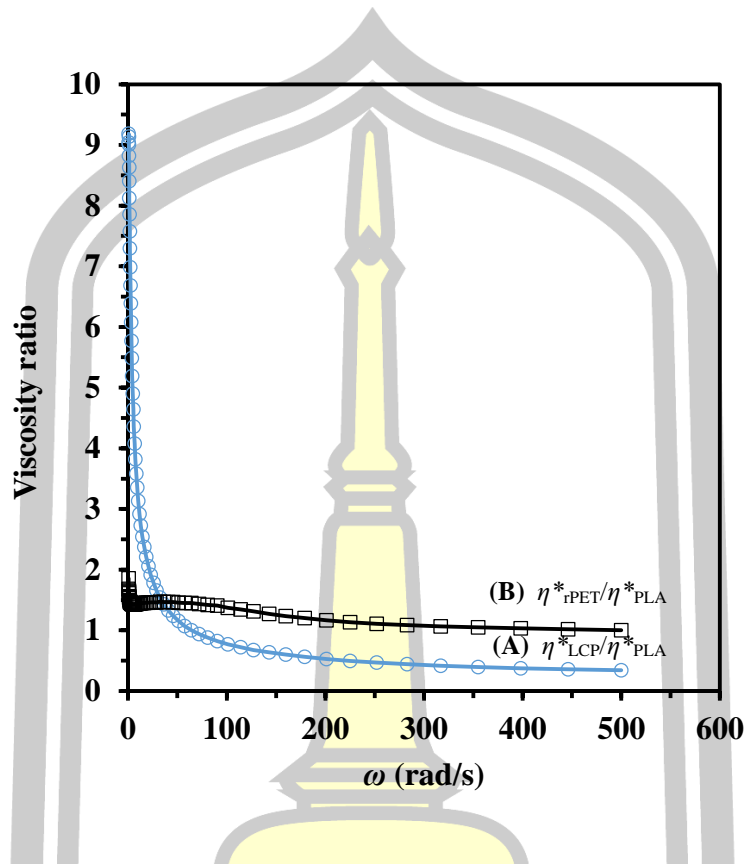


Figure 26. Viscosity ratio versus ω for (A) PLA-LCP and (B) PLA-rPET blending systems, measured at 225 and 260°C, respectively.



4.5 Viscosity ratios of rPET/PE and PLA/PE blends

The viscosity ratios as a function of frequency for the PE-PLA at 225°C and PE-rPET blend systems at 260°C are evaluated and are presented in Figure 27. The viscosity ratios of both composite systems sharply increase from 0.002 to 0.14 as the frequency increases from 0-500 rad/s. However, the viscosity ratios of both composite systems are comparable and much lower than unity, suggesting that the deformation of both rPET and PLA dispersed phases would occur in PE matrix phase.

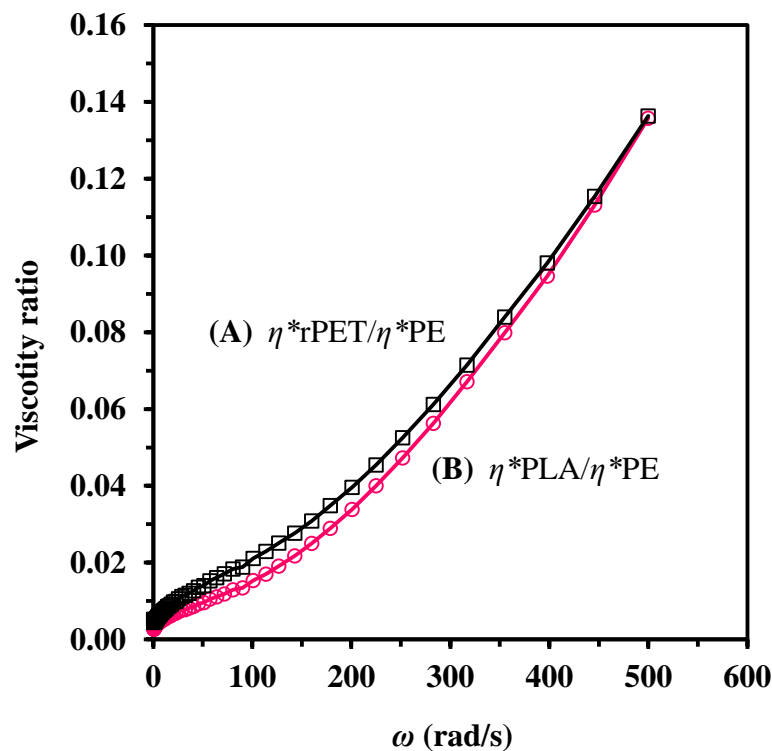


Figure 27. Viscosity ratio versus ω for (A) PE-PLA and (B) PE-rPET blending systems, measured at 225 and 260°C, respectively.

4.6 Effect of LCP and rPET minor contents on morphology of the PLA-based composite strands

It is well known that the final properties of the fiber reinforce polymer composite depend on its phase morphology which is affected by several important factors such as rheological behavior, composition, interfacial tension, processing condition and fabrication techniques. In the present study, the morphology of the fracture surface is studied by means of SEM. Figure 28 shows the SEM micrographs of the fracture surfaces for the PLA/LCP and PLA/rPET extruded strands containing various LCP and rPET contents. For LCP-containing composites, most of the LCP domains appeared as droplets. With increasing LCP contents, increasing in LCP droplet size is observed due to the intramolecular coalescence of molten LCP phase that occurs during extrusion. Moreover, pull-out trace of LCP is clearly observed arising from poor compatibility between PLA and LCP. In the case of the PE/rPET system, most of rPET domains appear as small droplets and the diameter of rPET domains seems to progressively increase with increasing rPET contents. Interestingly, the domain size of the rPET is much smaller than that of the LCP, due to the difference in the melt viscosity and intrinsic nature of two polymers.

As seen from the morphological results that both LCP and rPET minor phase can be dispersed as droplets in PLA matrix. Therefore, the fibrillation of both dispersed phases is expected to occur after further process using hot drawing process. Unfortunately, the fiber of both PLA based-composites could not be obtained after hot drawing process has been tried. The difficulty of fiber fabrication of the PLA-based composites may arise from the intrinsic properties of PLA such as low melt strength etc. Therefore, the PE/PLA composites prepared using PLA as the minor phase is the interesting novel system with expectation of ease of processing.

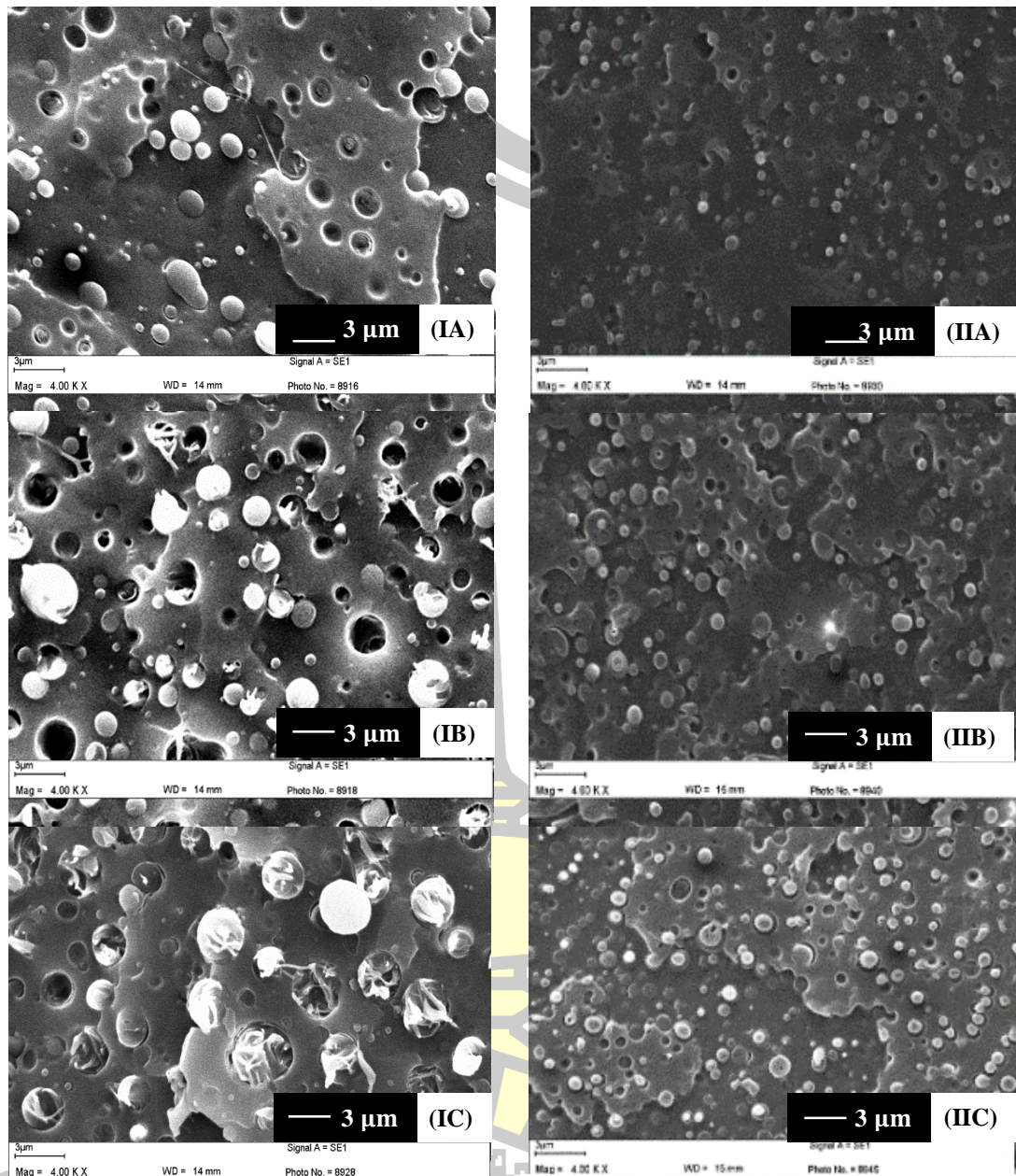


Figure 28. SEM micrographs of the fracture surface for PLA/LCP (column I) and PLA/rPET (column II) blends containing (A) 10, (B) 20, and (C) 30 wt% dispersed phase.

4.7 Effect of PLA contents on morphology of the PE based-composite

Figure 29 shows SEM micrographs of the fracture surface for the PE/PLA extruded strands containing various PLA contents. Most of PLA domains appear as small droplets. The diameter of PLA domains seems to progressively increase with increasing PLA loading and lies in the range of 0.2 to 1.0 μm . The pull-out traces of PLA droplets are observed on the fracture surface due to low adhesion at the interface between PLA and PE phases. According to the results of the viscosity ratio shown earlier (Figure 26), it may be expected, from the low viscosity ratios for the PE/PLA systems, that the fibrillar morphology could be obtained from these blend systems. However, the fact that PLA was broken down into small droplets may be due to the high viscosity of the system and limited coalescence. Furthermore, the deformation of the dispersed-phase droplets into fibrillation structures or coalescence of the dispersed-phase domains generally depends on the ratio between the viscous forces (that tend to elongate the droplets) and the interfacial forces (that tend to keep the drop spherical). This ratio is frequently described by the Capillary number (Ca) which is defined by [93].

$$Ca = \frac{\eta_m \dot{\gamma}}{(\sigma/b)} \quad (4.1)$$

Where η_m is the viscosity of the matrix, $\dot{\gamma}$ is the shear rate, b is the initial diameter of dispersed droplets, and σ is the interfacial tension between the matrix and dispersed phase. Meanwhile, the lower the viscosity ratio, the higher the possibility of forming fibrillary morphology would be. The viscosity ratio will now be examined as it is one of the criteria which have been used to determine the possibility of fibril formation of the dispersed phase. The viscosity ratio for PE/PLA is lower than 0.14, the fibrillation of the rPET domains is not clearly observed in as-extruded strand. According to Equation (4.1), there can be two possibilities that cause the Ca to be low. They are small initial diameter (b) of the dispersed phase and the high interfacial tension. However, the fibrillation of PLA can be expected to occur if higher shear or elongational force during processing is applied.

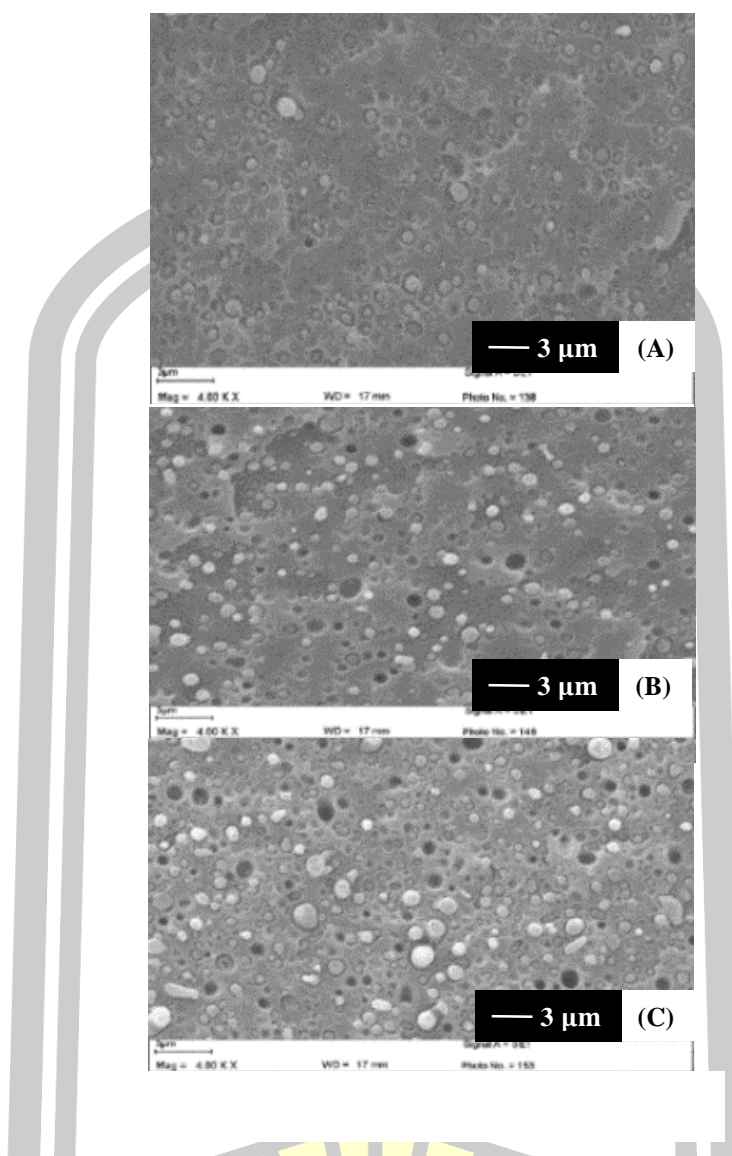
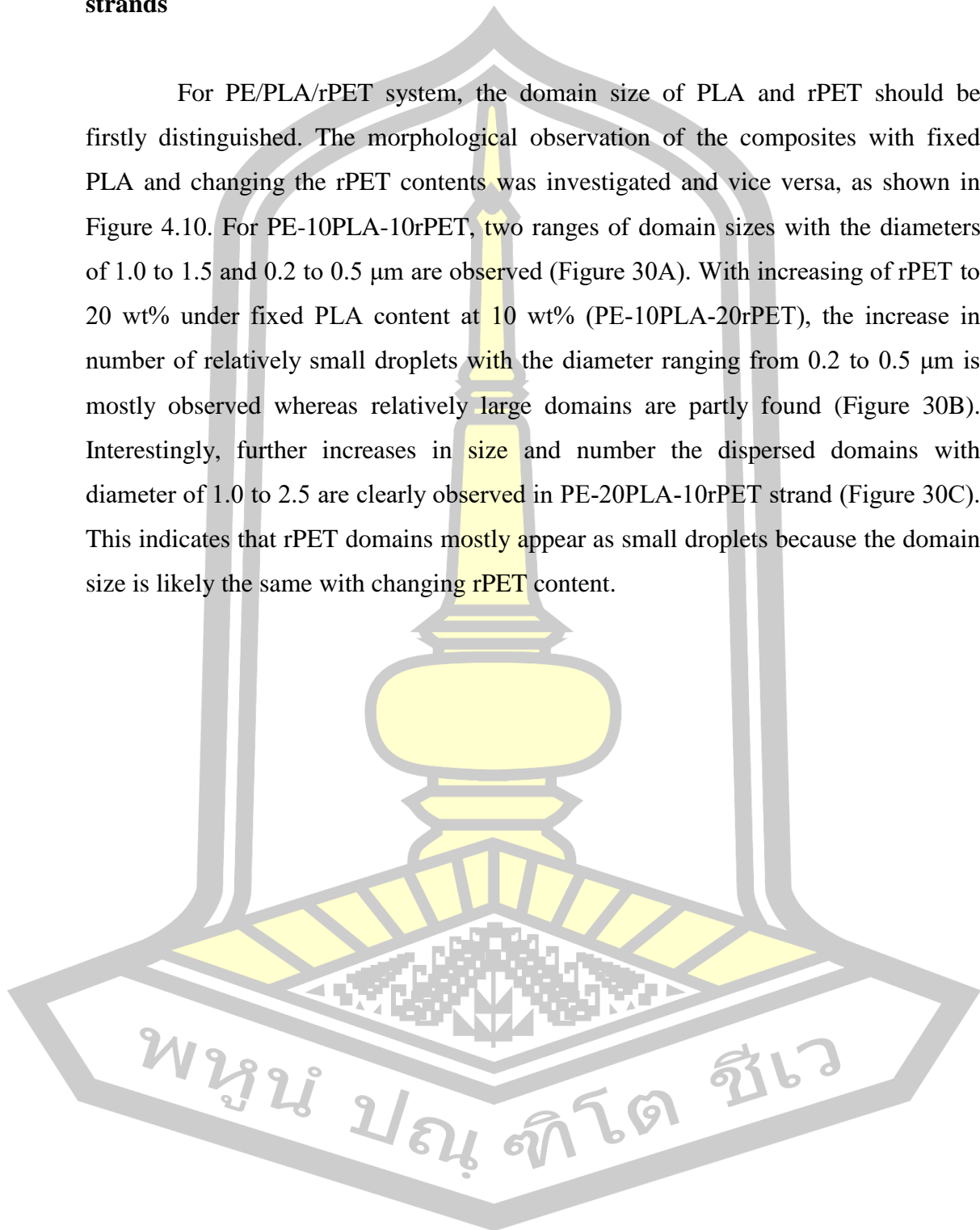


Figure 29. SEM micrographs of the fracture surface for PE/PLA blends containing (A) 10, (B) 20, and (C) 30 wt% dispersed phase.



4.8 Effect of rPET contents on morphology of the PE/PLA/rPET extruded strands

For PE/PLA/rPET system, the domain size of PLA and rPET should be firstly distinguished. The morphological observation of the composites with fixed PLA and changing the rPET contents was investigated and vice versa, as shown in Figure 4.10. For PE-10PLA-10rPET, two ranges of domain sizes with the diameters of 1.0 to 1.5 and 0.2 to 0.5 μm are observed (Figure 30A). With increasing of rPET to 20 wt% under fixed PLA content at 10 wt% (PE-10PLA-20rPET), the increase in number of relatively small droplets with the diameter ranging from 0.2 to 0.5 μm is mostly observed whereas relatively large domains are partly found (Figure 30B). Interestingly, further increases in size and number the dispersed domains with diameter of 1.0 to 2.5 are clearly observed in PE-20PLA-10rPET strand (Figure 30C). This indicates that rPET domains mostly appear as small droplets because the domain size is likely the same with changing rPET content.



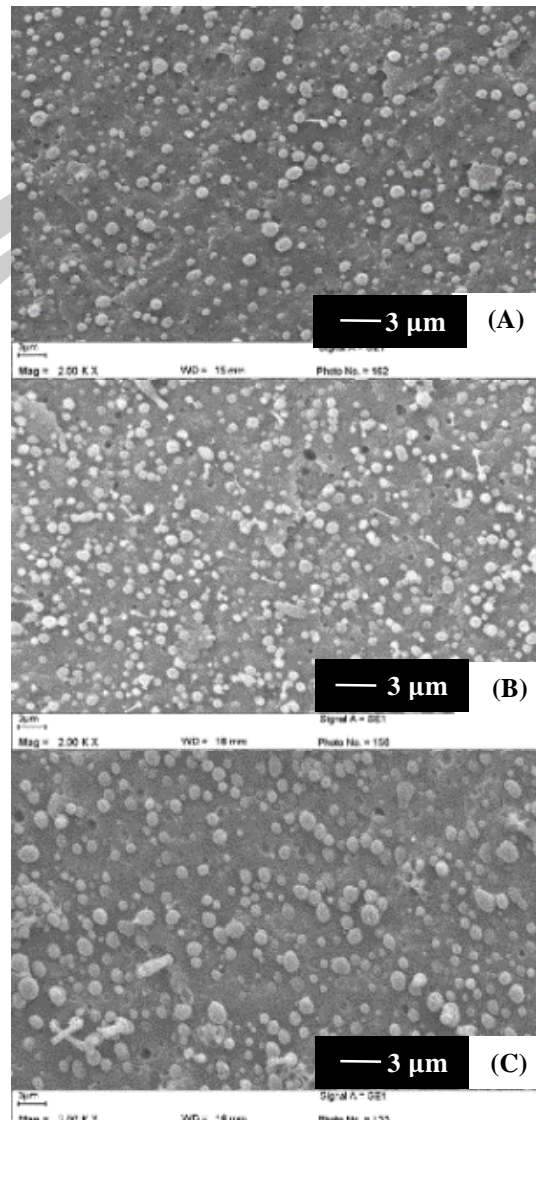


Figure 30. Fracture surfaces of the extruded strands for PE-10PLA-10rPET (A), PE-10PLA-20rPET (B) and PE-20PLA-10rPET (C).

พหุพันธ์ ปณ. ทีโตน ซีเว

4.9 Effect of PE-g-MA compatibilizer on morphology of the PE/PLA and PE/PLA/rPET extruded strands

The effect of compatibilizer loading on morphology of PE-10PLA and PE-10PLA-10rPET extruded strands are shown in Figure 31. In this study, the contents of PE-g-MA were used as 5 wt%. With the presence of compatibilizer, both of the PLA and rPET domains show smaller size of dispersed phase with diameters of domains are mostly lower than 0.5 μm when compared with the uncompatibilized blends. In case of PE-10PLA-10rPET (Figure 31IB) and PE-10PLA-10rPET-5MA (Figure 31IIB), PLA domains appeared as the larger size droplets whereas smaller droplets belong to rPET phase. Moreover, the addition of compatibilizer has a little effect on the PE-10PLA-10rPET morphology of the composites.

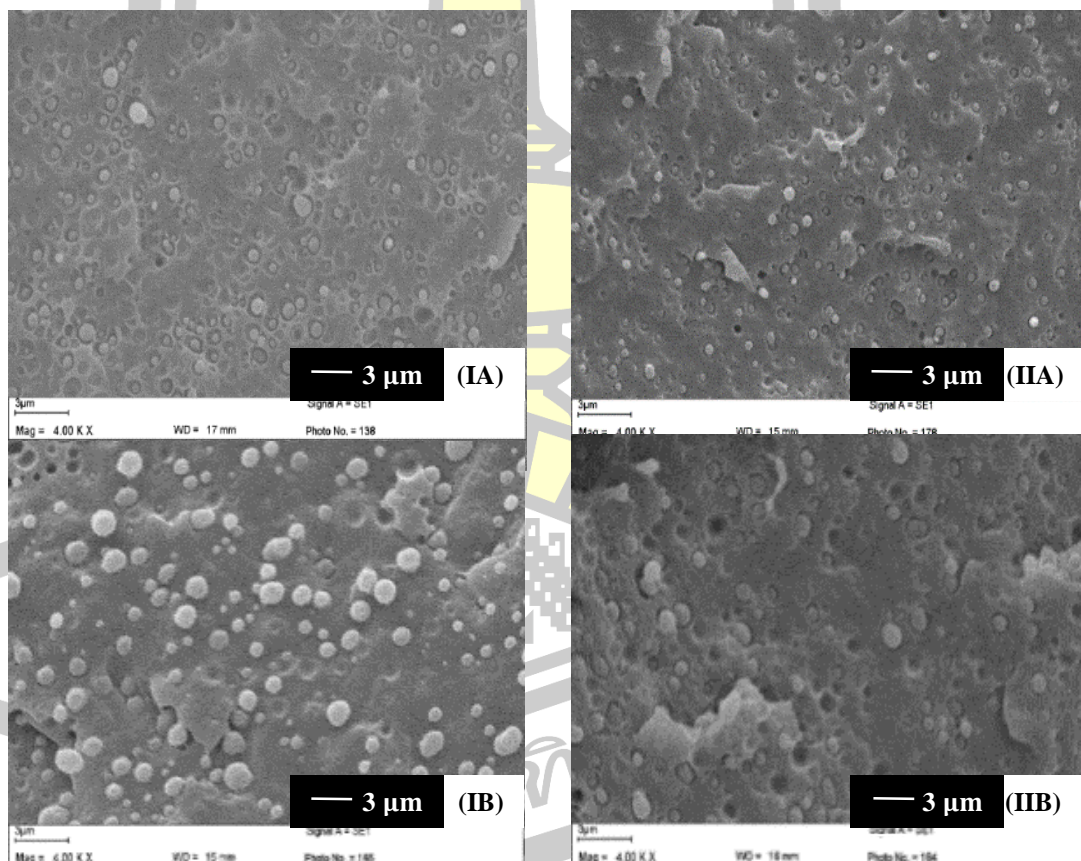
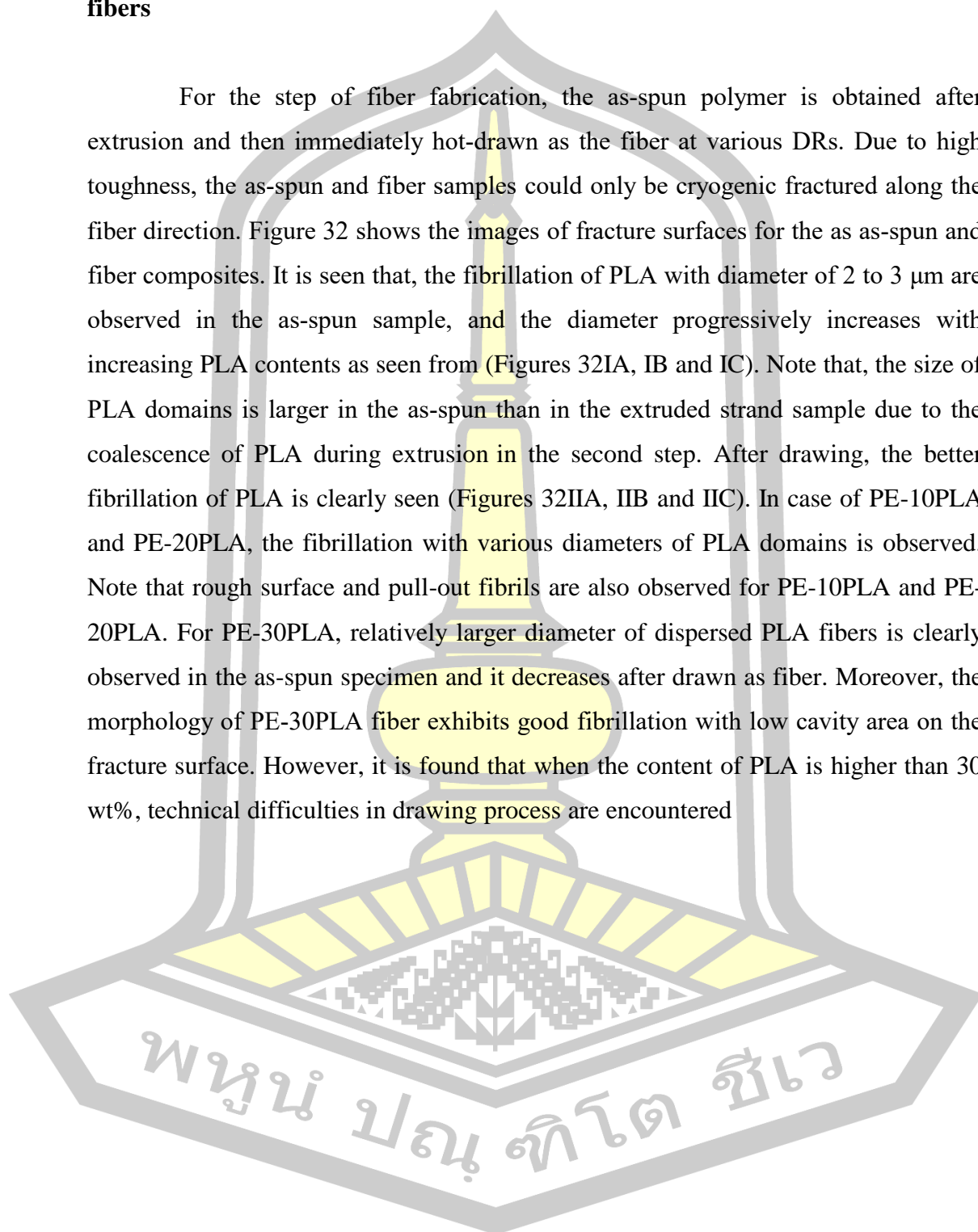


Figure 31. The fracture surface of uncompatibilized (column I) and compatibilized (column II) samples for PE-10PLA (row a), PE-10PLA-10rPET (row b).

4.10 Effect of PLA contents on morphology of the PE/PLA as-spun and drawn fibers

For the step of fiber fabrication, the as-spun polymer is obtained after extrusion and then immediately hot-drawn as the fiber at various DRs. Due to high toughness, the as-spun and fiber samples could only be cryogenic fractured along the fiber direction. Figure 32 shows the images of fracture surfaces for the as-spun and fiber composites. It is seen that, the fibrillation of PLA with diameter of 2 to 3 μm are observed in the as-spun sample, and the diameter progressively increases with increasing PLA contents as seen from (Figures 32IA, IB and IC). Note that, the size of PLA domains is larger in the as-spun than in the extruded strand sample due to the coalescence of PLA during extrusion in the second step. After drawing, the better fibrillation of PLA is clearly seen (Figures 32IIA, IIB and IIC). In case of PE-10PLA and PE-20PLA, the fibrillation with various diameters of PLA domains is observed. Note that rough surface and pull-out fibrils are also observed for PE-10PLA and PE-20PLA. For PE-30PLA, relatively larger diameter of dispersed PLA fibers is clearly observed in the as-spun specimen and it decreases after drawn as fiber. Moreover, the morphology of PE-30PLA fiber exhibits good fibrillation with low cavity area on the fracture surface. However, it is found that when the content of PLA is higher than 30 wt%, technical difficulties in drawing process are encountered



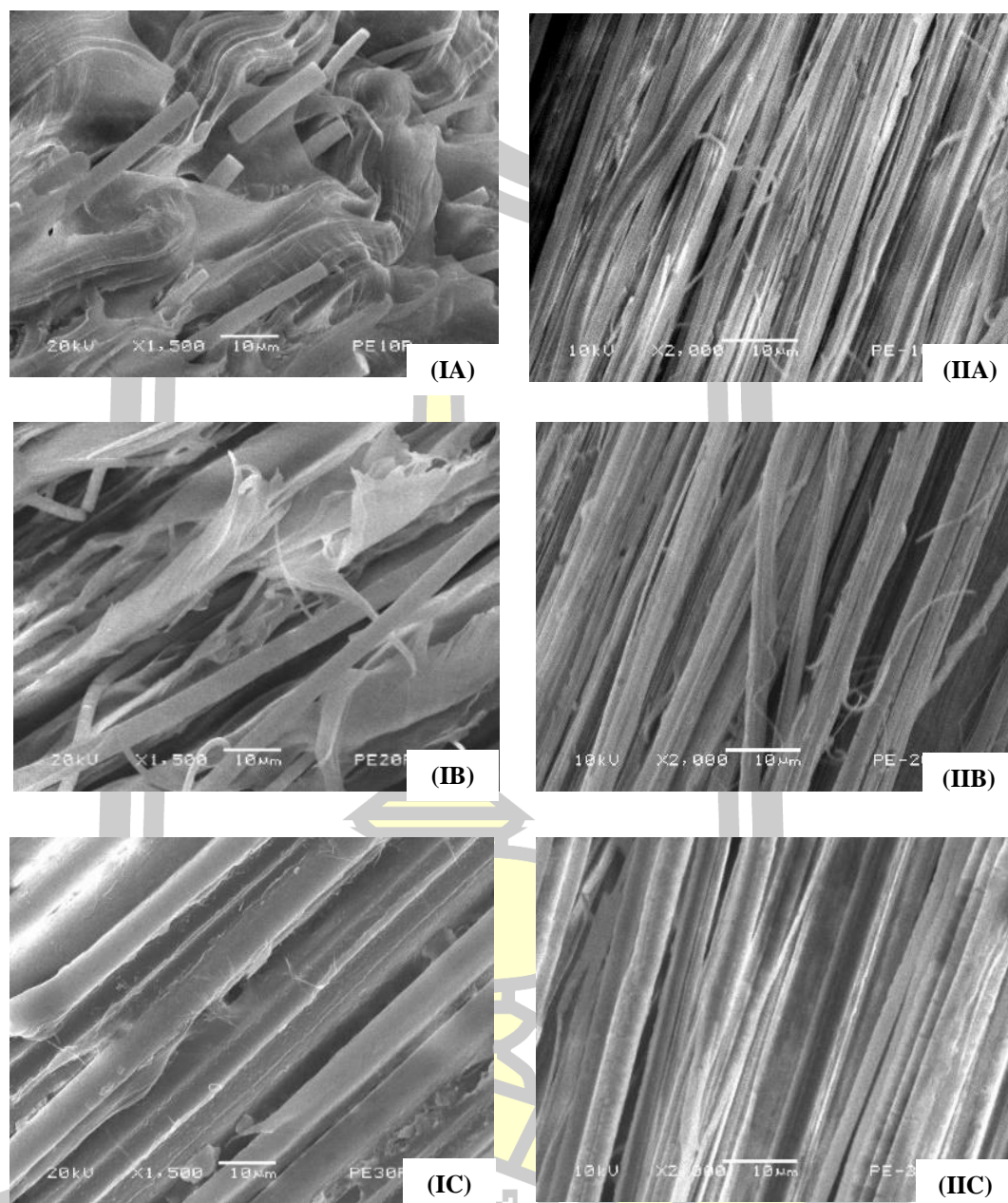


Figure 32. Fracture surface of the as-spun samples (column I) and its composite fibers (column II) of PE-10PLA (A), PE-20PLA (B) and PE-30PLA (C), drawn at DR = 20.

4.11 Effect of PE-g-MA compatibilizer on morphology of the PE/PLA and PE/PLA/rPET as-spun and drawn fibers

Figure 33 shows SEM images of fracture surface in longitudinal direction for the as-spun (column I) and drawn fibers (column II) of uncompatibilized (row A) and compatibilized composites (row B). For PE-10PLA as-spun fiber (Figure 33IA and IB), the diameters of PLA fibrils in the compatibilized system are mostly smaller than those of the uncompatibilized one. For the compatibilized composite (Figures 33IB) and IIB), the number of pulled-out PLA fibrils decreases when compared with the uncompatibilized drawn fibers. Moreover, low area of cavity between the fibrils causing from pull-out effect is found at the fracture surface.

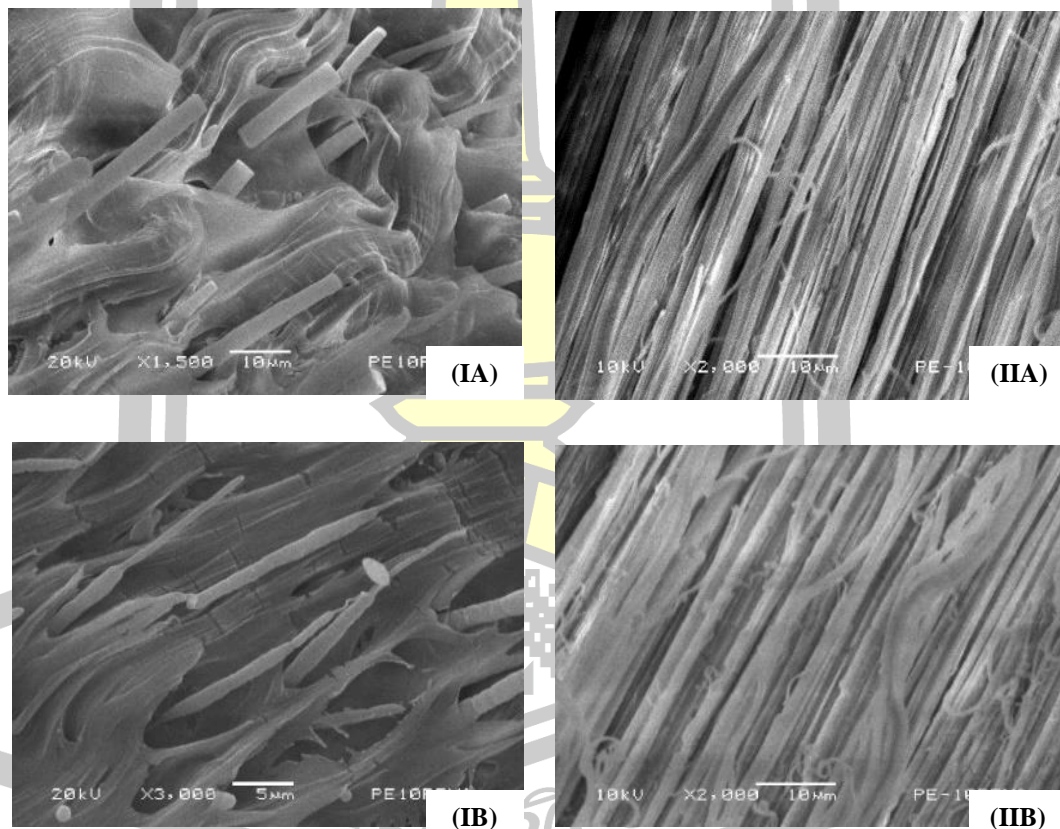


Figure 33. Fracture surfaces of the as-spun (column I), and DR20-fiber (column II) samples for PE-10PLA (row A) and PE-10PLA-5MA (row B).

For as-spun samples of PE/PLA/rPET composites (Figure 34), small droplets mostly belonging to rPET dispersed phase are observed, whereas PLA phase is mostly elongated in this step similar to PE/PLA system (Figure 33IA). The droplets appeared in the as-spun samples are mostly deformed into microfibrils after fabricating as fiber (Figure 34IIA and IIB). Note that, decrease in pull-out fibrils of rPET is observed on the matrix surface. Moreover, low area of cavity between the fibrils causing from pull-out effect is found at the fracture surface of PE-10PLA-10rPET-5MA composites (Figure 34 IIB). This results from the dense packing of the dispersed domains under applied high elongational force during hot drawing process. However, the addition of PE-g-MA compatibilizer has a little effect on the morphology of the rPET containing composite.

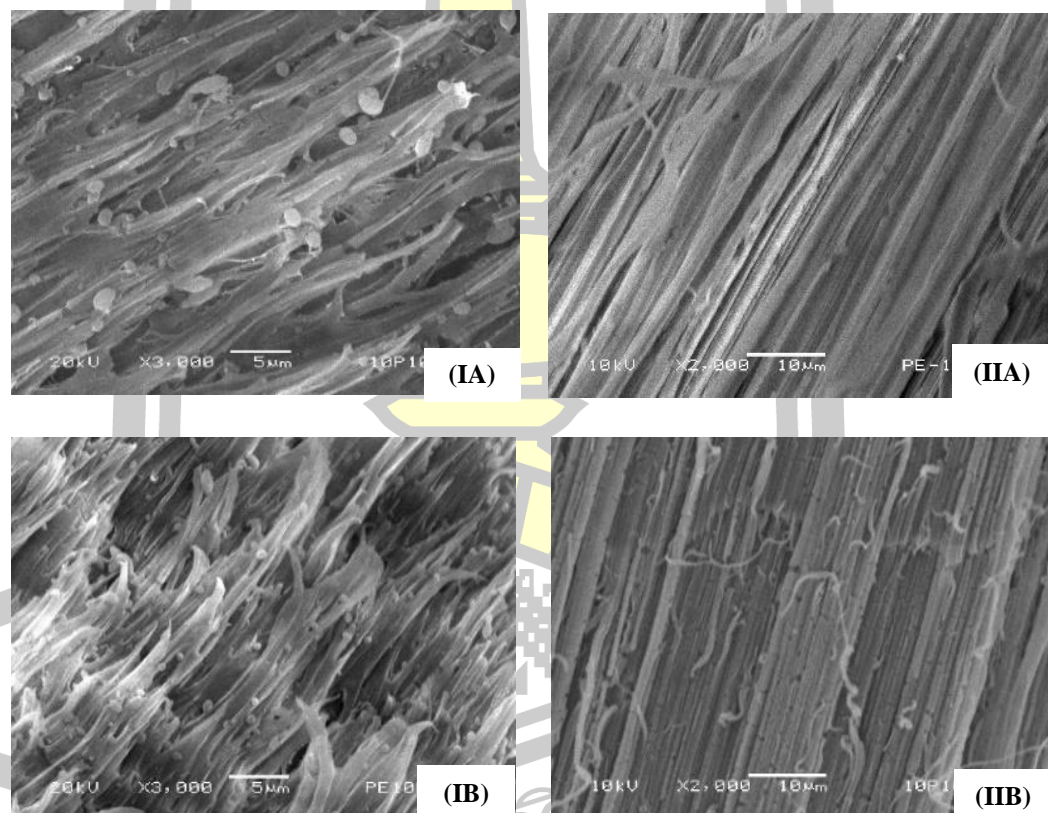


Figure 34. Fracture surfaces of the as-spun (column I), and DR20-fiber (column II) samples for PE-10PLA-10rPET (row A), PE-10PLA-10rPET-5MA (row B).

Figure 35 shows the surface images for the composite fibers. Smooth surface is observed for PE-10PLA (Figure 35A). The rough surface of the fibers is progressively found with PLA loading (Figure 35B) and C). For rPET-containing composite fibers (Figure 35D and E), the smooth surface is also observed. These results suggest that the smooth surface of the composite fibers is attainable at 10 wt% PLA and 10 wt% rPET loadings.

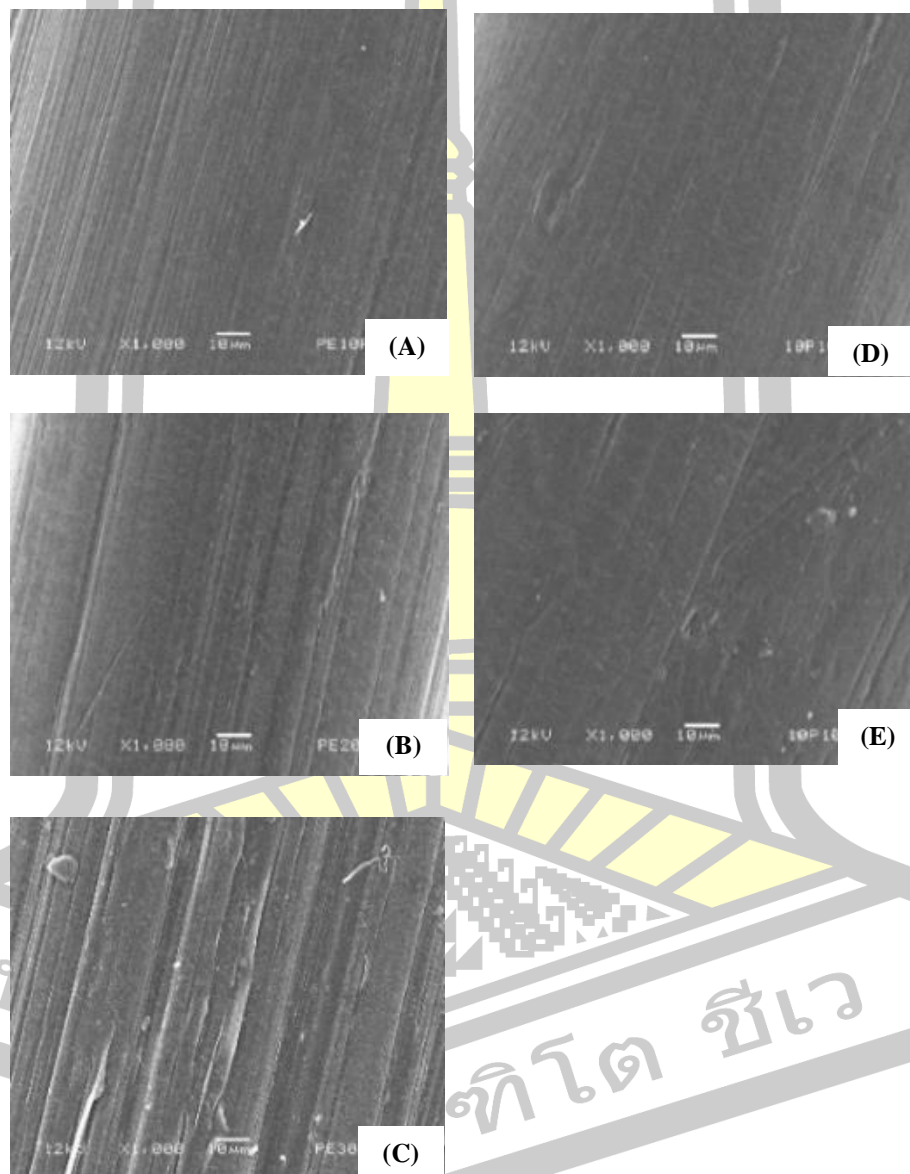


Figure 35. SEM images of fiber surfaces for PE-10PLA (A), PE-20PLA (B), PE-30PLA (C), PE-10PLA-10rPET (D) and PE-10PLA-10rPET-5MA (E).

4.12 Effect of draw ratios on morphology of PE/PLA/rPET composite fibers

The fracture surfaces along the fiber direction of PE/PLA/rPET composite fibers at selected draw ratios of 12, 14, and 20 are shown in Figures 36. The good fibrillation of both PLA and rPET dispersed phases was observed with increasing draw ratio. By taking a look on fracture image of PE-10PLA-10rPET composite fiber at draw ratio of 12 (Figure 36A), a number of cracks on fibrils perpendicular to the fibril direction and large area of fiber pull-out trace are clearly observed. The better fibrillation of is found by drawing at higher draw ratio, e.g. at DR = 14 (Figure 36B). Meanwhile, relatively small fibrils attributing to rPET are additionally observed with stretching at draw ratio of 14. With drawing using draw ratio as high as 20 (Figure 36C), the absence of cracking trace on the fibrils, less pull-out fibrils resulting in decreased cavity area on the matrix surface are clearly observed.

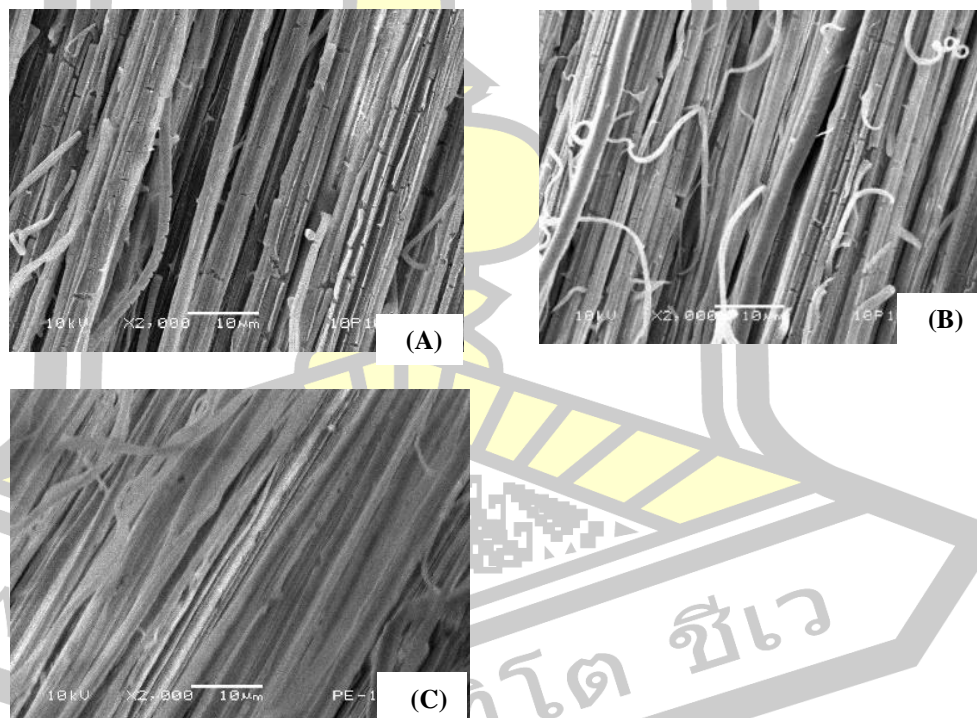


Figure 36. Fracture surface of PE-10PLA-10rPET composite fibers drawn at DR = 12 (A), 14 (B), and 20 (C).

4.13 Tensile properties of polymers

4.13.1 Effect of PLA contents on tensile properties of the as-spun composites

Figure 37 shows the tensile behavior for PE-10PLA, PE-20PLA and PE-30PLA in comparison with PE. The stress reported here is the nominal (engineering) stress, that is, the force divided by the cross-section area of the initial undeformed state. Under uniaxial stretching, all as-spun samples exhibit plastic behavior. The yielding points of all as-spun samples are clearly seen at the strain $< 10\%$. The yield stress of as-spun samples lies in the range of 16-23 MPa. It is interesting to note that the yielding behavior of the polymers occur in the narrow strain range (sharp peak) when compared with those of the as-spun PE (broad peak) (Figure 37B). In the same meaning, the neck point of as-spun PE-20PLA and PE-30PLA appears at the lower strain when compared with that of the neat PE matrix. This indicates that the presence of PLA could restrict the sliding of molecular chains, resulting in the shift of the neck point to lower strain [6]. This results in yielding effect at lower strain with increasing PLA contents. The secant modulus of all as-spun samples are nearly the same (Figure 37C) whereas the ultimate strength of the polymers lies in the range 16-13 MPa and depends on the PLA contents (Figure 37D). From stress-strain curves, it is seen that PE and PE-10PLA exhibit high elongation ($>1000\%$ strain), whereas the elongation at break of the composites PE-20PLA and PE-30PLA remarkably drops to ~ 55 and $\sim 10\%$, respectively, due to the loss of connectivity for matrix phase with high PLA loading.

4.13.2 Effect of PE-g-MA compatibilizer on tensile properties of PE-10PLA and PE-10rPET as-spun composites

Figure 4.18 shows the stress - strain curves, secant modulus and ultimate strength of PE, PE-10PLA, PE-10PLA-5MA and PE-10rPET-5MA as-spun composites. The yielding points of all samples are clearly seen at strain $< 10\%$ and the yielding stress lies in the range of 16-20 MPa. The stress of as-spun PE-10PLA is slightly higher than that of all samples as seen from Figures 38A and B. Moreover, it is seen that the secant modulus and ultimate strength of PE-10PLA-5MA and PE-10rPET-5MA are lower than those of PE-10PLA (Figures 38C and D). These results

suggest that the presence of PE-g-MA compatibilizer slightly affects the tensile properties of as-spun composites.

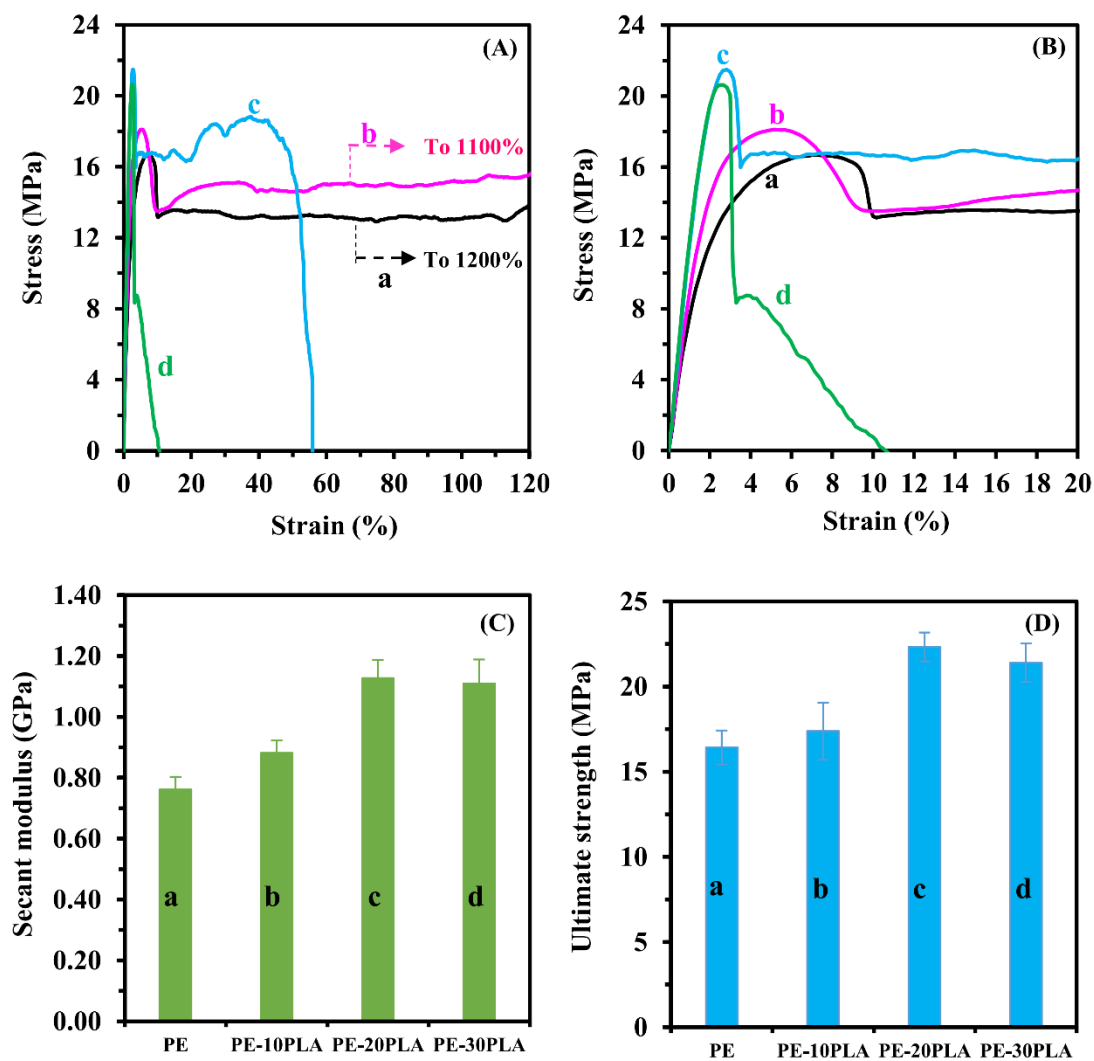


Figure 37. Stress-strain curves (A), stress-strain curves with expanded strain region from 0 to 20% (B), secant modulus (C), and ultimate strength (D) for the as-spun samples of PE (a), PE-10PLA (b), PE-20PLA (c), and PE-30PLA (d).

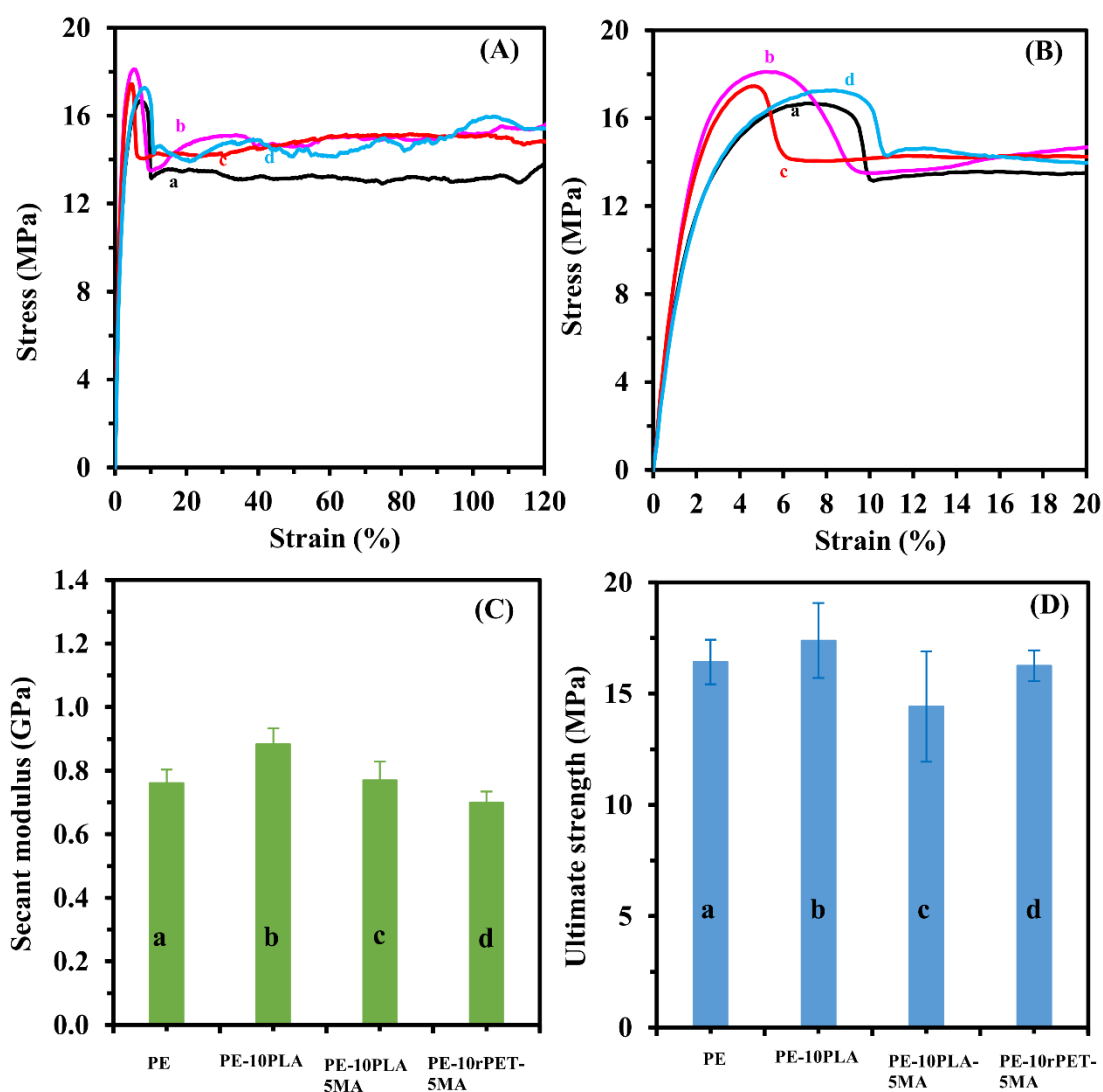
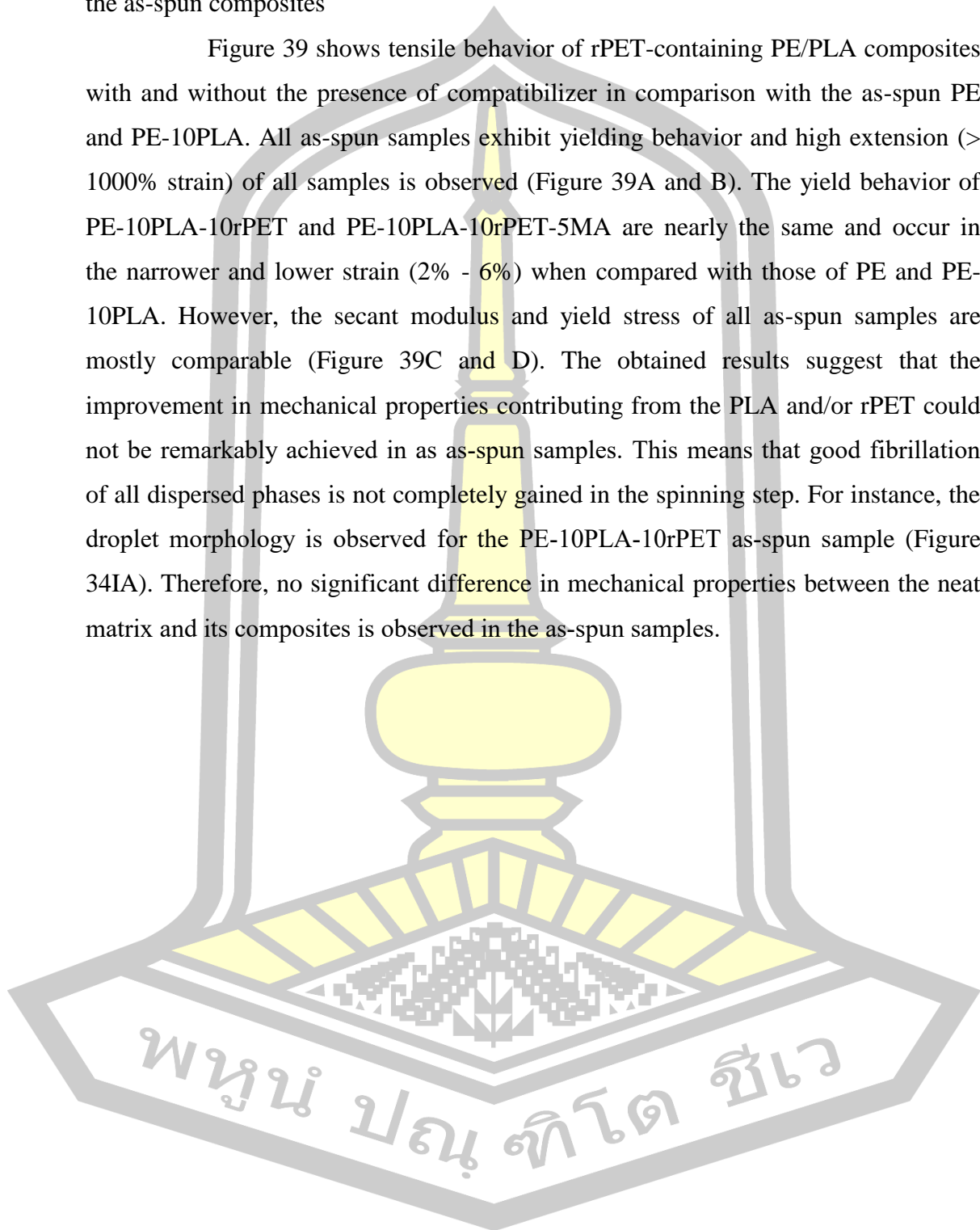


Figure 38. Stress-strain curves (A), stress-strain curves with expanded strain region from 0% to 20% (B), secant modulus (C), and ultimate strength (D) for the as-spun samples of PE (a), PE-10PLA (b), PE-10PLA-5MA(c), and PE-10rPET-5MA (d).

4.13.3 Effect of rPET and PE-g-MA compatibilizer on tensile properties of the as-spun composites

Figure 39 shows tensile behavior of rPET-containing PE/PLA composites with and without the presence of compatibilizer in comparison with the as-spun PE and PE-10PLA. All as-spun samples exhibit yielding behavior and high extension (> 1000% strain) of all samples is observed (Figure 39A and B). The yield behavior of PE-10PLA-10rPET and PE-10PLA-10rPET-5MA are nearly the same and occur in the narrower and lower strain (2% - 6%) when compared with those of PE and PE-10PLA. However, the secant modulus and yield stress of all as-spun samples are mostly comparable (Figure 39C and D). The obtained results suggest that the improvement in mechanical properties contributing from the PLA and/or rPET could not be remarkably achieved in as-spun samples. This means that good fibrillation of all dispersed phases is not completely gained in the spinning step. For instance, the droplet morphology is observed for the PE-10PLA-10rPET as-spun sample (Figure 34IA). Therefore, no significant difference in mechanical properties between the neat matrix and its composites is observed in the as-spun samples.



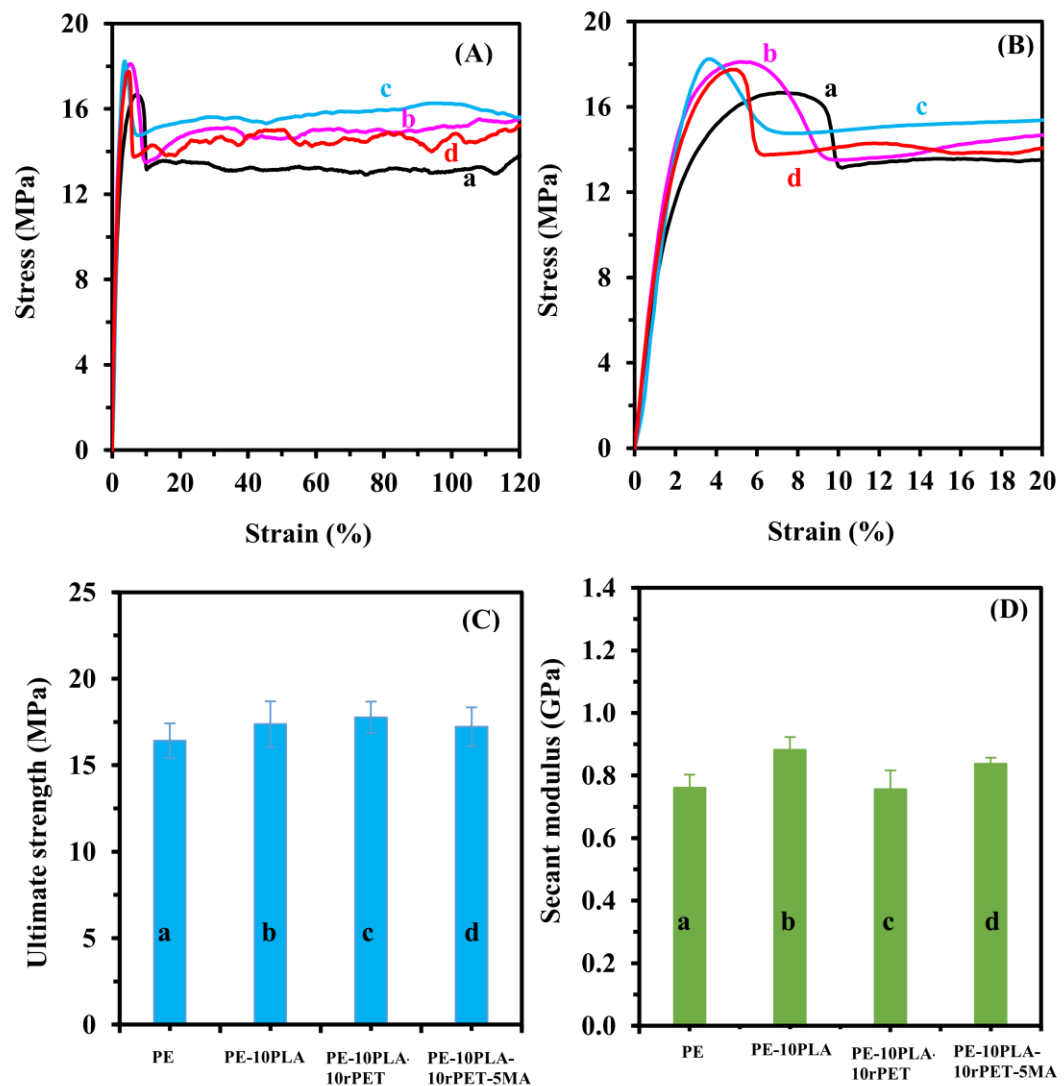
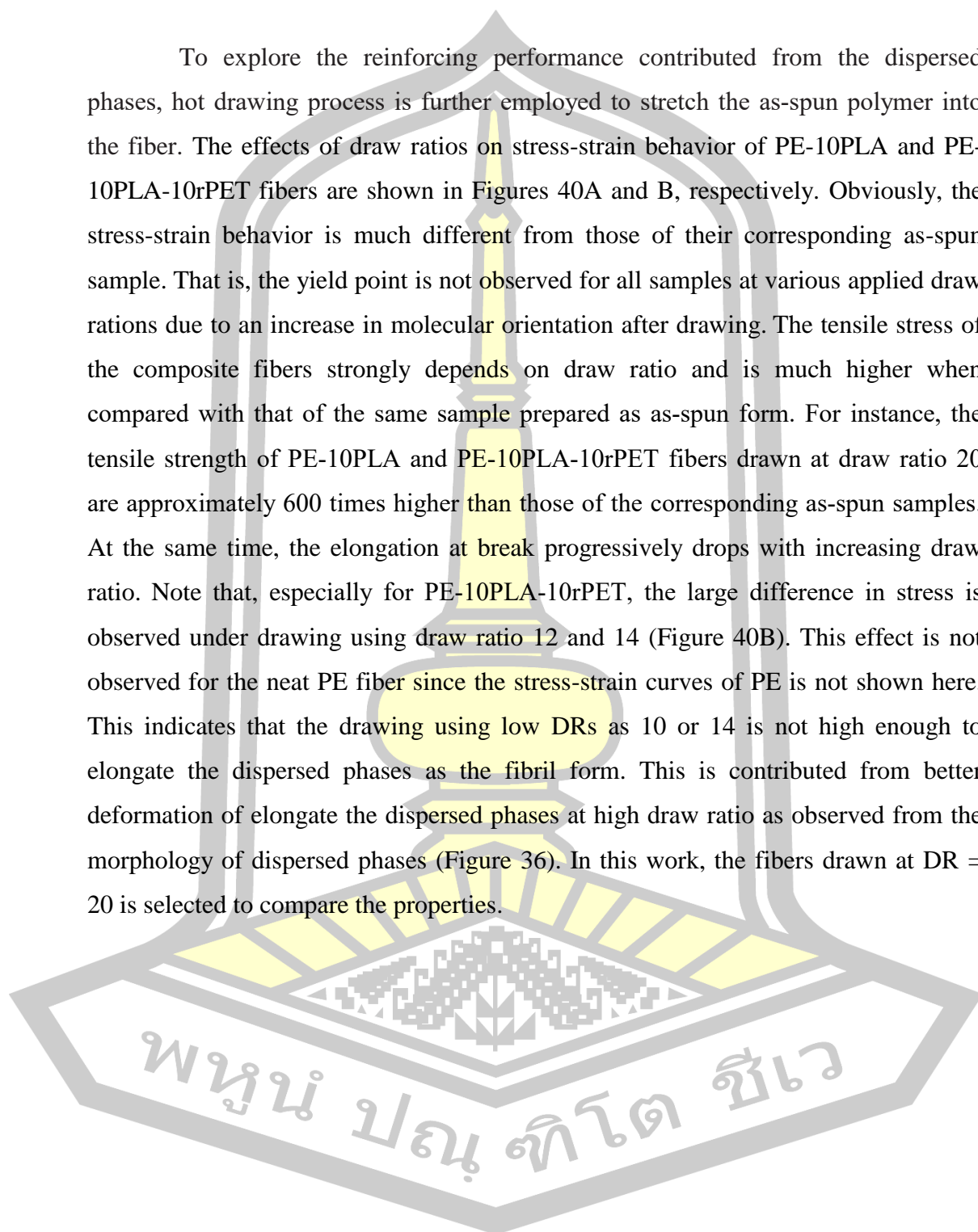


Figure 39. Stress-strain curves (A), stress-strain curves with expanded strain region from 0% to 20% (B), secant modulus (C), and ultimate strength (D) for the as-spun samples of PE (a), PE-10PLA (b), PE-10PLA-5MA(c), and PE-10rPET-5MA (d).

พหุ ประถมศึกษา

4.14 Effect of draw ratios on stress-strain behavior of the polymer fibers

To explore the reinforcing performance contributed from the dispersed phases, hot drawing process is further employed to stretch the as-spun polymer into the fiber. The effects of draw ratios on stress-strain behavior of PE-10PLA and PE-10PLA-10rPET fibers are shown in Figures 40A and B, respectively. Obviously, the stress-strain behavior is much different from those of their corresponding as-spun sample. That is, the yield point is not observed for all samples at various applied draw ratios due to an increase in molecular orientation after drawing. The tensile stress of the composite fibers strongly depends on draw ratio and is much higher when compared with that of the same sample prepared as as-spun form. For instance, the tensile strength of PE-10PLA and PE-10PLA-10rPET fibers drawn at draw ratio 20 are approximately 600 times higher than those of the corresponding as-spun samples. At the same time, the elongation at break progressively drops with increasing draw ratio. Note that, especially for PE-10PLA-10rPET, the large difference in stress is observed under drawing using draw ratio 12 and 14 (Figure 40B). This effect is not observed for the neat PE fiber since the stress-strain curves of PE is not shown here. This indicates that the drawing using low DRs as 10 or 14 is not high enough to elongate the dispersed phases as the fibril form. This is contributed from better deformation of elongate the dispersed phases at high draw ratio as observed from the morphology of dispersed phases (Figure 36). In this work, the fibers drawn at DR = 20 is selected to compare the properties.



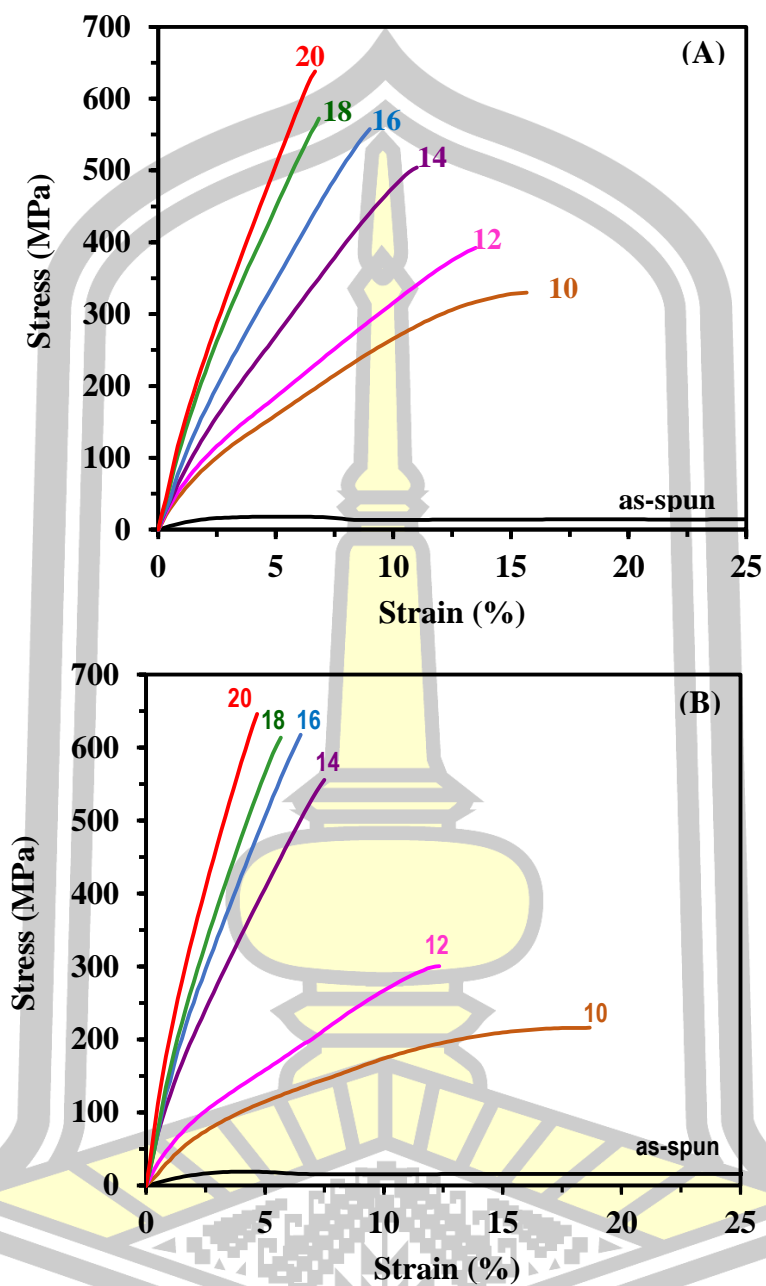
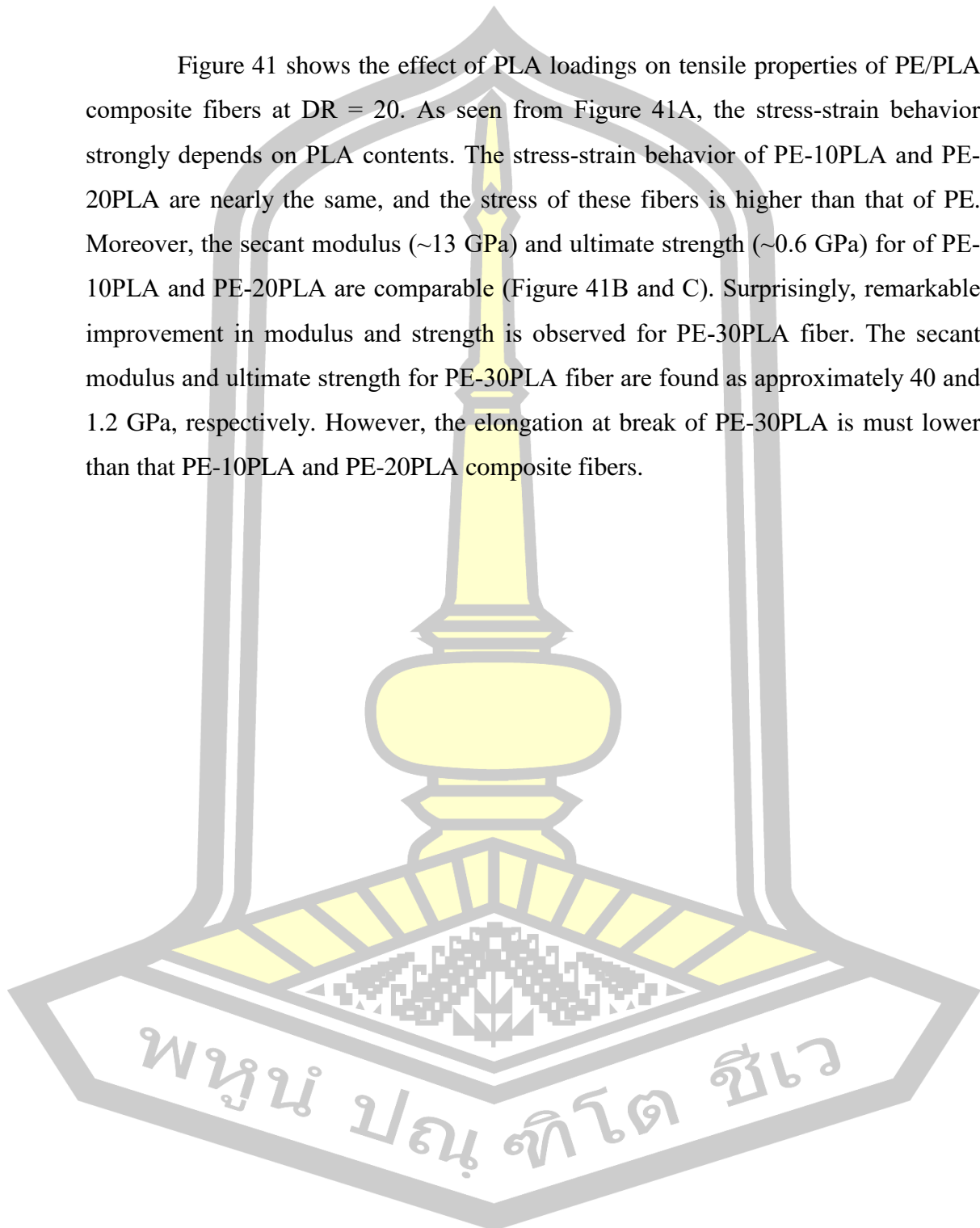


Figure 40. Effect of draw ratios on stress-strain behavior for PE-10PLA (A) and PE-10PLA-10rPET (B) composite fibers.

4.15 Effect of PLA contents on tensile properties of polymer fibers

Figure 41 shows the effect of PLA loadings on tensile properties of PE/PLA composite fibers at DR = 20. As seen from Figure 41A, the stress-strain behavior strongly depends on PLA contents. The stress-strain behavior of PE-10PLA and PE-20PLA are nearly the same, and the stress of these fibers is higher than that of PE. Moreover, the secant modulus (~13 GPa) and ultimate strength (~0.6 GPa) for of PE-10PLA and PE-20PLA are comparable (Figure 41B and C). Surprisingly, remarkable improvement in modulus and strength is observed for PE-30PLA fiber. The secant modulus and ultimate strength for PE-30PLA fiber are found as approximately 40 and 1.2 GPa, respectively. However, the elongation at break of PE-30PLA is must lower than that PE-10PLA and PE-20PLA composite fibers.



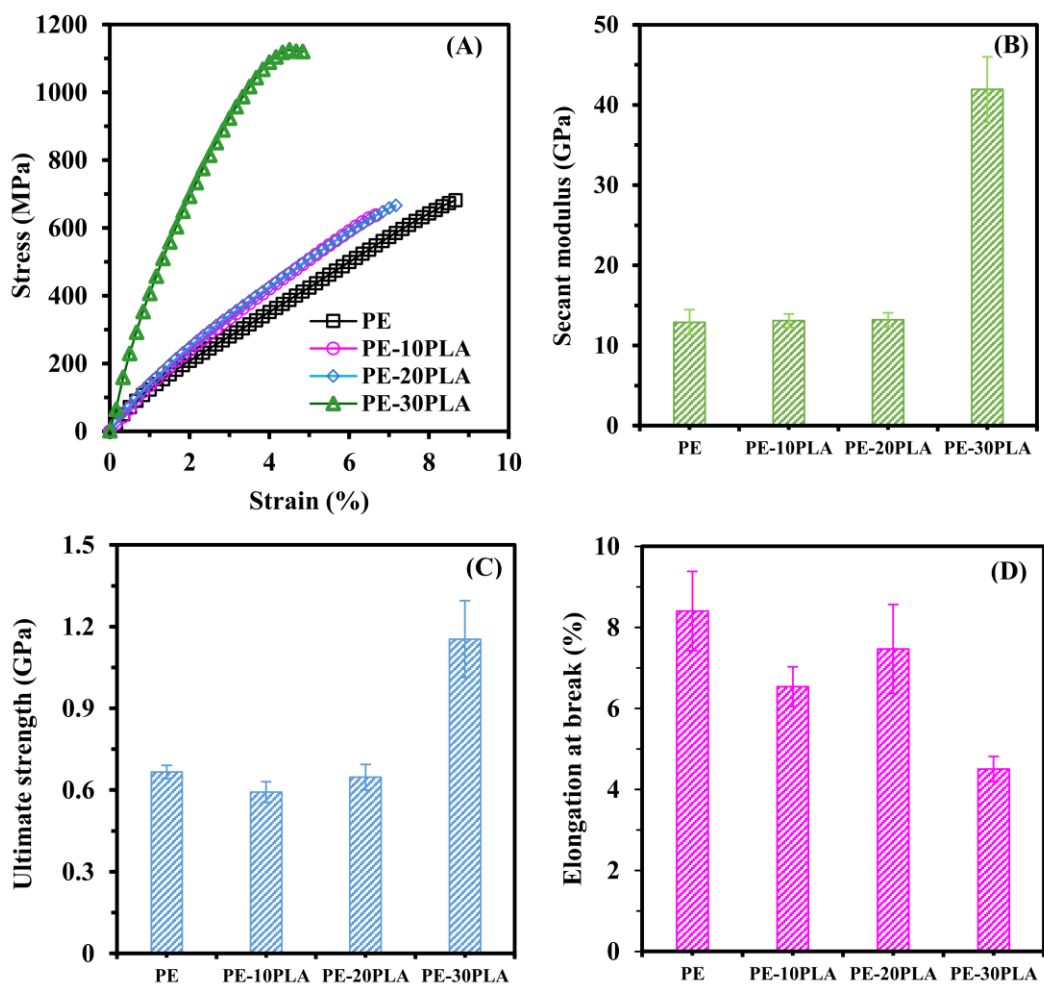
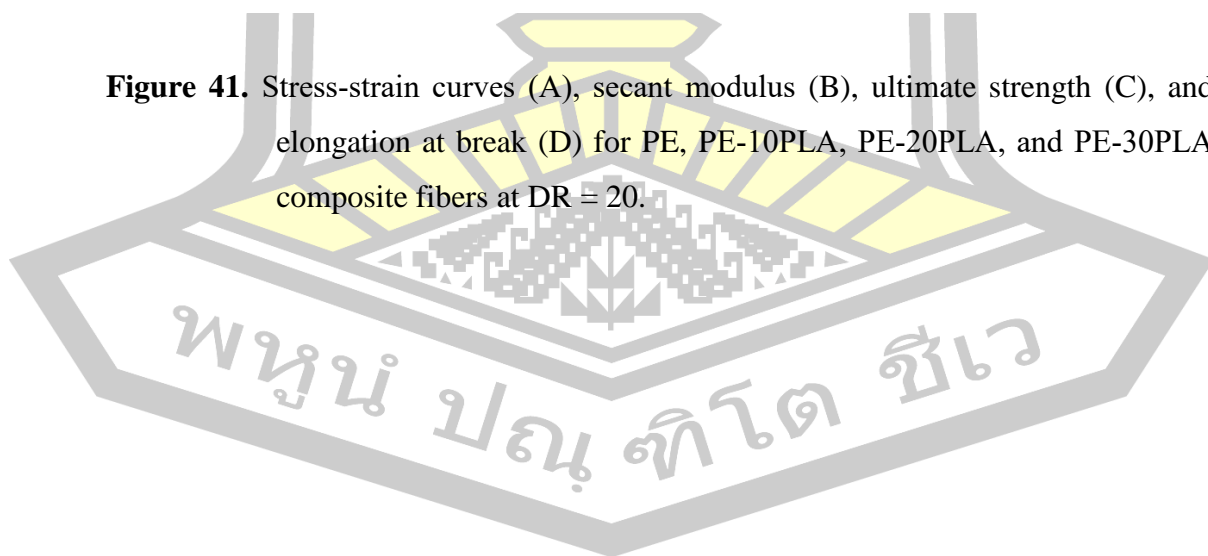
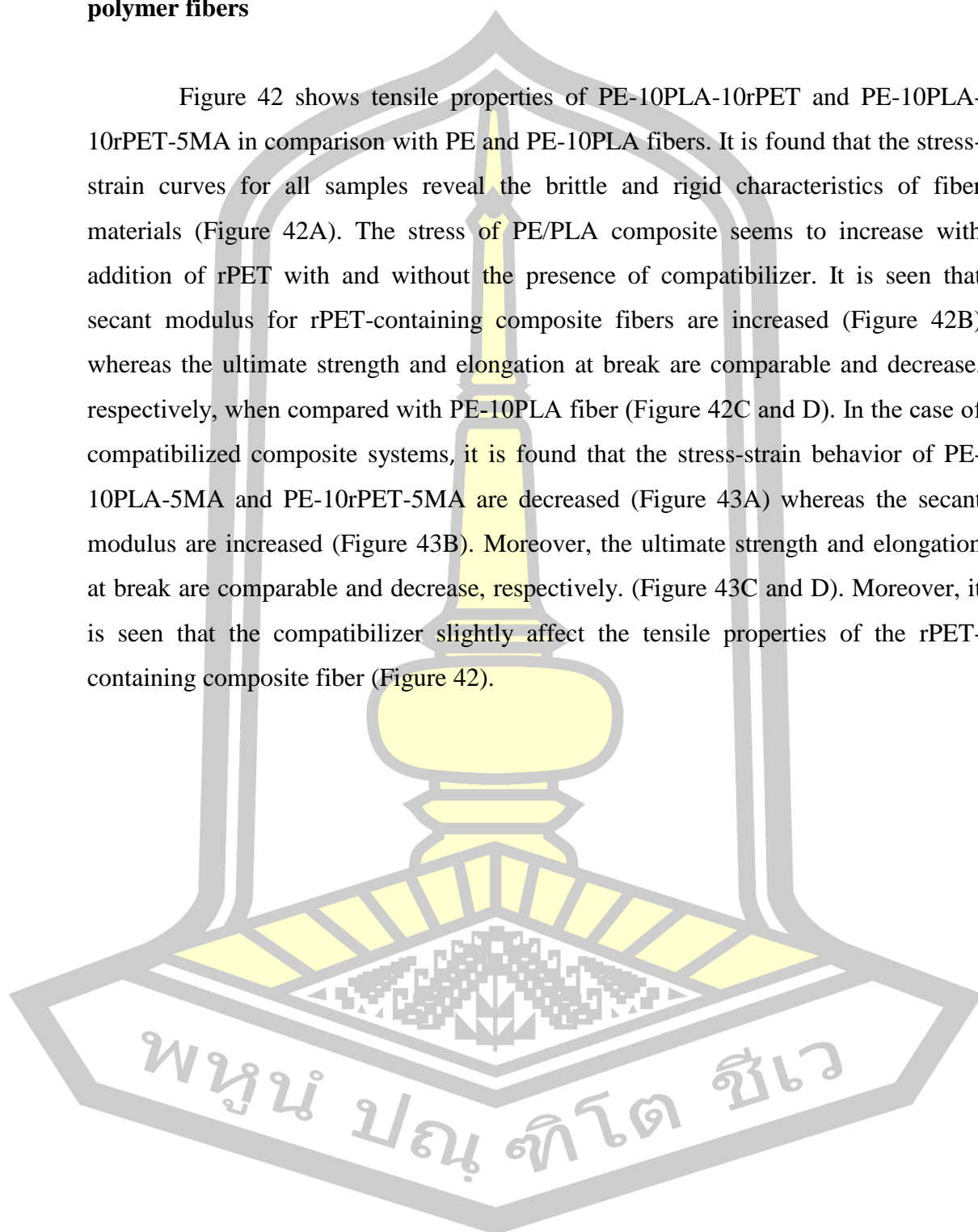


Figure 41. Stress-strain curves (A), secant modulus (B), ultimate strength (C), and elongation at break (D) for PE, PE-10PLA, PE-20PLA, and PE-30PLA composite fibers at DR = 20.



4.16 Effect of rPET and PE-g-MA compatibilizer on tensile properties of polymer fibers

Figure 42 shows tensile properties of PE-10PLA-10rPET and PE-10PLA-10rPET-5MA in comparison with PE and PE-10PLA fibers. It is found that the stress-strain curves for all samples reveal the brittle and rigid characteristics of fiber materials (Figure 42A). The stress of PE/PLA composite seems to increase with addition of rPET with and without the presence of compatibilizer. It is seen that secant modulus for rPET-containing composite fibers are increased (Figure 42B) whereas the ultimate strength and elongation at break are comparable and decrease, respectively, when compared with PE-10PLA fiber (Figure 42C and D). In the case of compatibilized composite systems, it is found that the stress-strain behavior of PE-10PLA-5MA and PE-10rPET-5MA are decreased (Figure 43A) whereas the secant modulus are increased (Figure 43B). Moreover, the ultimate strength and elongation at break are comparable and decrease, respectively. (Figure 43C and D). Moreover, it is seen that the compatibilizer slightly affect the tensile properties of the rPET-containing composite fiber (Figure 42).



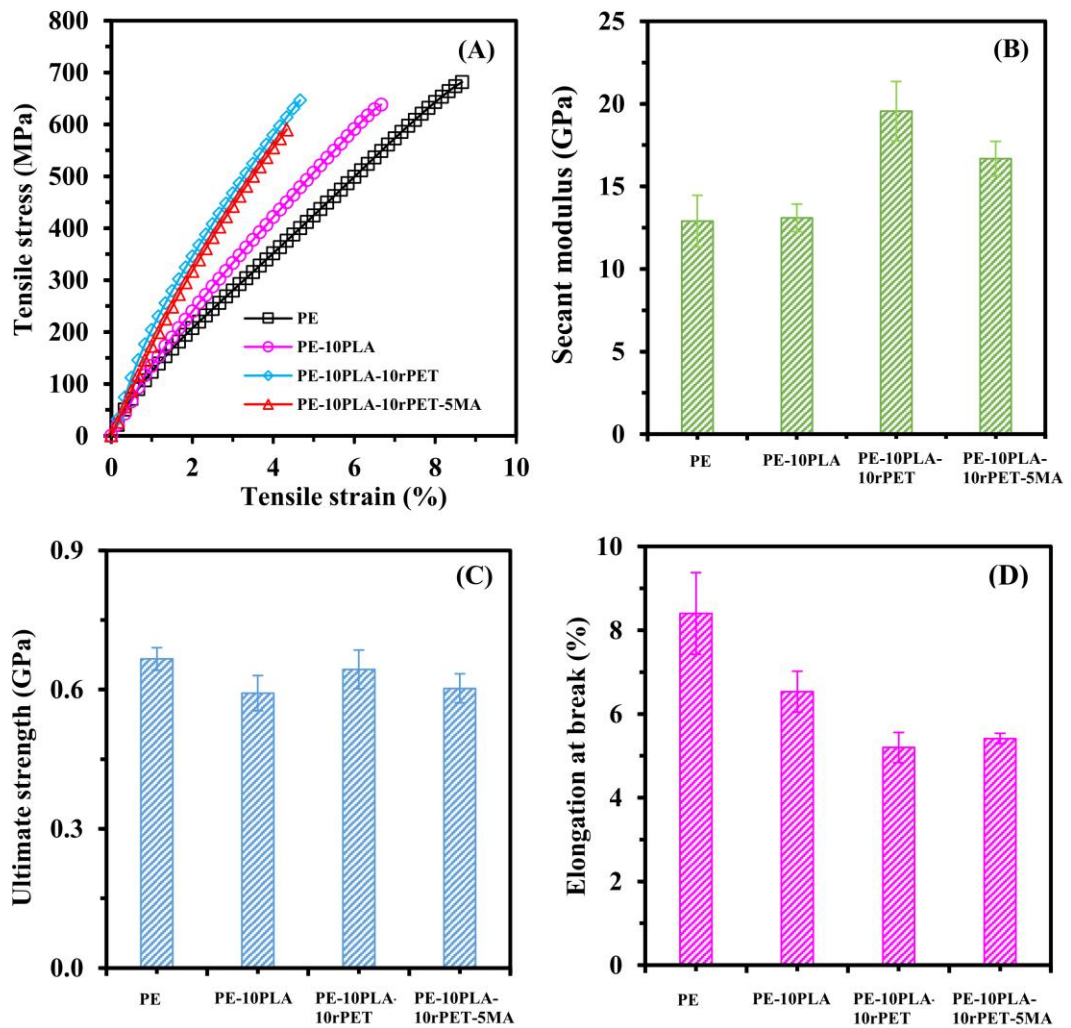
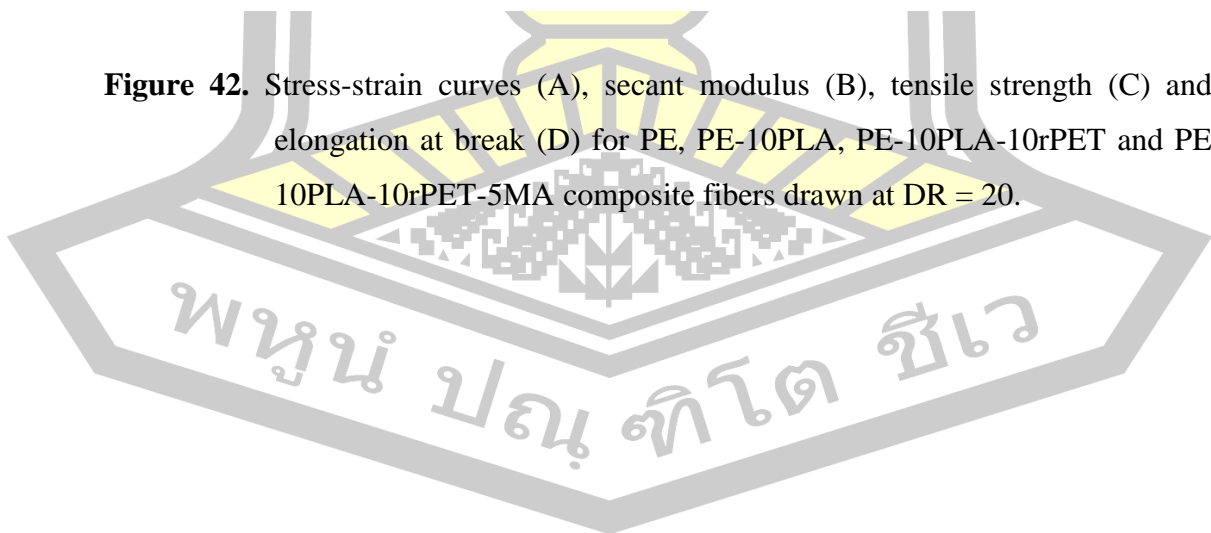


Figure 42. Stress-strain curves (A), secant modulus (B), tensile strength (C) and elongation at break (D) for PE, PE-10PLA, PE-10PLA-10rPET and PE 10PLA-10rPET-5MA composite fibers drawn at DR = 20.



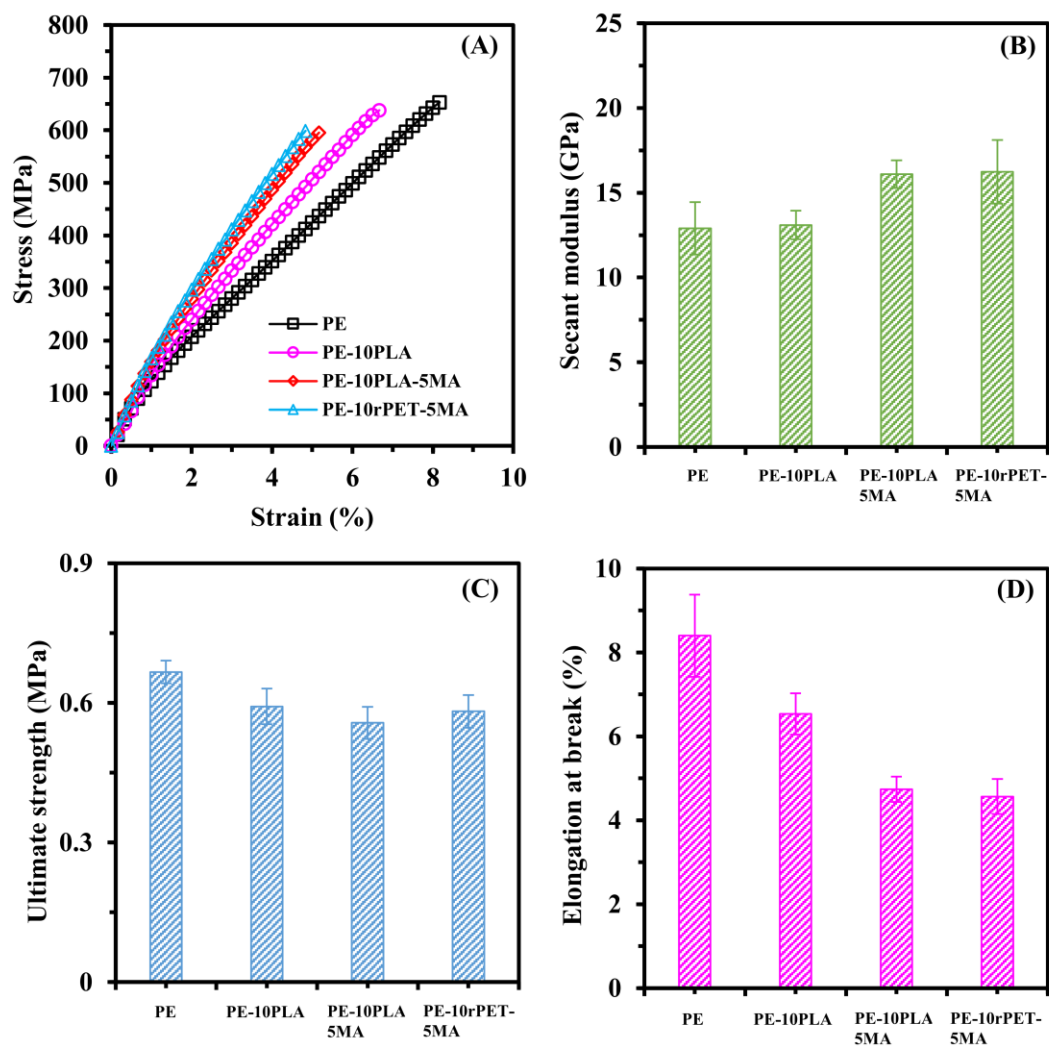


Figure 43. Stress-strain curves (A), secant modulus (B), tensile strength (C) and elongation at break (D) for PE, PE-10PLA, PE-10PLA-5MA and PE-10rPET-5MA composite fibers drawn at DR = 20.

พหุบัณฑิต ชีวะ

4.17 Effect of rPET and LCP on tensile properties of polymer fibers

Figure 44 shows the stress-strain curves and tensile properties of PE-10PLA-10rPET and PE-10PLA-10LCP in comparison with PE and PE-10PLA fibers. The stress of PE-10PLA-10LCP composite is higher than those of PE-10PLA and PE-10PLA-10rPET (Figure 44A). It is seen that secant modulus and ultimate strength for PE-10PLA-10rPET and PE-10PLA-10LCP composite are comparable and increased, respectively when compared with PE-10PLA fiber (Figure 44B and C). However, the elongation at break of LCP- and rPET containing composites are decreased (Figure 44D).

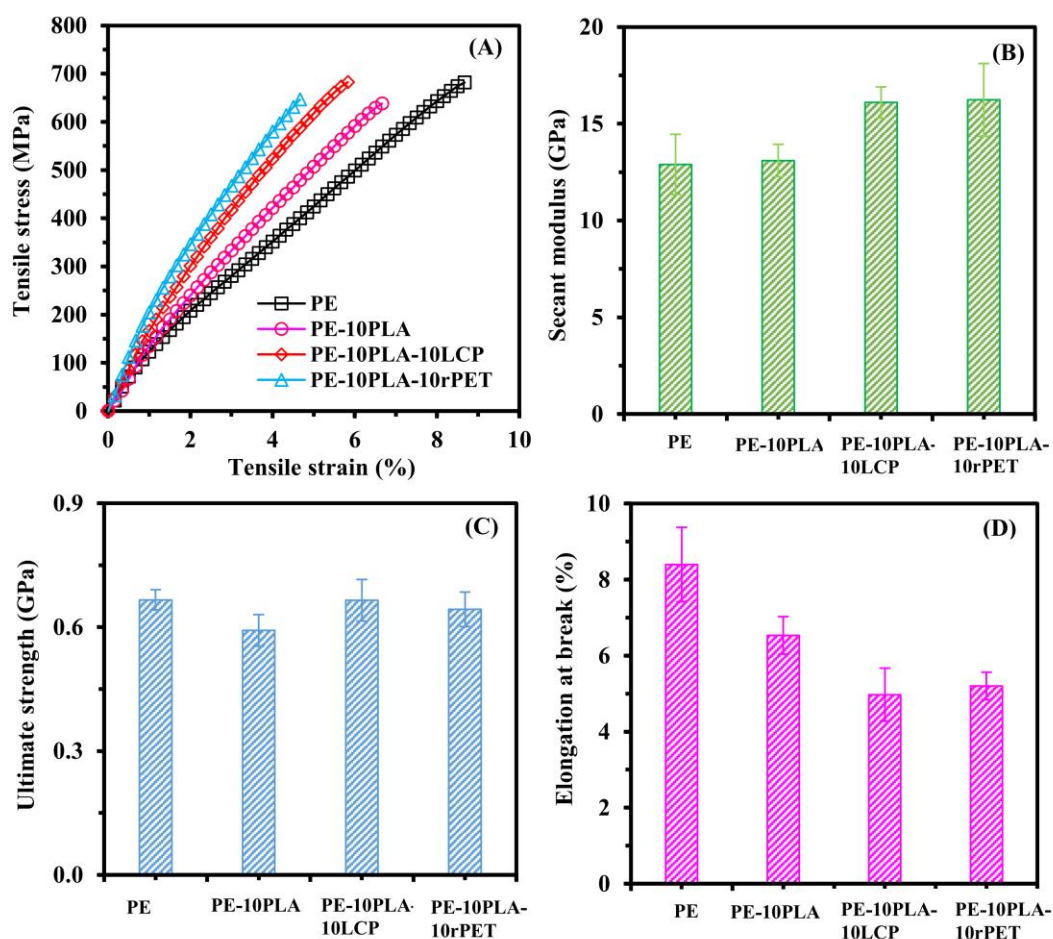


Figure 44. Stress-strain curves (A), secant modulus (B), ultimate strength (C), and elongation at break (D) for PE, PE-10PLA, PE-10PLA-10LCP, and PE-10PLA-10rPET composite fibers at DR = 20.

4.18 Discussion on reinforcing performance

To explore the reinforcing effect contributed from the different reinforcing materials, the secant modulus and ultimate strength of composite fibers prepared using the same or nearly the same line of process were quantitatively compared in Table 2 and mechanical properties of the implant produced are listed in the Table 3. The properties of polypropylene-based composite fibers are also compared as it was prepared using the same hot drawing process, and the same rPET was used as reinforcing component for the PP-based composite fibers [38]. Moreover, the properties of LCP- and rPET used as the dispersed phases for PE-based composite fibers with and without the presence of SEBS-g-MA [6] are comparatively shown here. For our previous studies, the mechanical properties of the PP-based or PE-based composites fibers strongly depend on the types of dispersed phases, compatibilizer, and drawing ability. In this work, the maximum DR of 20 could be obtained for PE/PLA and PE/PLA/rPET systems. Therefore, although drawing ability PE-based composite fibers previously investigated can be carried out at higher DR, the tensile properties of the all fibers are compared at $DR = 20$. For the previous studies, dispersed LCP or rPET domains and compatibilizer slightly affect the secant modulus and ultimate strength for the PP-based systems [38].

Mechanical properties for composite fiber prepared in this work several polymeric materials used in load-bearing application are compared in the Table 3. In the same line of application, the secant modulus and ultimate stress of PE/PLA/rPET systems are higher than those of other polymeric materials. Actually, the composite fibers prepared in this study will be further fabricated as the laminates using film-stacking method. Therefore, the final mechanical properties for the laminate of the fiber composites are expected to slightly decrease.

Table 2. Comparison of secant modulus and ultimate stress for various thermoplastic-based composite fibers.

Composite System	Secant Modulus (GPa)	Ultimate Stress (GPa)	Reference
PP-based (melt drawing: DR = 12)			
PP/LCP	8.2	0.36	[36]
PP/rPET	8.9	0.41	[36]
PP/LCP/SEBS-g-MA	10.2	0.39	[36]
PP/rPET/SEBS-g-MA	8.3	0.54	[36]
PE-based (melt drawing: DR = 20)			
PE/LCP	1.5 (max. 1.6/DR22.5)	0.51 (max. 0.51/DR20)	[6]
PE/rPET	1.4 (max. 1.5/DR22.5)	0.41 (max. 0.45/DR25)	[6]
PE/LCP/SEBS-g-MA	3.0 (max. 3.5/DR30)	0.41 (max. 0.51/DR35)	[6]
PE/rPET/SEBS-g-MA	2.8 (max. 6.5/DR35)	0.51 (max. 0.58/DR27.5)	[6]
PE/PLA	12.6	0.58	This work
PE/PLA	19.8	0.65	This work
PE/PLA/rPET/PE-g-MA	17.5	0.57	This work
Other relevant composites			
HDPE/GF (injection) ^a	1.4	0.043	[94]
PP/PALF (sheet)	1.5	0.033	[95]
HDPE/Clay ^b	22.5 (max. 37.5/DR30)	1.30 (max. 1.30/DR30)	[96]

The contents of the dispersed components and maleate compatibilizers used are 10 and 5 wt%, respectively

^aThe content of GF (E 968A) is 20 wt%, and the modulus reported here is elastic modulus.

^bThe content of clay is 3 wt%.

พหุ ประถมศึกษา

Table 3. Comparison of mechanical properties of different human tissues, ceramics and polymeric materials used for load-bearing.

Composite System	Young's (C)/Compression (M)/modulus (GPa)	Tensile strength (GPa)	Reference
Cortical bone	14-20 (M)	0.5-1.5	[97]
Cancellous bone	0.05-0.5 (M)	0.1-0.2	[97]
PLA/PCL (scaffold) ^a	14 (C)	1.4	[98]
PLA/HA (injection) ^b	-	0.063-0.075	[99]
HAp/PLA (film) ^c	3.44 (C)	0.048	[100]
HAP/PLA (scaffold) ^d	0.149 (C)	0.087	[101]
PE/Bioglass® ^e (sheet) ^e	2.54 (M)	0.021	[102]
HA/PE (scaffold bone) ^f	4.4 (M)	0.08	[103]
HA/PEEK (injection) ^g	16.0 (M)	0.69	[104]
PE/PLA/rPET/PE-g-MA (fiber)	17.5 (M)	0.57	This work

^aThe content of PCL is 30 wt%.

^bThe content of HA is 5 wt%

^cThe content of HAp is 20 wt%.

^dThe content of HAP is 50 wt%.

^eThe content of Bioglass® is 40 wt%.

^fThe content of PE is 20 wt%.

^gThe content of HA is 40 wt%.

พหุ ประถมศึกษา

4.19 Composition of thermal stability of extruded strands, as-spun and drawn fibers

The effect of processing step on the thermal stability of polymer products is investigated. The dynamic TG curves of PE-10PLA-10rPET composites in the form of strands, as-spun and fibers are presented in Figure 45. The TG measurements were carried out in nitrogen and in air at a heating rate of 10°C/min. In nitrogen, the similar shape of the TG curves for all samples are observed. In air, the drawn fiber seem to show lower thermal stability when compared with the strand and as-spun samples. To clearly compare the thermal stability between PE-10PLA and PE-10PLA-10rPET preparation in the forms of strand and drawn fiber the TG curves of the two forms and present in Figure 46, the additional presence of rPET clearly improved the stability of the polymer composites both in the forms of strand and drawn fiber. In comparison with drawn fiber, the sample prepared in the form of extruded exhibits slightly higher thermal stability.

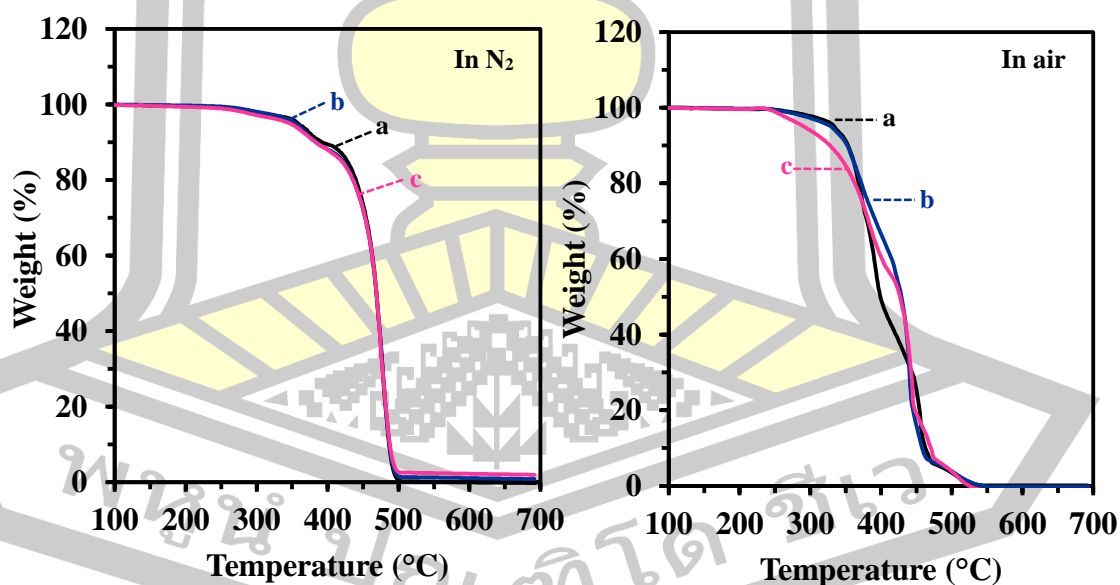


Figure 45. Dynamic TG curves of PE-10PLA-10rPET composite systems in the forms of extruded strand (a), as-spun (b) and drawn fiber (c) at a heating rate 10°C/min in nitrogen and air.

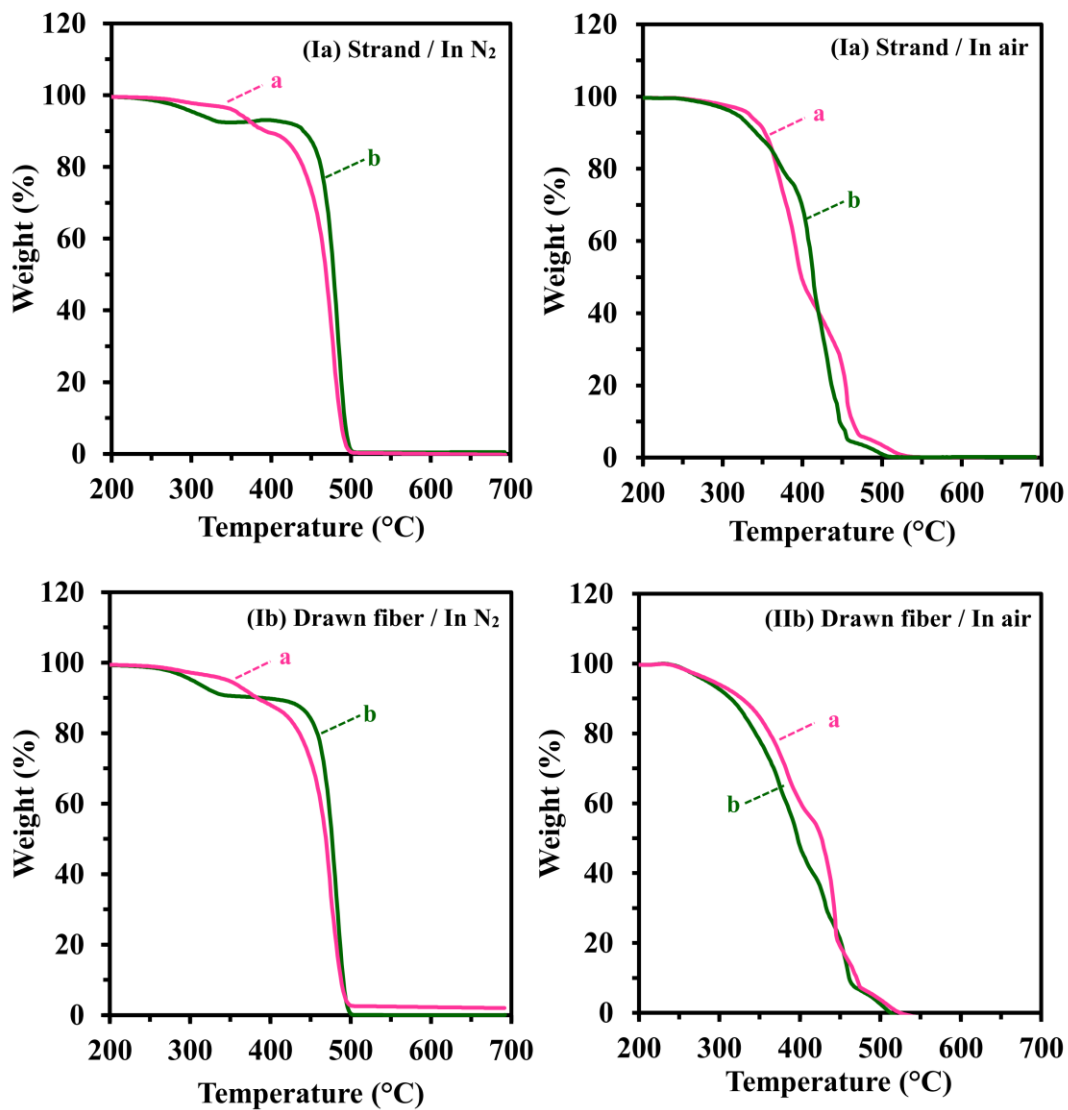
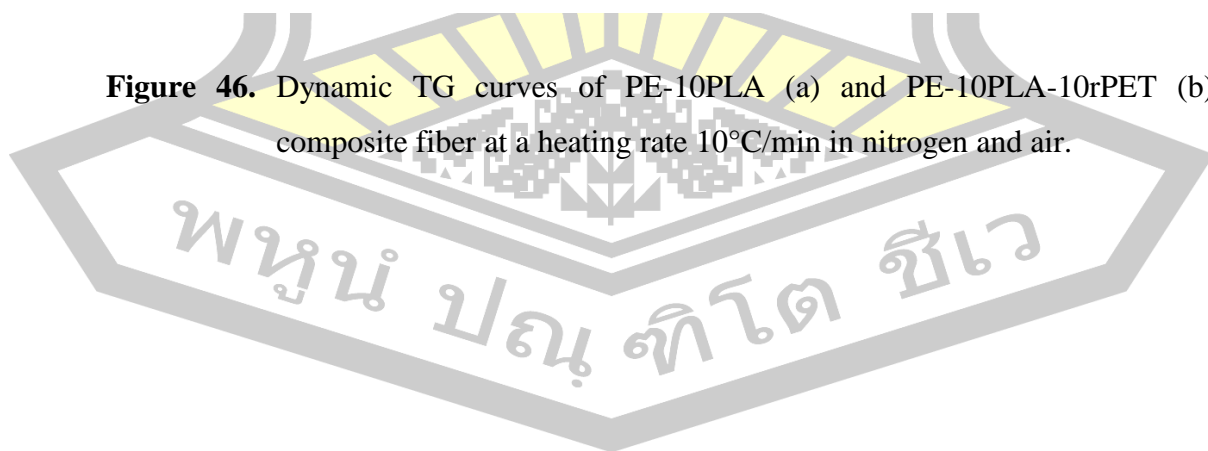


Figure 46. Dynamic TG curves of PE-10PLA (a) and PE-10PLA-10rPET (b) composite fiber at a heating rate 10°C/min in nitrogen and air.



4.20 Effect of PLA contents on nonisothermal decomposition behavior

Normally, polymers must encounter elevated temperatures at almost every stage in manufacturing, compounding, and processing stages, in service, and during repairing step. Therefore, an understanding of thermal stability and thermal decomposition behavior of polymer is an essential information for the development and extension of their applications. In the present study, TGA is performed to gain some understanding of the effect of the PLA on thermal decomposition of the PE-10PLA blends. The nonisothermal TG curves of the polymers are presented in Figure 47IA and IIA. The TG measurements are carried out in nitrogen and in air at a heating rate of 10°C/min. The TG curves of each sample remarkably reveal the different profiles. In nitrogen, the nonisothermal TG profile of PE reveals only a single weight-loss step at the temperature range of 400-500°C (Figure 47IA). The degradation mechanism of PE involves primary random scission pathway and chain branching and is responsible for the propene product and the other gives rise to 1-hexene [105]. Moreover, the mechanism begins at the weak link site along the polymer chain once thermally induced scission has occurred. Although random scission is a primary degradation pathway in PE, it can also result in polymer chain branching. Both scission and branching occur simultaneously giving rise to a single mass loss step. The single step of weight loss around 300-400°C is observed for PLA. Normally, the thermal degradation of PLA is complex and involves the generation of significant amounts of volatile products e.g., cyclic oligomers, lactides, carbon dioxide, acetaldehyde, ketene and carbon monoxide [106, 107]. For the composites, at least two weight-loss steps are observed around 350 and 450°C, involving the degradation of PLA and PE, respectively. Moreover, the weight-loss content according to the first step progressively increases with increasing PLA content. In air (Figure 47IIA), all samples start to degrade at around 300°C and multi-minor steps of weight loss are observed for the composite samples due to the complex degradation mechanisms. In comparison with PE, the composites seem to degrade at lower temperature with increasing PLA contents. To compare the results of the decomposition characteristics in a more quantitative way, the nonisothermal decomposition data of all samples are compared and summarized in Table 4. T_{onset} represents the onset degradation

temperature. T_{max} represents the temperature at the maximum weight loss rate, $(d\alpha/dt)_{max}$. The subscripts 1 and 2 represent the first- and second-major stages of the degradation, respectively. It is seen that T_{onset} and T_{max} of all polymers are mostly higher in nitrogen than in air. In fact, the thermal stability of polymer in air is somewhat lower than that in nitrogen. However, the situation that polymer has been exposed in air is more common than in nitrogen during real processing and application. T_{max1} of the composites seems to mostly increase with addition of the dispersed phases indicating the efficiency contribution from the dispersed phase. Note that, $(d\alpha/dt)_{max1}$ of the composites are much lower than those of the neat PLA polymer. Moreover, $(d\alpha/dt)_{max1}$ of the composites progressively increases with increasing PLA contents. Note that, $(d\alpha/dt)_{max2}$ of the composites progressively increase with increasing PLA contents and $(d\alpha/dt)_{max2}$ of the composites are much higher than $(d\alpha/dt)_{max1}$.

The DSC traces of degradation for the PE, rPET and the composites in nitrogen and in air are shown in Figure 47IB and IIB and Table 5, respectively. T_m and ΔH_m represent the melting temperature and melting enthalpy, respectively, whereas T_d and ΔH_d represent the peak temperature and the enthalpy associated with the thermal degradation process. It is seen that the DSC profiles of the samples are different in nitrogen and in air, arising from the different degradation mechanisms. The DSC curve of PE in nitrogen (Figure 47IB) shows melting endotherm with a minimum at 139°C. After this point, PE exhibits a broad endotherm and stretches up to $\approx 480^\circ\text{C}$. In the case of the PLA dispersed phase, the melting and broad endotherm peak at $\approx 155^\circ\text{C}$ and 370°C , respectively. These degradation peaks are near the region of maximum weight loss in the TGA data. In nitrogen, although the degradation temperatures of PLA dispersed phases is lower than that of the neat PE, the incorporation of 10 wt% PLA into PE results in a slight increase of degradation temperature (T_d) of the composites when compared with the neat matrix. Under heating in air, it is seen that not only the endothermic process but also the exothermic one occur during degradation for the neat PE and the composites. This is due to the fact that the concurrent and further degradation mechanisms in air tend to additionally involve the formation reaction. It is noticed that the DSC curve of PE shows melting endotherm with a minimum at $\approx 140^\circ\text{C}$ in air. A very broad degradation exotherm that

stretches from 350 to 500°C is observed and the DSC trace shows a large peak whose maximum is at $\approx 390^\circ\text{C}$. As seen from Table 5, the T_d decrease with increasing PLA dispersed phase contents. Under dynamic heating in nitrogen and in air, the thermal decomposition enthalpy (ΔH_d) of composites are lower than that of the neat PE matrix.

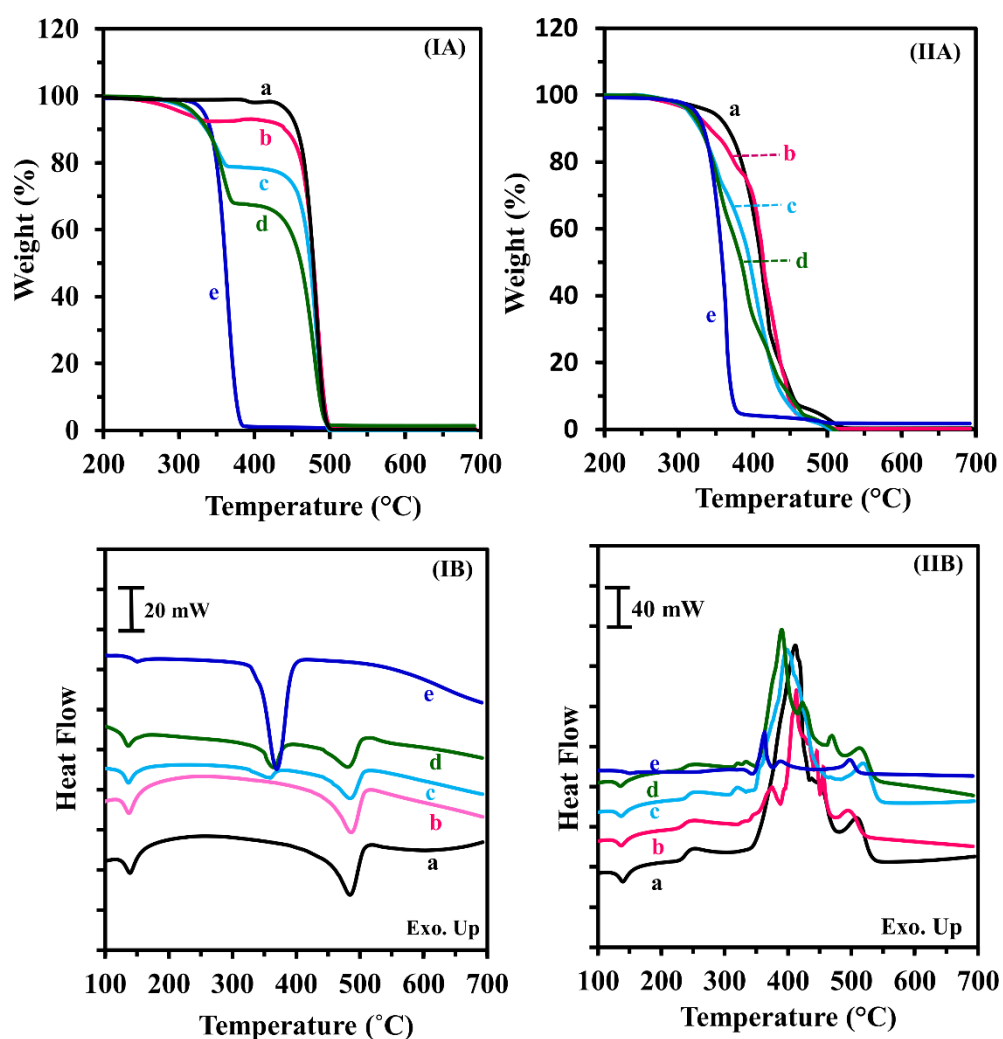


Figure 47. Dynamic TG curves (row I) and Simultaneous DSC curves (row B) for PE-PLA blends containing of (a) 0, (b) 10, (c) 20, (d) 30 and (e) 100 wt% dispersed phase at a heating rate $10^\circ\text{C}/\text{min}$ in nitrogen (column I) and in air (column II).

Table 4. Thermal decomposition data of PE/PLA composites under thermal degradation in nitrogen and in air.

Sample	T_{onset1} (°C)	T_{onset2} (°C)	T_{max1} (°C)	T_{max2} (°C)	$(d\alpha/dt)_{max1}$ (%/min)	$d\alpha/dt)_{max2}$ (%/min)	Char yield at 600 °C (wt%)
In Nitrogen							
PE	461	-	483	-	35.2	-	0.19
PE-10PLA	258	459	311	486	0.84	31.6	0.42
PE-20PLA	314	462	355	483	4.87	27.0	0.00
PE-30PLA	330	451	360	479	8.38	19.0	1.39
PLA	345	-	366	-	30.5	-	0.53
In Air							
PE	373	-	408	-	16.8	-	0.34
PE-10PLA	328	-	342	371	2.63	4.32	0.15
PE-20PLA	324	-	352	392	8.51	12.1	0.00
PE-30PLA	325	-	357	386	11.1	12.7	0.00
PLA	337	-	362	-	34.9	-	1.83

Table 5. Simultaneous DSC data of PE/PLA composites under thermal degradation in nitrogen and in air.

Sample	T_{m1} (°C)	ΔH_{m1} (kJ/g)	T_{m2} (°C)	ΔH_{m2} (kJ/g)	T_d (°C)	ΔH_d (kJ/g)
In nitrogen						
PE	139	0.07	-	-	484	0.79
PE-10PLA	137	0.06	-	-	486	0.51
PE-20PLA	136	0.11	360	0.08	484	0.51
PE-30PLA	136	0.08	365	0.22	481	0.37
PLA	151	0.01	-	-	369	1.11
In Air						
PE	140	0.10	-	-	412	6.55
PE-10PLA	136	0.07	-	-	413	0.40
PE-20PLA	136	0.06	-	-	399	0.37
PE-30PLA	136	0.05	-	-	390	5.03
PLA	155	0.02	-	-	364	0.21

4.21 Effect of rPET, LCP and PE-g-MA compatibilizer on nonisothermal decomposition

The effects of rPET, LCP and PE-g-MA compatibilizer on thermal stability in nitrogen and in air are also investigated as shown in Figures 48IA and IIA, respectively. Moreover, the thermal decomposition data all samples were quantitatively presented in Table 6. T_{onset} represents the onset degradation temperature. T_{max} represents the temperature at the maximum weight loss rate, $(da/dt)_{max}$. The subscripts 1 and 2 represent the first- and second-major stages of the degradation, respectively. In nitrogen, the nonisothermal TG profile of neat polymers reveals only a single weight-loss, whereas the composite reveals the two weight-loss step at the temperature range around 350-480 °C (Figure 48IA). Under dynamic heating in air (Figure 48IIA), the first major and the second minor weight-loss steps of PE, rPET and LCP are observed. Moreover, multi-minor steps of weight loss are observed for the composite samples, indicating that the degradation process is more complex in air than in nitrogen. The thermal resistance of PE-10PLA-10rPET is not significantly affected by compatibilizer. As seen from Table 4.5, it is seen that T_{onset1} and T_{max1} of PE-10PLA-10rPET are somewhat higher than the PE-10PLA-10LCP. It is found that $(da/dt)_{max1}$ of PE-10PLA-10rPET are lower than the PE-10PLA-10LCP. However, the addition LCP or rPET into PE/PLA composites are much higher than that of PE-10PLA both in nitrogen and in air. The results suggest the improved thermal stability of the composites, contributing from rPET and LCP.

The simultaneous DSC traces of thermos-oxidative degradation for the neat polymers and its composites are shown in Figures 4.28IB and IIB. The corresponding peak temperature (T_d) and enthalpy (ΔH_d) associated with the major degradation stage of all materials are also presented in Table 7. It is seen that the DSC profiles of the samples are different in nitrogen and in air, arising from the different degradation mechanisms. It is seen that the addition of the dispersed phases into PE does not affect the T_m of PE. In nitrogen, the degradation temperatures (T_d) of LCP- and rPET-containing PE/PLA are lower than those of the neat PE and PE/PLA. In air, T_d and ΔH_d of PE-10PLA-10LCP are much higher than that of PE-10PLA-10rPET.

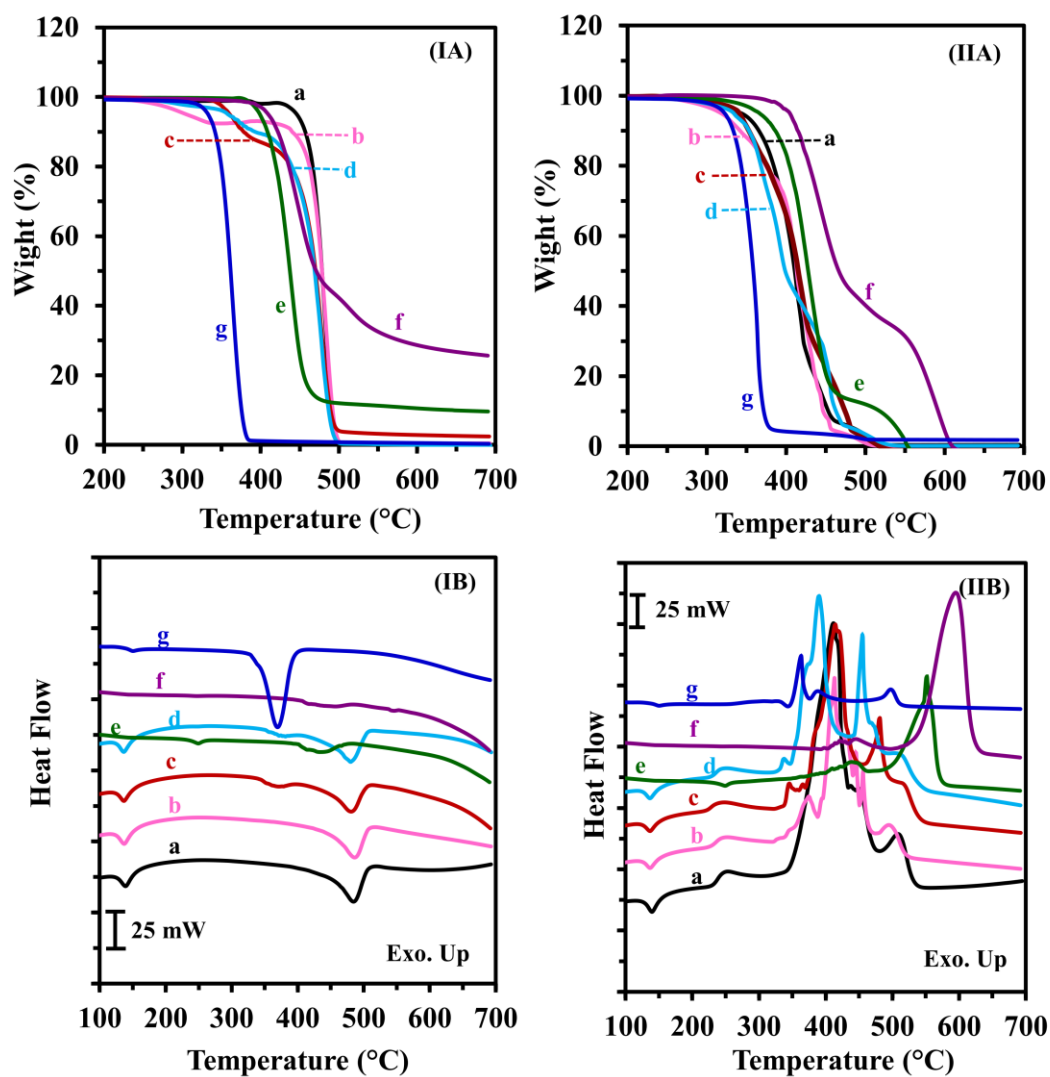


Figure 48. Dynamic TG curves (row A) and Simultaneous DSC curves (row B) of (a) PE, (b) PE-10PLA, (c) PE-10PLA-10LCP, (d) PE-10PLA-10rPET, (e) rPET (f) LCP and (g) PLA at a heating rate of 10 °C/min in nitrogen (column I) and in air (column II).

พหุบัณฑิต ชีวะ

Table 6. Thermal decomposition data of neat polymers and its composites in nitrogen and in air.

Sample	T_{onset1} (°C)	T_{onset2} (°C)	T_{max1} (°C)	T_{max2} (°C)	$(d\alpha/dt)_m$ $_{ax1}$ (%/min)	$d\alpha/dt)_{ma}$ $_{x2}$ (%/min)	Char yield at 600 °C (wt%)
In Nitrogen							
PE	461	-	483	-	35.2	-	0.19
PE-10PLA	258	459	311	486	0.84	31.6	0.42
PE-10PLA-10rPET	364	448	375	478	1.92	24.9	0.00
PE-10PLA-10LCP	352	489	369	478	3.30	23.3	2.85
PE-10PLA-10rPET- 5MA	348	445	374	480	2.86	22.8	0.73
PLA	345	-	366	-	30.5	-	0.53
rPET	409	-	440	-	21.1	-	10.5
LCP	418	-	448	-	9.90	-	28.7
In Air							
PE	373	-	408	-	16.8	-	0.34
PE-10PLA	328	-	342	371	2.63	4.32	0.15
PE-10PLA-10rPET	349	-	334	362	2.46	18.8	0.13
PE-10PLA-10LCP	342	-	342	362	4.18	4.74	0.00
PE-10PLA-10rPET- 5MA	350	-	355	372	5.81	10.0	0.00
PLA	337	-	362	-	34.9	-	1.83
rPET	397	-	429	548	16.1	4.98	0.00
LCP	409	-	440	586	9.14	7.05	4.15

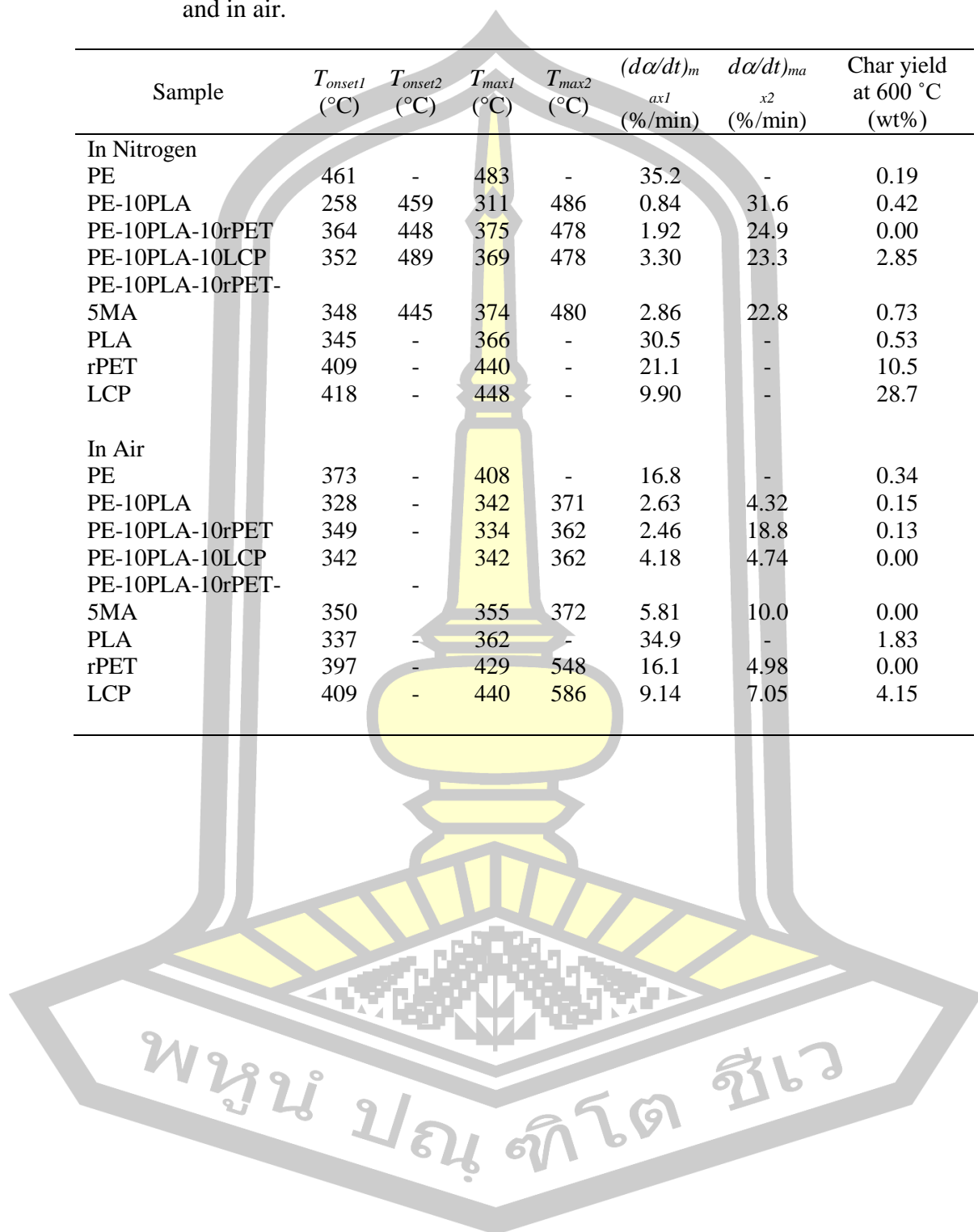
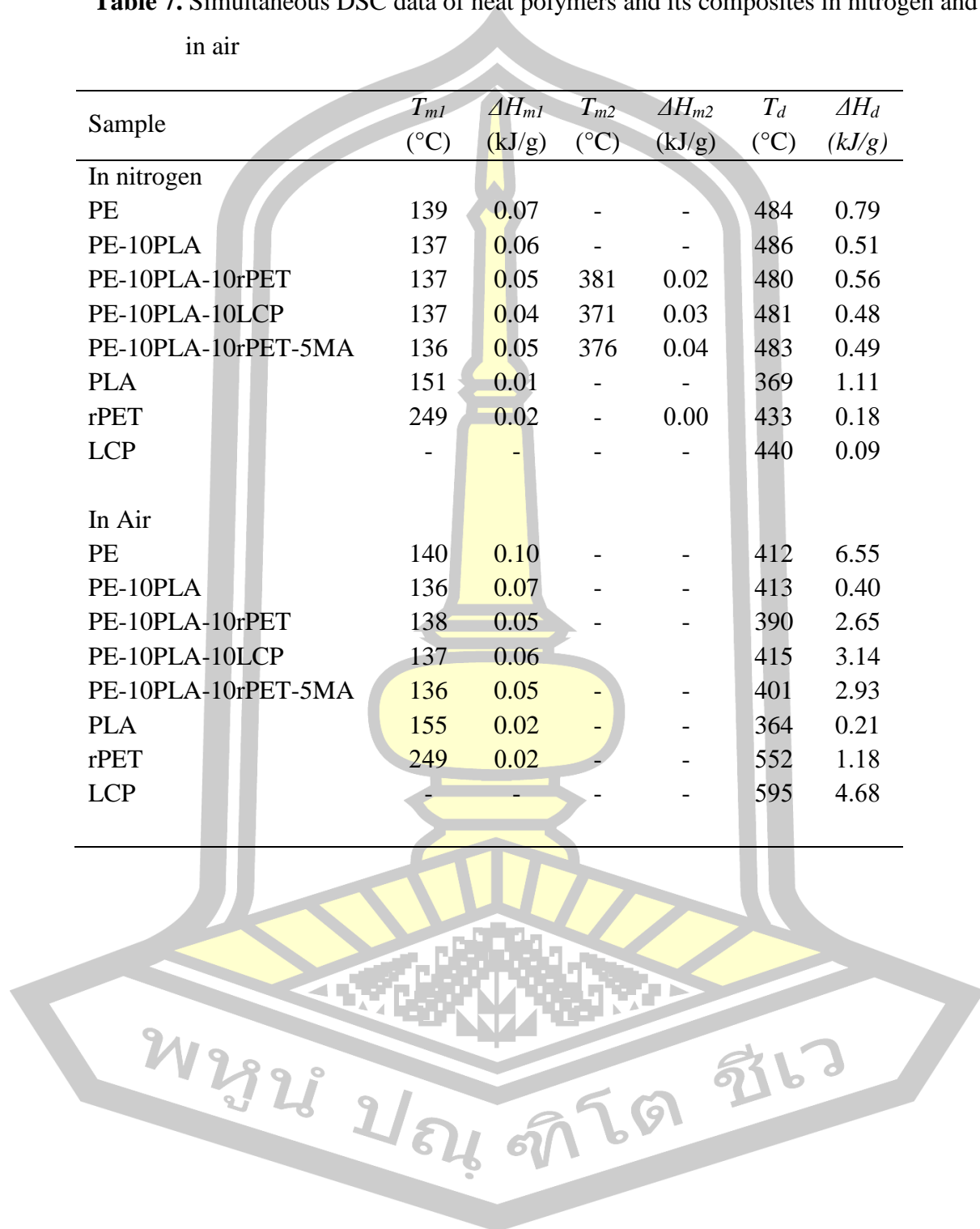


Table 7. Simultaneous DSC data of neat polymers and its composites in nitrogen and in air

Sample	T_{m1} (°C)	ΔH_{m1} (kJ/g)	T_{m2} (°C)	ΔH_{m2} (kJ/g)	T_d (°C)	ΔH_d (kJ/g)
In nitrogen						
PE	139	0.07	-	-	484	0.79
PE-10PLA	137	0.06	-	-	486	0.51
PE-10PLA-10rPET	137	0.05	381	0.02	480	0.56
PE-10PLA-10LCP	137	0.04	371	0.03	481	0.48
PE-10PLA-10rPET-5MA	136	0.05	376	0.04	483	0.49
PLA	151	0.01	-	-	369	1.11
rPET	249	0.02	-	0.00	433	0.18
LCP	-	-	-	-	440	0.09
In Air						
PE	140	0.10	-	-	412	6.55
PE-10PLA	136	0.07	-	-	413	0.40
PE-10PLA-10rPET	138	0.05	-	-	390	2.65
PE-10PLA-10LCP	137	0.06	-	-	415	3.14
PE-10PLA-10rPET-5MA	136	0.05	-	-	401	2.93
PLA	155	0.02	-	-	364	0.21
rPET	249	0.02	-	-	552	1.18
LCP	-	-	-	-	595	4.68



4.22 Effect of the polymer in the forms of strand, as-spun and drawn fibers on thermal properties

The thermal behavior of PE phase in the sample are studied by DSC. To clearly elucidate the effect of strand, as-spun and draw ratios at DR 20, the DSC traces and the DSC data of PLA pellet, PE-10PLA in the forms of extruded strand, as-spun sample and drawn fiber and PE-drawn fiber shown in Figure 49 and Table 8. The DSC curve of polymer samples shows melting exothermic. It is seen the endothermic peak associated with the fusion of the crystalline fraction of PLA is observed at about 150 and this peak is not clearly observed in the PLA-containing composites. The T_m and ΔH_m of samples are slightly shifted to higher temperature with in the forms of drawn fiber. When PE-10PLA composite in the forms of drawn fiber, the degree of crystallinity of PE phase increased. Note that, T_m , ΔH_m and X_c of neat PE and PE-10PLA composite in the forms of drawn fiber are comparable.

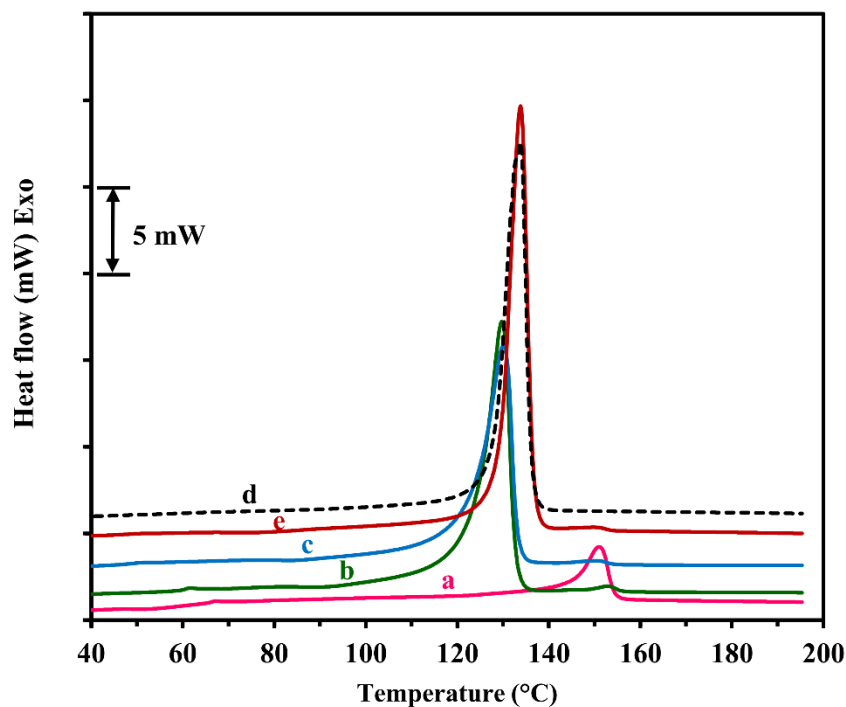


Figure 49. DSC curves of PLA pellet (a), PE-10PLA in the forms of extruded strand (b), as-spun sample (c) and drawn fiber (d) and PE-drawn fiber (e). The fibers were selected at DR=20.

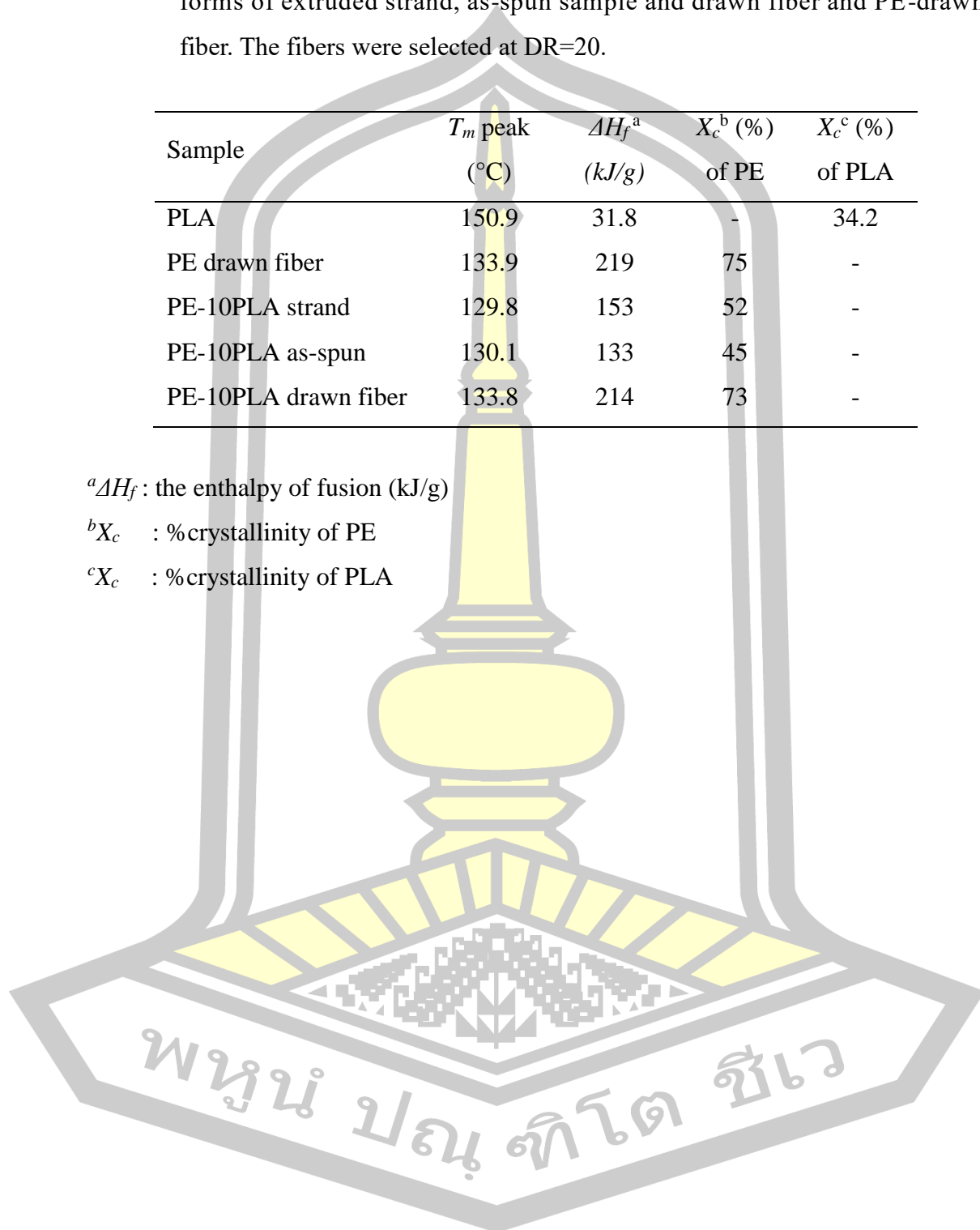
Table 8. Melting temperature and %crystallinity of PLA pellet, PE-10PLA in the forms of extruded strand, as-spun sample and drawn fiber and PE-drawn fiber. The fibers were selected at DR=20.

Sample	T_m peak (°C)	ΔH_f^a (kJ/g)	X_c^b (%) of PE	X_c^c (%) of PLA
PLA	150.9	31.8	-	34.2
PE drawn fiber	133.9	219	75	-
PE-10PLA strand	129.8	153	52	-
PE-10PLA as-spun	130.1	133	45	-
PE-10PLA drawn fiber	133.8	214	73	-

$^a\Delta H_f$: the enthalpy of fusion (kJ/g)

bX_c : %crystallinity of PE

cX_c : %crystallinity of PLA



4.23 Effect of PLA contents on x-ray diffraction of polymers

As seen from the tensile properties of PE-30PLA composite fiber that the tensile stress is much higher than those of PE, PE-10PLA, PE-20PLA and PE-30PLA. To more support the explanation, the XRD was performed.

The XRD patterns of PE, PE-10PLA, PE-20PLA and PE-30PLA fibers (DR=20) in meridinal and horizontal directions at DR=20 are shown in Figure 50. As seen from Figure 50A, PE has main reflection peaks at 16.9° (monodimic, (040), 21.5° (orthorhombic, 110) and 23.8° (orthorhombic, 200). The next two weak peaks are found at $2\theta = 30.0^\circ$ and $2\theta = 36.5^\circ$ attributing to reflection planes (210) and (020), respectively. In addition, there are several other weak reflection planes in the range of $2\theta = 38^\circ$ to $2\theta = 60^\circ$. These results are in good agreement with reported values of PE previously communicated. [108, 109]. It is seen that the intensity of XRD patterns are higher in meridinal than in equatorial direction. This may be due to the better molecular orientation in the meridinal (stretching direction of fiber) direction. The two crystalline characterization peaks (110) and (200) was progressively reduced in intensity with PLA loading. It is surprising that the peak at $2\theta = 16.9^\circ$ is observed for PE fiber, overlapping with (200/100) plans of PLA (α -form, orthorhombic unit cell) [110]. Moreover, (010) α plans of PLA is observed at $2\theta = 14.8^\circ$. Surprisingly, the XRD peaks especially, at 16.9° of PE-20PLA show much higher in meridinal than in equatorial direction indicating good orientation of PLA domains. However, no significant change of the mentioned peaks is observed for PE-30PLA. This may arise from the existing of cavities between fibers packing preparation.

To evaluate the relative effect contributed from PLA loading, the ratios of peak intensity at $2\theta = 21.5^\circ$ (110) to $2\theta = 23.8^\circ$ (200) and $2\theta = 16.9^\circ$ in meridinal direction and calculated as shown in Table 9. It is seen that the peak intensity ratios of $2\theta = 21.5^\circ / 2\theta = 23.8^\circ$ are not significantly different with PLA loading. Interestingly, the peak intensity ratio of $2\theta = 21.5^\circ / 2\theta = 16.9^\circ$ of PLA-30PLA dramatically drops compared with those of PE and PE-10PLA. This means that increase in crystallinity of PLA is observed with high content PLA loading. The obtained XRD results are in good agreement with the tensile properties.

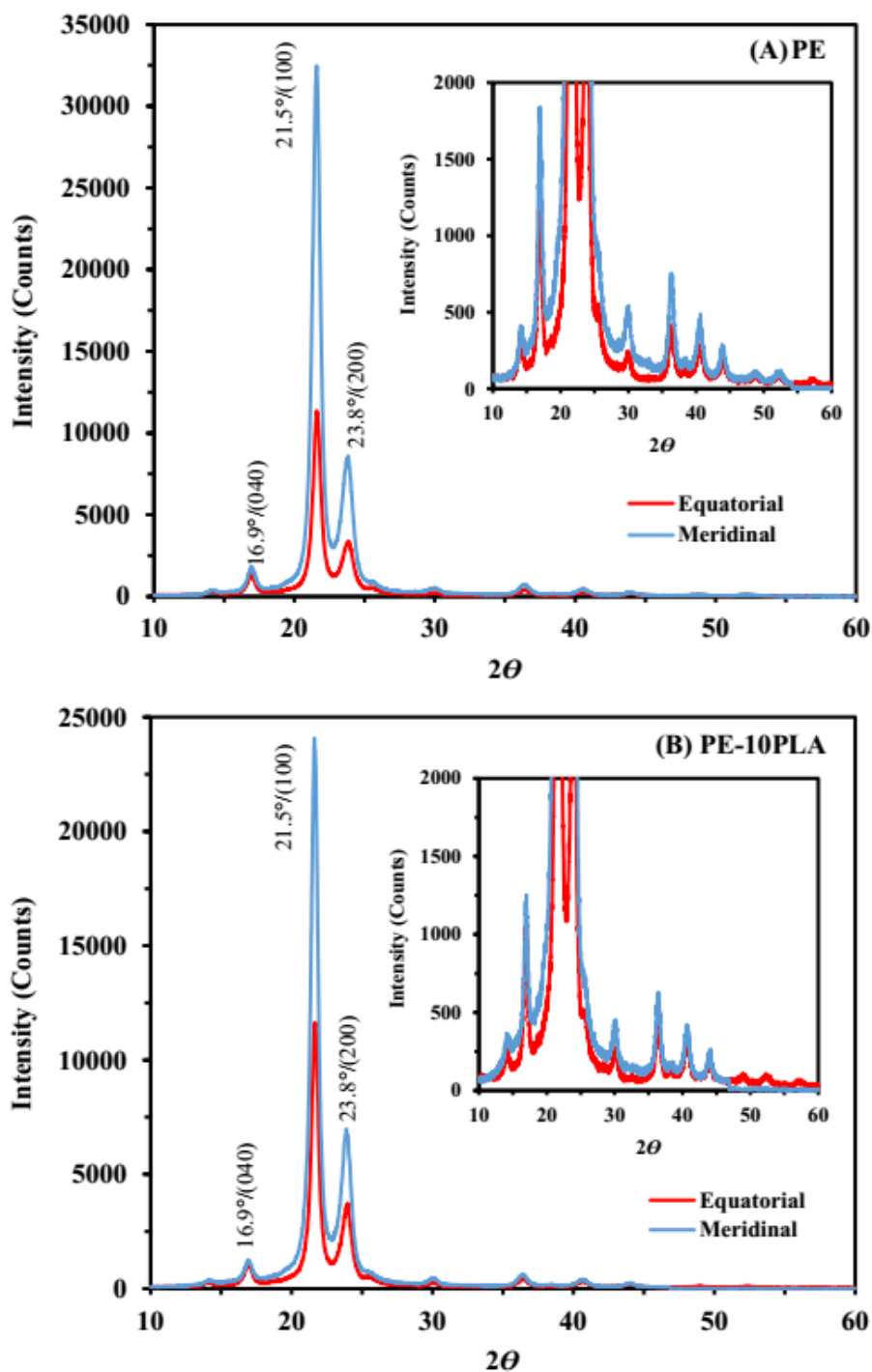


Figure 50. X-ray patterns for PE (A), PE-10PLA (B), PE-20PLA (C) and PE-30PLA (D) drawn fibers in equatorial and horizontal directions. All fibers were drawn at DR = 20.

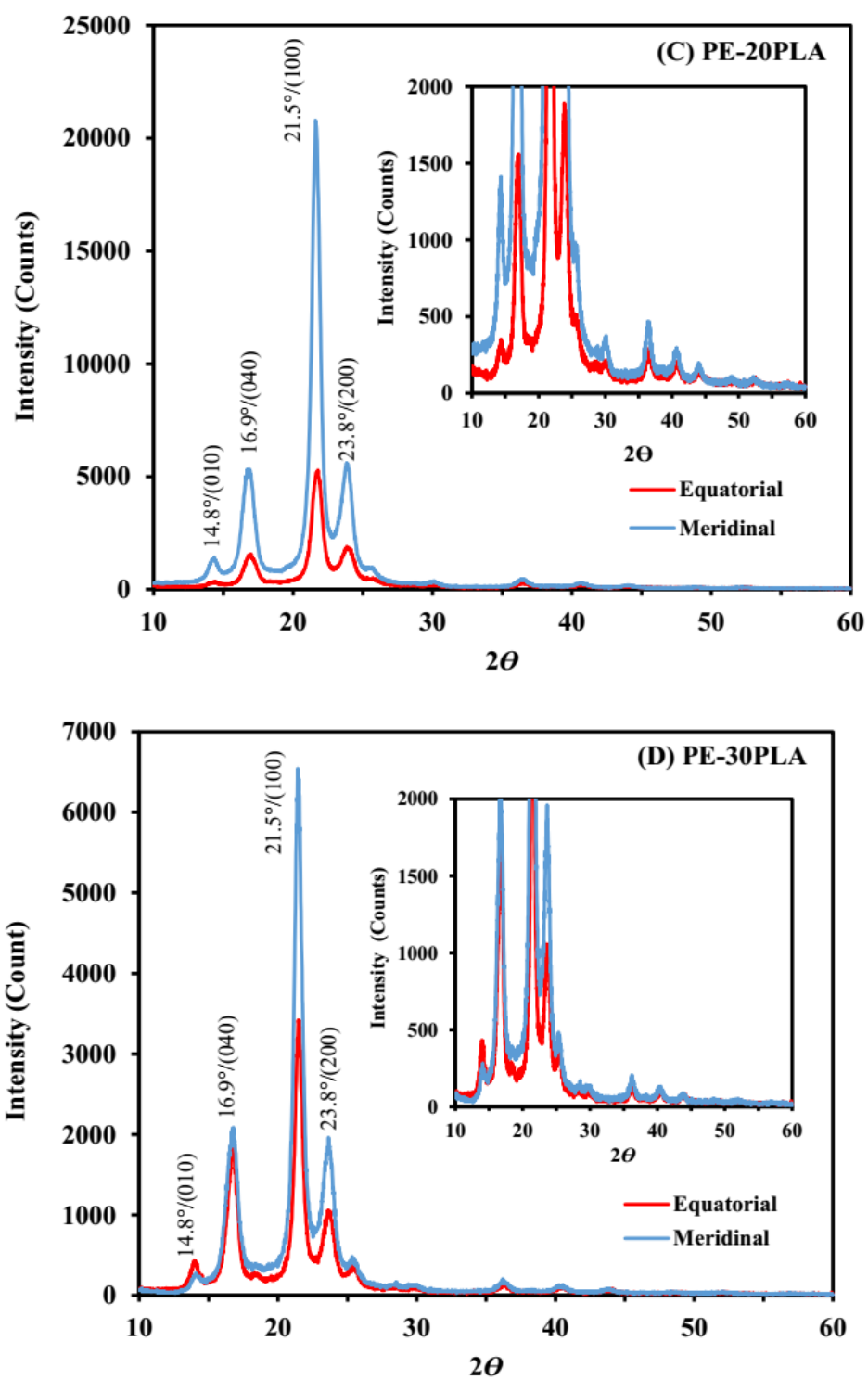
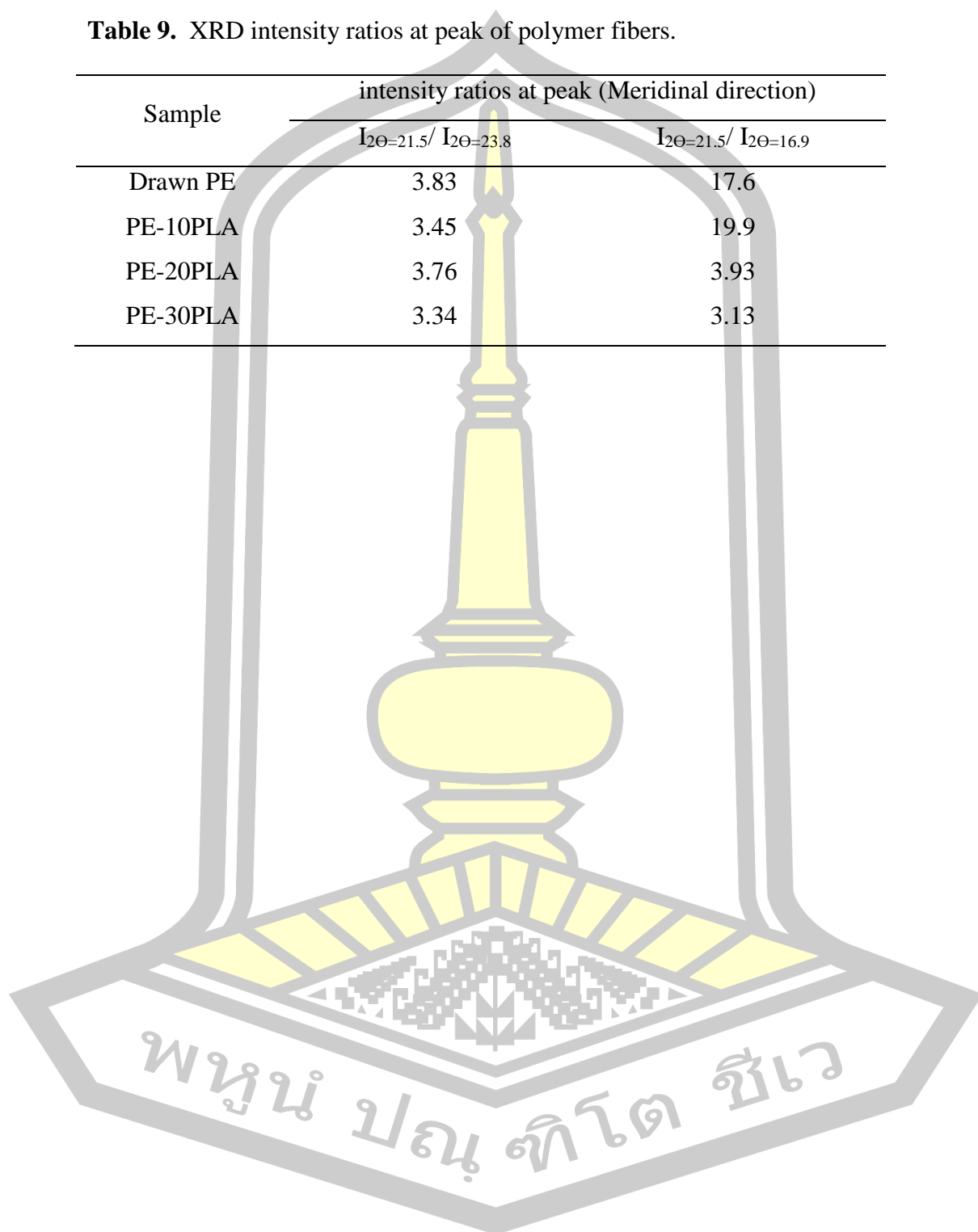


Figure 50 (continued).

Table 9. XRD intensity ratios at peak of polymer fibers.

Sample	intensity ratios at peak (Meridinal direction)	
	$I_{2\theta=21.5}/I_{2\theta=23.8}$	$I_{2\theta=21.5}/I_{2\theta=16.9}$
Drawn PE	3.83	17.6
PE-10PLA	3.45	19.9
PE-20PLA	3.76	3.93
PE-30PLA	3.34	3.13



CHAPTER 5

CONCLUSIONS

5.1 Conclusions

From the whole results of the present study, the following conclusions can be drawn;

1. The rheological results showed that the PLA, rPET, PLA-10LCP and PLA-20LCP exhibited Newtonian behavior while the non-Newtonian behavior is observed for LCP or rPET containing blends. The elongated LCP domains were clearly observed in an extruded strands with addition of LCP concentration while the elongated domains were not observed for PLA-rPET system.

2. The incorporation of small amount of PLA (20-30 wt%) into PE significantly lowered the melt viscosity of the blend system. The viscosity ratio of PE/PLA and PE/rPET systems were nearly the same and lied between 0-0.14 under applied angular frequency of about 0-500 rad/s. The presence of rPET and compatibilizer showed slightly effect on the rheological characteristics of PE/PLA systems.

3. Both PLA and rPET domains in as extruded strand were mostly found in the form of droplets. The domain size of PLA is mostly larger than that of rPET due to less compatibility of PLA and PE matrix. The fibrillation of PLA was observed in the as-spun sample whereas rPET appeared as droplets. Fibrillation of PLA and rPET domains was obviously observed for the composite fibers.

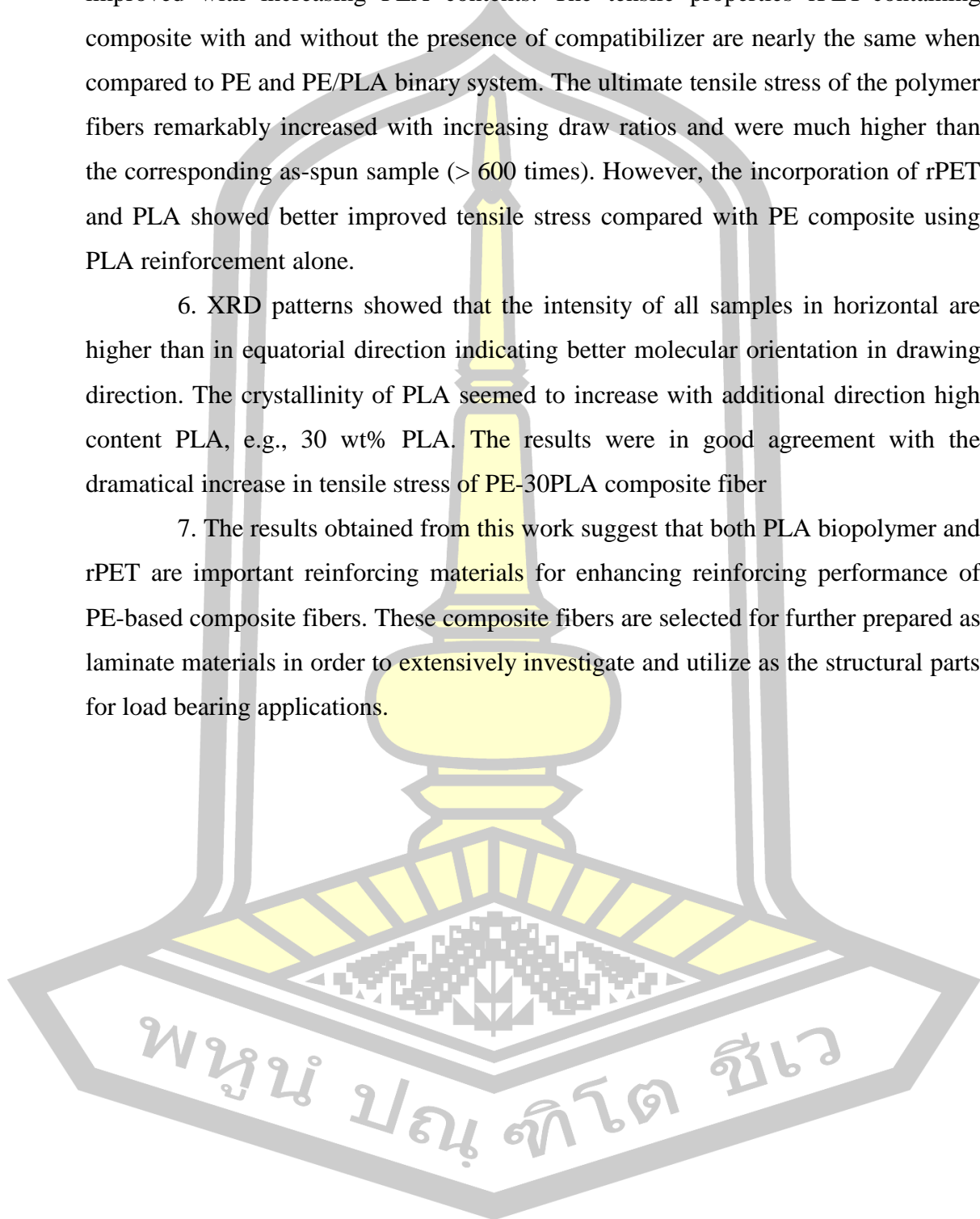
4. Thermal stability of the composites seemed to progressively decrease with PLA loading both in nitrogen and in air atmospheres. It is seen that the addition of rPET into PE/PLA clearly improved the thermal stability of the composite the further incorporation of compatibilizer slightly affected the stability compared with the rPET-containing composite.

5. From tensile results, the narrower strain range at yield point for the as-spun polymers and the decrease in elongation were observed with PLA loadings.

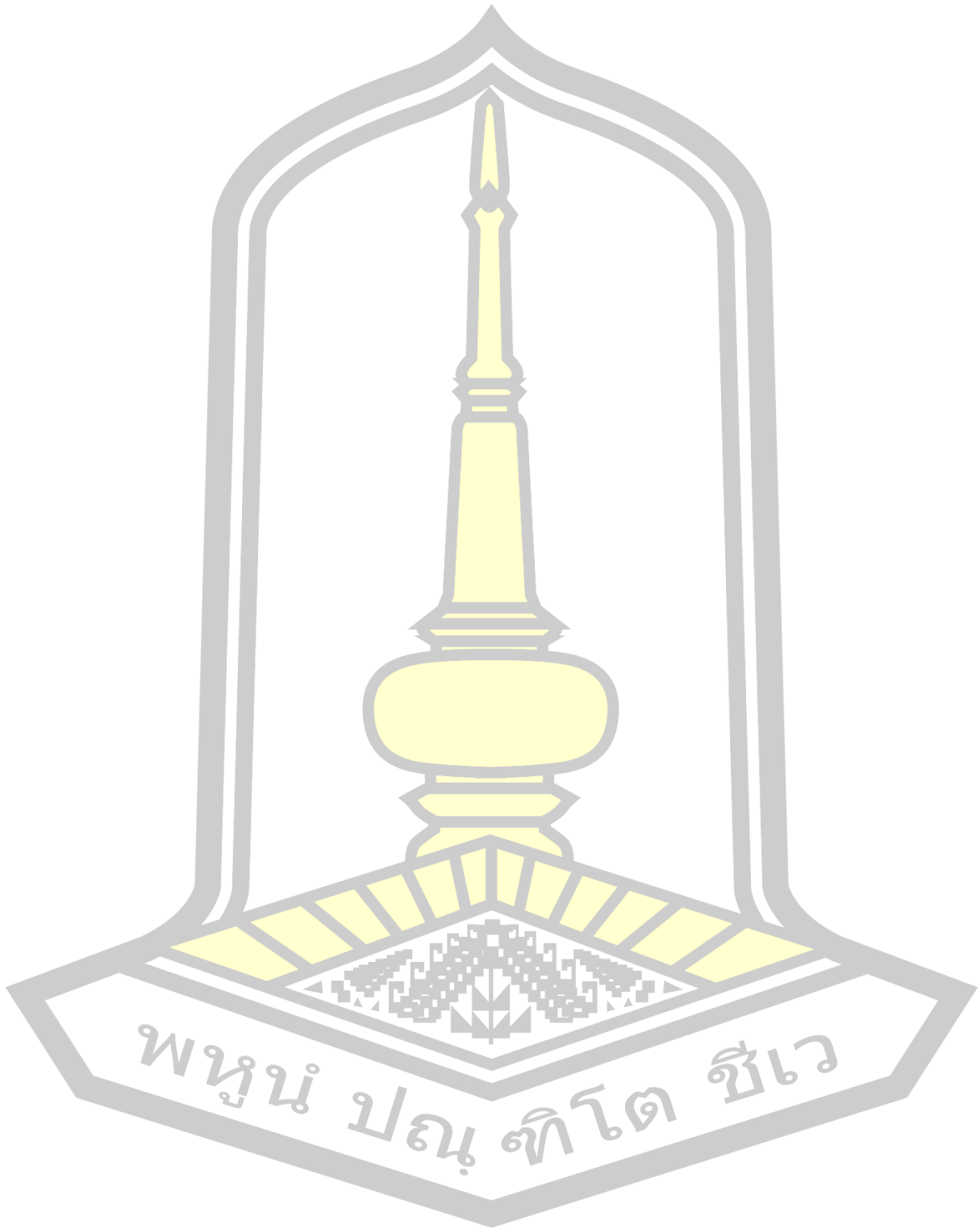
Moreover, secant modulus and ultimate strength of the as-spun samples were slightly improved with increasing PLA contents. The tensile properties rPET-containing composite with and without the presence of compatibilizer are nearly the same when compared to PE and PE/PLA binary system. The ultimate tensile stress of the polymer fibers remarkably increased with increasing draw ratios and were much higher than the corresponding as-spun sample (> 600 times). However, the incorporation of rPET and PLA showed better improved tensile stress compared with PE composite using PLA reinforcement alone.

6. XRD patterns showed that the intensity of all samples in horizontal are higher than in equatorial direction indicating better molecular orientation in drawing direction. The crystallinity of PLA seemed to increase with additional direction high content PLA, e.g., 30 wt% PLA. The results were in good agreement with the dramatical increase in tensile stress of PE-30PLA composite fiber

7. The results obtained from this work suggest that both PLA biopolymer and rPET are important reinforcing materials for enhancing reinforcing performance of PE-based composite fibers. These composite fibers are selected for further prepared as laminate materials in order to extensively investigate and utilize as the structural parts for load bearing applications.



REFERENCES



REFERENCES

1. Awaja F, Pavel D. Recycling of PET. *Eur Polym J.* 2005; 41(7): 1453-1477.
2. Park S, Kim S. Poly (ethylene terephthalate) recycling for high value added textiles. *Fash Text.* 2014; 1: 1-17.
3. Sulyman M, Haponiuk J, Formela K. Utilization of Recycled Polyethylene Terephthalate (PET) in Engineering Materials: A Review. *Int J Environ Sci Dev.* 2016; 7(2): 100-108.
4. Ochi T, Okubo S, Fukui K. Development of recycled PET fiber and its application as concrete-reinforcing fiber. *Cem Concr Compos.* 2007; 29(6): 448-455.
5. Kim SB, Yi NH, Kim HY, Kim JHJ, Song YC. Material and structural performance evaluation of recycled PET fiber reinforced concrete. *Cem Concr Compos.* 2010; 32(3): 232-240.
6. Kayaisang S, Saikrasun S, Amornsakchai T. Potential Use of Recycled PET in Comparison with Liquid Crystalline Polyester as a Dual Functional Additive for Enhancing Heat Stability and Reinforcement for High Density Polyethylene Composite Fibers. *J Polym Environ.* 2013; 21(1): 191-206.
7. Kayaisang S, Amornsakchai T, Saikrasun S. Potential utilization of recycled PET in comparison with liquid crystalline polymer as an additive for HDPE based composite fibers: Comparative investigation on mechanical performance of cross-ply laminates. *J Polym Eng.* 2013; 33(9): 793-802.
8. Garlotta D. A Literature Review of Poly (Lactic Acid). *J Polym Environ.* 2002; 9(2): 63-84.
9. Auras R, Harte B, Selke S. An overview of polylactides as packaging materials. *Macromol Biosci.* 2004; 4(9): 835-864.
10. Rasal RM, Janorkar AV, Hirt DE. Poly(lactic acid) modifications. *Prog Polym Sci.* 2010; 35(3): 338-356.

11. Jamshidian M, Tehrany EA, Imran M, Jacquot M, Desobry S. Poly-Lactic Acid: Production, applications, nanocomposites, and release studies. *Compr Rev Food Sci Food Saf.* 2010; 9(5): 552-571.
12. Murariu M, Dubois P. PLA composites: From production to properties. *Adv Drug Deliv Rev.* 2016; 107: 17-46.
13. Hamad K, Kaseem M, Deri F. Melt Rheology of Poly(Lactic Acid)/Low Density Polyethylene Polymer Blends. *Adv Chem Eng Sci.* 2011; 1(4): 208-214.
14. Sodergard A, Stolt M. Properties of lactic acid based polymers and their correlation with composition. *Prog Polym Sci.* 2002; 27: 1123-1163.
15. Bitinis N, Verdejo R, Maya EM, Espuche E, Cassagnau P, Lopez-Manchado MA. Physicochemical properties of organoclay filled polylactic acid/natural rubber blend bionanocomposites. *Compos Sci Technol.* 2012; 72(2): 305-313.
16. Castro-Aguirre E, Iñiguez-Franco F, Samsudin H, Fang X, Auras R. Poly(lactic acid)-Mass production, processing, industrial applications, and end of life. *Adv Drug Deliv Rev.* 2016; 107: 333-366.
17. Balakrishnan H, Hassan A, Wahit MU, Yussuf AA, Razak SBA. Novel toughened polylactic acid nanocomposite: Mechanical, thermal and morphological properties. *Mater Des.* 2010; 31(7): 3289-3298.
18. Ployetchara N, Suppakul P, Atong D, Pechyen C. Blend of polypropylene/poly(lactic acid) for medical packaging application: Physicochemical, thermal, mechanical, and barrier properties. *Energy Procedia.* 2014; 56(C): 201-210.
19. Reddy N, Nama D, Yang Y. Polylactic acid/polypropylene polyblend fibers for better resistance to degradation. *Polym Degrad Stab.* 2008; 93(1): 233-241.
20. Anderson KS, Lim SH, Hillmyer MA. Toughening of polylactide by melt blending with linear low-density polyethylene. *J Appl Polym Sci.* 2003; 89(14): 3757-3768.

21. Holz N, Goizueta G, Ciapati N. Linear Low-Density Polyethylene Addition to Polypropylene/Elastomer Blends: Phase Structure and Impact Properties. *Polym Eng Sci.* 1993; 3(22): 2765-2770.
22. Hassan A, Wahit MU, Chee CY. Mechanical and morphological properties of PP/NR/LLDPE ternary blend-effect of HVA-2. *Polym Test.* 2003; 22: 281-290.
23. Hamad K, Kaseem M, Deri F. Rheological and mechanical characterization of poly(lactic acid)/polypropylene polymer blends. *J Polym Res.* 2011; 18(6): 1799-1806.
24. Biresaw G, Carriere CJ. Compatibility and mechanical properties of blends of polystyrene with biodegradable polyesters. *Compos Part A Appl Sci Manuf.* 2004; 35(3): 313-320.
25. Hamad K, Kaseem M, Deri F. Rheological and mechanical properties of poly(lactic acid)/polystyrene polymer blend. *Polym Bull.* 2010; 65(5): 509-519.
26. Balakrishnan H, Hassan A, Wahit MU. Mechanical, Thermal, and Morphological Properties of Polylactic Acid/Linear Low Density Polyethylene Blends. *J Elastomers Plast.* 2010; 42: 223-239.
27. Singh G, Bhunia H, Rajor A, Jana RN, Choudhary V. Mechanical Properties and Morphology of Polylactide, Linear Low-Density Polyethylene, and Their Blends. *J Appl Polym Sci.* 2010; 118: 496-502.
28. Razak SIA, Sharif NFA, Rahman WAA. Biodegradable Polymers and their Bone Applications : A Review. *Int J Eng Sci.* 2012; 12(1): 31-49.
29. Luise RR. Application of High Temperature Polymers. Luise RR, editor. New York: CRC Press; 1997. 25 p.
30. Charles, E, Carraher J. Polymer chemistry. 4th ed. New York: Marcel Dekker; 1996.
31. PK M. Fiber-reinforced composites: Materials, Manufacturing, and Design. 3rd ed. New York: CRC Press; 2007.

32. Evstatiev M, Fakirov S, Krasteva B, Friedrich K, Covas JA, Cunha AM. Recycling of poly(ethylene terephthalate) as polymer-polymer composites. *Polym Eng Sci.* 2002; 42(4): 826-835.
33. Mbarek S, Jaziri M, Carrot C. Recycling Poly(ethylene terephthalate) Wastes: Properties of Poly(ethylene terephthalate)/Polycarbonate Blends and the Effect of a Transesterification Catalyst. *Polym Eng Sci.* 2006; 46(10): 1378-1386.
34. La Mantia FP, Botta L, Morreale M, Scaffaro R. Effect of small amounts of poly(lactic acid) on the recycling of poly(ethylene terephthalate) bottles. *Polym Degrad Stab.* 2012; 97(1): 21-24.
35. Saikrasun S, Limpisawasdi P, Amornsakchai T. Comparative study on phase and properties between rPET/PS and LCP/PS in situ microfibrillar-reinforced composites. *J Polym Res.* 2009; 16(4): 443-454.
36. Sunan S, Panpirada L, Taweechai A. Effect of LCP and rPET as Reinforcing Materials on Rheology, Morphology, and Thermal Properties of in situ Microfibrillar-Reinforced Elastomer Composites. *J Appl Polym Sci.* 2009; 112: 1897-1908.
37. Sombatdee S, Saikrasun S, Amornsakchai T. Phase behavior and thermal properties of polypropylene in situ reinforced with liquid crystalline polymer and rPET. *J Reinf Plast Compos.* 2009; 28(24): 2983-2998.
38. Sombatdee S, Amornsakchai T, Saikrasun S. Reinforcing performance of recycled PET microfibrils in comparison with liquid crystalline polymer for polypropylene based composite fibers. *J Polym Res.* 2012; 19(3): 1-13.
39. Kayaisang S, Amornsakchai T, Saikrasun S. Influence of liquid crystalline polymer and recycled PET as minor blending components on rheological behavior, morphology, and thermal properties of thermoplastic blends. *Polym Adv Technol.* 2009; 20(12): 1136-1145.
40. Fowler PA, Hughes JM, Elias RM. Biocomposites: technology, environmental credentials and market forces. *J Sci Food Agric.* 2006; 86: 1781-1789.

41. Mohanty AK, Misra M, Drzal LT. Sustainable Bio-Composites from renewable resources: Opportunities and challenges in the green materials world. *J Polym Environ.* 2002; 10(1-2): 19-26.
42. Yu L, Dean K, Li L. Polymer blends and composites from renewable resources. *Prog Polym Sci.* 2006; 31: 576-602.
43. Faruk O, Bledzki AK, Fink HP, Sain M. Biocomposites reinforced with natural fibers: 2000-2010. *Prog Polym Sci.* 2012; 37(11): 1552-1596.
44. Jayaraman K. Manufacturing sisal – polypropylene composites with minimum fibre degradation. *Compos Sci Technol.* 2008; 63(2003): 367-374.
45. Li Y, Hu C, Yu Y. Interfacial studies of sisal fiber reinforced high density polyethylene (HDPE) composites. *Compos Part A Appl Sci Manuf.* 2008; 39(4): 570-578.
46. Li X, Tabil LG, Oguocha IN, Panigrahi S. Thermal diffusivity, thermal conductivity, and specific heat of flax fiber-HDPE biocomposites at processing temperatures. *Compos Sci Technol.* 2008; 68(7-8): 1753-1758.
47. Wang H, Chang R, Sheng K chuan, Adl M, Qian X qun. Impact Response of Bamboo-Plastic Composites with the Properties of Bamboo and Polyvinylchloride (PVC). *J Bionic Eng.* 2008; 5: 28-33.
48. Singha AS, Rana RK. Natural fiber reinforced polystyrene composites: Effect of fiber loading, fiber dimensions and surface modification on mechanical properties. *Mater Des.* 2012; 41: 289-297.
49. Alvarez VA, Terenzi A, Kenny JM, Vázquez A. Melt rheological behavior of starch-based matrix composites reinforced with short sisal fibers. *Polym Eng Sci.* 2004; 44(10): 1907-1914.
50. Wong S, Shanks R, Hodzic A. Interfacial improvements in poly(3-hydroxybutyrate)-flax fibre composites with hydrogen bonding additives. *Compos Sci Technol.* 2004; 64(9): 1321-1330.

51. Arbelaz A, Fernández B, Valea A, Mondragon I. Mechanical properties of short flax fibre bundle/poly(ϵ -lactone-caprolactone) composites: Influence of matrix modification and fibre content. *Carbohydr Polym.* 2006; 64(2): 224-232.
52. Liu L, Yu J, Cheng L, Qu W. Mechanical properties of poly(butylene succinate) (PBS) biocomposites reinforced with surface modified jute fibre. *Compos Part A Appl Sci Manuf.* 2009; 40(5): 669-674.
53. Lunt J. Large-scale production, properties and commercial applications of polylactic acid polymers. *Polym Degrad Stab.* 1998; 59(1): 145-152.
54. Hamad K, Kaseem M, Yang HW, Deri F, Ko YG. Properties and medical applications of polylactic acid: A review. *Express Polym Lett.* 2015; 9(5): 435-455.
55. Avinc O, Khoddami A. OVERVIEW OF POLY (LACTIC ACID) (PLA) FIBRE Part I : Production , Properties , Performance , Environmental Impact , and End-use Applications of Poly(lactic acid) Fibres. *Fibre Chem.* 2009; 41(6): 16-25.
56. Jiang L, Zhang J, Wolcott MP. Comparison of polylactide/nano-sized calcium carbonate and polylactide/montmorillonite composites: Reinforcing effects and toughening mechanisms. *Polymer.* 2007; 48(26): 7632-7644.
57. Evagelia K, Michel N, Panayiotis G. Comparative Study of PLA Nanocomposites Reinforced with Clay and Silica Nanofillers and Their Mixtures. *J Appl Polym Sci.* 2011; 122(3): 1519-1529.
58. Piekarska K, Sowinski P, Piorkowska E, Haque MMU, Pracella M. Structure and properties of hybrid PLA nanocomposites with inorganic nanofillers and cellulose fibers. *Compos Part A Appl Sci Manuf.* 2016; 82: 34-41.
59. Bledzki AK, Jaszkievicz A, Scherzer D. Mechanical properties of PLA composites with man-made cellulose and abaca fibres. *Compos Part A Appl Sci Manuf.* 2009; 40(4): 404-412.
60. Xia X, Liu W, Zhou L, Liu H, He S, Zhu C. Study on flax fiber toughened poly (lactic acid) composites. *J Appl Polym Sci.* 2015; 132(38): 1-10.

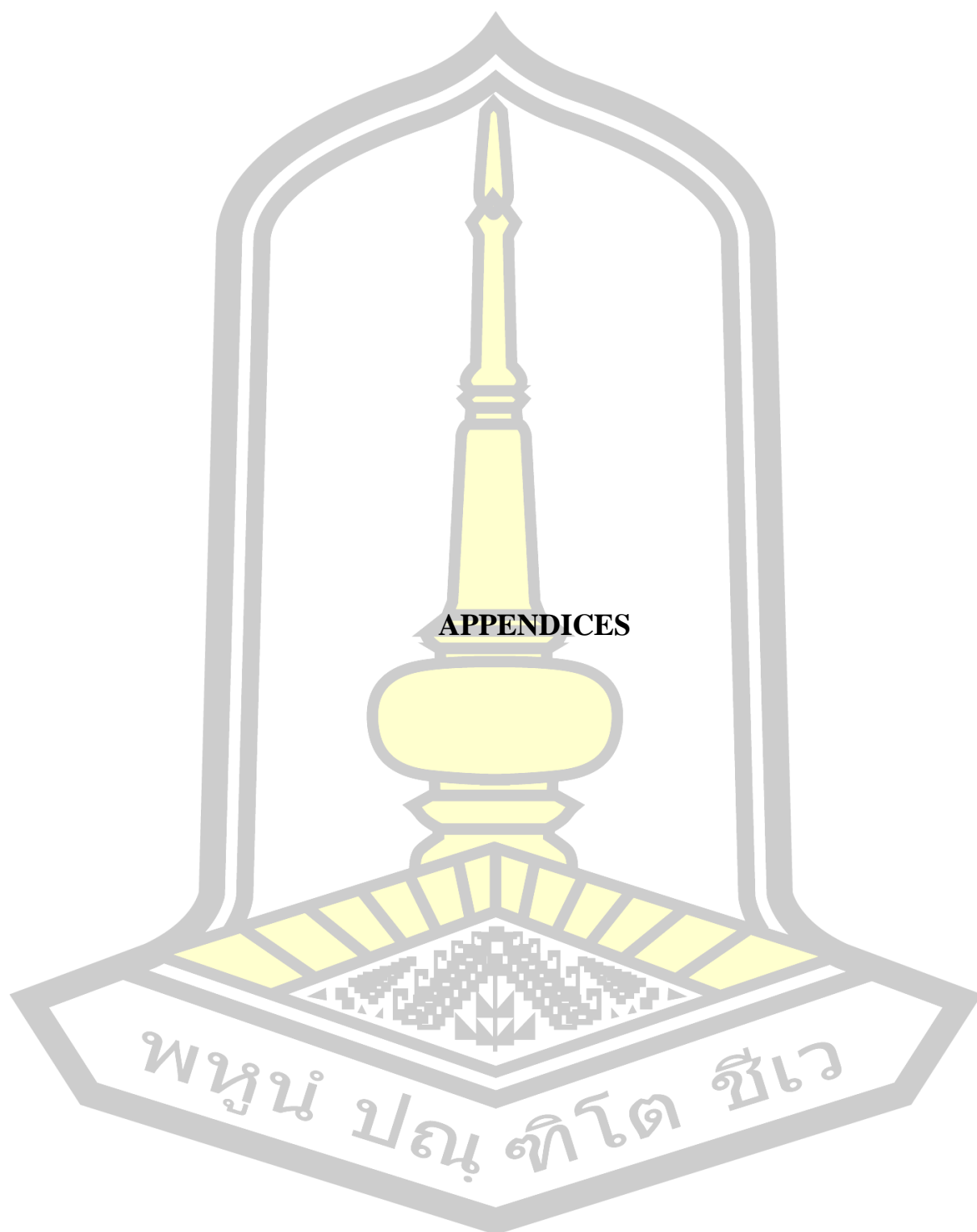
61. Li K, Mao B, Cebe P. Electrospun fibers of poly(ethylene terephthalate) blended with poly(lactic acid). *J Therm Anal Calorim.* 2014; 116(3): 1351-1359.
62. Saini P, Arora M, Kumar MNVR. Poly(lactic acid) blends in biomedical applications. *Adv Drug Deliv Rev.* 2016; 107: 47-59.
63. Pawar RP, Tekale SU, Shisodia SU, Totre JT, Domb AJ. Biomedical Applications of Poly (Lactic Acid). 2014; 4(1): 40-51.
64. Sankaran KK, Krishnan UM, Sethuraman S. Axially aligned 3D nanofibrous grafts of PLA-PCL for small diameter cardiovascular applications. *J Biomater Sci Polym Ed.* 2014; 25(16): 1791-1812.
65. Mi HY, Salick MR, Jing X, Jacques BR, Crone WC, Peng XF, et al. Characterization of thermoplastic polyurethane/polylactic acid (TPU/PLA) tissue engineering scaffolds fabricated by microcellular injection molding. *Mater Sci Eng C.* 2013; 33(8): 4767-4776.
66. Ramdhanie LI, Aubuchon SR, Boland ED, Knapp DC, Barnes CP, Simpson DG, et al. Thermal and Mechanical Characterization of Electrospun Blends of Poly(lactic acid) and Poly(glycolic acid). *Polym J.* 2006; 38(11): 1137-1145.
67. Gendron R. *Thermoplastic foam processing: Principle and development.* New York: CRC Press; 2005.
68. Anderson KS, Hillmyer MA. The influence of block copolymer microstructure on the toughness of compatibilized polylactide/polyethylene blends. *Polymer.* 2004; 45(26): 8809-8823.
69. Yoo TW, Yoon HG, Choi SJ, Kim MS, Kim YH, Kim WN. Effects of compatibilizers on the mechanical properties and interfacial tension of polypropylene and poly(lactic acid) blends. *Macromol Res.* 2010; 18(6): 583-588.
70. Choudhary P, Mohanty S, Nayak SK, Unnikrishnan L. Poly(L-lactide)/polypropylene blends: evaluation of mechanical, thermal, and morphological characteristics. *J Appl Polym Sci.* 2011; 121(6): 3223-3237.

71. Lai SM, Lan YC, Wu WL, Wang YJ. Compatibility improvement of poly(lactic acid)/thermoplastic polyurethane blends with 3-aminopropyl triethoxysilane. *J Appl Polym Sci*. 2015; 132(30): 1-9.
72. Mallick PK. *Fiber-Reinforced*. 3rd ed. New York: CRC Press; 2008.
73. Dealy JM, Wissbrun KF. *Melt Rheology and Its Role in Plastics Processing: Theory and Application*. Norwell: Chapman & Hall/CRC; 1999.
74. Gupta VB, Kothari VK. *Manufactured Fibre Technology*. London: Chapman & Hall/CRC; 1997.
75. Nielsen L. *Polymer rheology*. New York: Marcel Dekker Inc; 1977.
76. Saikrasun S, Bualek-Limcharoen S, Kohjiya S, Urayama K. Thermotropic liquid-crystalline copolyester/thermoplastic elastomer in situ composites. I. Rheology, morphology, and mechanical properties of extruded strands. *J Appl Polym Sci*. 2003; 89(10): 2676-2685.
77. Mark HF. *Encyclopedia of Polymer Science and Engineering*. New York: Wiley; 1987.
78. Hatakeyama T, Quinn FX. *Thermal Analysis Fundamentals and Applications to Polymer Science*. 2nd ed. New York: John Wiley & Sons; 1999.
79. Nielsen L, Landel R. *Mechanical properties of polymer and composite*. 2nd ed. New York: Marcel Dekker Inc; 1996.
80. Navarro R, Tirre L, Kenny JM, Jimenez A. Thermal degradation of recycled polypropylene toughened with elastomers. *J Degrad Stab*. 2003; 82: 279-290.
81. Pramoda KP, Chung TS, Liu SL, Oikawa H, Yamaguchi A. Characterization and thermal degradation of polyamide and polyamide liquid crystalline polymer. *Polym Degrad Stab*. 2000; 67: 365-374.
82. Xu QW, Man HC, Lau WS. The effect of a third component on the morphology and mechanical properties of liquid-crystalline polymer and polypropylene in situ composites. *Compos Sci Technol*. 1999; 59(2): 291-296.

83. Thomas S, Shanks R, Chandrasekharakurup S. Nanostructure polymer blends. USA: Elsevier Inc; 2014.
84. Fultz B, Howe J. Transmission electron microscopy and diffractometry of materials. New York: Verlag Berlin Heidelberg; 2013.
85. Sombatdee S, Saikrasun S, Amornsakchai T. Effects of polylactic acid and rPET minor components on phase evolution, tensile and thermal properties of polyethylene-based composite fibers. *Polym Adv Technol*. 2018; 29: 1123-1137.
86. Harris AM, Lee EC. Improving Mechanical Performance of Injection Molded PLA by Controlling Crystallinity. *J Appl Polym Sci*. 2008; 107: 2246-2255.
87. Srithep Y, Nealey P, Turng L-S. Effects of Annealing Time and Temperature on the Crystallinity and Heat Resistance Behavior of Injection-Molded Poly(lactic acid). *Polym Eng Sci*. 2012; 1-9.
88. Wunderlich B. *Macromolecular Physics*. New York: Academic press; 1980.
89. Hsieh T, Tiu C, Hsieh K, Simon GP. Characterization of thermotropic liquid crystalline polyester/polycarbonate blends: Miscibility, rheology, and free volume behavior. *J Appl Polym Sci*. 2000;77:2319–30.
90. Isayev AI, Modic M. Self-Reinforced Melt Processible Polymer Composites: Extrusion, Compression, and Injection Molding. *Polym Compos*. 1987; 8(3): 158-175.
91. Blizzard KG, Baird DG. The Morphology and Rheology of Polymer Blends Containing a Liquid Crystalline Copolyester¹³. *Polym Eng Sci*. 2005; 27(9): 653-662.
92. Mehta A, Isayev AI. The Dynamic Properties, Temperature Transitions, and Thermal Stability of Poly(etheretherketone)- Thermotropic Liquid Crystalline Polymer Blends. *Polym Eng Sci*. 1991; 31(13): 963-970.

93. Seo Y, Kim KU. Study on the ternary blends of nylon 6, a thermotropic liquid crystalline polymer, and a thermoplastic elastomer. *Polym Eng Sci.* 1998; 38(4): 596-604.
94. AlMaadeed M, Ouederni M, Khanam P. Effect of chain structure on the properties of Glass fibre/polyethylene composites. *Mater Des.* 2013; 47: 725-730.
95. Kengkhetkit N, Amornsakchai T. A new approach to “Greening” plastic composites using pineapple leaf waste for performance and cost effectiveness. *Mater Des.* 2014; 55: 292-299.
96. Chantreasakul, S Amornsakchai T. High strength polyethylene fibers from high density polyethylene/organoclay composites. *Polym Eng Sci.* 2007; 47: 943-450.
97. Murugan R R. Development of nanocomposites for bone grafting. *Compos Sci Technol. Compos Sci Technol.* 2005; 65: 2385-2406.
98. Torabinejad B, Mohammadi-Rovshandeh, J Davachi M, Zamanian A. Synthesis and characterization of nanocomposite scaffolds based on triblock copolymer of L-lactide, ϵ -caprolactone and nano-hydroxyapatite for bone tissue engineering. *Mater Sci Eng, C.* 2014; 42: 199-210.
99. Liu Z, Chen Y, Ding W, Zhang C. Filling behavior, morphology evolution and crystallization behavior of microinjection molded poly(lactic acid)/hydroxyapatite nanocomposites. *Compos Part A.* 2015; 72: 85-89.
100. Wan Y, Wu C, Xiong G, Zuo G, Jin J, Ren K, et al. Mechanical properties and cytotoxicity of nanoplate-like hydroxyapatite/ polylactide nanocomposites prepared by intercalation technique. *J Mech Behav Biomed.* 2015; 47: 29-37.
101. Nejati E, Mirzadeh H, Zandi M. Synthesis and characterization of nano-hydroxyapatite rods/poly(L-lactide acid) composite scaffold for bone tissue engineering. *Compos Part A.* 2008; 39: 1589-1596.

102. Wang M, Hench L., Bonfield W. Bioglass®/high density polyethylene composite for soft tissue application: Preparation and evaluation. *J Biomed Mater Res.* 1998; 42: 577-586.
103. Sarsilmaz F, Orhan N, Unsaldi E, Durmus AS, Colakoglu N. A polyethylene-high proportion hydroxyapatite implant and its investigation in vivo. *Acta Bioeng Biomech.* 2007; 9(2): 9-16.
104. Abu Bakar MS, Cheang P, Khor KA. Tensile properties and microstructural analysis of spheroidized hydroxyapatite-poly(etheretherketone) biocomposites. *Mater Sci Eng, A.* 2003; 345: 55-63.
105. Vyazovkin S, Wight CA. Isothermal and Nonisothermal Reaction Kinetics in Solid: In Search of Ways toward Consensus. *J Phys Chem A.* 1997; 101(44): 8279-8284.
106. Nalbandi A. Kinetics of thermal degradation of polylactic acid under N₂ atmosphere. *Iran Polym J.* 2001; 10: 371.
107. Babanalbandi A, Hill D, Hunter D, Kettle L. Thermal stability of poly (lactic acid) before and after g -radiolysis. *Polym Int.* 1999; 48(10): 980-984.
108. Razmkhah K, Chmel N, Gibson M, Rodger A. Oxidized polyethylene films for orienting polar molecules for linear dichroism spectroscopy. *Analyst.* 2014; 139: 1372-1382.
109. Chouit F, Guelulati O, Boukhezar S, Harat A, Guerioune M, Badi A. Synthesis and characterization of HDPE/N-MWNT nanocomposite films. *Nanoscale Res Lett.* 2014; 9: 288.
110. Zhang H, Wang S, Zhang S, Ma R, Wang Y, Cao W, et al. Crystallization behavior of poly(lactic acid) with a self-assembly aryl amide nucleating agent probed by real-time infrared spectroscopy and X-ray diffraction. *Polym Test.* 2017; 64: 12-19.



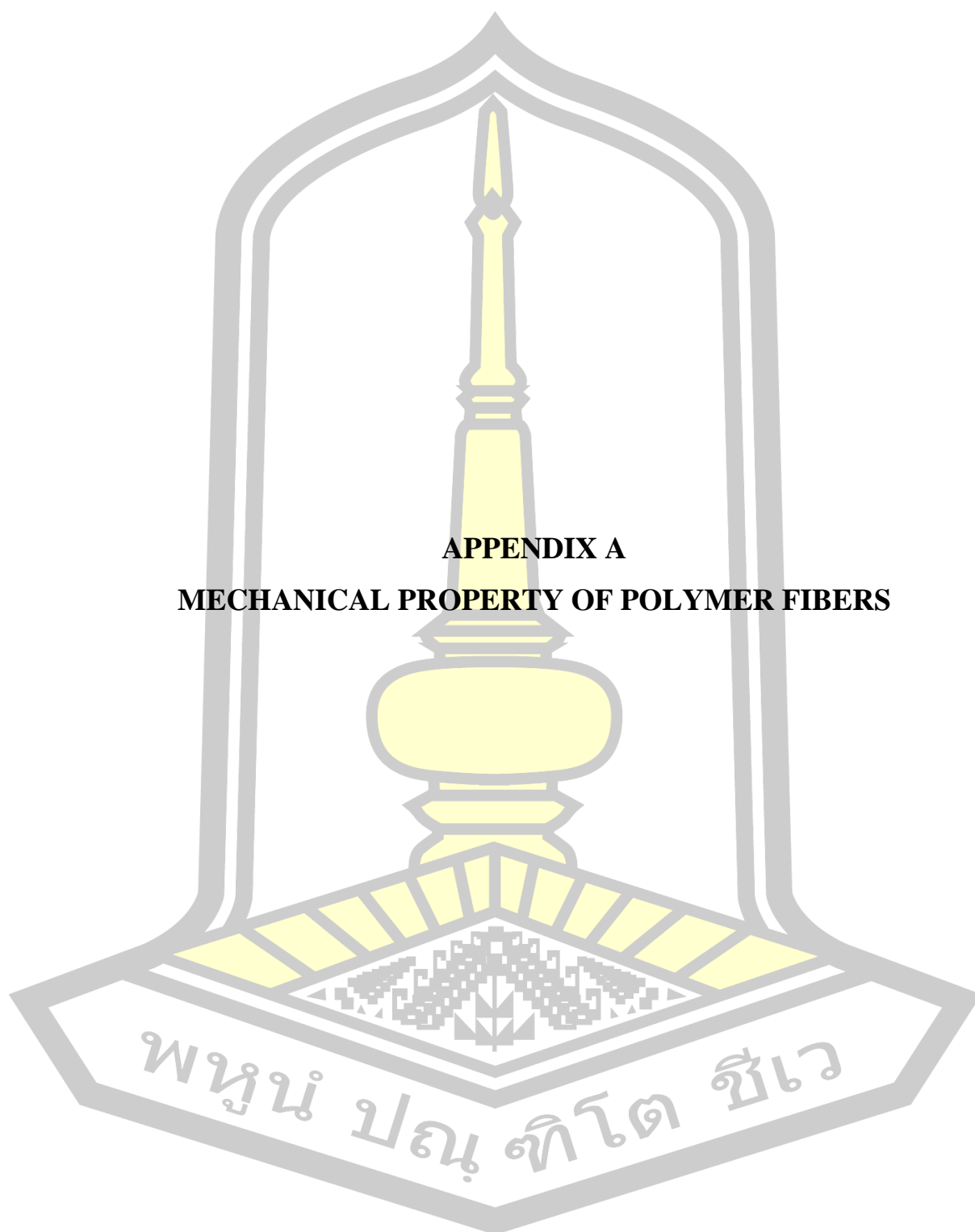


Table A1 Effect of PLA contents on secant modulus, tensile strength and elongation at break of the as-spun and composite fibers.

Sample	Secant modulus (GPa)	Tensile strength (MPa)	Elongation at break (%)
As-spun			
PE	0.76 ± 0.042	16.42 ± 0.996	7.40 ± 1.10
PE-10PLA	0.88 ± 0.041	17.38 ± 1.69	6.72 ± 1.13
PE-20PLA	1.13 ± 0.060	22.33 ± 0.840	3.26 ± 0.318
PE-30PLA	1.11 ± 0.080	21.40 ± 1.13	2.61 ± 0.273
Drawn fibers			
PE	12.9 ± 1.56	666.0 ± 24.4	8.40 ± 0.978
PE-10PLA	13.1 ± 0.840	592.3 ± 38.2	6.53 ± 0.490
PE-20PLA	13.2 ± 0.886	647.1 ± 46.7	7.47 ± 1.100
PE-30PLA	41.9 ± 4.07	1154.2 ± 140.5	4.50 ± 0.311

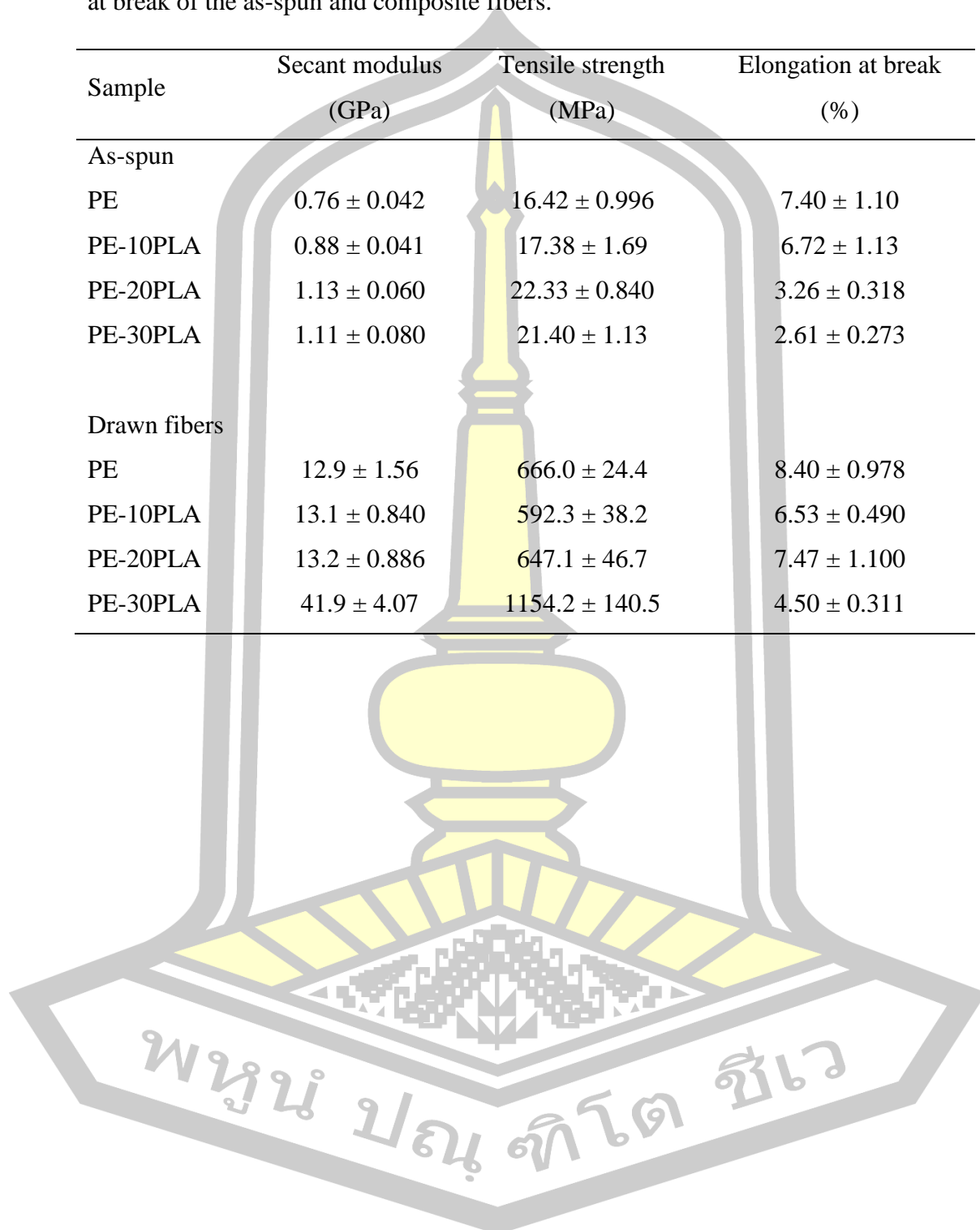


Table A2 Effect of rPET and compatibilizer on secant modulus, tensile strength and elongation at break of the as-spun and composite fibers.

Sample	Secant modulus (GPa)	Tensile strength (MPa)	Elongation at break (%)
As-spun			
PE	0.761 ± 0.042	16.4 ± 1.00	7.40 ± 1.10
PE-10PLA	0.882 ± 0.041	17.4 ± 1.33	5.24 ± 0.679
PE-10PLA-10rPET	0.756 ± 0.061	17.8 ± 0.91	3.93 ± 0.452
PE-30PLA-10rPET-5MA	0.838 ± 0.019	17.2 ± 1.12	4.02 ± 0.490
Drawn fibers			
PE	12.9 ± 1.55	666.0 ± 24.4	8.40 ± 0.978
PE-10PLA	13.1 ± 0.84	592.3 ± 38.2	6.53 ± 0.490
PE-10PLA-10rPET	19.6 ± 1.80	643.4 ± 41.8	5.20 ± 0.360
PE-30PLA-10rPET-5MA	16.7 ± 1.05	602.6 ± 31.2	5.42 ± 0.120

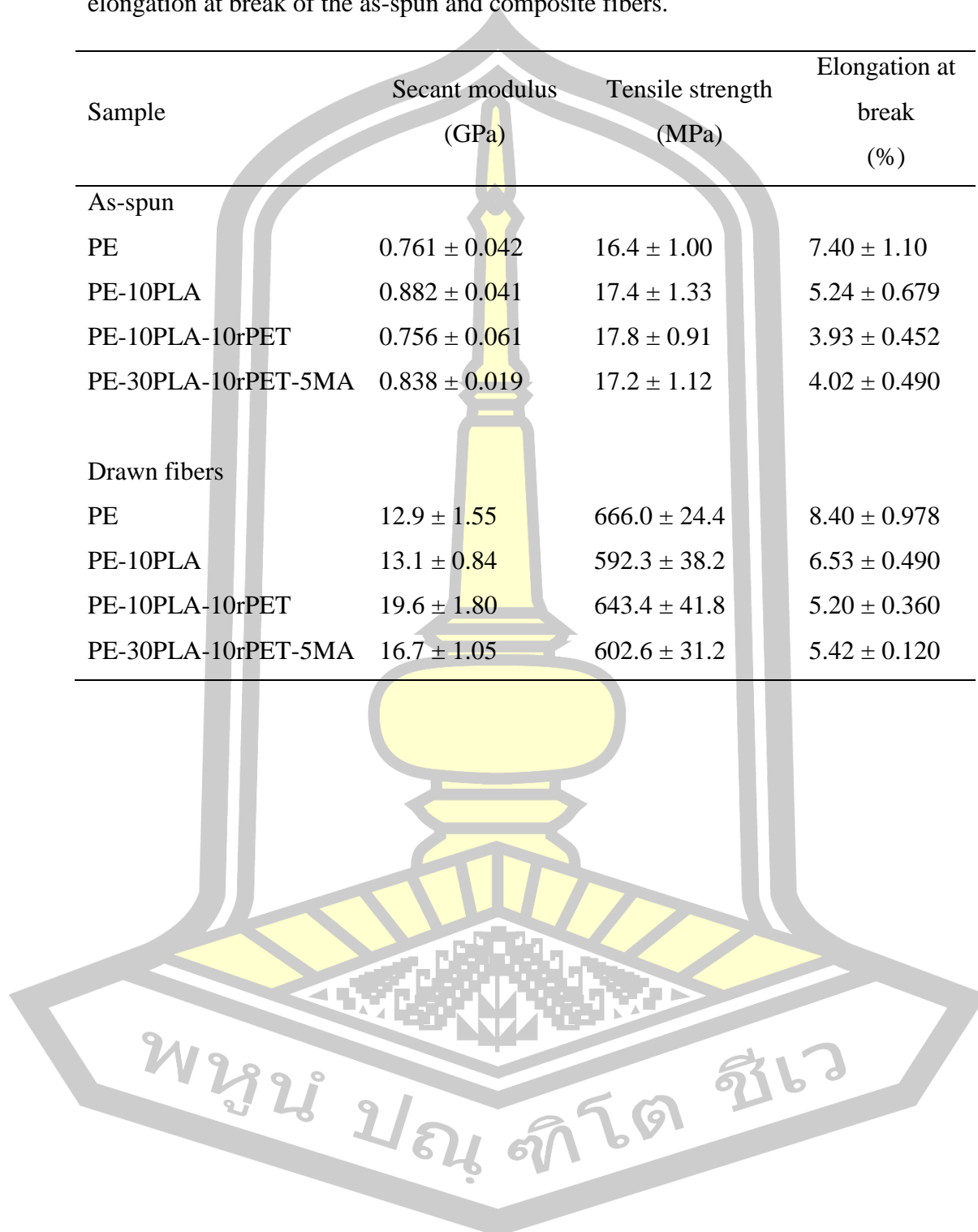


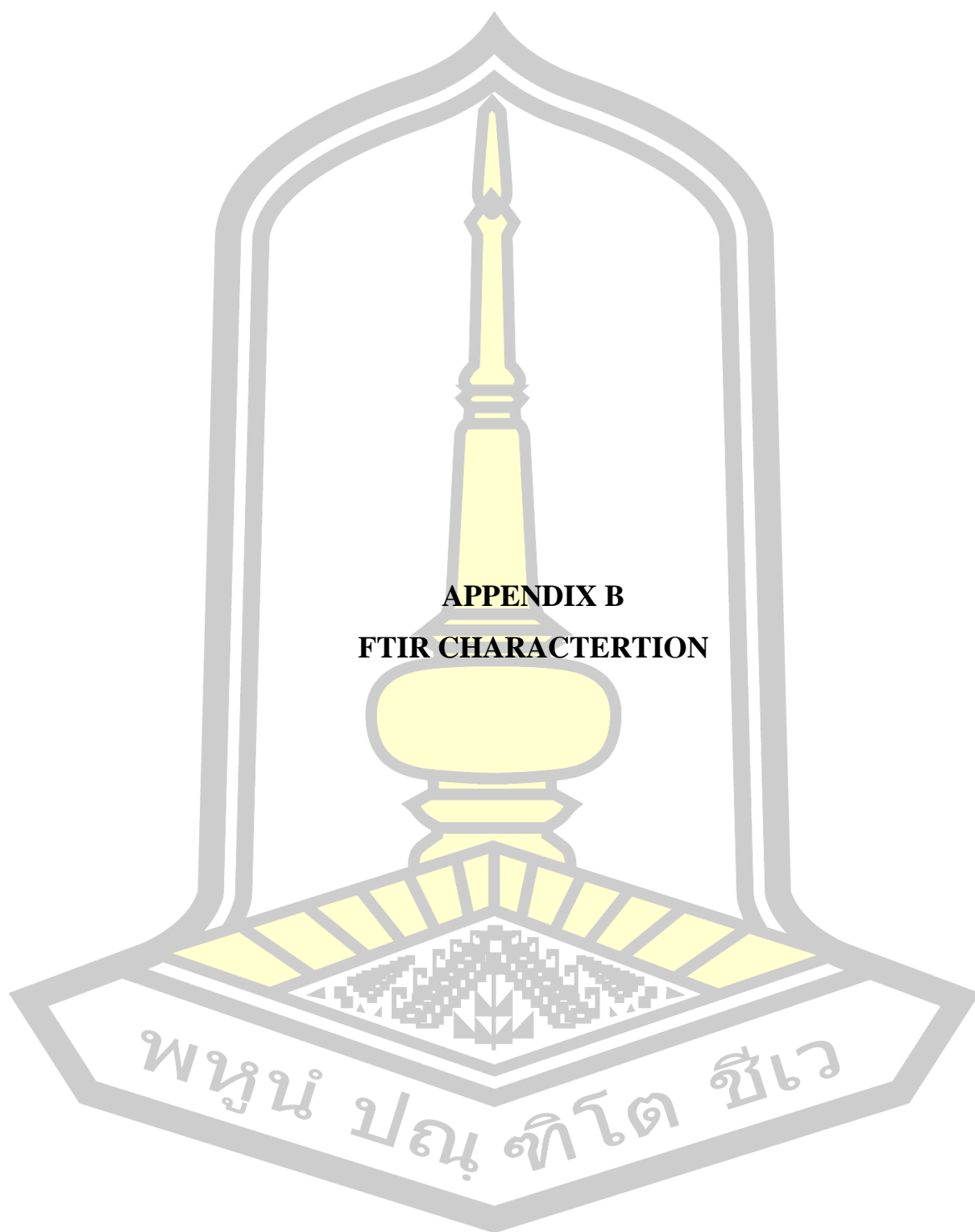
Table A3 Effect of draw ratios on tensile strength of polymer fibers.

Sample	Tensile strength (MPa)	
	PE-10PLA	PE-10PLA-10rPET
DR 10	318.5 ± 19.5	215.0 ± 6.57
DR 12	394.4 ± 14.9	306.1 ± 8.26
DR 14	502.2 ± 37.4	558.3 ± 23.1
DR 16	548.4 ± 11.9	615.8 ± 33.5
DR 18	599.6 ± 39.1	628.8 ± 23.7
DR 20	617.9 ± 45.0	643.4 ± 41.82

Table A4 Effect of rPET and LCP on secant modulus, tensile strength and elongation at break of the polymer fibers.

Sample	Secant modulus (GPa)	Tensile strength (MPa)	Elongation at break (%)
PE	12.9 ± 1.56	666.0 ± 24.4	8.40 ± 0.978
PE-10PLA	13.1 ± 0.840	592.3 ± 38.2	6.53 ± 0.490
PE-10PLA-10rPET	19.6 ± 1.80	643.4 ± 41.8	5.20 ± 0.360
PE-10PLA-10LCP	18.7 ± 1.68	665.0 ± 50.4	4.97 ± 0.694





APPENDIX B
FTIR CHARACTERIZATION

พหุจน์ ปณฺ ทิโต ชีเว

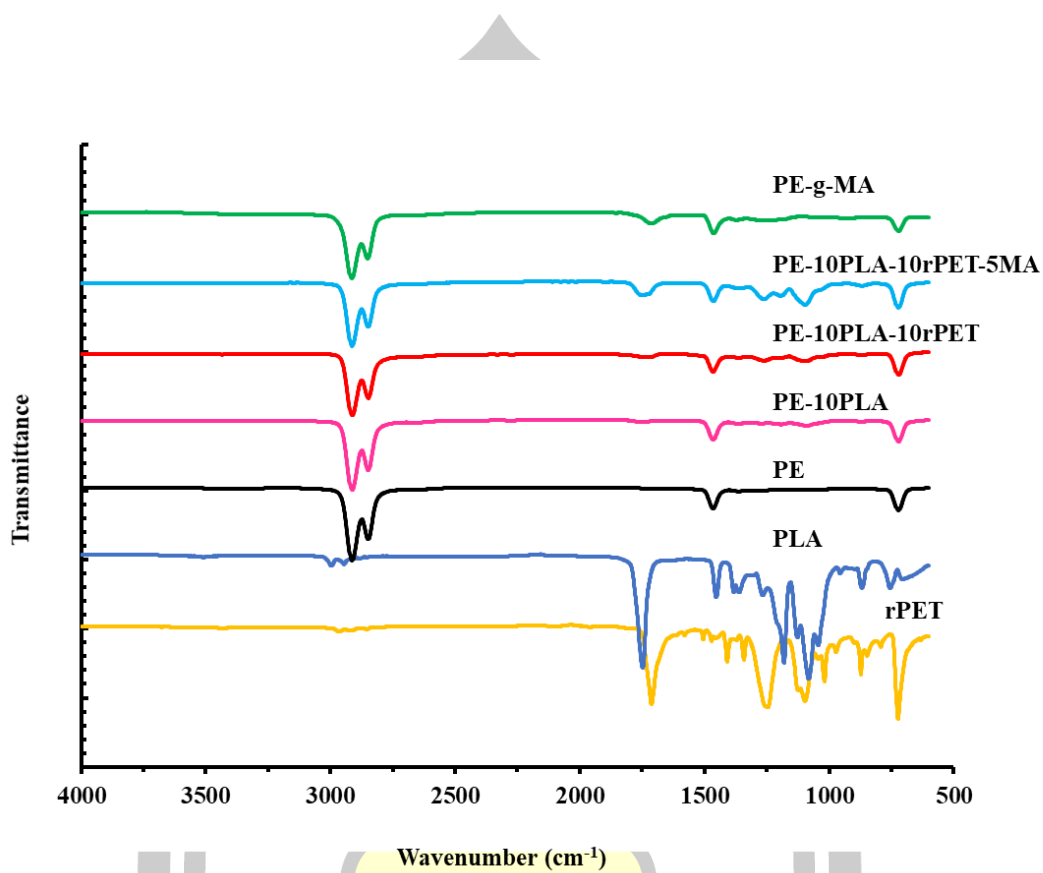
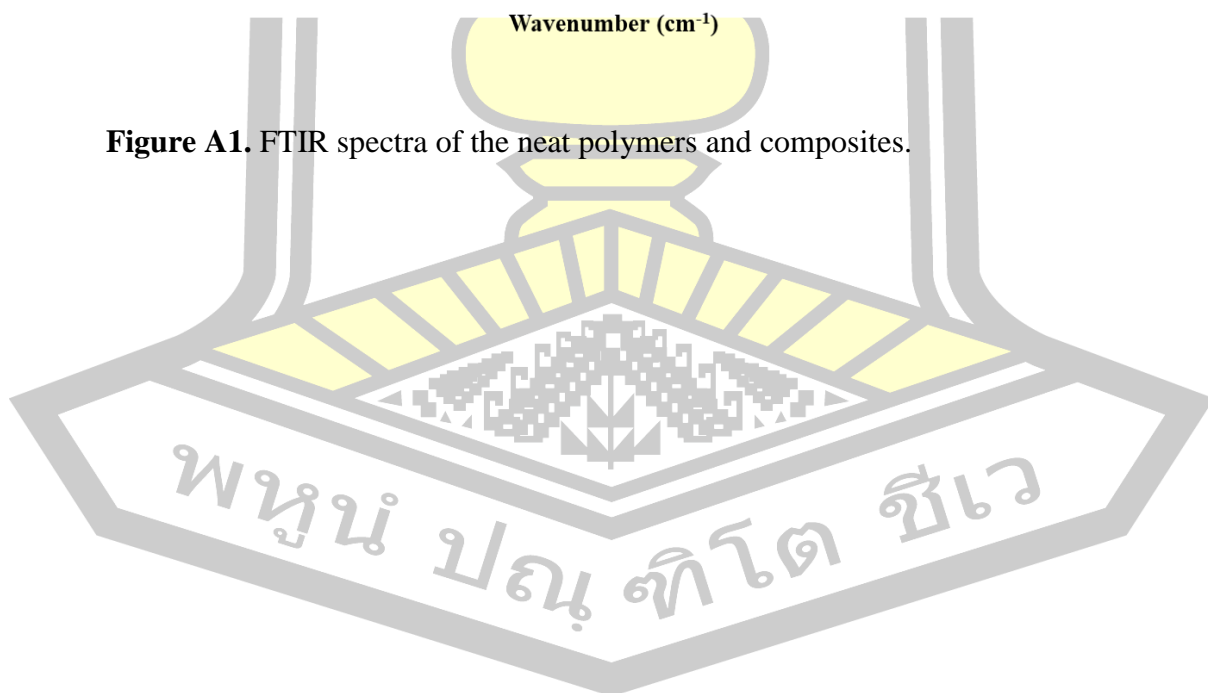
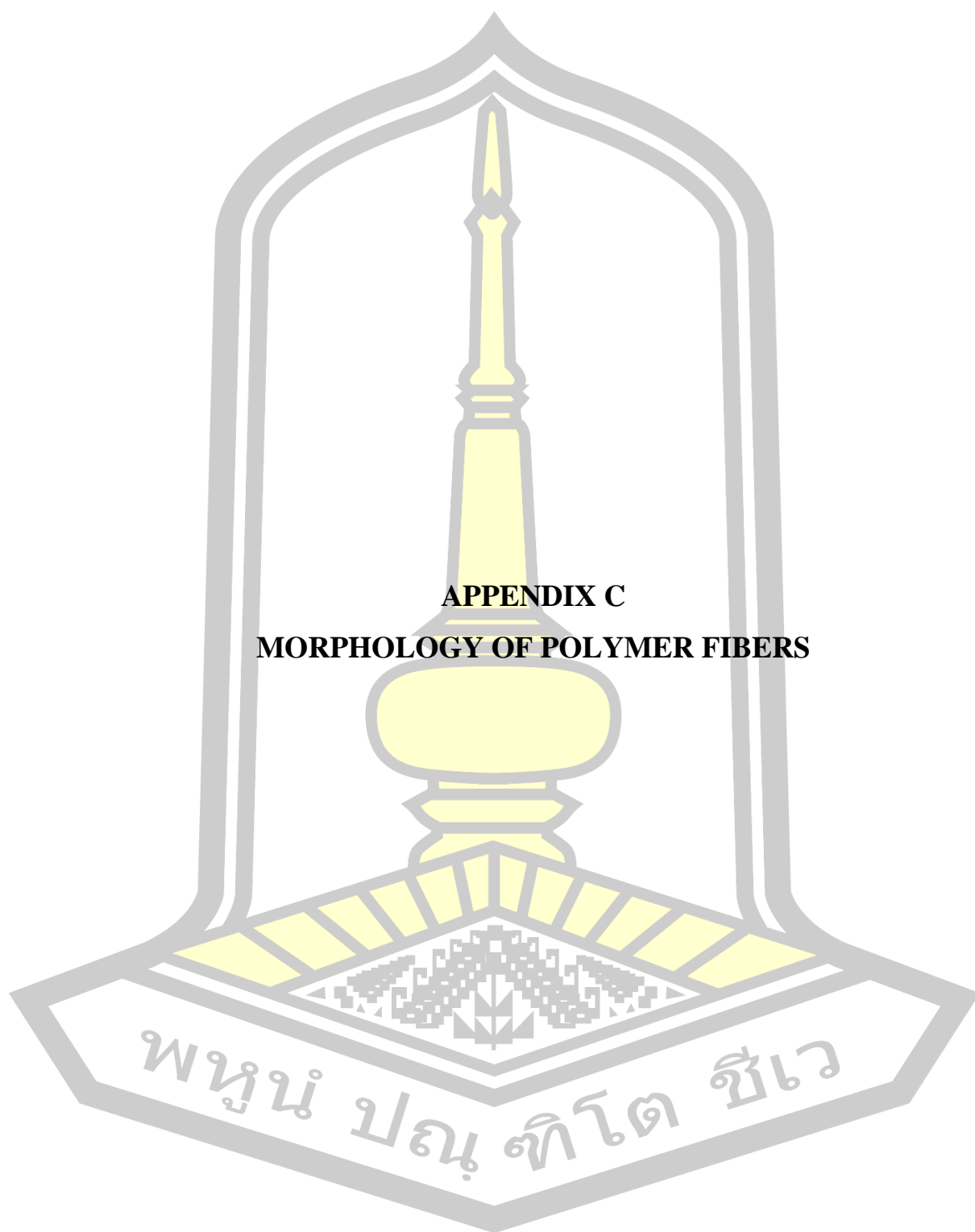


Figure A1. FTIR spectra of the neat polymers and composites.





APPENDIX C
MORPHOLOGY OF POLYMER FIBERS

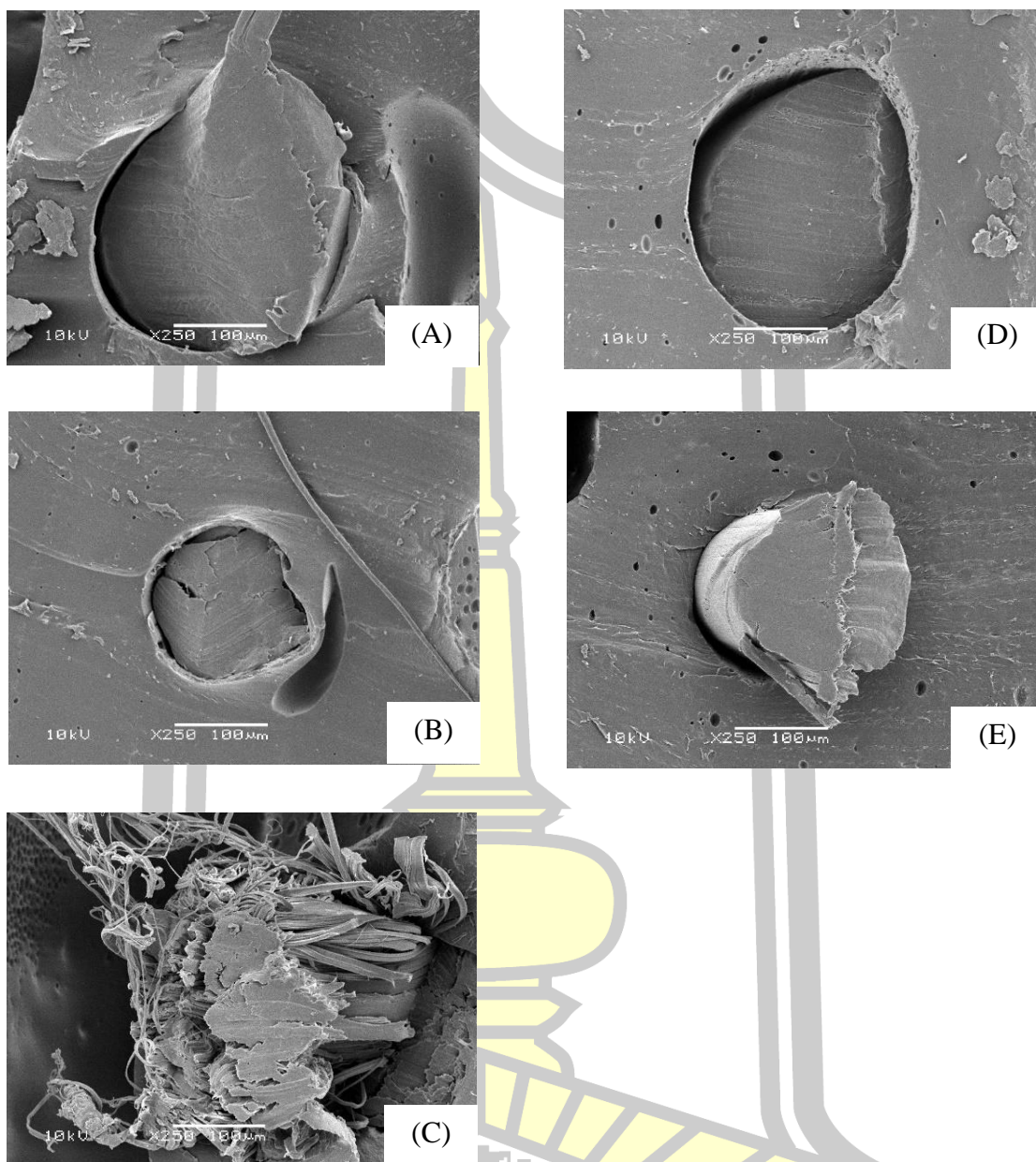
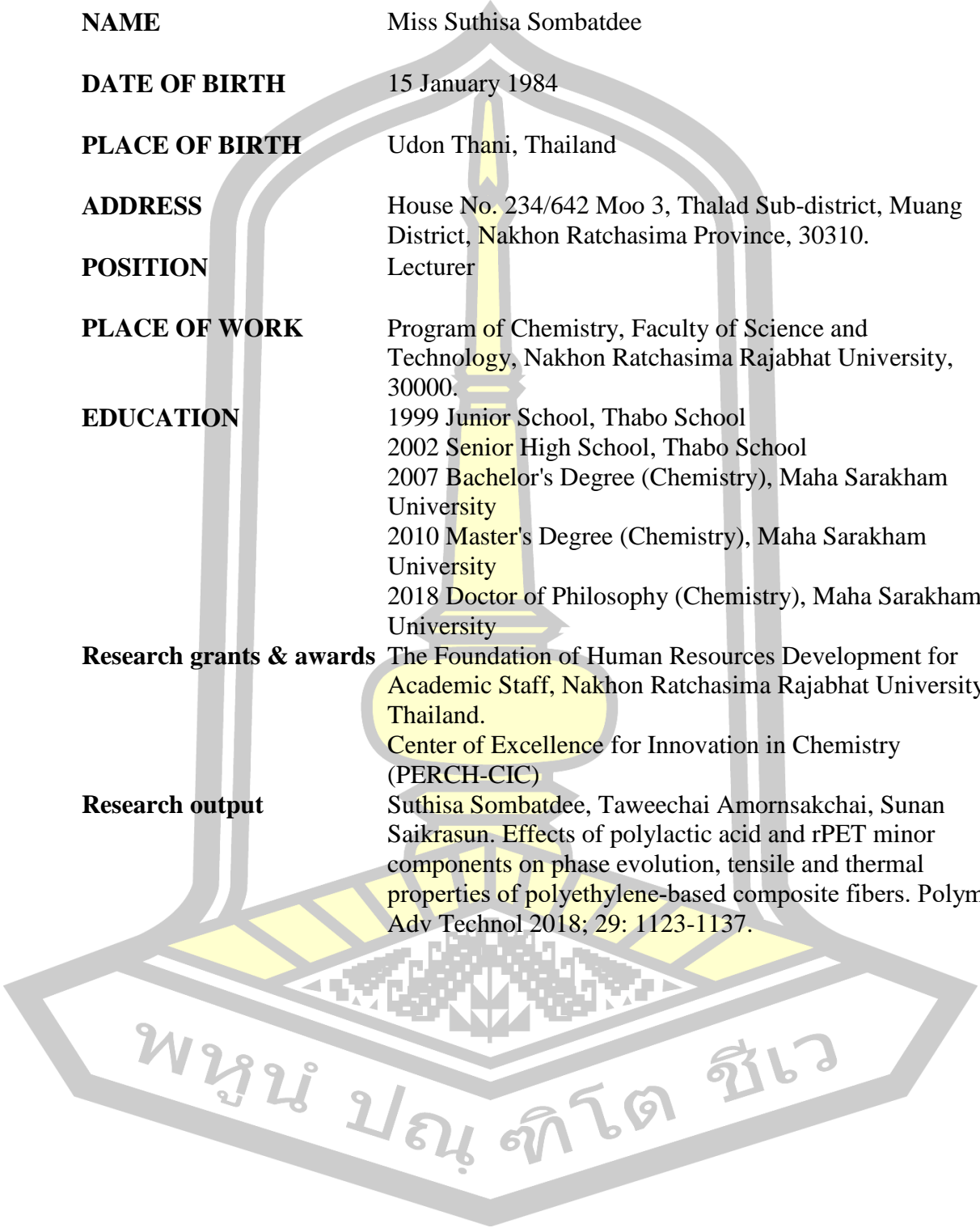


Figure A2. SEM images of fiber surfaces for PE-10PLA (A), PE-20PLA (B), PE-30PLA (C), PE-10PLA-10rPET (D) and PE-10PLA-10rPET-5MA (E).



NAME Miss Suthisa Sombatdee

DATE OF BIRTH 15 January 1984

PLACE OF BIRTH Udon Thani, Thailand

ADDRESS House No. 234/642 Moo 3, Thalad Sub-district, Muang District, Nakhon Ratchasima Province, 30310.

POSITION Lecturer

PLACE OF WORK Program of Chemistry, Faculty of Science and Technology, Nakhon Ratchasima Rajabhat University, 30000.

EDUCATION
1999 Junior School, Thabo School
2002 Senior High School, Thabo School
2007 Bachelor's Degree (Chemistry), Maha Sarakham University
2010 Master's Degree (Chemistry), Maha Sarakham University
2018 Doctor of Philosophy (Chemistry), Maha Sarakham University

Research grants & awards The Foundation of Human Resources Development for Academic Staff, Nakhon Ratchasima Rajabhat University, Thailand.
Center of Excellence for Innovation in Chemistry (PERCH-CIC)

Research output Suthisa Sombatdee, Taweechai Amornsakchai, Sunan Saikrasun. Effects of polylactic acid and rPET minor components on phase evolution, tensile and thermal properties of polyethylene-based composite fibers. Polym Adv Technol 2018; 29: 1123-1137.